# The Uptake of Acidic Gases on Ice

Thomas Huthwelker, Markus Ammann, and Thomas Peter

*Chem. Rev.*, **2006**, 106 (4), 1375-1444 • DOI: 10.1021/cr020506v

# The Uptake of Acidic Gases on Ice

Thomas Huthwelker,*,† Markus Ammann,† and Thomas Peter‡

*Laboratory for Radio- and Environmental Chemistry, Paul Scherrer Institute, CH-5232 Villigen, Switzerland, and Institute for Atmospheric and Climate Science, ETH Zurich, Universitätsstrasse 16, 8092 Zurich, Switzerland*

*Received July 25, 2005*

## *Contents*



† Paul Scherrer Institute.
‡ ETH Zurich.

10.1021/cr020506v CCC: $59.00 
Published on Web 04/12/2006

*God made solids, but surfaces were the work of the devil.*

Wolfgang Pauli

## *1. Introduction*

### 1.1. Objective of the Review

This paper reviews experimental and theoretical work on the nonreactive uptake of acidic trace gases such as HCl, $HNO_3$, HBr, HONO, and $SO_2$ on ice. The focus is on work performed within the last 15 years. Despite significant scientific efforts, the available data on total trace gas uptake, solubility, and diffusivity on or in ice scatter widely and show inconsistencies. This scatter might be caused by morphological differences, such as the degree of polycrystallinity or porosity of an ice film. In addition, the nature of the uptake process is not fully understood. Interpretations include the dissolution of trace gases into a "quasi-liquid layer", surface adsorption (Langmuir or BET-multilayer adsorption), the diffusion into the grain boundaries, and models that treat the uptake into porous ice films. We will review these theoretical concepts. Different methods for interpreting experimental data are considered as well, because they can cause inconsistencies among the published data sets. It is one aim of this review to seek consistencies and to illustrate inconsistencies among published data sets, hoping to stimulate further research to resolve such open questions.

Because the understanding of experimental data is deeply linked to the techniques used, we also review experimental techniques, with emphasis on two types of experiments:

Thomas Huthwelker studied physics at the University of Bonn (Germany). He performed his Ph.D. thesis at the Max-Planck-Institute for Chemistry in Mainz (Germany) with studies on uptake processes of HCl on ice under stratospheric conditions, using Knudsen cell experiments. After finishing his Ph.D., he was a postdoc at ETH Zürich (Switzerland) and simultaneously faculty adjunct at SUNY, Albany (USA), where he used ion beam analysis to study uptake processes on ice. His current work as researcher in the Surface Chemistry group at the Paul Scherrer Institute in Villigen (Switzerland) includes uptake processes on environmentally relevant surfaces.

Markus Ammann obtained his diploma in solid state physics from the Swiss Federal Institute of Technology in Zürich (ETH), Switzerland. He entered the field of aerosol research during his Ph.D. studies (ETH Zürich, 1988–1992, Research Supervisor, H. C. Siegmann), for which he developed a method of photoelectric charging of aerosol particles and applied it to volcanic aerosol emissions involving both laboratory and field work in a joint project of ETH Zürich and University of Catania, Italy. His current interest in heterogeneous atmospheric chemistry started during postdoctoral work first involving fundamental interaction studies of halide species with metal particles in gas suspension at Paul Scherrer Institute and later also dedicated to processes at the plant–atmosphere interface at the University of Bern. Since 1997, he has been head of the Surface Chemistry group of the Laboratory of Radio- and Environmental Chemistry at Paul Scherrer Institute, Villigen, Switzerland. His current activities include laboratory studies of mechanisms and kinetics of gas aerosol reactions and gas–ice partitioning.

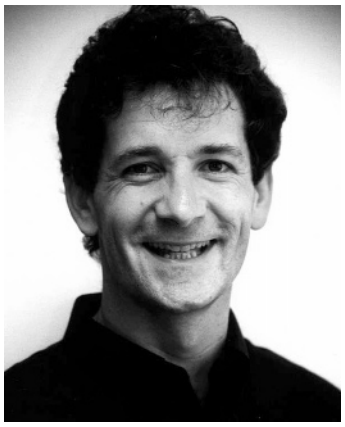

Thomas Peter studied physics at the University of Marburg and the Technical University of Munich, Germany, and at the University of Maryland, USA. In 1988 he received his Ph.D. for theoretical work on confinement fusion. In 1990 he began to study atmospheric chemistry and joined the Max Planck Institute for Chemistry in Mainz, where he led a group working on atmospheric aerosols. In 1995 he was appointed coordinator of the aerosol division of the German Ozone Research Program and a member of the steering committee of the high-flying aircraft Geophysica. Since 1997 he has been a member of the scientific steering group of SPARC, a project of the World Climate Research Program. He has been Professor for atmospheric chemistry at the Swiss Federal Institute of Technology (ETH) since 1999. With laboratory experiments, theoretical and modeling studies, and field campaigns, his group performs research on physicochemical processes of aerosol particles and trace gases, investigating their impact on the global atmosphere and climate.

First, we will consider direct experiments on the trace gas uptake on ice, such as experiments in Knudsen cells and flow tubes. Second, we will consider the various profiling techniques, which aim to determine the trace gas solubility and diffusion in the bulk or the near-surface region of poly- or single-crystalline ice. Some attention is also given to spectroscopic studies, which explore the formation of ions when acidic gases interact with ice. The latest technical developments based on synchrotron radiation are discussed briefly.

This review focuses on uptake processes of acidic trace gases on ice. Besides acid dissociation, we will not treat chemical reactions with other adsorbates or with the ice substrate itself. We also restrict this review to processes in the ice stability domain. The formation of hydrates is treated as considered necessary for understanding of the topic. Furthermore, we restrict this review to the partitioning between the gas and the solid phase. Therefore, we will treat surface adsorption, solubility, and diffusion of the trace gas. The uptake kinetics is considered as needed to understand the current data sets. Because the whole issue of measured uptake coefficients would be a review in itself, we exclude direct measurements of uptake coefficients from this review. This review puts some emphasis on hydrochloric acid, because most data are available for this system. In essence, it is a model system for the interaction of other strong acids, such as HBr or $HNO_3$, which are treated with less depth. In contrast to strong acids, we also treat $SO_2$ and HONO, which are less soluble in water and have lower affinity to ice.

## 1.2. Atmospheric and Environmental Relevance of the Trace Gas/Ice Interaction

There would be no life on Earth without the sunlight-driven water cycle. From rivers, oceans and natural ice surfaces water evaporates into the atmosphere, where it condenses as liquid droplets or ice and precipitates back to the Earth. Atmospheric ice occurs in many forms, such as micrometer-sized aerosol in cirrus clouds, graupel, or snowflakes of fascinating beauty. Most of the natural ice is located on the surface of the Earth as snow, firn, or glacial ice. Depending on climatic conditions, the natural ice may remain hundreds of years in mountain glaciers (e.g., ref 1) or even several hundred thousand years in the polar regions.[2]

Examples for atmospheric ice are cirrus clouds, which play an important yet only partly understood role in the Earth's radiation budget.[3] Another example is polar stratospheric clouds (PSCs), which form in the dry polar winter stratosphere at altitudes above 15 km. They consist of micrometer-sized sulfuric acid droplets, various acidic hydrates, and sometimes also water ice.[4,5] Both ice and ice-like surfaces (i.e., acidic hydrates) play a key role in atmospheric chemistry and climate research.

For example, the surface of polar stratospheric cloud material hosts reactions, such as reactions 1 and 2 below, that are important for the formation of the ozone hole.[6] It is important to note that many heterogeneous reactions occur on ice and ice-like surfaces and also on aqueous surfaces, only the reaction rates being different. Thus, studying ice may also shed light on the nature of ice-like surfaces. Most inorganic acidic gases, which are highly soluble in water, also have a strong affinity to ice surfaces. Thus, acidic gases are taken up into tropospheric rain or snow, leading to the environmental problem of acid precipitation.

These two major environmental issues, the formation of acid rain and the development of the ozone hole, triggered the research on the interaction of acidic trace gases with ice. This research field is also of key importance in the highly active field of climate research. Polar and alpine ice cores are used as a chemical archive for the Earth's atmospheric past.[7,8] Reading this archive, that is, to deduce the atmosphere's historic composition from the ice core, requires proper knowledge of how trace gases are taken up onto the surface of natural ice and finally built into the ice itself (see, for example, refs 9−12).

Furthermore, the recent discovery of a vigorous photochemical production of various trace gases, such as formaldehyde, acetaldehyde, NO, $NO_2$, and the acidic HONO in the polar snowpack, also poses the question of how acidic gases partition in the snowpack (see refs 12−15). The importance of the trace gas/snow interaction is underlined by the estimate that an equivalent of the whole atmospheric air is blown through the highly porous upper part of the snowpack[12] within a few months.

In the following section, we briefly discuss the role of the gases in the atmosphere that are treated in this review.

**Hydrochloric Acid (HCl).** Volcanic eruptions are a natural source of hydrochloric acid (HCl). Because it is highly soluble in water,[16,17] rain will wash HCl from the troposphere readily. The main sources for stratospheric HCl are industrially produced chlorofluorocarbons (CFCs). Because these substances are chemically inert and of low solubility in water, they can reach the upper stratosphere without being washed out. Here solar radiation cracks the CFCs into fragments, which undergo subsequent chemical reactions and, among other species, produce HCl. The heterogeneous reactions of HCl with chlorine nitrate ($ClONO_2$) or hypochlorous acid (HOCl) on PSC surfaces are

$$HCl \rightarrow H^+ + Cl^- \quad (1)$$

$$ClONO_2 + Cl^- \rightarrow Cl_2 + NO_3^- \quad (2)$$

$$HOCl + Cl^- \rightarrow Cl_2 + OH^- \quad (3)$$

where the neutral molecules in these reactions indicate gaseous species, which diffuse through the gas phase to and from the particle surface, whereas the ions indicate dissociated species, residing on (or slightly below) the particle surface. These reactions form molecular chlorine ($Cl_2$) during the polar winter. In the spring, once the sun rises, the photolysis of molecular chlorine initiates a chain of catalytic reactions that destroy ozone. Over Antarctica, these reactions may lead to an almost complete destruction of ozone, as a consequence of which the spring time ozone hole forms (for reviews of this topic, see refs 4, 6, 16, and 18−20).

Of all acidic trace gas interactions, the HCl/ice interaction has been studied most intensely. However, available measurements of the amount of HCl taken up onto the ice surface scatter from a few hundredths of a monolayer[21] to a few monolayers[22] for temperatures around 200 K. Although the existence of the heterogeneous reactions of HCl on ice surfaces is well established in laboratory studies, there are still inconsistencies[23] between the available data sets and unresolved controversies.[24−29]

**Hydrobromic Acid (HBr) and hydroiodic Acid (HI).** Methyl bromide ($CH_3Br$) is the main precursor for HBr in the atmosphere. It originates from biogenic processes in the ocean and from its use as a fumigant. HBr also originates from the anthropogenic emission of halons. In the strato-

sphere, methyl bromide and halons are photolyzed yielding atomic Br. A small fraction of the bromine is converted to HBr by reactions with $HO_2$ and HCHO (For detailed review, see ref 16). On polar stratospheric clouds, HBr dissociates and $Br^-$ may react with $ClONO_2$ to yield BrCl, another important compound for catalytic ozone destruction (upon photolysis). Hydroiodic acid (HI) is of some importance for the marine boundary layer chemistry[30] and possibly also for the stratospheric ozone.

HBr and other bromine compounds are of great importance to recent observations of ozone depletion events in polar regions,[13,31] and it has been argued that HBr is scavenged by aerosols and ice crystals,[32] leading to the release of $Br_2$, which is a key precursor for the catalytic ozone depletion.

**Nitric Acid ($HNO_3$).** Tropospheric nitric acid is mainly formed by oxidation of nitrogen oxides (NO, $NO_2$) originating from anthropogenic or natural combustion and lightning. Similar to HCl, $HNO_3$ is a highly water soluble strong acid with a strong affinity to ice. Thus, rain and snow will remove $HNO_3$ easily from the troposphere.

Stratospheric $HNO_3$ is produced by reaction of $NO_2$ with OH and by reaction 1. At sufficiently low temperatures, it dissolves in sulfuric acid aerosols.[33,34] Under most conditions, the stratosphere is too dry to form ice. However, there is sufficient $HNO_3$ in the stratosphere to allow for nitric acid trihydrate (NAT) at temperatures typically 7 K above the ice equilibrium temperature.[35] Similarly to ice and sulfuric acid, NAT particles act as catalytic surfaces hosting similar heterogeneous reactions.

Furthermore, the sedimentation of NAT or NAT-coated ice particles has been suggested to contribute to the denitrification of the stratosphere. This has been investigated in field,[36,37] modeling,[38] and laboratory studies.[39,40] Similarly, the partitioning and potential removal by sedimentation of $HNO_3$, which adsorbs on ice particles in cirrus clouds, have been suggested in modeling studies[41] and also based on measured $HNO_3$ uptake on ice surfaces in the laboratory.[42,43]

Nitric acid is also taken up onto snow, where it ionizes. The nitrate ions are believed to play a key role for the photochemical production of various nitrogen oxides (See refs 12, 14, and 44−47 and citations therein).

**Nitrous Acid (HONO).** This compound is recognized as a precursor for hydroxyl radicals in polluted urban air. The chemical processes leading to the formation of HONO are, however, still not well understood. Laboratory studies show that HONO formation occurs primarily on surfaces. Water also plays an important role in the conversion process as has been shown in the laboratory and recently also suggested in field experiments.[48] One possible source for HONO may be the surface of soot particles.[49,50] While the formation rate seems to be fast in the first minute of exposure with $NO_2$, a passivation of the surface rapidly slows down the formation afterward. Stratospheric HONO plays a role within halogen activation on particle surfaces, $X + HONO \rightleftharpoons OH + NOX$, with X = Cl or Br. In the stratosphere, NOX photodissociates rapidly to yield halogen atoms, which destroy ozone through catalytic chain reactions.[51] Besides natural source reactions, HONO is produced by combustion emission from aircraft engines operating in the upper troposphere or lower stratosphere.[52]

HONO is one of the key products from photochemical processes in snow, as it has been shown in field experiments in the Arctic,[45,53−55] and it has been pointed out that understanding the snow microphysics is of crucial importance for our understanding of arctic snow chemistry.

**Sulfur Dioxide ($SO_2$).** Most of the atmospheric $SO_2$ is due to anthropogenic emissions such as exhausts from fuel combustion. Natural sources include biomass burning and volcanic eruptions. Most of the atmospheric sulfur is emitted as $SO_2$, with some as hydrogen sulfide ($H_2S$) and dimethyl sulfide ($CH_3SCH_3$, DMS) or organic carbonyl sulfide (OCS) from biogenic processes.[16]

In contrast to HCl and $HNO_3$, sulfur dioxide is much less soluble in water.[56] However, dissolved sulfur dioxide is easily oxidized to sulfuric acid ($H_2SO_4$) by various atmospheric oxidants, mainly the hydroxy radical (OH) and also ozone ($O_3$) and hydrogen peroxide ($H_2O_2$). Because sulfuric acid is nonvolatile, the uptake of $SO_2$ into water or ice is practically unlimited, once enough oxidants are available, because the oxidation reactions are acid-catalyzed. Conversely, if there are not enough oxidants in the atmosphere, the solubility of the $SO_2$ in liquid droplets strongly depends on the liquid pH due to the equilibrium reaction $SO_2 + H_2O \rightleftharpoons HSO_3^- + H^+$. To some extent, in the absence of oxidants, $SO_2$ is also removed by dry deposition to snow[57,58]

In the absence of oxidants, the uptake of $SO_2$ on clean ice has a most exciting feature: the amount of uptake increases with increasing temperature, which is in contrast to classical adsorption processes.[59−62] This unique feature has not yet been observed with any other trace gas and deserves attention because it may point to a complex uptake process and the possible influence of surface or interfacial melting on trace gas uptake.

## 1.3. Microphysics of the Trace Gas Uptake

The uptake of trace gases by liquids is conceptually simple. The partitioning between gas and condensed phase is mostly governed by solubility, diffusion, and reaction of the trace gas in the liquid phase.[63−65] Only at extreme conditions, such as high chemical reactivity of the trace gas in the liquid or under high vapor pressures, adsorptive processes on the liquid surface can play a role.[66−69] General frameworks to model such processes have been developed and are summarized in several publications and reviews.[63−65,70,71]

For solid matter, the physical picture is less clear. Because the solubility of trace gases in solids is lower and the diffusion in solids is much slower (e.g., refs 72−74), the bulk contribution is less important than the surface adsorption.[75] Moreover, the trace gas uptake on ice is a composite process,[56,63,64,76,77] as illustrated in Figure 1. Molecules hitting the surface will either be reflected into the gas phase or be accommodated on the surface into different types of adsorption states. For acidic gases, these may just be weakly bound precursor states to a more strongly bound chemisorbed (e.g., fully hydrated or dissociated) state. They may also diffuse on the surface in the adsorbed state.[78] The ice might be porous, and transport processes into such pores might enhance the effective surface area and hence the overall uptake.[25,79] Moreover, in most experiments, neither the ice surface nor the ice bulk is a perfect crystal. The ice surface itself consists of atomically flat parts (terraces) but may have may steps and kink sites, especially at lower temperature, where no surface melting occurs. Crystalline imperfections can also be found in the bulk of the polycrystalline ice, where grain boundaries and triple junctions may serve as additional reservoirs for the uptake of trace elements.[9−11,80,81] To some extent, trace gases may also dissolve in the ice matrix itself.

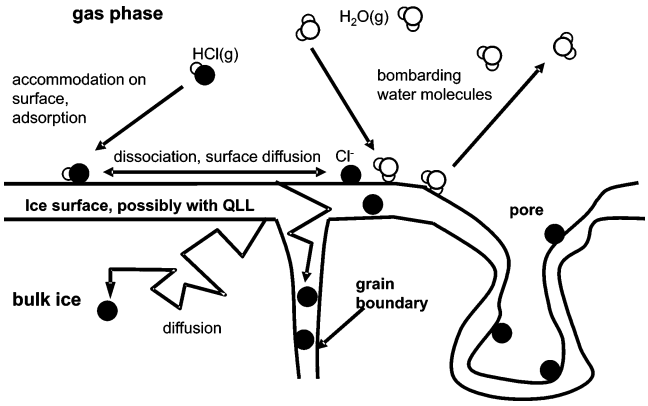


**Figure 1.** Conceivable processes for HCl uptake on ice: impingement of HCl molecules onto the surface, surface accommodation, adsorption, dissociation, surface diffusion, possible uptake into QLL or formation of a QLL by the presence of HCl, and diffusion into a crystal matrix and into grain boundaries. Simultaneous bombardment of the surface with water molecules.

In addition, it has been suggested that trace gases are taken up into the quasi-liquid layer (QLL) (e.g., refs 61 and 82−86).

## 1.4. The Nature of the Ice Surface

Research on the nature of the ice surface has a long and often controversial history. The existence of a disordered surface layer (or quasi-liquid layer, QLL) at temperatures close to the ice melting point had already been investigated in the middle of the 19th century by Faraday.[87,88] He studied the adhesion of two adjacent ice balls, each hanging at the end of an individual thread. The ice balls adhered to each other, while at the same time each could rotate around its center of mass. Faraday concluded that there was a mobile layer between the two ice surfaces. Today, surface disorder is a well explored phenomenon in solid-state physics,[89−91] and detailed reviews for metals[92] and ice[93,94] are available in the literature. In the following section, we describe the main findings of this research field with focus on the trace gas/ice interaction.

**The Physics of Surface Disorder.** Surface disorder is the breakup of the solid crystal structure in the upper $1-10^5$ monolayers closest to the solid−vapor interface.[92] The main feature of surface disorder, increasing disorder with rising temperature, is demonstrated in Figure 2, which shows a molecular dynamics simulation of surface disorder on ice. While at low temperatures, only the uppermost ice layer deviates from the ideal hexagonal ice lattice, both the intensity of the disorder and the depth of the disordered region increase with increasing temperature.

Surface disorder occurs on many solids at temperatures close to their melting points. The thermodynamic reason for surface melting is that the disorder reduces the total free energy of the entire system consisting of the crystalline bulk and the disordered surface layer (see refs 91, 93, and 95 and references therein). Different surface configurations may exist on different crystal facets of the same solid if they are energetically more favorable.[96] Lead (Pb) is an interesting illustration of this behavior: Surface disorder has been experimentally observed on most of the facets, except on the (111) and (100) facets.[97] Similar observations have been made for aluminum.[98,99] In case of lead, facets not showing any surface melting can be overheated by up to 120 °C above the metals' melting temperature.[100] Such effects have been corroborated in molecular dynamics studies.[101]

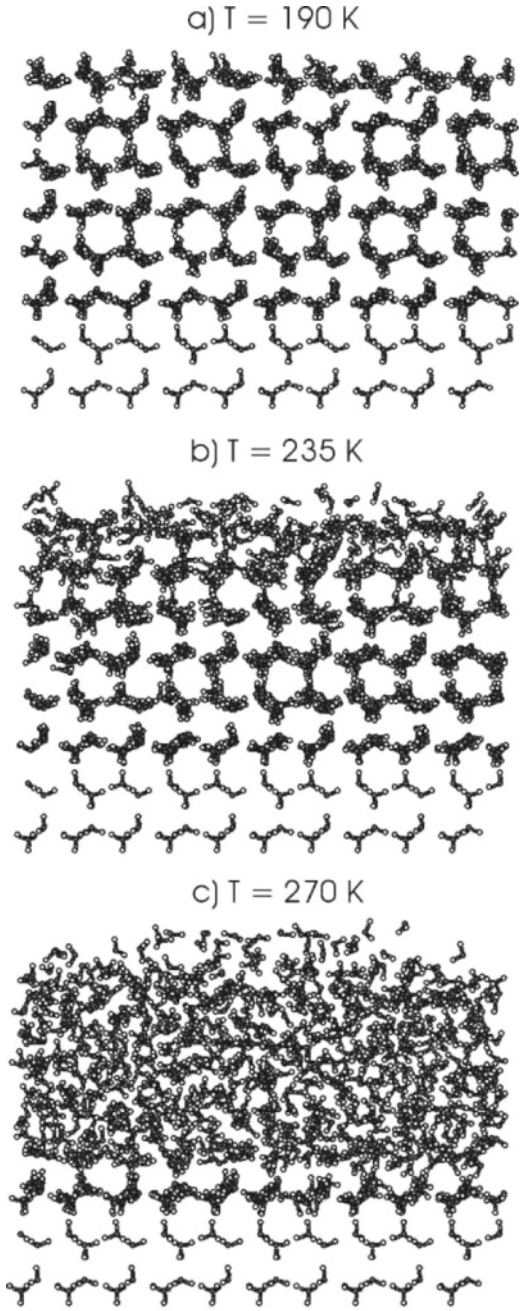


**Figure 2.** Molecular dynamics study of surface premelting on hexagonal ice. (Reprinted with permission from ref 361. Copyright 2001 Elsevier.)

Based on these results, surface melting can be considered as germ formation for the nucleation of the phase transition from the solid to the liquid state. Thus, surface disorder is responsible for the asymmetry that liquids, such as water, tend to supercool massively before the solid nucleates, whereas the solid cannot "superheat" in the presence of surface disorder. Therefore, the disordered layer has also been called the premelt layer. Because several names are used in the literature for the thin disordered layer on the surface of ice, we adopt the term "quasi-liquid layer" (QLL) in this review.

**Experimental Evidence for Surface Disorder on Ice.** There is compelling experimental evidence from various techniques that the near-surface region of ice differs from the crystalline ice bulk and moreover exhibits water-like properties. Surface conductivity measurements[102] show a high

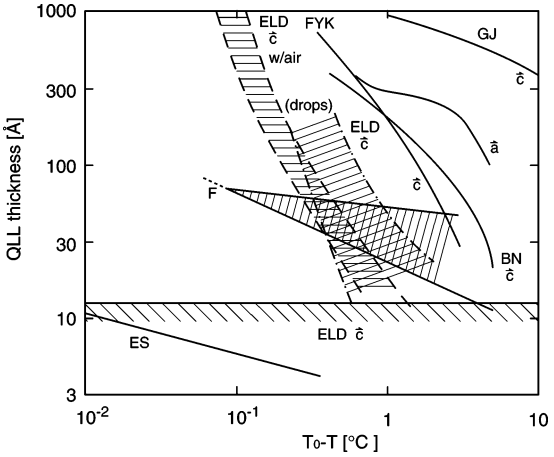


**Figure 3.** Thickness of the surface premelt layer, as derived from measurements and theoretical considerations: ELD,[104] FYK,[103] and BN,[105] ellipsometry; GJ,[114] proton channeling; F[116,117] and ES,[464] theoretical predictions; $\vec{a}$, basal surfaces; $\vec{c}$, prismatic surfaces. (Adapted with permission from ref 104. Copyright 1993 Elsevier.)

mobility in the surface region of ice. Ellipsometry on ice suggests the existence of a surface layer on the ice surface[103−105] with a refractive index between those of water and ice.[103] Furthermore, the nuclear magnetic resonance (NMR) signature (and thus the self-diffusion constant of water) in an interfacial layer was found to be between those of ice and water.[106] Surface-sensitive X-ray studies provided the first direct evidence that the surface layer is indeed disordered.[107−109] Measurements with atomic force microscopy on ice surfaces demonstrated the existence of a viscous surface layer on ice.[110,111] The infrared spectrum of the ice surface, as measured with attenuated total reflection spectroscopy, equals the one of water at the triple point, while it slowly changes to the one of ice when the temperature is decreased.[112] A similar result was obtained with the synchrotron-based near-edge X-ray absorption fine structures spectroscopy (NEXAFS) technique,[113] where a gradual change of the photoelectron spectrum from a water-like to an ice-like spectrum was observed when the temperature was decreased.

In all these studies, features of disorder were found close to the ice melting point, which disappeared when the temperature was lowered below a certain threshold. Thus, these studies indicate that the ice surface has water-like properties at the triple point but smoothly changes its nature to a more ice-like state when the temperature is lowered.

While the existence of a special layer on the ice surface has been experimentally confirmed in many studies for temperatures above −20 °C, the estimates for the layer thickness and threshold temperature vary widely (cf. Figure 3). At lower temperatures, disorder has also been observed. Using proton channelling, Golecki and Jaccard[114] showed that vibrations of oxygen atoms are larger in the near-surface region than in the bulk ice for temperatures as low as −50 °C. Recent studies using second harmonic generation suggest that surface disorder in the upper atomic layer on the ice surface may already exist at temperatures as low as 200 K on pure ice.[115]

The quantitative differences between these studies might be because different techniques are sensitive to different physical features of the surface layer. Some methods measure "bulk properties in the near-surface region of the ice surface", such as hardness and viscosity (AFM), refractive index (ellipsometry), or crystal order (surface-sensitive X-ray scattering). The sensitivity to thermal vibrations and the restriction to the outermost monolayer are the possible reason proton channelling and nonlinear optics techniques[115] showed evidence for disorder at temperatures much lower than the other techniques.

**Modeling Surface Disorder on Ice.** An early attempt to model surface melting on ice was made by Fletcher.[116,117] He estimated the energy reduction in the QLL, which is caused by the reorientation of the water molecules on the surface, and concluded that disorder at the ice surface should exist to temperatures as low as −30 °C. Modern models assume that surface melting occurs once a surface can be wetted by its own melt (e.g., refs 89, 91, 93, 94, 118, and 119 and citations therein). This concept predicts that the QLL disappears at low temperatures, while its thickness, $d_{qll}$, grows to infinity when the triple point temperature, $T_0$, of the solid is reached, where solid and liquid can coexist. For a system dominated by van der Waals forces, the relationship

$$d_{qll} \propto (T_0 - T)^{-1/3} \quad (4)$$

can be derived.[93]

The picture of a thin, homogeneous liquid layer with a sharp interface to the ice crystal matrix provides a conceptual idea to explain or predict properties of the ice surface. However, in reality, the disordered layer is probably not a film that is homogeneous in the direction perpendicular to the surface. This is indicated by molecular dynamics simulations, which show for aluminum[120] or ice[121−128] that the disordered surface layer exhibits a smooth transition from the rigid crystal lattice in the bulk of the ice toward the very disordered surface. It is noteworthy that realistic modeling of the ice surface by means of molecular dynamics has proven difficult, because, for example, the melting point of simulated ice is typically several tens of degrees too low.[125,127,128]

**Surface Disorder and Impurities.** It has been hypothesized that trace gases do not simply adsorb onto the ice surface but rather dissolve into the quasi-liquid ice surface (e.g., refs 61 and 82−86). Only a few studies deal with interaction of impurities with the QLL. Beaglehole[129] used bulk thermodynamic arguments and concluded that the QLL on ice should exist at lower temperatures than those in pure ice if a salt is present. Using the Derjaguin−Landau−Verwey−Overbeek theory (e.g., refs 130 and 131), Wettlaufer[132] investigated the importance of solute effects and showed that even small amounts of impurities may have profound effects on the QLL thickness.

The impact of impurities on the disordered layer has been demonstrated by ellipsometry, where the layer thickness changed once the ice was exposed to gaseous nitrogen.[104] Hydrocarbon contaminations[113] and salts[110] have been shown to strongly enhance the surface disorder of ice. There is also indirect experimental evidence that the trace gas/ice interaction is connected to the phenomenon of surface melting. Measurements of the adsorption of alkenes on ice showed that the enthalpy of adsorption at −35 °C changes abruptly to a value close to the enthalpy of dissolution in water, which was interpreted as the onset of surface melting of the ice surface.[133]

**Surface Defects.** Below a certain temperature threshold, surface premelting disappears and the ice surface becomes crystalline. While an ideal crystal forms atomically flat

crystal planes (terraces), on a real crystal, surface defects, such as steps or kink sites, are to be expected. Each of these sites may have an individual adsorption energy for adsorbing molecules, as it has been shown theoretically[134] for the HCl/ice system. For practical matters, data on trace gas uptake on ice always refer to an average uptake over all different sites, because the uptake to individual processes has been unaccessible in uptake experiments. However, we note that a roughening of the ice surface with time has been reported,[22,135] which may indicate that the surface configuration of the ice changes with time and, in turn, also the nature of the uptake process.

**Bulk Defects and Interfacial Reservoirs.** Polycrystalline ice consists of individual single crystalline grains and confined liquidlike reservoirs in grain boundaries and triple junctions, which are the lines where three grain boundaries meet. The latter are also called veins. When ice freezes, most impurities are expelled from the ice and accumulate in confined reservoirs in a second phase.[136−140] For example, sulfuric acid has been found in the veins of polar ice.[11] Also hydrochloric acid (HCl) has been localized in veins of laboratory ice after exposure to gaseous HCl.[10] The existence of liquid water[141,142] and ions[81] has been shown experimentally in veins of polycrystalline ice and in the necks of adjacent ice spheres.[143] Recently, it has been suggested that the impurity transport in liquid(-like) veins should be considered when interpreting polar ice cores.[144−146]

Such liquidlike inclusions in confined reservoirs are thermodynamically stable, that is, the chemical potential of all species must be equal in all phases. Depending on thermodynamic conditions (temperature, pressure, etc.), either a solid or a concentrated solution forms. Liquids in veins are further stabilized by the negative curvature of the ice−liquid interface inside the vein.[80] This interface phenomenon is comparable to the Kelvin effect, which leads to enhanced vapor pressure over small droplets (but is opposite in sign). Furthermore, disorder may be induced by the local force fields at the reservoir/ice interface, similarly as for the QLL.[94]

It is important to note that the interplay between impurities and surface forces is very complex. At high concentrations, bulk thermodynamics dominates and additional impurities will enhance the reservoir size. For very low impurity concentrations, however, the reservoir size may decrease with increasing impurity level, when the attractive part of the dispersion force starts competing with the repulsive screened Coulomb interaction.[147] These effects may be important when studying the trace gas uptake on ice. In confined reservoirs, additional impurities such as dissolved salts or nonvolatile acids will change the amount of trace gas uptake by two main effects. First, there is a chemical interaction between the trace gas taken up and the impurity in the ice, such as it has been observed for the uptake of $SO_2$ on doped ice[60] and interpreted by assuming liquid-phase chemistry.[84] Second, impurities may change the reservoir size. Because both effects occur simultaneously, synergistic effects may lead to unexpected effects of great importance in environmental research, because ice in nature always hosts a mixture of various impurities.

### *1.4.1. Controversies Connected to the Issue of Surface Melting*

There has been some controversy[86,148−152] about how to model the thermodynamics of the QLL and how to use this concept in environmental sciences.

**Homogeneity of the QLL.** The hypothesis that the disordered surface layer on ice can be modeled in terms of a homogeneous thin layer[93] has been criticized by Knight.[149] He did not question the existence of a disordered surface layer but the applicability of the wetting theory to model surface melting on ice. This theory requires the surface energies of both the ice−water interface and the water−gas interface (see section 2.2). He argued that these energies are ill defined quantities, because the QLL on ice is a nonhomogeneous region, in contrast to thin films on interfaces, for which wetting theory[131] has been designed originally.

**Gibbs' Phase Rule.** Knight[149] argued that the wetting concept violated the Gibbs' phase rule, because only at the triple point could three phases (liquid water, solid ice, and gas phase water) coexist. This argument was countered by Baker and Dash,[150] who pointed out that taking surface properties, such as the surface thickness, explicitly into account would introduce two additional independent (conjugated) variables (the surface energy, $\sigma$, and the surface area, $A$) into the thermodynamic equations. This allowed a further degree of freedom and thus the presence of an additional (two-dimensional) phase (see also section 2.2).

**Contact Angle of Water on Ice.** Another point of interest brought up by Knight[149] and by Fukuta and Lu[148] is that measurements of the water−ice contact angle (see citations in ref 149) do not show a vanishing contact angle. Therefore, water does not perfectly wet the ice surface. This point is corroborated by ellipsometric measurements[104] showing incomplete wetting[94] of the ice surface, that is, the thickness of the surface layer does not diverge to infinity when the temperature is increased to the ice melting point (in contrast to eq 38 below). Furthermore, the formation of droplets with a nonzero contact angle was observed in this study.

This issue has been taken up later by Makkonen,[153] who argued that the ice−liquid surface energy, $\sigma_{sv}$, cannot be determined by measuring the contact angle of water on ice if ice is covered by a disordered layer, because then the water drop would not rest on the dry ice surface but rather on top of the premelt layer. To resolve this issue, Makkonen[153] measured the contact angle of hot water (∼85 °C) on the crystalline ice surface at temperatures too low to exhibit surface melting. He arrived at a surface energy of $\sigma_{sv} = 73$ mJ m$^{-2}$, more than than 30 mJ lower than that previously determined.[154] Because thermodynamic equilibrium appears difficult to establish for a hot water droplet resting on a cold ice surface, such measurements deserve careful reinvestigation.

**Evaporation of Atmospheric Ice Particles.** Chen and Crutzen[86] suggested that a contaminated quasi-liquid layer reduces the ice vapor pressure and thus prolongs the evaporation of atmospheric ice particles. Baker and Nelson[152] commented that a surface layer on micrometer-sized atmospheric ice particles should be a few tenths of a nanometer thick and thus in equilibrium with the underlying ice. Because solubilities in ice were very low, no change of the ice vapor pressure and thus of the evaporation rate can occur. In their reply,[155] Chen and Crutzen admitted that a thin surface layer may be quickly in equilibrium with the underlying ice but argued that atmospheric ice was mostly out of thermodynamic equilibrium and possibly full of defects and solute inclusions, which could render equilibrium considerations questionable.

While the mechanism of how impurities change the properties of ice remained questionable, both groups pointed

toward the possibility that impurities might severely affect the evaporation of ice, as it was observed in early studies by Davy and Somorjai.[156] In current research, this issue is subject to many studies,[38,39,157−159] which are not the topic of this review.

## 2. Thermodynamics and Kinetics of the Trace Gas/Ice Interaction

### 2.1. Thermodynamics of Trace Gas Uptake

#### 2.1.1. Raoult's and Henry's Laws

Uptake processes, such as the dissolution of trace gases into liquid or solid condensed matter or adsorption onto its surface, are driven by the same thermodynamic principle. At thermodynamic equilibrium, the chemical potential

$$\mu_i = \left(\frac{\partial G}{\partial n_i}\right)_{T,p,n_j} \tag{5}$$

of each trace species $i$ must be equal in all phases.[160,161] For ideal mixtures, the chemical potential of species $i$ with mixing ratio $x_i$ is

$$\mu_i(T,p) = \mu_i^0(T,p) + k_B T \ln x_i \tag{6}$$

where $\mu_i^0$ is the Gibbs free energy needed to transfer one mole of $i$ from a selected standard state in a pure system at $(T_0,p_0)$ into the state at $(T,p)$. The term $k_B T \ln x_i$ describes the change of the chemical potential by diluting the pure substance with another substance. The mixing ratio of the $i$th species in the gas phase with total pressure $p$ is directly related to the partial pressure by $p_i = p x_{g,i}$. In this section, we use the mixing ratio as a unit for the amount of dissolved matter in the solid phase. For practical matters, often other units are more convenient, as described in Appendix A.

For a solvent, such as water or ice, the thermodynamic equilibrium conditions read

$$\mu_{c,w}^0 + k_B T \ln(1 - \sum_i x_i) = \mu_{g,w}^0 + k_B T \ln\frac{p_w}{p_v} \tag{7}$$

with indices g and c denoting the gas and the condensed phase, respectively. Here $x_i$ are the mixing ratios of the dissolved species in the condensed phase, $p_v$ is the vapor pressure of the pure condensed phase (i.e., pure water or ice), and $p_w$ is the vapor pressure of the condensed phase with a dissolved impurity. At the triple point (i.e., the pure system without an impurity as the standard state), we have $\mu_{c,w}^0 = \mu_{g,w}^0$ and find Raoult's law:

$$p_w(x_i) = p_v^0(1 - \sum_i x_i) \tag{8}$$

It is difficult to use eq 6 for the dissolved species because the term $\ln x$ diverges for $x \to 0$. To overcome this problem, an infinitely dilute solution is defined: The standard potential $\mu_i^0$ is split into two terms: $\mu_i^0 \equiv \mu_i^\infty + kT \ln f^\infty$, where a unity activity coefficient, $f^\infty$, is chosen in the limit of infinite dilution, that is, $f^\infty \equiv 1$ for $\lim x \to 0$. By this procedure, the standard state, $\mu_i^\infty$, of an infinitely dilute solution is defined. It corresponds to the free energy needed to dissolve a mole of trace gas in an infinite amount of solvent.

For infinite dilution ($f^\infty = 1$), eq 6 reads for the $i$th species

$$\mu_{c,i}^\infty + k_B T \ln x_{c,i} = \mu_{g,i}^0 + k_B T \ln\frac{p_i}{p} \tag{9}$$

and we find the equilibrium relation

$$x_{c,i} = \frac{p_i}{p} \exp\left(-\frac{\mu_{c,i}^\infty - \mu_{g,i}^0}{k_B T}\right) \tag{10}$$

This relationship is Henry's Law, suggesting a direct proportionality between the mixing ratio in the condensed phase and the vapor pressure above the solution (which in equilibrium is equal to the partial pressure):

$$h_i p_i = x_{c,i} \tag{11}$$

with $h = p^{-1} \exp[-(\mu_{c,i}^\infty - \mu_{g,i}^0)/(k_B T)]$. However, a strictly linear relationship between $x_{c,i}$ and $p_i$ is given only for dilute solutions (i.e., ideal solutions), in which $f^\infty = 1$ is independent of $x_{c,i}$. Conversely, electrolytic solutions are not ideal, because additional interactions, such as the Coulomb interaction between the ions (described by the Debye−Hückel theory) or near-range interaction potentials in more concentrated solutions,[17,34,161,162] occur between the ions in solution.

The most simple case of a nonlinear $p_i(x_{c,i})$ relationship can be obtained by acidic gases of the form HX (X = F, Cl, Br, I, $NO_3$, etc.), which may partially dissociate upon dissolution:[163]

$$HX \rightleftharpoons H^+ + X^- \tag{12}$$

In thermodynamic equilibrium, the energy balance of this process reads (cf. eq 9)

$$\mu_{g,HX}^0 + k_B T \ln\left(\frac{p_{HX}}{p}\right) = \mu_{H^+}^\infty + k_B T \ln x_{H^+} + \mu_{X^-}^\infty + k_B T \ln x_{X^-} \tag{13}$$

or

$$\hat{h}_{HX} p_{HX} = x_{H^+} x_{X^-} \tag{14}$$

with $\hat{h}_{HX} = p^{-1} \exp[-(\mu_{g,HX}^0 - \mu_{c,H^+}^\infty - \mu_{c,X^-}^\infty)/(k_B T)]$. For single strong acids dissolved in a solvent (e.g., in water), there is complete dissociation, that is, $x_{H^+} = x_{X^-}$. Thus, for a single strong acid, Henry's Law reads[164]

$$\hat{h}_{HX} p_{HX} = x_{X^-}^2 \tag{15}$$

In contrast to the dissolution into the very mobile matrix of liquids, trace molecules have to create space when entering a rigid crystal lattice. Typically, L-defects can be formed in the ice matrix by the added molecules.[154,165] The free energy $(\mu_{c,x_L}^\infty + k_B T \ln x_L)$ is needed to produce these defects in the ice (with mixing ratio $x_L$ of the L-defects and $\mu_{c,x_L}^\infty$, the corresponding standard potential). Adding this term into eq 13 and assuming that each acid molecule creates exactly one L-defect in the ice and dissociates completely, one can derive Henry's Law:

$$\hat{h}_{HX x_L} p_{HX} = x_{X^-}^3 \tag{16}$$

in complete analogy to eq 15. This yields the power law $x_i \propto p_i^{1/3}$.[166] Interestingly, a power law of the form $x_i \propto p_i^{1/2.73}$ has been found by Thibert and Dominé[73] for the dissolution of HCl in single crystals. Similarly, Seidensticker[167] determined an exponent between $^1/_2$ and $^1/_3$ from measuring the partition coefficient of HCl in ice growing from aqueous solutions. From these considerations, it becomes clear that the pressure dependence of uptake processes may yield important mechanistic information.

The Henry's Law constant can also be expressed in dimensionless units, and we define the dimensionless Henry's Law constant $H_d$ by $n_g H_d = n_c$, where $n_g$ and $n_c$ are the concentrations in the gas and the condensed phase, respectively (see also Appendix A).

### 2.1.2. Thermodynamics of Adsorption

For adsorption processes, the same thermodynamic principles as for the dissolution of a trace gas in a liquid must hold: the chemical potential of molecules in the gas phase

$$\mu_g = \mu_i^0 + k_B T \ln\frac{p}{p_0} \tag{17}$$

must equal the one of the adsorbed molecules

$$\mu_s = \mu_i^0 + k_B T \ln\frac{p_L}{p_0} + \Delta\mu_{ad} \tag{18}$$

Here, the standard state is chosen as the chemical potential $\mu_i^0$ of an an ideal gas at a pressure of 1 atm. The entropic term $\ln(p_L/p_0)$ accounts for the change in concentration upon transfer of the molecules from the gas phase (at pressure $p_0$) to the surface (at pressure $p_L$). Clearly, $\Delta\mu_{ad}$ depends on the definition of $p_L$.

Kemball and Rideal[168] consider an ideal three-dimensional gas at a pressure of 1 atm at a temperature of 0 °C with a thickness of $d_0 = 6$ Å as reference state for the adsorbate. The pressure $p_L$ in the surface layer can be converted to a surface concentration by $n_s = p_L/(k_B T) \times V_0/A_0$, where $V_0$ is the molar volume and $A_0 = V_0/d_0$. The chemical potential of an ideal gas is independent from the shape of its container. Thus, the change in chemical potential for transferring an ideal gas with pressure $p$ into a layer of thickness $d_0$ at pressure $p_L$ (i.e., to the surface concentration, $n_s$) is simply given by $\ln p_L/p_0$. The term $\Delta\mu_{ad}$ accounts for the additional change of free energy by the interaction of the adsorbed molecules with the substrate. The equilibrium condition $\mu_g = \mu_s$ leads to

$$K_p^0 \equiv \exp\left(-\frac{\Delta\mu_{ad}}{k_B T}\right) = \frac{n_s k_B T}{p d_0} \tag{19}$$

which defines the thermodynamic equilibrium constant $K_p^0$ relative to the reference state of an ideal gas at a pressure of 1 atm and a layer thickness of $d_0 = 6$ Å.[168]

Choosing a thickness of $d_0 = 6$ Å may appear arbitrary and other choices have been made in the literature. For example, de Boer[169] considered an ideal two-dimensional gas with all molecules having the same mean distance between each other as a reference state for the adsorbate, which leads to a different value for $\Delta\mu_{ad}$. Both methods contain arbitrary choices, thus when a free energy of adsorption is given, the reference state of the "ideal adsorbate" must be given. In this review, we follow the method of Kemball and Rideal, which has the advantage that the concept of a two-dimensional gas is not needed and that the surface concentration of the adsorbate, $n_s$, is introduced naturally.

The thermodynamic treatment assumes an average energy for the adsorption. On a microscopic scale, the ice surface may have a complex microstructure with many different types of adsorption sites, such as steps, kink sites, or terraces. Based on quantum mechanical and molecular dynamics simulations, the energy differences between the different surfaces were found to vary between 37 and 64 kJ/mol.[134]

### 2.1.3. Phase Diagrams

Matter manifests in different phases. For example, in the HCl−water system, a concentrated aqueous solution, a solid solution of HCl in ice or hydrates may form depending on the thermodynamic conditions, such as temperature, mixing ratio, and pressure.[73,74,170] These stability regions can be shown as phase diagrams. Phase diagrams are two-dimensional (sometimes three-dimensional) cross sections of the multidimensional thermodynamic space, which is a function of pressure, temperature, and mixing ratios of all involved species. The basic thermodynamic relationship to construct a phase diagram is that the chemical potential of each species must be equal in phase 1 and 2, when they are in equilibrium with each other, that is,

$$\mu_{1,i}(p,T,x_1,...,x_n) = \mu_{2,i}(p,T,x_1,...,x_n), \quad i = 1, n \tag{20}$$

Because the vapor pressure is a direct measure of the chemical potential (eq 9), the equality of the vapor pressure of two phases is sufficient to determine their coexistence. However, also other data, such as formation enthalpies, melting point depressions or heat capacities have been invoked to construct phase diagrams.[170,171]

As a first example, the melting point depression is illustrated in Figure 4, showing the $x-T$ phase diagram for the ice/$SO_2$ system.[172,173] For a $SO_2$ mixing ratio of 10%, there is a melting point depression of about 1 °C. Because the weak acid $SO_2$ has a low solubility in water, a solution with 1 mol % of $SO_2$ implies an $SO_2$ pressure in the gas phase of 0.1 bar. For higher trace gas pressures, new phases may form, in the case of $SO_2$, the hexahydrate.

For strong acids, such as HCl, HBr, and $HNO_3$, a similar picture applies. However, due to their higher effective solubilities[174] (caused by their larger tendency to dissociate), melting point depressions are 20−40 times stronger than those in aqueous $SO_2$ solutions before the formation of ionic hydrate crystals is enabled. Figure 5 shows the HCl−ice

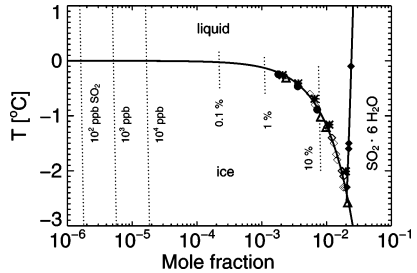


**Figure 4.** $SO_2$−ice phase diagram as a function of temperature and mole fraction of $SO_2$ in an aqueous $SO_2$ solution based on data taken from Gmelin.[173] Solid lines: coexistence curves between ice and an aqueous $SO_2$ solution and the $SO_2 \cdot H_2O$ hydrate, respectively. Dotted lines: constant $SO_2$ pressure lines in the gas phase. (Reprinted with permission from ref 172. Copyright 2001 Elsevier.)

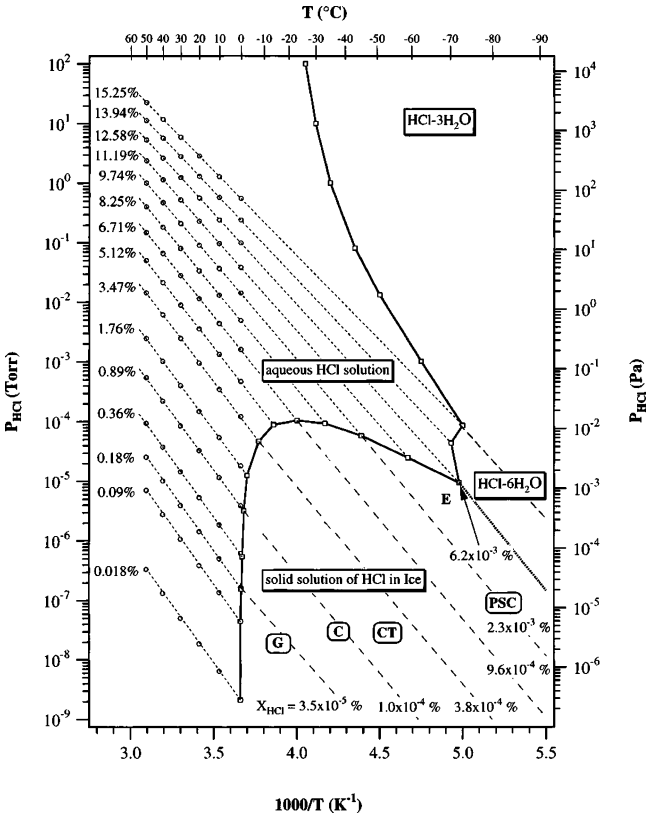


**Figure 5.** HCl phase diagram after Thibert and Dominé[73] with changes. The dashed and dotted lines are isosolubility lines in the ice phase and in water, respectively. The regions G, C, CT, and PSC mark HCl partial pressure and temperature conditions as typical for the Greenland troposphere, cirrus clouds, condensation trails of airplanes, and type II polar stratospheric clouds, respectively. (Adapted with permission from ref 73. Copyright 1997 American Chemical Society.)

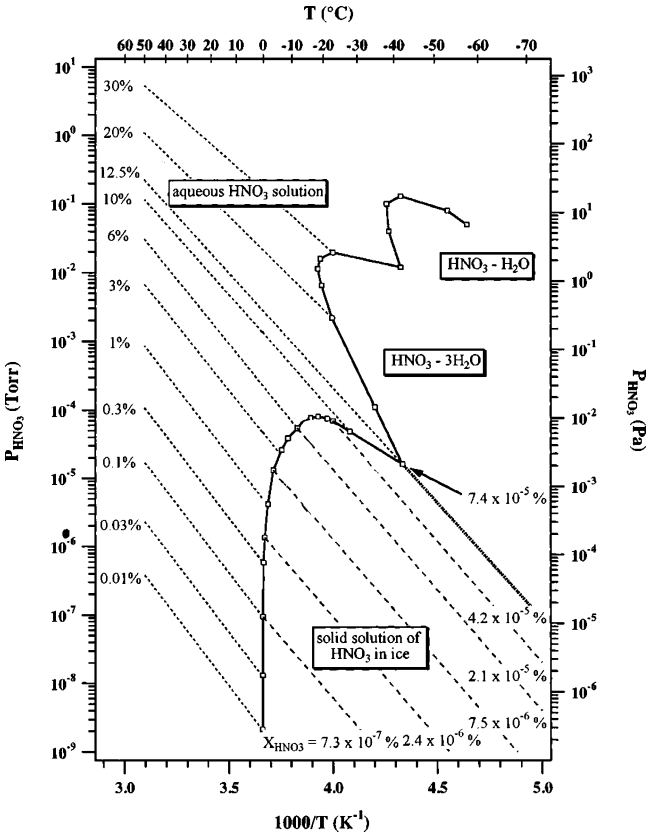


**Figure 6.** $HNO_3$ phase diagram after Thibert and Dominé.[74] The dashed and dotted lines are isosolubility lines in the ice phase and in water. (Adapted with permission from ref 74. Copyright 1998 American Chemical Society.)

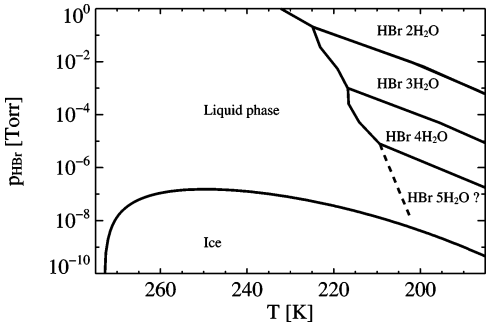


**Figure 7.** HBr phase diagram. The ice−liquid coexistence line is calculated using the model of Carslaw et al.;[17] hydrate locations are taken from Chu and Chu.[171]

phase diagram in the $T-p$ presentation constructed by Thibert and Dominé[73] based on data available in the literature.[170,175−180] For temperatures above 0 °C, an aqueous HCl solution is the only thermodynamically possible phase irrespective of the HCl partial pressure. The dotted lines show the HCl mixing ratio in the solution (percentages specify mole fractions). The ice/liquid coexistence curve reveals a depressed melting point with rising HCl pressure. At HCl pressures higher than $\sim 10^{-4}$ Torr, ice is no longer thermodynamically stable. Preexisting ice exposed to higher HCl pressures will simply melt. Moreover, the solubility strongly rises with decreasing temperature, as can be seen by reading the solution composition as a function of temperature at a constant HCl pressure. For partial pressures of $10^{-4}$ Torr, there is about 14% HCl in the solution at −70 °C. The strong rise of the HCl solubility with lower temperatures causes the surprising effect that ice exposed to constant $p_{HCl}$ can melt upon lowering of the temperature.[181]

The phase diagram (Figure 5) also shows the solubility of HCl in single crystals of ice, as determined by Thibert and Dominé[73] in experiments on the uptake of HCl from the gas phase. Obviously, in comparison to the liquid phase, the solubility is much lower in ice, on average by a factor of 5000.

Similarly, Figure 6 shows the phase diagram for the $HNO_3$ as derived by Thibert and Dominé[74] using data from the literature.[170,175,178−184] It shows the same principal features as the HCl phase diagram.

Less information is available for the HBr−water system. To date the HBr solubility in ice has not been measured. Chu and Chu[171] constructed the HBr phase diagram based on the freezing points of the di-, tri-, and tetrahydrate as determined by Pickering[175,185] and further thermodynamic data (refs 186 and 187). Figure 7 shows the phase diagram with hydrate stability domains as given by Chu and Chu[171] and the ice/liquid coexistence curve as calculated from a thermodynamic ion-interaction model.[17] This phase diagram has the same principal shape as the HCl/water phase diagram. It should be noted that the ice−liquid coexistence line is shifted toward lower partial pressures. Ice will melt at HBr partial pressures above $\sim 10^{-7}$ Torr, while for HCl the limit is at $10^{-4}$ Torr. This is because the solubility of HBr in water is about 3 orders of magnitude higher than that of HCl. Again, hydrates will form at low temperatures and high vapor

pressures. To our knowledge, currently there are no data in the literature for the HI−ice phase diagram.

## 2.2. The Thermodynamics of Surface Melting

In this section, we discuss the thermodynamic concepts for premelting. It is important to clearly distinguish between melting of a macroscopic liquid, which occurs only at temperatures *above* the triple point of ice, and premelting, which occurs at the solid interface at temperatures *below* the triple point due to the presence of surface forces. In any system, thermodynamic equilibrium is defined by the equality of the chemical potential of the *i*th species in every phase (solid (s), liquid (l), and gas (g))

$$\mu_{s,i}(p,T) = \mu_{l,i}(p,T) = \mu_{g,i}(p,T) \tag{21}$$

In absence of surface forces, these two equations have exactly one solution for the two variables $p$ and $T$, which defines the triple point. This mathematical formulation of the Gibbs phase rule clarifies that liquid water cannot exist in thermodynamic equilibrium in contact with ice and vapor unless the system is at its triple point, that is, at 6.1 hPa and 0.0075 °C. However, this conclusion is is only valid if wall and surface effects can be neglected, which introduces additional variables to eq 21[150] (see also paragraph "Gibbs' phase rule" in section 1.4.1).

**Surface Pressure.** The effects of walls and surfaces can be understood microscopically. Molecules in the bulk experience different microscopic forces by their nearest neighbors compared to molecules in near-surface region. This is because they have fewer interaction partners in the condensed phase (or more interaction partners are replaced by others outside of the solid in the vicinity of a wall).[130,188] These different force fields in the bulk and the surface layer lead to different energies, so the work

$$dU = -pdV \tag{22}$$

needed to compress a volume $dV$ will be different in the bulk and surface region. Thus, the pressure $p$ in the surface region differs from the pressure in the bulk according to eq 22. That surface and bulk pressures are different is a general feature of surfaces.[188]

**Thermodynamic Equation To Model the Wetting on Ice.** In a confined volume, such as in thin films, grain boundaries, or veins, the pressure difference between the bulk and the surface area can be treated using the concept of disjoining pressure.[130] The disjoining pressure may be defined as the difference between the "normal pressure in the film and the pressure in the homogeneous liquid at the same chemical potential as the film".[189] If the disjoining pressure in a liquid is negative, the film will wet the surface. Based on the wetting concept, equations for surface melting on ice have been derived.[93,118,119,150,190] Here we follow the presentation of refs 93 and 150.

The inner energy of a system including its surface is given by

$$U = TS - pV + \sigma(d)A \tag{23}$$

where $\sigma(d)$ is the energy per surface area in a QLL, which depends on the layer thickness $d$, $A$ is the total surface area, $S$ is the entropy, and $V$ is the total volume. Because the pressure in the surface region is not constant, we consider the appropriate thermodynamical potential, which is the grand canonical potential

$$\Phi = U - TS = -pV + \sigma A \tag{24}$$

In thermodynamic equilibrium, the conditions $d\Phi = 0, \Phi = \Phi_{max}$ for $(T,\mu)$ = constant must hold. Note that minimizing the Gibbs free energy, $G(T,p)$, would require $p$ and $T$ to be constant.

In the following, we use the indices q, l, and b to denote the surface layer, bulk liquid water, and bulk solid (ice), respectively. The total volume of the system consisting of bulk ice and the surface layer is $V = V_q + V_{ice}$, ($V_q$, surface layer volume; $V_{ice}$, bulk ice volume) and is assumed to be constant. Using the relation $V_{ice} = V - V_q = V - Ad$ in eq 24, we can calculate $\Phi$ for the whole system consisting of bulk and surface layer.

$$\Phi = -p_q V_q - p_{ice} V_{ice} + \sigma(d)A = Ad(p_{ice} - p_q) - p_{ice}V + \sigma(d)A \tag{25}$$

To find the equilibrium thickness $d$ of the surface layer, we minimize $\Phi$ with respect to $d$

$$\frac{\partial \Phi}{\partial d} = 0 \tag{26}$$

which leads to

$$p_q - p_{ice} = \frac{\partial \sigma(T,p,d)}{\partial d} \tag{27}$$

The chemical potential of water in the surface layer, $\mu_q$, can also be expressed by the Taylor expansion of that of liquid water, $\mu_l$

$$\mu_q(T,p_q) \cong \mu_l(T,p_q) \cong \mu_l(T,p_{ice}) + \left.\frac{\partial \mu_l}{\partial p}\right|_{T,p} (p_q - p_{ice}) \tag{28}$$

which we have started at the bulk ice pressure, $p_{ice}$, which equals the one in bulk water in contact with ice. This expansion assumes that the water molecules in the layer react on average on external pressure changes as they would do in bulk water. With eq 27 and the partial molar volume, $\alpha_w = \partial\mu_l/\partial p$, we find

$$\Delta\mu = \mu_q(T,p_q) - \mu_l(T,p_{ice}) = \alpha_w \frac{\partial \sigma}{\partial d} \tag{29}$$

and define the excess Gibbs free energy, $\Delta\mu$, which describes the free energy difference between a water molecule in bulk water and the one in a confined reservoir. This difference is because the pressure $p_q$ in the layer is different from the one in bulk water, as calculated in eq 28. From eq 28, it is clear that a surface layer can only be stable if the surface energy $\sigma(d)A$ actually lowers the energy of the system, that is,

$$\Delta\mu = \alpha_w \frac{\partial \sigma(T,p,d)}{\partial d} < 0 \quad \text{or} \quad p_q - p_{ice} < 0 \tag{30}$$

To evaluate the temperature dependence of $\Delta\mu$, we calculate

the expression $\Delta\mu(p,T)$ by Taylor expansion at the triple point $(T_0,p_0)$ as

$$\Delta\mu(T,p) = \Delta\mu(T_0,p_0) + \left.\frac{\partial\Delta\mu}{\partial T}\right|_{T_0,p_0}(T - T_0) + \left.\frac{\partial\Delta\mu}{\partial p}\right|_{T_0,p_0}(p - p_0) \quad (31)$$

Note that $\Delta\mu = \mu_q - \mu_l = \mu_{ice} - \mu_l$ because $\mu_{ice} = \mu_q$ holds in thermodynamic equilibrium. Moreover, the term $\Delta\mu(p_0,T_0)$ disappears at the triple point (infinitely thick surface layer, $\mu_l = \mu_{ice} = \mu_q$). In good approximation, the pressure term of the expansion can be neglected.[93,190] With use of the thermodynamic relation[191]

$$\frac{\Delta h}{T} = -\left.\frac{\partial\Delta\mu}{\partial T}\right|_{T_0,p_0} \quad (32)$$

the enthalpy is introduced. Thus, at the triple point, where $\Delta\mu(p_0,T_0) = 0$, we find by equating $\Delta\mu$ from eqs 29 and 31 and using the definition for the latent heat of melting, $l_m = h_l - h_i = -\Delta h > 0$

$$l_m\frac{T - T_0}{T_0} = \alpha_w\frac{\partial\sigma}{\partial d} \quad (33)$$

**Surface Energies.** For further evaluation, an explicit expression for the surface energy, $\sigma(d)$, is needed. Sticking to the model of a liquid in a thin layer, the surface energy $\sigma$ for a thickness $d$ can be written as[93]

$$\sigma(d) = \Delta\sigma f(d) + \sigma_{sv} \quad (34)$$

with

$$\Delta\sigma = \sigma_{lv} + \sigma_{ls} - \sigma_{sv} \quad (35)$$

Here $\sigma_{lv}$ is the liquid−vapor, $\sigma_{ls}$ the liquid−solid, and $\sigma_{sv}$ the solid−vapor (i.e., without a QLL or surface layer) surface energy.[192] The thickness dependence of the surface energy $\sigma(d)$ must show the thick film limit $\lim_{d\to\infty}\sigma(d) = \sigma_{lv} + \sigma_{ls}$ and the dry surface limit $\lim_{d\to 0}\sigma(d) = \sigma_{sv}$. A surface layer can form if $\sigma_{lv} + \sigma_{ls} < \sigma_{sv}$ or equivalently (for a monotonic function $f(d)$) $\partial\sigma/\partial d < 0$, as shown above. The explicit functional dependence of $f(d)$ can be derived using the microscopic force laws. For van der Waals interaction, we have[130]

$$f(d) = 1 - \frac{a_0^2}{d^2} \quad (36)$$

For short-range interactions (i.e., for exponential microscopic force), one finds[93]

$$f(d) = 1 - e^{-\delta d} \quad (37)$$

where $\delta$ is an inverse interaction length.

**QLL Thickness.** Using the explicit form for the surface energy (eq 34), one can find the temperature dependence of the layer thickness for van der Waals forces from eq 33

$$d \approx \left(\frac{2\alpha_w\Delta\sigma a_0^2}{l_m}\frac{T_0}{T - T_0}\right)^{1/3} \quad (38)$$

($a_0$ is the diameter of a water molecule), whereas for short-range forces

$$d \approx \frac{1}{\delta}\ln\left(\frac{\delta\alpha_w\Delta\sigma}{l_m}\frac{T_0}{T - T_0}\right) \quad (39)$$

Note that $\Delta\sigma < 0$. Both expressions reveal the divergence of $d$ upon temperature approaching the melting point. A deeper discussion of QLL thermodynamics can be found in several other publications.[89,93,119,130]

**Application to Grain Boundaries and Veins.** In a similar way, the thermodynamics of confined reservoirs, such as grain boundaries or veins, can be treated.[141,142,193,194] Now, the pressure in the confined reservoir is determined by the curvature of the reservoir. In a cylindrical geometry, the pressure in a vein can be calculated from the vein radius, $r_v$:

$$p_c - p = \frac{\sigma_{ls}}{r_v} \quad (40)$$

where $p_c$ is the pressure in the confined reservoir. By introduction of this pressure difference in eq 27, the radius of a vein can be calculated as

$$r_v = \frac{\alpha_w\sigma_{ls}}{l_m}\frac{T_0}{T - T_0} \quad (41)$$

A more detailed treatment of vein thermodynamics, including the influence of impurities, has been given by Nye[193] and Mader.[141] For dissolved nonvolatile substances, it was shown[141,193] that the melting point depression $\Delta T$ in a vein follows the proportionality

$$\Delta T \propto \frac{1}{r_v} \quad (42)$$

Recently, these and similar concepts have been used to model the transport of impurities in polar ice[144−146] and to explain the temperature dependence of sulfur dioxide uptake into packed ice beds.[172]

## 2.3. Kinetics of Gas Uptake When Ice Is Exposed to a Gaseous Environment

The thermodynamics and kinetics of gas uptake are closely related to each other because thermodynamic properties, such as the surface coverage or the solubility, are experimentally determined in kinetic experiments. Thus, we discuss the kinetic concepts needed to interpret uptake experiments.

### *2.3.1. Mass Accommodation Coefficient, Surface Adsorption Coefficient, and Uptake Coefficient*

The flux density of molecules of species $i$ in an ideal gas colliding with a surface is given by the simple gas kinetic expression

$$j_{coll,i} = \frac{\bar{v}n_{g,i}}{4} \quad (43)$$

Here, $n_{g,i}$ is the gas molecular density directly above the liquid surface and $\bar{v} = (8k_BT/(\pi m_i))^{1/2}$ is the mean thermal velocity of the gas molecules with mass $m_i$.

Even on a fresh surface, which is not yet covered by molecules of the adsorbing/absorbing species, a certain fraction of the striking molecules is reflected into the gas phase (due to mismatch of the electronic orbitals of the

colliding molecules). The probability for a molecule to be accommodated on the surface when striking it is often described by the mass accommodation coefficient, $\alpha_c$. Different definitions have been used in the literature; here we present the definition as formulated by the Subcommittee on Gas Kinetic Data Evaluation of the IUPAC (http://www.iupac-kinetic.ch.cam.ac.uk)

$$\alpha_c = \frac{\text{number of gas molecules entering the condensed phase in unit time}}{\text{number of gas molecules striking the interface in unit time}} \quad (44)$$

To use this definition, the meaning of "to enter the condensed phase" must be defined. Unfortunately, for historic reasons, this has been done differently for uptake processes on liquid and solid interfaces.

**Surface without Internal Structure.** If the liquid interface is considered without any internal structure, a molecule enters the condensed phase if it dissolves into the liquid just below the interface. Historically, the mass accommodation coefficient, $\alpha_c$, was introduced in this way to describe uptake processes on liquids.[63,64,195] Analogously, one can use the mass accommodation coefficient for uptake processes on ice. Here, $\alpha_c$ is the probability of a molecule to be adsorbed on the surface when striking it. Thus, when the solid or liquid surface is considered without any further structure, $\alpha_c$ simply describes the probability for a molecule not to be reflected into the gas phase. Here the use of $\alpha_c$ is the same on liquids and solids.

**Mass Accommodation on Liquid Surfaces with Internal Structure.** When uptake processes on liquids were investigated, it was realized that the transfer of a gas-phase molecule into the liquid phase is a composite process, which includes the adsorption of the gas molecule on the liquid surface as first step and subsequent dissolution as second step. The adsorption of trace gases on liquids has been demonstrated for both organic[196] and highly soluble inorganic trace gases.[66] The mass accommodation coefficient can be estimated with variants of the precursor model (see section 2.3.4), which include surface adsorption of trace gases on the liquid.[69,197−199] In such models, the mass accommodation coefficient, $\alpha_c$, describes the overall transfer of a gas-phase molecule into the liquid phase, consistent with the definition of $\alpha_c$ for uptake processes on structureless surfaces, as described in the last paragraph.

**Mass Accommodation on Solid Interfaces with Internal Structure.** Also uptake processes on solids are composite processes, consisting of molecular adsorption, migration to a stronger bound surface state, possibly hydration and subsequent dissociation, and to a lesser extent also dissolution just below the surface. Indeed, in molecular beam experiments, several uptake channels have been experimentally observed. For example, most of the unreflected HCl molecules rest for a time scale of a millisecond or more on the ice surface, while only a small percentage of HCl molecules are trapped for a very short time scale of a few microseconds before desorbing back into the gas phase.[200,201] Thus, in principle, the uptake of a gas molecule on the ice surface can also be considered as series of subsequent adsorption steps. After a first weekly bound physisorption, transfer to a stronger bound state follows. This two step process can be described with the precursor model (see section 2.3.4), as it has been used by several authors to model uptake processes on ice.[78,202,203] While conceptually and mathematically equivalent to uptake models for liquid interfaces, the mass accommodation coefficient is used differently on solid and liquid interfaces. On liquids, $\alpha_c$ is the probability for the overall process, including surface adsorption and subsequent dissolution. In contrast, for uptake processes on ice, $\alpha_c$ is used as the probability for the very first physisorption step only.

**Surface Accommodation Coefficient, $S_0$.** To resolve these different definitions, it has been suggested to introduce a new term, the term surface accommodation coefficient $S_0$.[71] Here, $S_0$ is the probability for a molecule to reside on the surface at least for a time scale as short as a molecular vibration ($\sim 10^{-12}$ s). This process may be called physisorption and refers to the very first step of the uptake process.

**Use of $\alpha_c$ in This Review.** In this review, we use the mass accommodation coefficient, $\alpha_c$, for trace gas uptake on ice as it is done in most of the ice literature. Here $\alpha_c$ is used for the probability for a molecule not to be reflected when striking the surface. In this definition, $\alpha_c$ and $S_0$ are equal.

**Uptake Coefficient $\gamma$.** Saturation effects as the partial coverage of available surface sites in case of surface adsorption lead to an immediate reduction of the net flux $j_{net,i}$ onto the surface even below the value $j_{in,i} = \alpha_{c,i} j_{coll,i} = \alpha_{c,i} \bar{v}_i n_{g,i}/4$. In addition, already dissolved or adsorbed molecules may desorb back into the gas phase, further reducing the net flux taken up onto the solid. Thus, in an experiment, only a fraction smaller than the mass accommodation coefficient, $\alpha_{c,i}$, will be taken up. This experimentally observed fraction is called the uptake coefficient, $\gamma$, which is defined by

$$\gamma_i(t) \equiv \frac{j(t)_{net,i}}{j_{coll,i}} = j(t)_{net,i} \frac{4k_B T}{p_{g,i} \bar{v}_i} \quad (45)$$

Equations 45 and 44 are related via

$$\gamma_i(t \rightarrow 0) = \alpha_{c,i} \quad (46)$$

for uptake on fresh (i.e., previously unexposed) surfaces. Clearly, this limit will hold for experimental time scales in the duration of a molecular vibration ($10^{-12}$ s). In practical experiments with Knudsen cells or flowtubes, the shortest experimentally accessible time scales are often much longer (milliseconds and longer), and the initial uptake coefficient in an experiment does not necessarily equal the mass accommodation coefficient. Thus, care must be taken when interpreting the initial uptake coefficient in uptake experiments.

In experimental setups, for example, Knudsen cells and flow tubes, the uptake coefficient, $\gamma_i(t)$, is the only experimentally accessible quantity, whereas individual processes, such as adsorption, dissolution, or diffusion, remain unresolved. For environmental applications, it might be seductive to think that the measurement of an uptake coefficient should suffice to characterize an environmental system. However, proper modeling is required not only to deduce the principal physical parameters from a measured uptake coefficient but also to take into account the often extremely different time scales (seconds to months) and surface properties (single vs polycrystalline, porosity) prevailing in natural and artificial systems.

### *2.3.2. Surface Boundary Condition: The Hertz–Knudsen Equation*

The net flux, $j_{net,i}$, of molecules between the gas phase (partial pressure $p^s_{g,i}$, the exponent s indicates that the

pressure is the one just at the interface) and condensed matter with vapor pressure $p_{v,i}$ can be calculated using flux matching arguments.[204] The incoming flux $j_{in,i} = \alpha_{c,i}\bar{v}_i p^s_{g,i}/(4k_BT)$ is readily calculated from the partial pressure. In thermodynamic equilibrium ($p^s_{g,i} = p_{v,i}$), the flux of molecules evaporating from the solid into the gas phase with flux $j_{out,i} = -\alpha_{c,i}\bar{v}_i p_{v,i}/(4k_BT)$ must equal the incoming flux, $j_{in,i}$. Under the assumption that the condensing and evaporating fluxes are independent also under nonequilibrium conditions, we find the Hertz−Knudsen equation for the net flux onto the planar ice surface:

$$j_{net,i} = \frac{\alpha_{c,i}\bar{v}_i}{4k_BT}(p^s_{g,i} - p_{v,i}) \tag{47}$$

which describes growth and evaporation of ice. Similarly, the Hertz−Knudsen equation also can be used to describe the surface kinetics of trace gases dissolving in condensed matter. When an impurity with concentration $n_{c,i}$ is dissolved in condensed matter, this species has a vapor pressure $p_{v,i} = n_{c,i}k_BT/H^*_{d,i}$. Here $n_{c,i}$ is the concentration of the dissolved species just below the surface, and $H^*_{d,i}$ is the effective dimensionless Henry's Law constant. Thus, the net flux through the surface is

$$j_{net,i} = \frac{\alpha_{c,i}\bar{v}_i}{4}\left(\frac{p^s_{g,i}}{k_BT} - \frac{n_{c,i}}{H^*_{d,i}}\right) \tag{48}$$

The Hertz−Knudsen equation is an approximation since it assumes the validity of the ideal gas law even under nonequilibrium conditions. Under extreme conditions, the net flux may become high enough to substantially deplete the gas phase, and deviations from the ideal gas law may occur. Such effects were taken into account by using Enskog's development of the Boltzmann equation,[205−207] and this led to a modified equation for the net flux through the surface:

$$j_{net,i} = \frac{\bar{\alpha}_{c,i}}{1 - 0.5\bar{\alpha}_{c,i}}\frac{\bar{v}_i}{4}\left(\frac{p^s_{g,i}}{k_BT} - \frac{n_{c,i}}{H_{d,i}}\right) \tag{49}$$

where $\bar{\alpha}_{c,i}$ is the mass accommodation coefficient averaged over all the velocities of the (not necessarily thermally distributed) gas molecules distribution. More sophisticated treatments of the kinetics of evaporation and chemical reactions on surfaces have been reviewed elsewhere.[208]

### 2.3.3. Adsorption and the Langmuir Equation

Due to the limited number of adsorption sites, saturation effects may occur during adsorption. This effect can be modeled using the Langmuir adsorption isotherm.[188] Let $n_{sites}$ be the total number of sites on the surface (those already occupied and those still available). If there are $n_{s,i}$ molecules adsorbed on the surface, the fraction $\theta_i = n_{s,i}/n_{sites}$ is called the surface coverage. Although $n_{sites}$ is specific for a certain gas, the typical density of sites on the surface is about $10^{15}$ molecules cm$^{-2}$. Often, and also in this review, this number is adopted for $n_{sites}$ (see also ref 209).

The net flux between gas and surface is given by an expression similar to the Hertz−Knudsen equation, eq 47, that is, $d\theta_i/dt = j_{net,i}/n_{sites}$. However, the flux onto a surface with surface coverage $\theta_i$ is reduced by the factor $(1 - \theta_i)$ due to already occupied sites. Assuming the desorbing flux, eq 47, proportional to the surface coverage $\theta_i$, we can formulate the differential equation for the surface coverage $\theta_i$ as

$$\frac{d\theta_i}{dt} = \frac{p_{g,i}}{k_BT}\frac{k_{ad,i}}{n_{sites}}(1 - \theta_i) - k_{d,i}\theta_i \tag{50}$$

Here we have used the definition $k_{ad,i} \equiv \alpha_{c,i}\bar{v}/4$. For thermodynamic equilibrium, that is, $d\theta_i/dt = 0$, the equilibrium surface coverage can be calculated readily:

$$\theta_{eq,i} = \frac{K_{L,i}p_{g,i}}{1 + K_{L,i}p_{g,i}} \tag{51}$$

Equation 51 is the Langmuir isotherm and $K_{L,i} = k_{ad,i}/(k_{d,i}n_{sites}k_BT)$ is the Langmuir adsorption constant. For the low coverage limit (i.e., for $(1 - \theta_i) \approx 1$), we find from eq 50 the linear relation between pressure and coverage

$$\frac{\theta_i}{p} = K_{L,i} = \frac{k_{ad,i}}{k_{d,i}n_{sites}k_BT} \tag{52}$$

similar to Henry's Law for the dissolution of trace gases into liquids (eq 11). Comparison of the kinetic definition in eq 52 with the thermodynamic definition in eq 19 relates the thermodynamic Langmuir constant, $K^0_p$, to the one derived in eq 52 by

$$K^0_p = K_{L,i}\frac{n_{sites}k_BT}{d_0} \tag{53}$$

The time-dependent solution of the surface coverage (eq 50) is

$$\theta_i(t) = \theta_{eq,i} + (\theta_i(0) - \theta_{eq,i})\, e^{-\lambda_i t} \tag{54}$$

with the time constant

$$\lambda_i = \frac{p_g}{k_BT}\frac{k_{ad,i}}{n_{sites}} + k_{d,i} \tag{55}$$

Note that the characteristic time for equilibration rises with the lowering of the partial pressure. With the definition for $\gamma$ in eq 45, the uptake coefficient can be calculated readily (assuming $\theta_i(0) = 0$ and using $j_{in,i} = n_{sites}\, d\theta_i/dt$)

$$\gamma_i(t) = \alpha_{c,i}\, e^{-\lambda_i t} \tag{56}$$

**Adsorption with Dissociation.** If the adsorbed species dissociates, the adsorption isotherm may be derived assuming complete dissociation of the adsorbing species.[210] If one assumes that a molecule occupies two sites and that all sites are equivalent, the saturation term $(1 - \theta_i)$ has to be squared and also the desorption rate is quadratic in $\theta_i$ to account for the recombination. Thus, the differential equation for the surface kinetics reads

$$\frac{d\theta_i}{dt} = \frac{p_{g,i}}{k_BT}\frac{k_{ad,i}}{n_{sites}}(1 - \theta_i)^2 - k_{d,i}\theta_i^2 \tag{57}$$

For equilibrium conditions, the adsorption isotherm is readily calculated as

$$\theta = \frac{K_{\mathrm{LD},i} p^{1/2}}{1 + K_{\mathrm{LD},i} p^{1/2}} \tag{58}$$

where $K_{\mathrm{LD},i} = (k_{\mathrm{ad},i}/(k_{\mathrm{d},i} n_{\mathrm{sites}} k_{\mathrm{B}} T))^{1/2}$ is the Langmuir equilibrium constant.

Both the dissociative and nondissociative adsorption isotherms have been used to model the uptake of HCl and $HNO_3$ on ice and the chemical reaction of HCl on the surface of ice and various solid hydrates (see, for example, refs 77, 174, and 211−215 and citations therein). Recently, an adsorption isotherm has been suggested[21] to describe the adsorption of HCl on ice for wide range of HCl pressure, including the thermodynamic stability domain of both ice and hydrates.

**Other Isotherms.** In real systems, mere Langmuir type adsorption is rarely found. To describe further adsorption on top of an already adsorbed monolayer, multilayer concepts such as one derived by Brunnauer, Emmet, and Teller[216] (BET) or the Frenkel−Halsey−Hill (FHH) adsorption isotherms are used. In essence, the BET isotherm describes the adsorption of a gas from low pressures ($p_{\mathrm{g},i} < p_{\mathrm{v},i}$) to full condensation of the gas on the substrate ($p_{\mathrm{g},i} \simeq p_{\mathrm{v},i}$). It is routinely used to determine the surface area of porous materials. For reviews, see refs 188 and 210.

### 2.3.4. Precursor Model

Trace gases are taken up onto a surface with several individual steps, such as adsorption, subsequent dissociation, and possibly dissolution into the bulk. This complex system may be described by the precursor model, which we illustrate for a two-step process consisting of adsorption on the surface and subsequent dissolution into the bulk, as it has been used to model the uptake kinetics of the HCl uptake on ice.[213,214,217,218] The kinetic equations for this system read for the surface

$$\frac{\mathrm{d}\theta_i}{\mathrm{d}t} = \frac{p_{\mathrm{g},i}}{k_{\mathrm{B}} T} \frac{k_{\mathrm{ad},i}}{n_{\mathrm{sites}}} (1 - \theta_i) - k_{\mathrm{d},i} \theta_i - k_{\mathrm{s},i} \theta_i + k_{i,\mathrm{s}} n_i (1 - \theta_i) \tag{59}$$

and the bulk phase

$$\frac{\mathrm{d}n_i}{\mathrm{d}t} = k_{\mathrm{s},i} \theta_i - k_{i,\mathrm{s}} n_i (1 - \theta_i) \tag{60}$$

While a general solution for these coupled nonlinear equations cannot be given easily, approximate solutions can be derived. Assuming irreversible dissolution ($k_{i,\mathrm{s}} n_i = 0$), a steady state on the surface ($\mathrm{d}\theta_i/\mathrm{d}t = 0$), and the low coverage limit ($1 - \theta_i$) $\approx 1$, the uptake coefficient can be derived as[202,203]

$$\gamma_i = \frac{\alpha_{\mathrm{c},i}}{1 + \dfrac{k_{\mathrm{d,i}}}{k_{\mathrm{s},i}}} \tag{61}$$

Assuming an Arrhenius-like temperature dependence for the desorption constant ($k_{\mathrm{d},i} \equiv A_{\mathrm{d},i} \exp(-\Delta E_{\mathrm{d},i}/(k_{\mathrm{B}} T))$ and the dissolution rate ($k_{\mathrm{s},i} \equiv A_{\mathrm{s},i} \exp(-\Delta E_{\mathrm{s},i}/(k_{\mathrm{B}} T))$, one finds a non-Arrhenius-like temperature dependence for the uptake coefficient

$$\gamma = \frac{\alpha_{\mathrm{c},i}}{1 + \dfrac{A_{\mathrm{d},i}}{A_{\mathrm{s},i}} \exp\left(-\dfrac{\Delta E_{\mathrm{d},i} - \Delta E_{\mathrm{s},i}}{k_{\mathrm{B}} T}\right)} \tag{62}$$

which has been used to model the uptake coefficient of HCl[213] and the kinetics of gas pulses on ice[217] in a Knudsen cell.

It should be noted that the formulation in eq 59 interprets the rate constants $k_{\mathrm{s},i}$ and $k_{i,\mathrm{s}}$ as the kinetic constants of the surface bulk exchange. We note that using this interpretation, eq 61 has also been used to analyze uptake processes on liquids.[219] In contrast, Hynes et al.[213] interpreted the precursor as a weakly bound state with the second uptake step as the ionization of HCl on the ice. In this picture, $n_i$ would not be the concentration in the bulk phase just below the interface but the surface concentration of the strongly bound state, while $\theta$ would be the coverage of the weakly bound precursor state.

Fluckiger et al.[217] interpreted the kinetics of acid uptake using two states at the surface and a third state in the condensed phase but stressed that the physical nature of these states (bulk or surface) cannot be easily inferred from the kinetic data alone. In contrast, Huthwelker et al.[214] interpreted the second state as a bulk state. In both studies, the uptake kinetics of HCl could be modeled. The reason for this is that both physical pictures lead to mathematically equivalent equations. Thus, using the precursor model does not easily allow one to infer the nature of the uptake process. Rather, independent techniques are needed to understand the physical nature of the uptake process.

### 2.3.5. Diffusion into the Bulk

In addition to adsorption processes, molecules may be taken up by diffusion as well. There are a variety of different conceivable reservoirs, such as grain boundaries, pores in vapor deposited ice, or the ice crystal matrix itself (see section 7). While the molecular transport processes may be dramatically different in these different reservoirs, the nature of diffusion is the same in all cases, namely, a stochastic transport mechanism governed by Brownian motion, which is described by the diffusion equation

$$\frac{\partial n(x,t)}{\partial t} = -D \frac{\partial^2 n(x,t)}{\partial^2 x} \tag{63}$$

While the diffusion equation describes the kinetics of a stochastic transport process, the meaning of the diffusion constant $D$ depends on the physical system. For the diffusion into the ice crystal, solid-state diffusion constants need to be used; for the diffusion into grain boundaries or micropores, diffusion constants need to be formulated or measured for this specific system. For some conditions also, several diffusive processes, such as the diffusion into the ice crystal, grain boundaries, and pores, may occur simultaneously. Because the diffusion equation is linear, we can sum the individual diffusive flows (with $D_j$ = diffusion constant of individual diffusion process and $\beta_j$ = relative contribution of each process, where $\sum \beta_j = 1$). This leads to a diffusion equation with the effective diffusion constant $D = \sum_j \beta_i D_i$

$$\frac{\partial n(x,t)}{\partial t} = -\sum_j \beta_j D_j \frac{\partial^2 n(x,t)}{\partial^2 x} = -D \frac{\partial^2 n(x,t)}{\partial^2 x} \tag{64}$$

Hence, the solution of the diffusion eq 63 will be applicable also to describe the kinetics of systems with several simultaneous diffusion processes. When modeling the diffusion of a trace gas into solid matter with several reservoirs, we use the effective diffusion constant $D$ and the effective solubility. The effective solubility can be described by the dimensionless Henry's Law constant $H_d$, which is defined by $H_d n_g = n_c$. Here $n_c$ is the concentration of the trace gas in the condensed phase averaged over all reservoirs.

It is important to note that the kinetics of an uptake process may look like a diffusion process, while the fundamental uptake process is surface adsorption. One example is the uptake into highly microporous ice. Here molecules diffuse into the micropores with diffusive kinetics, while the fundamental uptake process is the adsorption on the pore walls.

For some initial boundary conditions, the diffusion equation can be solved analytically (for review, see refs 65, 220, and 221). To model the diffusion of a trace gas into unexposed condensed matter (i.e., with $n(x,t=0) = 0$, where the interface is at $x = 0$), we assume that no kinetic resistance exists at the solid−gas interface. Furthermore, it is assumed that there is a constant concentration in the gas phase, just at the solid surface, and that Henry's Law is valid during all times at the interface: $n(x=0) = H_d n_g(x=0)$ (see eqs 11 and 124) is valid at the surface. For these conditions, the time-dependent solution for the concentration profile of the diffusing species in the ice is[220,221]

$$n(x,t) = H_d n_g\left[1 - \mathrm{erf}\left(\frac{x}{2\sqrt{Dt}}\right)\right] \tag{65}$$

By calculation of the flux density, $j = -D\,\partial n(x,t)/\partial x$, at the surface (i.e., for $x \rightarrow 0$) and use of eq 45, the uptake coefficient is readily calculated[65] as

$$\gamma(t) = \frac{4H_d\sqrt{D}}{\bar{v}\sqrt{\pi t}} \tag{66}$$

If the dissolving gas dissociates, the uptake coefficient depends on the partial pressure. As shown in the appendix, the Henry's Law constant for a dissociating gas is $H_d^* \approx (KH_d^0 k_B T/p)^{1/2}$ (see eq 130). If we assume that the gas/liquid equilibrium at the interface establishes itself infinitely fast, we can approximate the uptake coefficient for a dissociating gas as[222]

$$\gamma(t,p) \approx \frac{4}{\bar{v}}\left(\frac{k_B TKH_d^0}{p}\right)^{1/2}\sqrt{\frac{D}{\pi t}} \tag{67}$$

### 2.3.6. Resistor Model To Describe Uptake Processes

Equations 66 and 67 predict an infinitely large uptake during the initial stage of the diffusion, which is physically impossible because the maximum transport toward a surface is limited by the gas kinetic bombardment at given partial pressure, $p_i$. This surface resistance to mass accommodation must be added into the description of the trace gas uptake process.

The coupling of this surface resistance with the diffusion into the bulk can be treated using the resistor model,[56,223] see also refs 23, 56, 66, 67, 69, and 223−225. The net flux, $j_{net}$, through an interface with surface resistance (mass accommodation coefficient $\alpha_c$) is expressed by the Hertz−Knudsen eq 48. Within time $t$, the trace gas will diffuse into a depth $x = (Dt/\pi)^{1/2}$.[226] To couple diffusion and surface resistance, we assume that the trace element concentration, $n_c^s$, is constant in space in the depth $x$. Limited by surface resistance, within time $t$ a total of $n_c x = j_{net} t$ molecules can cross the surface. From this condition and the diffusive depth $x$, we estimate the average surface concentration in the depth $x$ by $n_c^s = j_{net} t/x = j_{net}(\pi t/D)^{1/2}$. Using this expression, we can eliminate $n_c^s$ in eq 48. From the net flux, $j_{net} = \bar{v}p_g/(4k_B T)$, the uptake coefficient is readily calculated as

$$\frac{1}{\gamma(t)} = \frac{1}{\alpha_c} + \frac{\bar{v}}{4H}\sqrt{\frac{\pi t}{D}} \tag{68}$$

This result shows that the uptake process can be interpreted in terms of an electrical analogue, the resistor model. In this model, the uptake process is considered as a series of two resistors. The resistivity is given by the inverse uptake coefficient of the individual process, in this case $1/\gamma_{surf} = 1/\alpha_c$ to describe the mass accommodation and $1/\gamma_{diff} = (\bar{v}/(4H_d))(\pi t/D)^{1/2}$ (cf. eq 66) for the diffusion.

However, it should be pointed out that the resistor model in eq 68 is only an approximation. The full analytical solution for the uptake coefficient of a system consisting of diffusive and surface resistance is[227]

$$\gamma(t) = \exp(\tau^2)\,\mathrm{erf}(\tau) \tag{69}$$

with $\tau = (t/t_0)$ and $t_0 = (4H_d D^{1/2}/(\alpha_c \bar{v}))^2$, which has the limits $\gamma(t \rightarrow 0) = \gamma_{surf} = \alpha_c$ and $\gamma(t > t_{char}) = \gamma_{diff}$ with the characteristic time $t_{char} > (4H_d^* D^{1/2}/(\alpha_c \bar{v}))^2$. Comparing the full solution with the resistor model shows that the resistor model works extremely well if one process dominates, while for the presented case, deviations in the 20% range can be found in the intermediate regime (the deviation may be different in other cases). Thus, the resistor model can be used safely to calculate the uptake coefficient in regimes where one process dominates, while it provides approximate solutions in intermediate regimes. Consequently, it allows easy identification of different uptake regimes, as has been demonstrated recently in applications including chemical reactions on aerosols.[224]

More complex situations may be treated as well, as we demonstrate for a system with coupled diffusion and adsorption. The mathematical formulation must reflect the physical picture we have from the system. One picture is to interpret the uptake as a two step process. First, the molecules are adsorbed by a Langmuir type adsorption, as described in eq 56. Once the molecules are adsorbed on the surface, they can diffuse into the bulk reservoir, such as the ice bulk or grain boundaries. Thus, the incoming molecules need to fill two reservoirs: the ice surface and the bulk sinks. The uptake coefficient can be split into a bulk and a surface part: $\gamma(t) = \gamma_{bulk}(t) + \gamma_{surface}(t)$. If we assume that diffusive losses to the bulk are too small for significant depletion of the surface, we can calculate the surface contribution directly from eq 56 by $\gamma_{surface} = \alpha_c \exp(-\lambda t)$. There are two resistances for a gas-phase molecule to diffuse into the bulk. First, there is mass accommodation, which is described by the mass accommodation coefficient ($\alpha_c$). The overall probability for a molecule to be first adsorbed on the surface and then in a second step enter the bulk phase is given by the product of the mass accommodation coefficient, $\alpha_c$, and the fraction of equilibrated surface at time $t$, which is described by $\theta(t)/\theta_e$

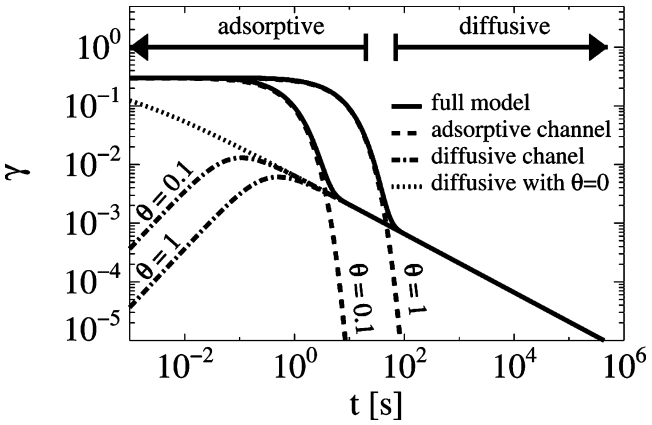


**Figure 8.** Uptake coefficient as a function of time calculated using the resistor model (eq 70 for a temperature of 200 K and an HCl partial pressure of $10^{-6}$ Torr). Two cases, with equilibrium coverages of $\theta = 0.1$ and $\theta = 1$, are presented. For both cases, we choose $H_d^* D^{1/2} = 1$ ms$^{-1/2}$ (cf. Figure 27). Two regimes are visible: During the initial period, uptake by surface adsorption dominates (dashed line), and uptake by diffusion occurs only after there is significant adsorption on the surface (dashed−dotted line). Once the surface is saturated, there is only uptake by diffusion.

$= (1 - \exp(-\lambda t))$ (eq 54). By replacing $\alpha_c$ with this product in eq 68, we find $1/\gamma_{bulk} = 1/(\alpha_c(1 - \exp(-\lambda t))) + (\bar{v}/(4H_d))(D/(\pi t))^{1/2}$ and can formulate the uptake coefficient for the overall system

$$\gamma(t) = \gamma_{bulk}(t) + \gamma_{surface}(t) = \frac{1}{\frac{1}{\alpha_c(1 - e^{-\lambda t})} + \frac{\bar{v}}{4H_d}\sqrt{\frac{\pi t}{D}}} + \alpha_c e^{-\lambda t} \quad (70)$$

Similar equations for the steady-state conditions can be found in refs 67 and 225. In Figure 8, we plot the uptake coefficient as calculated from eq 70 for typical values for the HCl uptake on ice. Two regimes are visible. During the very initial period, the uptake is limited by the mass accommodation coefficient, $\alpha_c$. This corresponds to the limit $\lim_{t\to 0} \gamma(t) = \alpha_c$. During this period, the surface is filled by adsorbing molecules until the equilibrium coverage, $\theta_e$, is reached. The higher $\theta_e$, the longer it takes to fill the surface. Surface adsorption dominates the uptake process if the condition $((1 - \exp(-\lambda t))(1/\alpha_c + (\bar{v})/(4H_d)\sqrt{\pi t/D})^{-1} \ll \alpha_c \exp(-\lambda t)$ holds; now eq 70 reduces to $\gamma(t) \approx \alpha_c \exp(-\lambda t)$. Once the surface is equilibrated, the uptake is dominated by diffusion. For $\lim_{t\to\infty} = (4H_d/\bar{v})(D/\pi t)^{-1/2}$, we find the diffusive limit, as formulated in eq 68. This example demonstrates that using the resistor model allows one to identify different kinetics regimes in uptake processes.

## 3. Experimental Techniques I: Kinetic Analysis of the Gas Phase

Early estimates in the 1960s and 1970s of the uptake of trace species on atmospheric ice[228] have been obtained from studies of the equilibrium between ice and aqueous solutions.[136,138,167] In such experiments, ice is grown from a solution and the composition in the ice and the liquid phase is determined afterward, for example, by ion chromatography. The ratio of the concentrations in the liquid and the ice phase is called partition coefficient. After 1985, triggered by the recognition that heterogeneous processes on polar stratospheric clouds are essential for the formation of the ozone hole,[6,18] methods to study uptake and reaction on ice in direct contact with the gas phase have been developed, which usually require the application of sophisticated techniques.

Two techniques, the Knudsen cell and the flow tube, play a major role in the investigation of heterogeneous processes, such as nonreactive uptake processes or heterogeneous chemical reactions. Both techniques have originally been developed to study gas-phase reactions,[229−231] but with some adaptation they also allow the investigation of multiphase processes.

### 3.1. Knudsen Cells

Originally, the Knudsen cell has been designed to study fast gas-phase radical reactions.[229] Knudsen cells have been used to study heterogeneous chemical reactions[6,75,232−234] relevant for stratospheric chemistry. Furthermore, the uptake of trace gases on aqueous sulfuric acid[235−237] and ice[22,214,238−244] has been investigated in Knudsen cells.

In essence, a Knudsen cell is a low-pressure flow reactor with an inlet for trace gases and the possibility to analyze the gas phase composition as function of time. It is used in the Knudsen regime with total pressures so low (typically below about 1 mTorr) that the mean free path of the gas molecules is larger than the dimensions of the cell. In contrast to flow tubes, which operate at higher pressures, the advantage is that effects of gas phase diffusion do not kinetically limit the gas uptake and therefore do not complicate the analysis of the experimental data. The limits of such ideal gas flow conditions in tubular Knudsen cells have been investigated by use of Monte Carlo simulations.[245] Disadvantages may result from higher sensitivities to wall effects (see below). Also, 1 mTorr corresponds to the vapor pressure of ice at 190 K. Therefore, in a Knudsen cell, only experiments referring to ice under upper tropospheric and stratospheric conditions can be performed.

**Experimental Realization.** Figure 9 shows the setup of a Knudsen cell experiment as developed by Caloz et al.[238] Typically, a Knudsen cell setup consists of three parts: (1)

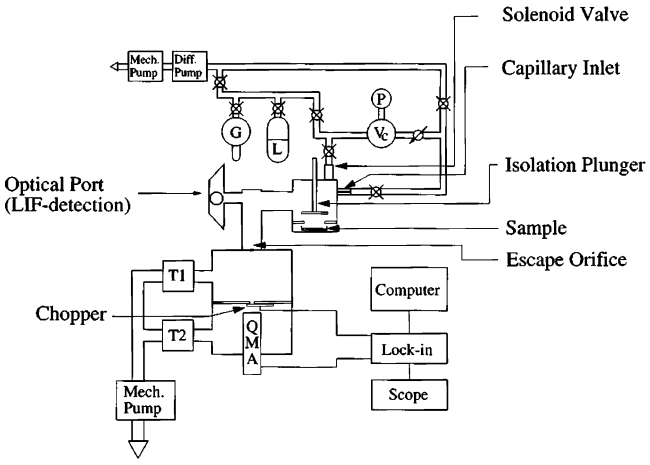


**Figure 9.** Setup of a Knudsen cell experiment with an optical port for gas-phase analysis: QMA, quadrupole mass sepctrometer; T1 and T2, valves; the chopper allows in situ subtraction of background signals in the mass spectrometer; an isolation plunger is used for covering the sample; the escape orifice defines the gas flow through the Knudsen cell. (Reprinted with permission from F. Caloz, F. F. Fenter, K. D. Tabor, and M. Rossi, *Review of Scientific Instruments, 68*, 3172 (1997). Copyright 1997, American Institute of Physics.)

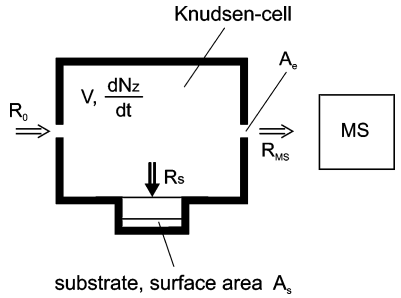


**Figure 10.** Fluxes in a Knudsen cell; see text for discussion.

a gas-flow system to bring vapors with the required partial pressures into the cell, (2) the Knudsen reactor itself, and (3) a gas analysis system, for example, a mass spectrometer. Some setups also invoke IR spectroscopy to analyze the sample.[22,43,246]

**Using Knudsen Cells.** Figure 10 illustrates the principal concept of a Knudsen cell when used as a flow system. A plunger, which is the valve, allows sealing of the substrate from the main chamber. For uptake experiments, a Knudsen cell can be used with a constant gas flow. Opening the plunger allows exposure of the substrate to the gas phase. From the loss rate after opening the plunger, both the rate and total amount of the uptake can be determined (see section 5.1). Knudsen cells have also been used in other configurations. For example, with short gas pulses, the rate constants can be determined.[241,247] An alternative method uses large porous surfaces and very small gas flows[21] into the mass spectrometer. If the amount of trace gas taken up on the ice surface is large compared to the loss by pumping into the mass spectrometer, the vapor pressure above the ice can be measured directly. Thus, for a known ice surface area and total amount of HCl taken up, measurements of the gas partial pressure above the surface directly yield the gas−solid partitioning.

**Gas Control.** The upper part of Figure 9 shows the gas flow system, which is pumped by a diffusion pump. Vapors can be taken from gaseous and liquid sources. There are several methods to let gases into the cell: either a capillary inlet or a needle valve to establish a constant flux through the Knudsen cell or a solenoid valve, which allows injection if gas pulses into the cell.

**Temperature Control.** When high vapor pressure materials, such as ice, are investigated, humidification and temperature control are necessary. Temperature control can be achieved by using commercial circulation coolers, in which a refrigerated liquid such as ethanol, methanol, or cycloheptane is circulated. Temperatures below −100 °C are difficult to reach, because the viscosity of the circulated liquid increases with lower temperature. Furthermore, the liquids are easy to inflame and may form explosive gas mixtures. Such obstacles can be overcome by liquid nitrogen cooled systems,[39,238] such as the one illustrated in Figure 11. Here, liquid nitrogen cooled gas is flowed along a heat exchanger. A computer controlled resistive heating coil between the sample and the heat exchanger allows one to establish a constant temperature of the sample. The whole system is surrounded by a vacuum for thermal insulation.

**Unwanted Wall Effects.** When a Knudsen cell is used, adsorption on the cell walls must be considered. Acidic gases strongly adsorb on metal walls. Nitric acid may decompose into nitrogen oxides ($NO_x$).[248] When heterogeneous reactions are investigated, measurements can be performed under

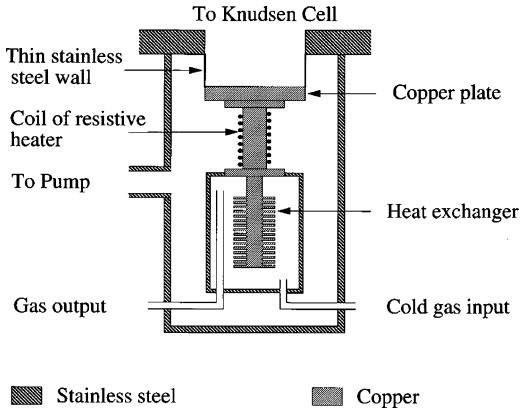


**Figure 11.** Low temperature support for a Knudsen cell. Temperature is controlled by resistive heating against a cold reservoir. Insulation vacuum and thin stainless steel walls at the copper substrate holder avoid input of heat. (Reprinted with permission from F. Caloz, F. F. Fenter, K. D. Tabor, and M. Rossi, *Review of Scientific Instruments*, *68*, 3172 (1997). Copyright 1997, American Institute of Physics.)

steady-state conditions so that wall losses after saturation play no role. However, measuring nonreactive uptake poses a more delicate problem, since no steady state evolves, so uptake onto walls competes directly with uptake onto the substrate surface. In such experiments, the overall uptake onto the walls must be small compared to the uptake onto the substrate. The importance of such effects has been demonstrated by Hanson and Mauersberger, when reinvestigating previous work[35] with refined methods.[249]

Several approaches have been used trying to reduce the influence of wall effects. Gold coatings have been brought onto metal surfaces to reduce the reactivity of metal surfaces. Also coatings with Teflon[236] have been used. Due to the possibly high porosity of wax and Teflon such coatings must be very thin, otherwise there will be a diffusive loss into the coating. Also pure glass systems with and without coating have been used.[214,238,250]

## 3.2. Flow Tubes

Another tool to study the uptake of acidic gases on ice is the flow tube. As the Knudsen cell, it was originally designed to study gas-phase reactions[230,231] and later also applied to study heterogeneous reactions, using various different setups (e.g., see refs 83, 231, 234, 251, and 252).

**Experimental Realization.** Figure 12 shows a typical setup. The flow tube itself consists of a cylindrical tube, which is coated with ice. An inert buffer gas (e.g., helium or nitrogen) mixed with a trace gas passes through the flow tube with typical pressure between 1 and 10 Torr.

Trace gases (water vapor, acids, or both) are fed into the flow tube either via a movable injector or through special ports (as is the case in Figure 12). At the end of the tube, the gas-phase composition is measured. If the reactive gas is brought into the tube via an injector, the length of the exposed substrate can be chosen by moving the injector. A typical operating procedure is to move the injector initially downstream of the surface to avoid premature exposure of the ice surface. Then the injector is pulled back to expose the ice surface. If the reacting trace gas is brought into the cell via an additional port, the adsorption of the reactant gas in the injector can be prevented. Furthermore, the injector can be kept out of the inner part of the tube during the experiment to avoid heating of the ice substrate and the gas

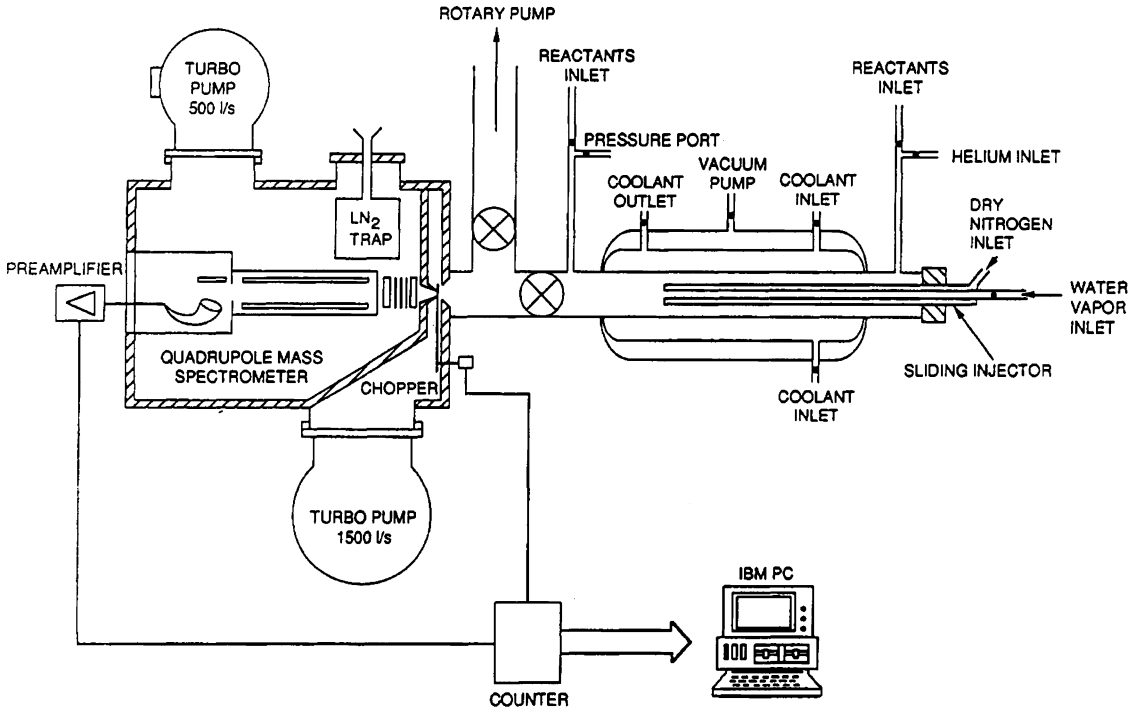


**Figure 12.** Setup of flow tube experiment after Chu et al.[252] Note the conceptual similarity with the Knudsen cell experiment (Figure 9). The right side of the figure shows a flow tube with gas supplies. Note that, in other setups also, the trace gases are brought into the reactor via a movable injector. The left side shows the principle of using a differentially pumped mass spectrometer with a chopper to subtract the background from the ion source online. (Reprinted with permission from ref 252. Copyright 1993 American Chemical Society.)

by the warm injector. Due to the uptake onto the wall, the trace gas pressure at the end of the flow tube drops, and the uptake coefficient can be derived from this drop.

**Substrate Preparation in Flow Tubes.** Ice substrates in flow tubes have been made mainly by two methods. In early studies, ice has been grown by vapor deposition (e.g., refs 28, 83, and 252). There has been some controversy about the influence of the porosity of vapor grown ice on its reactivity (see section 8.1). Therefore, much smoother ice films can be made in a two-step procedure.[42,213,215,253−255] First, the glass flow tube is cleaned and roughened with an aqueous HF solution, then this glass surface is wetted with a thin water film, which is cooled to freeze ice.

**Gas-Phase Diffusion.** If the gas passes through the flow tube under laminar flow conditions, according to the Hagen−Poiseuille Law, the gas will flow faster the further away it is from the walls or the injector. However, if the diffusion perpendicular to the flow direction is fast, the plug flow assumption is justified and all matter in the gas flow will be transported with the same velocity everywhere in the flow tube.

The interplay between diffusive and advective transport defines basic requirements for a flow tube. The characteristic time $\tau$ for a molecule to diffuse across a tube of diameter $d$ is $\tau = d^2/D$ with gas-phase diffusion constant $D$. Plug flow conditions occur if the distance $d = v\tau$ by which the gas flows along the tube during the time $\tau$ is less than the tube diameter, that is, $v\tau < d$. Eliminating $\tau$ from these two relations yields the criterion $D > vd$. At the same time, the gas-phase diffusion must not be too fast, that is, not faster than the flow velocity, $D < vL$. Otherwise, the concentration of the trace species in the gas phase along the axis of the tube will be almost constant (and the flow-tube equations, see below, cannot be used). In summary, the condition to construct a flow tube is $vd < D < vL$. For example, for a tube diameter of 2 cm, 10 cm length, and a gas velocity of 100 cm $s^{-1}$, gas-phase diffusion constants in the range of 200 cm $s^{-2} < D <$ 1000 cm $s^{-2}$ are acceptable, and this confines the total pressure to values around 1 Torr.

If reaction rates on the walls are fast, gas-phase diffusion will reduce the transport of trace gases toward the walls. Methods to account for the gas-phase diffusion are described in section 5.2 (See "Case II: Transport Limitations by Gas-Phase Diffusion"). For methods to estimate diffusion constants, we refer to refs 256−260.

## 3.3. Packed Ice Bed Experiments

Another method to study the uptake of trace gases on ice is the packed ice bed technique. In principle, a packed ice bed is a flow tube filled with porous ice. Packed ice beds have been originally designed to study the uptake of trace gases onto snow-like ice[59,60,84,261−265] or natural snow.[266]

A packed ice bed is made in the following manner. Distilled water is nebulized with an ultrasonic nebulizer above a Dewar flask containing liquid nitrogen. The fine mist falls into the liquid nitrogen, where it is frozen as fine amorphous ice spheres with typical diameters of some 100 $\mu$m. These ice spheres are filled into a glass tube. Care must be taken during freezing and transport of the ice through laboratory air to avoid contamination problems. For example, when the ice is used to study the uptake of $SO_2$, no oxidants, such as $H_2O_2$, should have contact with the ice or the fine mist. This can be avoided by producing and keeping the ice in a controlled atmosphere of pure gas.

In the next step, the ice is sintered for a period of several days at temperatures between −5 and −15 °C. This ensures that the originally amorphous ice is crystalline when the uptake experiment id performed. Furthermore, because the ice surface is extremely mobile, the several day period will stabilize the shape of the ice surface.[267] The ice used in a packed ice bed is porous and has a very high surface area.

The total surface area can reach several square meters, much higher than that in a flow tube or a Knudsen cell. To measure the ice surface area in packed ice beds, different methods have been applied, including optical techniques,[60] measurements of the permeability,[59] and BET measurements,[265] which were originally developed for measurements on natural snow.[268−270] The BET measurements showed that the high surface area in the packed ice bed experiments is mainly caused by the large number of individual ice spheres.[265] This is in contrast to the microporosity of the vapor deposited ice film, which has pores on scales of a few micrometers. Due to their high surface area, packed ice beds are specially suited to study uptake and reaction of weakly reactive or adsorptive gases (such as relatively weak acids, e.g., $SO_2$).

The ice-filled tube is connected to a gas flow system in a similar manner as a flow tube. A gas is routed through the packed ice bed and the signal at the end of the packed ice bed is monitored with an appropriate gas analysis system. Often gas specific detectors are used, such as a flame photometric detector for gases such as $SO_2$.

To determine the total uptake, two methods can be applied. The time evolution of the trace gas concentration at the tube exit, the so-called breakthrough curve, can be monitored and the uptake can be calculated by integration of the signal.[59] When this method is used, care must be taken to account for possible drift effects. Another method is to use the breakthrough curve to assess the saturation of the packed ice bed but to determine the total uptake by liquid-phase analysis of the melted ice bed.[60] This allows a better quantification of uptake rates, which are small compared to the flux of molecules passing the ice bed.

The analysis of the kinetics in a packed ice bed experiment is hampered by its porosity and the possibility of diffusive processes. Simple evaluation methods assuming diffusion in planar geometry on the surface of the porous matter[172] or modeling the ice surface by spheres have been used.[264] More complex models, which take various shapes of the pores into account, have also been presented.[271]

## 3.4. Methods To Analyze the Gas Phase

### *3.4.1. Mass Spectroscopy*

The analysis of the gas phase is often performed using mass spectroscopy. The principles of mass spectroscopy are detailed elsewhere.[272] In brief, a mass spectrometer works in three steps. A small portion of the gas to be analyzed is brought as a molecular beam into the ion source. Here it is ionized, either by ion impact or by chemical ionization, leading to characteristic fragments. For example, HCl fragments into the positive ions $^{35}Cl$, $H^{35}Cl$, $^{37}Cl$, $H^{37}Cl$. Determination of these fragments allows identification of the gas. In a second step, the ions are electrically accelerated into a mass filter, either a magnet or a quadrupole. The mass filter sorts the ion beam by $e/m$, the ratio of the fragment mass and charge. In the third step, the ions are detected either with a Faraday cup, measuring the charge of the ion beam, or with a secondary electron multiplier, counting each impacting ion. However, to analyze acidic gases in an ambient of water vapor, special modifications are needed, which are discussed below.

**Pressures.** The pressure in the mass spectrometer has to be low enough to allow the existence of an ion beam from the ion source through the mass filter into the detector, that is, the mean free path must be larger than that distance.

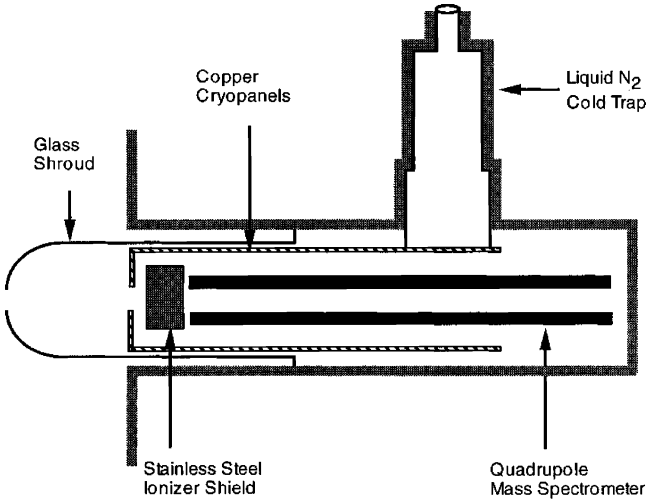


**Figure 13.** Mass spectrometer with cryoshield after Foster et al.,[135] as an alternative to a chopped system. The cryoshield effectively pumps water and, to some extent, trace gases to reduce the overall background in the mass spectrometer. (Reprinted with permission from ref 135. Copyright 1997 American Chemical Society.)

Further constraints arise because secondary electron multipliers and the filaments of the ion source require total pressures of less than $10^{-5}$ Torr to avoid destruction. Systems with a Faraday cup might be run at a pressure up to $10^{-4}$ Torr, however, on the cost of decreased sensitivity. Flow tubes are operated at pressures of 1−10 Torr. The total pressure in a Knudsen cell is in the mTorr regime. In both cases, differential pumping between reactor and mass spectrometer is needed.

**Backgrounds.** When acidic gases are analyzed in a humid environment, specific problems are caused by the stickiness of water and the acidic gases to metal surfaces in the mass spectrometer. In a vacuum system, hydrocarbons and water are the main residual gases. Hydrocarbons originate from pump oils in the vacuum system. Water is usually difficult to pump because of its finite solubility in pump oils (the amount of dissolved water is given by the humidity at the high pressure side of the pump). If a turbo pump is used, water will adsorb on the rotors, which also makes pumping difficult. By similar reasons, the sticky acidic gases are usually difficult to pump out of a vacuum system. Thus, with conventional vacuum systems, the analysis of acidic gases in a humid environment is difficult, because high background levels of the gases under investigation may occur.

The most prominent techniques to overcome these problems are to use cryopanels in the mass spectrometer, to use cryogenic pumps, or to subtract the background by modulating the beam with a chopper.

**Cryopanels.** The setup used by Foster et al.[135] is shown in Figure 13. Here a cryopanel encloses the quadrupole and the ion source. The cryopanel has a temperature of about 130 K. Due to the low ice vapor pressure at such temperatures all water molecules will be trapped. Thus, all water is effectively pumped, and a pressure of about $10^{-6}$ can be maintained in the ionization region. As acidic gases are effectively taken up on ice, these gases will be pumped by the growing ice at the cryoshield.

**Cryopumps.** Another method to overcome wall effects in a mass spectrometer is to use cryopumps. Such pumps can be bought from the shelf. A special type of cryopumps has been originally designed to analyze stratospheric air in balloon flights[273,274] and has been used by several

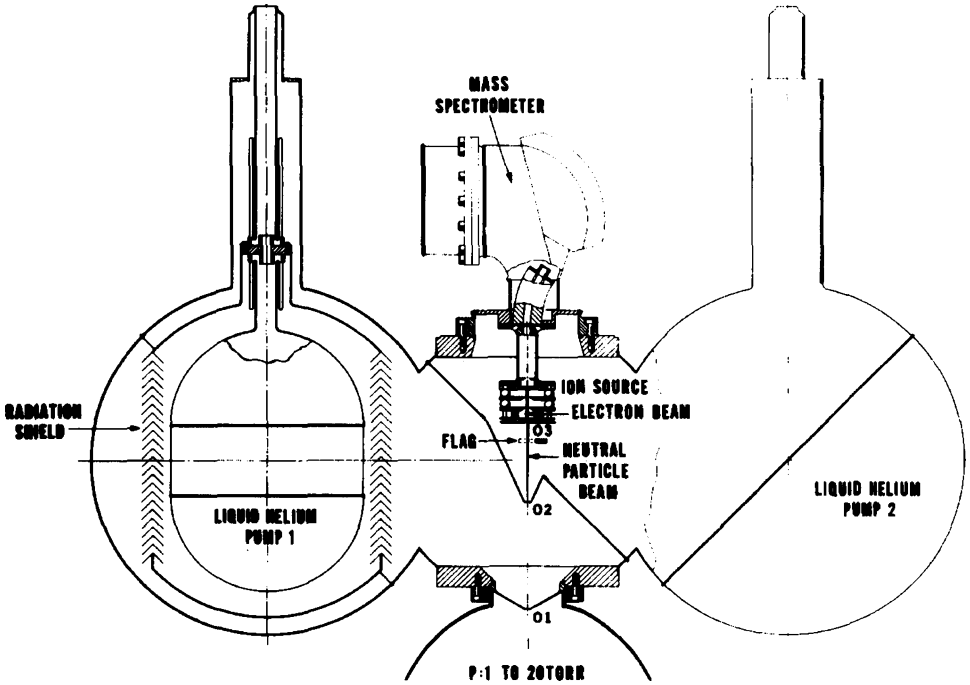


**Figure 14.** Setup for a mass spectrometer using liquid helium as a cryopump for effective background reduction. This type of setup has been used in field studies in balloon experiments and in laboratory experiments.[249] (Reprinted with permission from K. Mauersberger and R. Finstad, *Review of Scientific Instruments*, *50*, 1612 (1979). Copyright 1979, American Institute of Physics.)

authors.[35,249,275−277] Figure 14 shows the concept. The differential pumping is realized in two stages. Both stages are pumped with liquid helium pumps. The advantage of such systems is not only the high pumping speed. At liquid helium temperatures, all gases with the exception of helium itself will condense almost perfectly. Thus, a very low background on all lines in a mass spectrometer spectrum can be achieved and maintained during operation.

**Beam Modulation.** Finally, the modulation of the atomic beam with a chopper has been applied to overcome the problem of a high background. Figure 12 illustrates the principle. Again, there are two differential pumping stages between the reactor region and the ion source in the mass spectrometer. The gas enters the ion source via two orifices, one at the exit of the flow reactor and the other one at the entrance to the high vacuum region where the ion source is. A chopper between these two orifices modulates the beam. The open position measures the incoming gas with the background; the closed position measures only the background. Using lock-in amplification, the background is subtracted directly during the measurement. Different versions of this technique have been used for flow tubes[252,278] and Knudsen cells.[214,238]

### 3.4.2. Chemical Ionization Mass Spectroscopy (CIMS)

Chemical ionization mass spectroscopy (CIMS) uses ion−molecule reactions. For example, the reaction $CO_3^- + HNO_3 \rightarrow NO_3^- + OH + CO_2$[279] allows detection of $HNO_3$ by observation of the $NO_3^-$ ion in the mass spectrometer. Other reaction schemes involving various ions (e.g., $SF_6^-$, $F^-$, $I^-$) have been used to detect different molecules by various authors (for example, see refs 280−283).

The advantage of CIMS is that it is highly specific for the detection of a certain molecule. This is in strong contrast to the ionization by electron impact, where different molecules may have the same major mass fragment peaks (for example, both $ClONO_2$ and $NO_2$ fragment to mass $m/e$ = 46). CIMS allows one to distinguish between these molecules. Furthermore, the ionization can be made at high pressures, that is, in the flow tube or the reaction chamber itself, which reduces unwanted backgrounds from molecules desorbing from the mass spectrometer walls.

## 4. Experimental Techniques II: Analysis of the Condensed Phase

When a Knudsen cell or a flow tube is used, only the gas phase is measured upstream and downstream of its contact with the condensed phase. Therefore, these techniques allow one to measure only the time-dependent uptake coefficient, $\gamma(t)$, but cannot provide direct mechanistic information about the surface or volume processes involved (adsorption, solubility diffusivity, reactivity, etc.). Often, physical models must be applied to interpret the observed kinetics in the gas phase. For example, when surface uptake is assumed, the total uptake can be determined by integrating the loss from the gas phase, while uptake coefficients can be calculated from the steady-state signal, or the product $H_d D^{1/2}$ can be calculated by fitting the experimentally measured breakthrough curve to a proper theoretical model. However, this method of analysis is often difficult. For example, in a specific case, it may remain ambiguous whether the breakthrough curve is "better" fitted by assuming adsorption to the surface of a substrate or diffusive uptake into the bulk of the sample is the better assumption, or a superposition of both. In such cases, the relative ease of the gas-analysis-based methods is paid for by fundamental weaknesses in the identification of the process in the condensed phase. At current, the nature of the uptake of trace gases on ice is not well established. Thus, methods have been developed to study the condensed phase composition while a trace gas is taken up onto ice.

First of all, spectroscopic techniques to probe the condensed phase have been employed, most notably infrared

spectroscopy[284−286] and second harmonic generation.[287−289] IR spectroscopy probes the molecular vibrations; thus, it is well suited to study molecules and molecular ions, but single atoms or single atomic ions cannot be studied. While IR spectroscopy allows one to obtain mechanistic information on processes taking place in the first few monolayers below the surface (i.e., to a depth penetrated by the IR light), second harmonic generation or sum frequency generation enables one to probe molecules of an individual species residing on the surface (e.g., by analysis of its dangling bonds). These spectroscopic techniques provide important information about the nature of the interaction process, such as the formation of hydrates or the state of dissociation, but not necessarily on the amount of uptake. Therefore, we will not further consider these techniques in the current review.

Several other techniques have been employed to determine the amount of uptake by condensed phase analysis. In an early work, the liquid−ice partitioning has been determined by freezing bulk aqueous solutions and subsequent chemical analysis of the ice phase.[136−139,167] However, because this method yields only bulk information, sectioning techniques have been employed to study diffusivity and solubility of trace elements separately. By cutting the ice sample into thin slices a resolution ranging from a few millimeters[290] to about 20 $\mu$m[73,74,291] has been reached. Later, better resolutions could be achieved by using diverse laser desorption techniques.[292,293] Finally, in very recent experiments, Rutherford backscattering (RBS) has been demonstrated to be a capable method to study uptake processes on ice in situ and nondestructively.[172,294] A few of the more prominent ones of these techniques will be outlined in the following sections.

## 4.1. Laser-Induced Thermal Desorption (LITD)

Laser-induced thermal desorption has been used by several authors[135,292] to determine the composition of vapor deposited ice with coadsorbing trace species. In the setup of Berland et al.,[292] a $CO_2$ laser is used to evaporate a sample with short (∼100 ns) laser pulses with energies of a few millijoules applied to spot sizes of 0.6−1 mm. Ice substrates are made by vapor deposition onto an $Al_2O_3$ target. The laser beam is partially absorbed in the ice sample and, more importantly, in the $Al_2O_3$ in the sample holder by a two-photon transition. By this procedure, it is ensured that the complete energy of the laser pulse is used to evaporate the sample. Upon illumination, the substrate evaporates rapidly, and the vapor is analyzed in a mass spectrometer. To reach high sensitivity, the substrate holder and the ion source of the mass spectrometer has to be in a line of sight. This ensures that evaporated molecules enter the ion source without prior wall contact. As the sample is totally evaporated, the overall composition is determined.

## 4.2. Profiling by Sectioning Ice Samples

One of the first measurements of the diffusion constant in ice has been performed by Krishnan and Salomon.[290] These authors froze a cylinder of ice from deionized and distilled water in a plexiglass tube. On top of this ice sample, a cap of ice was frozen that was doped with radioactive $H^{36}Cl$. This sample was stored in a cold bath at a constant temperature to allow the diffusion of the radioactive HCl into the ice sample. After several hours, the sample was cut into pieces and the radioactivity of each piece was measured. From the activity in each piece, a concentration profile was inferred and the diffusion constant calculated.

In similarity to this early approach, Dominé et al.[291] developed a method to measure solubility and diffusivity of HCl and $HNO_3$ in ice single crystals. In essence, ice single crystals were brought into a stainless steel chamber and exposed to a controlled atmosphere of HCl with proper humidification. After some weeks, the ice crystals were cut into about 25 $\mu$m thin slices with a lathe and melted. The trace gas concentration in each slice was determined by liquid-phase analysis, and the concentration profile was derived. In section 7.1, we describe some controversy related to potential experimental pitfalls when this method is used. When these long-lasting experiments are performed, procedures for crystal handling and the correct humidification must be applied.

**Crystal Handling.** In a first step, ice single crystals were grown using a modified Bridgeman method.[73] The crystals were cut into pieces of about 4 cm length in a walk-in cold room. These pieces were frozen onto a specially designed sample holder, which can be mounted into the lathe. The lathe was used to give the samples a flat shape with an accuracy of 5 $\mu$m. The samples were mounted into the reaction chamber and annealed for several hours at −3 °C. Then the temperature was adjusted to the desired value, and an $HCl/H_2O$ mixture was passed through the chamber with the $H_2O$ in the gas phase adjusted to the equilibrium vapor pressure of the ice. The HCl was then taken up by diffusion onto the ice sample for a period of several months.

**Humidification of the Crystals.** The humidification of the ice crystals is most critical when performing these experiments. At a temperature of −20 °C, the ice vapor pressure is around 0.2 Torr. Thus, based on kinetic gas theory, about $10^5$ monolayers are exchanged per second with the gas phase. If the water vapor pressure has a mismatch of 0.01% with the ice vapor pressure about 1 $\mu$m of ice might grow per hour. Because the ice crystals are kept in the vapor phase for periods of several months, it is clear that proper temperature control is crucial when performing these experiments.

Dominé et al.[291] approach this problem by immersing both the reaction chamber and a condenser into the same temperature controlled ethanol bath. The water content in a nitrogen/water mixture is chosen slightly above the ice vapor pressure. This additional amount of water freezes in the condenser unit before entering the diffusion chamber to ensure correct humidification.

## 4.3. Profiling by Laser Resonant Desorption (LDR)

Laser resonant desorption (LDR) has been used by Livingston et al.[293] to determine the concentration profile in very thin ice samples. Ice is evaporated by means of short laser pulses, and the gas-phase composition of the evaporating ice is determined using mass spectroscopy. Figure 15 shows an overview of the experimental setup.

While in the LITD technique described above the wavelength is chosen for maximum absorption in the aluminum sample holder, leading to complete evaporation of the ice, the distinct difference in LDR experiments is that the wavelength of the laser light is chosen for maximum absorption in the ice. Laser light from an Er:YAG laser with a wavelength of 2.94 $\mu$m is highly absorbed by the O−H stretching vibration of the water molecule. The penetration depth at this wavelength is about 0.8 $\mu$m. Thus, with a short laser pulse with nanosecond duration, the upper layer of the

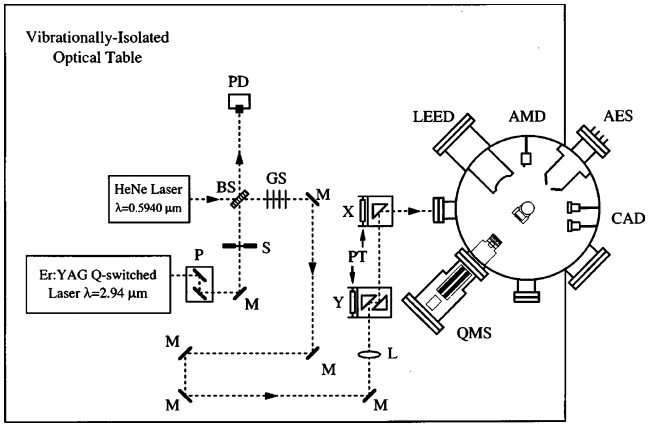


**Figure 15.** Setup for laser resonant desorption (LDR) depth profiling (from ref 293): AES, Auger electron spectrometer; AMD, alkali metal dispenser; BS, beam splitter; CAD, capillary array doser; GS, glass slides; L, $CaF_2$ lens; LEED, low-energy electron diffraction spectrometer; M, mirror; P, periscope assembly; PD, photodiode; PT, piezoelectric translator; QMS, quadrupole mass spectrometer; S, shutter. (Reprinted with permission from ref 293. Copyright 2000 American Chemical Society.)

ice can be evaporated. Analysis of the evaporating gas phase allows determination of the composition. With a sequence of laser pulses, layer by layer of the ice can be evaporated, and a concentration profile of a trace element can be determined. During the profiling experiment, the ice is cooled to temperatures around 140 K, where the ice vapor pressure is negligible.

## 4.4. Rutherford Backscattering (RBS)

Rutherford backscattering (RBS) has been used to probe the near-surface region (depth $\approx 1$ $\mu$m) of HCl doped ice and to investigate hydrate formation on ice surfaces.[294−296] This technique allows one to monitor processes in the near-surface region of ice in situ and nondestructively with a depth resolution of a few 100 Å. This is a compelling advantage compared to other profiling methods, which destroy the ice sample upon analysis.

Rutherford backscattering and other ion-beam-based techniques are routinely used to analyze the near-surface composition of solid, low-vapor pressure materials. Because the technique and its applications are reviewed in detail elsewhere,[297,298] we give only a brief description. When RBS is used, monoenergetic $He^+$ ions (typically 2 MeV) are shot onto the substrate under investigation. When travelling through matter, the remaining electron is stripped from the $He^+$ ion, and it becomes a $He^{2+}$ ion. The energy spectrum of the backscattered $He^{2+}$ ions is measured. This energy spectrum can be analyzed in detail using the physics principles of backscattering, which is simple and solely follows the laws of classical physics. If a $He^{2+}$ ion hits an atomic nucleus (which is usually much heavier than the incident light $He^{2+}$ ion), it transfers some of its energy to the target nucleus and will be scattered backward with a lower energy. The energy transfer to the target nucleus is determined by the conservation of energy and momentum. Therefore, the backscattered energy is a measure for the mass of the target nucleus. The spectrum of ions, which are backscattered on an infinite thin (monolayer) multielemental target consists of a series of peaks, each representing the mass of one of the elements. On targets of finite thickness, the $He^{2+}$ ions lose energy when penetrating through the substrate in interactions with the substrate electrons before hitting a target nucleus. This energy loss is a measure of the depth of the scattering event. Thus, an RBS spectrum contains information about the elemental composition and the distribution of the elements as a function of the depth. A favorable situation occurs, when heavy elements dissolve into a matrix of light matter, such as the uptake of HCl in ice. Now, the high-energy portion of the energy spectrum, for

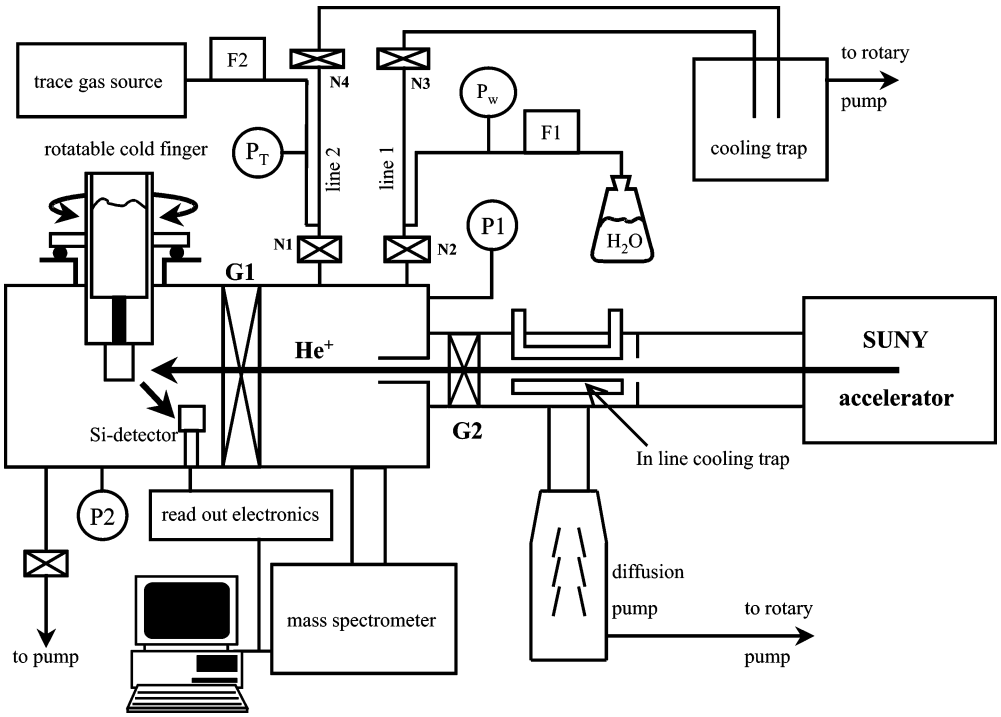


**Figure 16.** Setup for using RBS to investigate trace gas uptake on ice. High energy ions are produced in the SUNY accelerator. N1 and N2, needle valves to control the trace gas flux into the cell; G1 and G2, gate valves; $P_W$, $P_L$, and $P_Z$, pressure heads; the Si detector measures the spectrum of backscattered ions. (Reprinted with permission from ref 295. Copyright 2002 Elsevier.)

backscattering energies between the one of the heavy and the light elements can be interpreted as a direct measurement of the concentration profile of the heavy element, which can be thoroughly analyzed using established methods.[299]

As standard RBS is used at pressures smaller than $10^{-6}$ Torr to investigate low-pressure solids, the standard RBS setup needs some modifications to be usable on high vapor pressure solids, such as ice or aqueous solutions. Most notably, good differential pumping is needed between the source of the $He^+$ ion accelerator and the ice chamber[294,295] to secure proper vacuum in the accelerator region. Figure 16 shows a setup to apply RBS on ice and sulfuric acid.[294,295] Here, the Knudsen cell technique has been combined with RBS. This setup allows establishment of a well controlled temperature, and the gas mixing system is used to expose the ice target to a defined trace gas vapor. In this way, the diffusion of HCl into ice samples has been observed.

### 4.5. Radioactive Tracer Techniques

Radioactively labeled nitrogen oxides have been used to study uptake processes on atmospheric aerosols and ice.[49,265,300] The production of radioactive nitrogen requires a proton accelerator facility. When a proton beam (11 MeV) hits a high-pressure oxygen target, the short-lived isotope $^{13}N$ is produced via the nuclear reaction ($^{16}O(p,\alpha)^{13}N$). Based on this reaction, radioactively labeled nitrogen oxides are produced on a routine basis[301] at the Paul-Scherrer Institute. The radioactive isotope $^{13}N$ is produced in the form $^{13}NO$ near the target and transported to the laboratory, where it is further chemically converted to other nitrogen oxides, such as $^{13}NO_2$, $HO^{13}NO$, or $H^{13}NO_3$, for use in standard setups for heterogeneous chemistry experiments. Several types of experiments on trace gas uptake on ice can be performed using radioactive tracers.

In a thermochromatograpy experiment,[302] a buffer gas containing a radioactively labeled trace gas is passed through a flow tube where a temperature gradient, ranging from about 200 K to liquid nitrogen temperature, is applied along the flow direction. Because the temperature is well defined along the flow tube, temperature and tube position are well correlated. The gas flows from high to lower temperatures. Because the residence time exponentially rises with decreasing temperature, the migration velocity of the molecules slows substantially around a certain molecule-specific temperature (and location in the flow tube). Here, they accumulate, and a peak activity distribution is found, which can be detected easily with a scintillation counter. The trapping temperature is characteristic for the adsorption properties of the adsorbing gas and allows calculation of the adsorption enthalpy based on linear gas chromatography theory and an appropriate adsorption model. This approach can also be applied to a classical isothermal flow tube run with radioactively labeled trace gases. By scanning the radioactivity during the uptake process, one can monitor the migration of the trace gas through the flow tube in situ as function of time,[303] and kinetic adsorption models can be tested.

### 4.6. Synchrotron Radiation Based Techniques

During the last years, synchrotron based methods have found increasing importance in environmental science.[107−109,113,304−312] Synchrotron radiation (SR) has an extremely bright continuous spectrum, ranging from IR radiation up to hard X-rays. Thus, a variety of different techniques can be used, ranging from surface-sensitive X-ray photoelectron spectroscopy (XPS) to various brands of X-ray absorption spectroscopy (such as X-ray absorption near-edge structure, XANES, or surface-extended X-ray absorption fine structure, SEXAFS) or surface-sensitive diffraction techniques. With its (fine) tunable energy, precise spectroscopic analysis of the fine structure of electronic states and thus the nature of the chemical bonding is possible. Furthermore, with the use of ultrafast femtosecond spectroscopy, it is possible to directly study fast processes, such as the dissolution of electrons in water.[308,309] While synchrotron based techniques become more easily accessible to ordinary users, they are not suited for routine determination of the total amount or the kinetics of uptake processes. However, SR has great potential to explore the mechanism of uptake processes. For example, glancing incidence X-ray reflection has been used to confirm the surface disorder on ice surfaces,[107−109] photo-stimulated desorption near-edge X-ray absorption fine structure (PSD-NEXAFS) has been used to directly observe the dissociation of HCl on ice surfaces[313] and to prove that surface disorder is strongly influenced by hydrocarbon impurities.[113] Furthermore, recent X-ray absorption experiments showed that there is molecular HCl on the ice surface at very low temperature and that after HCl adsorption the hydrogen network weakens, which in turn will lead to further sites for adsorption and dissociation of HCl.[312] However, these experiments have been done at very low temperatures, possibly under hydrate stability conditions, and it would be of great interest to perform similar experiments in the ice stability domain.

## *5. Methods: Analysis of Flow Tube and Knudsen Cell Measurements*

When the uptake of acidic gases onto ice is measured, long-lasting uptake processes have been observed by many authors.[42,60,83,250,252] It is noteworthy that in the case of packed ice beds, such tailing has been observed for acidic gases but not for nonpolar substances. Thus, the tailing appears characteristic for the interaction of acids with ice. Its physical reason is unclear and attempts have been made to explore the nature of the uptake processes by analyzing its kinetics. In the following section, we summarize equations to analyze the kinetics in flow tube, Knudsen cell, and packed ice bed experiments, which are of use in tackling this problem.

### 5.1. Knudsen Cell Experiments

**Fluxes in the Knudsen Cell.** Figure 10 depicts the fluxes in a Knudsen cell. We denote the number of molecules in the cell with $N_c$. The flux (in molecules $s^{-1}$) into the cell and onto the substrate and the one leaving the cell at the exit hole are denoted by $R_0$, $R_S$, and $R_{MS}$, respectively. The continuity equation for the cell reads

$$\frac{dN_c}{dt} = R_0(t) - R_S(t) - R_{MS}(t) \tag{71}$$

The outflow from the cell into the mass spectrometer is proportional to the number of molecules in the cell, which defines the escape rate, $k_e$, by the equation

$$R_{MS}(t) = k_e N_c \tag{72}$$

**First-Order Wall Loss.** There are specific situations, such as the first-order loss onto the substrate, when the kinetics in the Knudsen cell can be analyzed without the assumption of quasi-stationarity. Using the abbreviation $k_{ad} = \alpha_c\bar{v}/4$, we calculate the flux, $R_S$, onto the substrate as

$$R_S = k_{ad}\frac{A_S}{V_c}N_c \tag{73}$$

The mass balance in the Knudsen cell reads

$$\frac{dN_c}{dt} = -k_e N_c - k_{ad}\frac{A_S}{V_c}N_c + R_0 \tag{74}$$

For the initial condition, $N_c(t) = N_0$, the general solution of this equation is

$$N_c(t) = (N_0 - R_0\tau)\exp\left(-\frac{t}{\tau}\right) + R_0\tau \tag{75}$$

where we have used the abbreviation $\tau = (k_e + k_{ad}A_S/V_c)^{-1}$. This equation describes the response of a Knudsen cell to changes of the influx $R_0$. It is clear from this equation that the first-order rate constant cannot be measured if $k_{ad}A_S/V_c \ll k_e$. Thus, the adsorption time must be fast compared to the outflow out of the cell.

Special cases of this equation include the kinetics of a gas flowing out of the cell ($N_c(t=0) = N_0$, $R_0 = 0$)

$$N_c(t) = N_0\exp\left(-\frac{t}{\tau}\right) \tag{76}$$

This equation has been used[314] to determine the escape rate, $k_e$, experimentally and to measure the adsorption constant, $k_{ad}$, for HCl, HBr, and HI.

**Calculation of Total Uptake on the Substrate.** The simplest way to analyze uptake experiments is to calculate the uptake per surface area, $n_{tot}(t)$, by numerical integration of the breakthrough curve

$$n_{tot}(t) = \int_0^t \frac{R_S(t')}{A_s}\,dt' \tag{77}$$

This method will work if the end of the uptake process is clearly determinable. However, in uptake experiments with ice, the measured signals often show long tailing, which makes it hard to determine the point in time when equilibrium has been reached.[172] For discussion of this issue, see section 8.4.4.

**Quasi-Stationarity.** The time-dependent continuity eq 71 cannot easily be solved analytically, except for first-order loss processes onto the substrate. Analytical solutions can be found for steady-state conditions (i.e., for $dN_c/dt = 0$). The term $dN_c/dt$ can also be neglected if the condition $|(R_0 - R_{MS} - R_S)| \gg |(dN_c/dt)|$ holds. This means that the difference between source and sink terms in the cell is large compared to the exchange of molecules due to the filling/emptying of the cell. Hence the substrate and not the exchange kinetics governs the time dependence. This is the quasi-stationary approximation, which allows treatment of slow, time-dependent uptake processes, such as the diffusion into the substrate. Then we can approximate eq 71 by

$$R_S \approx R_0 - R_{MS} \tag{78}$$

Only for strict steady-state conditions, that is, for complete time independence of all processes, we can write $R_S(t) = R_0 - R_{MS}$. In the following, we use the steady-state condition, but all equations are also valid for quasi-stationary conditions as approximation.

For a given size, $A_e$, of the exit aperture, the flux $R_{MS}$ is calculated readily from the pressure, $p_c$, using the ideal gas law ($p_cV_c = N_ck_BT$)

$$R_{MS} = \frac{A_e p_c}{\sqrt{2\pi m k_B T}} \equiv k_e N_c = k_e\frac{p_c V_c}{k_B T} \tag{79}$$

This equation defines the escape rate $k_e$, which is the inverse residence time of a molecule in the Knudsen cell. It depends on the mass of the gas molecules

$$k_e = \frac{A_e}{V_c}\sqrt{\frac{k_B T}{2\pi m}} \tag{80}$$

The flux $R_{MS}$ can be calculated directly from the partial pressure and the escape rate; thus the partial pressure is a direct measure for the flux $R_{MS}$. An uptake experiment in a Knudsen cell has two stages. First, the pressure, $p_0$ (and thus $R_0$), in the cell is measured with closed plunger. In the second step, the plunger is opened, and the pressure in the Knudsen cell changes to the pressure $p_r$ because the substrate acts as sink. The flux $R_S$ onto the substrate can be calculated from $p_0$ and $p_r$

$$R_S = \frac{k_e V_c}{k_B T}(p_0 - p_r) \tag{81}$$

Using the mean thermal velocity, $\bar{v} = (8k_BT/(\pi m))^{1/2}$, and the gas kinetic impingement rate on the substrate during uptake, $R_{S,max} = A_S\bar{v}p_r/(4k_BT)$, the uptake coefficient (cf. eq 45) is

$$\gamma = \frac{R_S}{R_{S,max}} = \frac{4k_e}{\bar{v}}\frac{V_c}{A_S}\frac{p_0 - p_r}{p_r} \tag{82}$$

This equation establishes the desired relationship between the unknown $\gamma(t)$ and the measured pressure $p_r(t)$, as well as other instrumental parameters. Equivalently, the temporal development of the partial pressure in the cell can be written as

$$p_r = \frac{p_0}{1 + \dfrac{\bar{v}A_s}{4k_e V_c}\gamma} \tag{83}$$

Note that all equations in this paragraph are valid approximations for the quasi-stationary condition ($|(R_0 - R_{MS} - R_S)| \gg |(dN_c/dt)|$), that is, for uptake processes with slow time dependence.

**Diffusive Uptake of a Nondissociating Species.** Because the diffusion is a slow time-dependent process, we use the quasi-stationary approximation (see paragraph "Quasi-Stationarity" in section 5.1). The diffusive loss of a gas onto a planar substrate is calculated by the time-dependent uptake coefficient (eq 66). Using this expression in eq 83 allows calculation of the time dependence of

the pressure in the Knudsen cell:

$$p_r(t) = \frac{p_0}{1 + \frac{A_S}{V_c k_e}\frac{H_d\sqrt{D}}{\sqrt{\pi t}}} \quad (84)$$

This approach has been used to determine $H_dD^{1/2}$ for HCl in sulfuric acid solutions under stratospheric conditions[235] and to analyze the uptake of HCl onto ice in Knudsen cell experiments.

**Diffusive Uptake of a Dissociating Species.** For a dissociating species, the solubility changes with the pressure $p_r$ in the cell ($H_d^* \approx (k_B T_s K H_d^0/p_r)^{1/2}$, see eq 130). Using the quasi-stationary approximation, we insert eq 67 into eq 83 and derive the time dependence of the partial pressure $p_r$ in the Knudsen cell as

$$p_r(t) = p_0\left(1 + \frac{\zeta^2}{2t}\right) \pm \sqrt{p_0\left(1 + \frac{\zeta^2}{2t}\right) - {p_0}^2} \quad (85)$$

where

$$\zeta = \frac{A_s}{V_c k_e}\sqrt{\frac{k_B T_s K H_d^0}{p_0}}\sqrt{\frac{D}{\pi}} \quad (86)$$

The solutions for the diffusive uptake have a negative sign in eq 85. The positive branch would describe a source. Note that the quantity $(k_B T K H_d^0 D/p_0)^{1/2}$ corresponds to $H_dD^{1/2}$ in eq 66. These equations have been used to analyze the uptake of HCl onto vapor deposited ice in a Knudsen cell.[250] To determine $H_d^*D^{1/2} = (k_B T K H_d^0 D/p_0)^{1/2}$ for a dissociating species from a Knudsen-cell experiment, it is best to use the linearity of $\gamma(t)(p_0/p_r(t))^{1/2} = \bar{v}H_d^*D^{1/2}/4 \times (\pi t)^{1/2}$.

**Asymptotic Fitting Method.** While the equations for diffusive uptake have been used successfully for studying the diffusive uptake of acidic gases into liquids, the nature of uptake processes on ice is not yet established (see section 8). Surface adsorption, diffusion, or a slow restructuring of the surface might occur simultaneously. Asymptotic fitting[172,214] of the latter part of the breakthrough curve has been used to analyze breakthrough curves with long-lasting tailing.

The method is illustrated in Figure 17. The breakthrough curve shows diffusion-like tailing and additional uptake during the initial part of the uptake process (Figure 17, upper panel). By fitting the equation for diffusion-like kinetics (eq 84) to the last part of the signal, one can determine $H_dD^{1/2}$. To first order, the nondiffusive component is the difference between total and diffusive uptake. This approach is only an approximation, because it does not take into account the complex kinetics of simultaneous adsorption and diffusion during the initial stage of the uptake. Complete numerical modeling of the system yields a conceptually equal but quantitatively slightly different result.

**"Dope and Probe" Experiments.** The methods described above analyze the uptake kinetics in the gas phase without any information about the solid phase. Evidence that HCl is indeed taken up into the bulk ice could be derived from the "dope and probe" technique as developed by Flückiger et al.[241,247,314]

A dope and probe experiment is performed in a Knudsen cell in two subsequent steps. First, in the dope period, the ice surface is exposed to a defined amount of HX (X = Cl, Br, or I). Then the plunger is closed for a defined period of time. During this time, adsorbed HX diffuses to a certain depth of the ice. With the plunger kept closed, a constant flux of $XONO_2$ is flowed through the Knudsen cell. Then, the plunger is opened, and the ice is probed with gaseous $XONO_2$. Two simultaneous heterogeneous reactions occur on the ice surface. The adsorbed HX is converted to $X_2$ by the titration reaction (with reaction rate $k_1$)

$$XONO_2(g) + X^-(s) \rightarrow X_2(g) + NO_3^-(s) \quad (87)$$

At the same time, the water molecules of the ice are converted by the hydrolysis reaction (reaction rate $k_2$)

$$XONO_2(g) + H_2O(s) \rightarrow HOX(g) + H^+NO_3^-(g) \quad (88)$$

Figure 18 shows the production of gaseous $Cl_2$ immediately after exposure of the ice to $ClONO_2$. Reaction 87 is expected to happen on the surface itself because $XONO_2$ will not easily

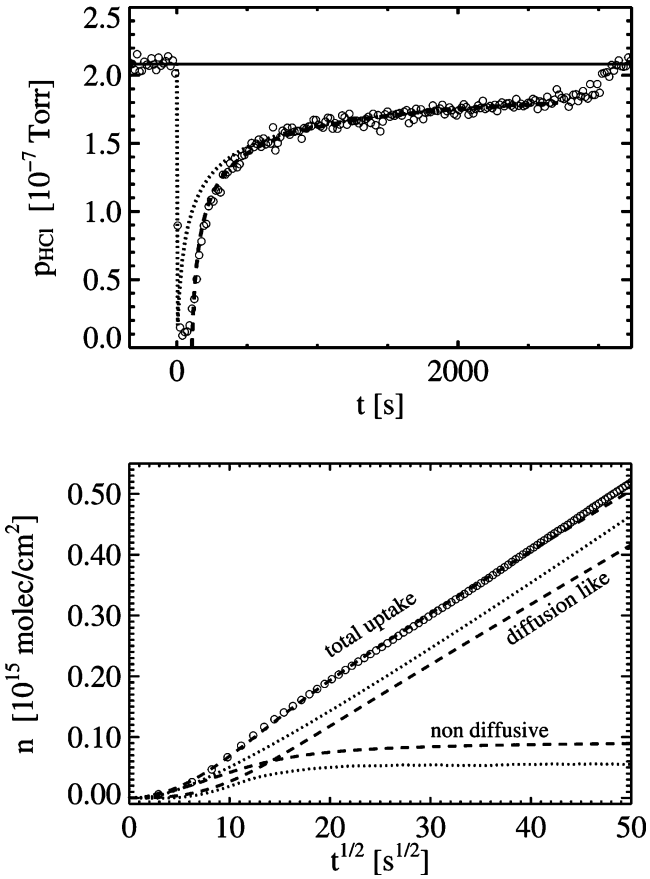


**Figure 17.** Upper panel: Breakthrough curve in a Knudsen cell experiment at 188 K. At $t = 0$ s the plunger is opened and the HCl exposure starts; at $t = 3000$ s the plunger is closed again. To first order, the difference between the dotted and dashed curves was used as an estimate for the surface uptake. Lower panel: total, diffusion-like, and nondiffusive uptake per surface area as a function of $t^{1/2}$. Circles, experimental data; dotted line, simulated breakthrough curve, based on $H_d^*D^{1/2}$, as determined by asymptotic fitting from the tailing of the breakthrough curve, i.e., for $t > 1000$ s using eq 67; dashed line, breakthrough curve simulated with a full numerical model assuming both diffusion and Langmuir adsorption occurring at the ice surface (see Figure 28 for comparison). (Reprinted with permission from ref 214. Copyright 2004 American Chemical Society.)

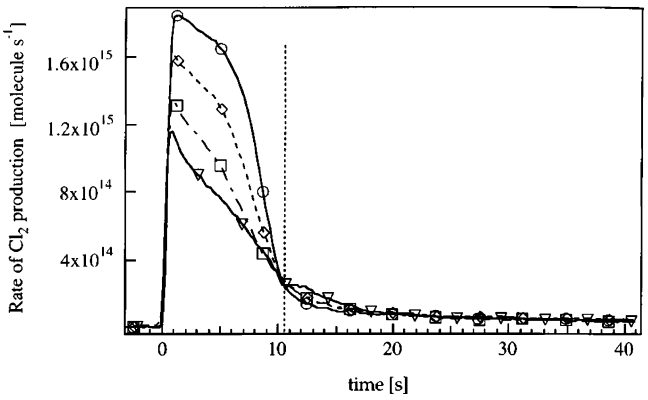


**Figure 18.** Production of $Cl_2$, after exposure of HCl doped ice with $ClONO_2$, for different time delays $\Delta t$ between HCl exposure and probing with $ClONO_2$: open circles, 2 min; diamonds, 5 min; squares, 10 min; triangles, 20 min. With increasing time $\Delta t$, the amount of HCl in the surface region reduces due to diffusion into the depth of the ice. Dotted line: crossing point of the four traces. (Reprinted with permission from ref 241 (Figure 9). Copyright 2000 American Chemical Society.)

dissolve into the ice. Once the main $X_2$ burst is gone, because there is no or little HX available for reaction with $XONO_2$, the hydrolysis reaction starts. Both evaporation of the ice (no water is fed into the Knudsen cell) and hydrolysis vaporize the ice, and HX, which diffused into the ice between the dope and the 'probe' periods is brought to the surface where it is converted to $X_2$ (reaction 88). Thus, the $X_2$ burst can be interpreted as a direct measurement of the HX concentration profile in the ice and thus allows one to estimate the diffusion depth of HX into ice.

**Pulsed Valve and Repetitive Pulse Experiments (RPE).** In a pulsed valve experiment, the ice is exposed to one short gas pulse, and the kinetics of the response allows one to infer information about the adsorption kinetics and the mass accommodation process (eq 75).

Repetitive pulse experiments (RPE) are an extension of this method. Here, the ice is exposed to a series of gas pulses with a defined repetition frequency. By mass balancing, the total HCl loss onto the ice between two pulses can be calculated from the time-dependent signals. Because the surface is brought into a steady state by continually repeated gas pulses, the ice surface itself must be saturated, and the authors concluded that there is a continuous diffusive loss into the ice. By estimating the diffusion depth using dope and probe experiments, one can determine the diffusion constant.

**Correction of Measured Partial Pressures due to Temperature Differences in the Cell.** If the pressure measurement and the substrate are made at different temperatures in the same system, the measured pressure needs to be corrected. This can be seen readily from the ideal gas law, when it is assumed that the gas phase is at temperature $T_c$ and the substrate is at temperature $T_S$. With the Hertz−Knudsen equation (cf. eq 47), we find for the flux balance at the surface $j_{net} = \alpha_c p_c/(2mk_BT_c)^{1/2} - \alpha_c p_v/(2mk_BT_S)^{1/2}$. In thermodynamic equilibrium, when there is no net growth or evaporation of the sample, we have $j_{net} = 0$ and consequently $p_c(T_c) = (T_c/T_S)p_v(T_S)$. The pressure in the warmer Knudsen cell is higher than the ice vapor pressure. For a wall temperature of $T_c = 300$ K and a substrate temperature of $T_S = 200$ K, this leads to a 22% effect. However, this simple treatment is only justified if the gas temperature dominates the flux onto the ice without changing the average gas temperature. This situation occurs if the Knudsen cell walls are large compared to the substrate surface. If this is not the case, semiempirical expressions[315] may be used, as has been done by Hanson and Mauersberger.[249]

## 5.2. Flow Tube Equations

In flow-tube experiments, a trace gas in a carrier gas is passed through a tube, which is typically coated with ice, onto which the trace gas is taken up. The trace gas partial pressure is monitored at the tube exit as a function of time. This so-called breakthrough curve is analyzed to determine the total uptake onto the substrate or to investigate the kinetics of the uptake process. In contrast to a Knudsen cell, which is operated at low pressures (at least below a few millitorr), a flow tube requires a carrier gas for operation. Thus, when the transport in a flow tube is modeled, several processes must be considered: advection and diffusion in the gas phase and the uptake onto the surface and possibly into the bulk of the condensed matter. Furthermore, for laminar flow conditions, a velocity profile in the flow tube evolves. If the gas flows in the $x$-direction, the processes in a flow tube of radius $R$ can be described by this differential equation:

$$\frac{\partial n(x,r,t)}{\partial t} = 2v\left(1 - \frac{r^2}{R^2}\right)\frac{\partial n(x,r,t)}{\partial x} + D_g\left(\frac{\partial^2}{\partial r} + \frac{1}{r}\frac{\partial}{\partial r} + \frac{\partial^2}{\partial^2 x}\right)n(x,r,t) + S(x,r,t) \quad (89)$$

Here $v$ is the mean (plug flow) gas velocity, $D$ is the gas-phase diffusion constant, and $S(x,r,t)$ is a term describing sinks and sources at the flow tube wall and of possible gas-phase reactions. Unfortunately, this partial differential equation can only be solved analytically for special cases, such as steady-state conditions and simplified assumptions for the source and sink terms.

**Calculation of the Total Uptake.** The simplest analysis is to calculate the total uptake onto a surface by numerical integration of the measured breakthrough curve. For a flow tube with cross section $A_F$, flow velocity $v$, and particle density $n$ at the tube exit,

$$\dot{N} = A_F n v \quad (90)$$

molecules leave the flow tube. If the entrance concentration is $n_0$ molecules $m^{-3}$, the total loss onto the substrate can be calculated by numerical integration of the breakthrough curve $n(t)$

$$N_{loss}(t) = A_F v \int_{t=0}^{t} [n_0 - n(\hat{t})]\, d\hat{t} \quad (91)$$

When this equation is used, criteria to determine the end of the uptake process must be invoked. Because breakthrough curves for acidic gases can show a very long tailing, the end of the uptake process may be ill defined.[42,172,214] For discussion, see section 8.4.4.

**The Quasi-Stationary Approximation.** The breakthrough curve in uptake experiments is time-dependent. If the temporal development of the breakthrough curve is slow, the quasi-stationary approximation can be made in a similar way as we have explained for the treatment in a Knudsen

cell (see section 5.1 and ref 316). Then eq 89 reads

$$0 = 2v\left(1 - \frac{r^2}{R^2}\right)\frac{\partial n(x,r,t)}{\partial x} + D_g\left(\frac{\partial^2}{\partial r} + \frac{1}{r}\frac{\partial}{\partial r} + \frac{\partial^2}{\partial^2 x}\right)n(x,r,t) + S(x,r,t) \quad (92)$$

For further analysis of this equation, we distinguish between fast and slow diffusion.

**Case I: Fast Diffusion.** If the gas-phase diffusion is fast enough that it does not limit the transport toward the tube walls, we can introduce two simplifications. First, we ignore the velocity profile in the gas phase. Second, the diffusion perpendicular to the flow direction is ignored.

Often the sink term, $S(x,r,t)$, is simply proportional to the concentration in the gas phase. A simple example is a first-order gas-phase reaction ($S(x,t) = -k_I n(x)$) or the irreversible loss of molecules onto the flow tube wall with the net flux $j_{net} = \gamma n_g/(\bar{v}4)$ (see, for example, eq 43). We calculate the change in concentration in an infinitesimal element of length d$x$, with surface area d$A$ and volume d$V$ and find for the sink term $S(x,r,t) = j_{net}(x,t)\ \mathrm{d}A/\mathrm{d}V$. Using the definition

$$\tau(t) = \frac{V_c}{A}\frac{4}{\bar{v}\gamma(t)} \quad (93)$$

we can write for the sink term

$$S(x,r,t) = \frac{n(x,t)}{\tau(t)} \quad (94)$$

Here we define the time $t$ such that the uptake process starts at $t = 0$; then the use of $t$ in eqs 92 and 94 are equal. With use of this expression for $S(x,t)$, eq 92 reduces to the ordinary differential equation

$$0 = v\frac{\partial n(x,t)}{\partial x} + D_g\frac{\partial^2 n(x,t)}{\partial^2 x} + \frac{n(x,t)}{\tau(t)} \quad (95)$$

which can be solved readily. The general solution is

$$n(x,t) = A\exp(\delta_1 x) + B\exp(\delta_2 x) \quad (96)$$

with the time constants

$$\delta_{1,2} = -\frac{v}{2D_g} \pm \sqrt{\left(\frac{v}{2D_g}\right)^2 - \frac{1}{D_g\tau(t)}} \quad (97)$$

Determination of the parameters $A$ and $B$ in eq 96 requires two boundary conditions. For a concentration of $n(x{=}0) = n_0$ and vanishing concentration at infinity, the general solution is

$$n(x) = n_0\exp(\delta_1 x) \quad (98)$$

The diffusion in the flow direction can be ignored if the condition

$$\frac{n(x,t)}{\tau(t)} + v\frac{\partial n(x,t)}{\partial x} \gg D_g\frac{\partial^2 n}{\partial^2 x} \quad (99)$$

holds. Then, for the boundary condition $n(x{=}0,t) = n_0$, eq 95 reduces to a first-order ordinary differential equation with the solution

$$n(x,t) = n_0\exp\left[-\frac{x}{v\tau(t)}\right] \quad (100)$$

Note that this solution can also be found from eq 97 by calculating the limit for $D \to 0$.[317] When diffusion in the flow direction in the flow tube (eq 100) is ignored, the solution is

$$n(x,t) = n_0\exp\left(-\frac{x}{v}\frac{A}{V}\frac{\bar{v}}{4}\gamma(t)\right) \quad (101)$$

where $\gamma(t)$ is the experimentally observed uptake coefficient. When uptake processes of trace gases on ice are investigated, several processes, such as surface adsorption or diffusion into the ice bulk or grain boundaries, may occur simultaneously. The uptake coefficient for this coupled system may be approximated by (cf. eq 70)

$$\gamma(t) = \frac{1}{\dfrac{1}{\alpha_c(1 - e^{-\lambda t})} + \dfrac{\bar{v}}{4H_d}\sqrt{\dfrac{\pi t}{D}}} + \alpha_c e^{-\lambda t} \quad (102)$$

If quasi-stationary conditions hold, this expression may be introduced into eq 101 to calculate the signal at the exit of the flow tube. Simple expressions for the flow tube equations can be found for certain limits. For example, asymptotically we find for $t \to \infty$ the diffusive limit for the flow tube equation

$$\frac{n(t)}{n_0} = \exp\left(-\frac{x}{v}\frac{A}{V}\frac{H_d\sqrt{D}}{\sqrt{\pi t}}\right) \quad (103)$$

We note that this equation could also directly be derived by using the uptake coefficient for a mere diffusive process (eq 66). This equation has been used to determine the product $H_d D^{1/2}$ for the dissolution of HCl in cold sulfuric acid solutions.[318]

Another extreme case occurs in the limit $t \to 0$. Now, eq 101 reads

$$\frac{n(t)}{n_0} = \exp\left(-\frac{x}{v}\frac{A}{V}\alpha_c\right) \quad (104)$$

Similarly, in the intermediate regime, when the condition $((1 - \exp(-\lambda t))(1/\alpha_c + (\bar{v})/(4H_d)\sqrt{\pi t/D})^{-1} \ll \alpha_c\exp(-\lambda t)$ holds (see section 2.3.6), we find adsorption kinetics dominant, and the flow tube equation reads

$$\frac{n(t)}{n_0} = \exp\left(-\alpha_c\frac{x}{v}\frac{A}{V}e^{-\lambda t}\right) \quad (105)$$

(This equation could also directly be derived from the expression for the uptake coefficient, $\gamma(t) = \alpha_c\exp(-\lambda t)$, with $\lambda = p_g k_{ad}/(k_B T n_{sites}) + k_d$ and $k_{ad} = \alpha_c\bar{v}/4$ as formulated in eq 56). It is noteworthy that under some conditions this equation may violate the condition of quasi-stationarity, especially during the initial fast period of the uptake process.

It is important to note that such equations need to be used with care. At present, the experimentally observed tailing in breakthrough curves was found to follow a $t^{1/2}$ law (see section 8.4.4), as formulated in eq 103. However, because the reservoir for diffusion is not yet established experimentally, the physical meaning of the quantity $H_d D^{1/2}$ is not clear.

**Table 1. Different Methods To Model Wall Reactions and Gas Phase Diffusion in Flow Tube Experiments[a]**

| author | diffusion radial | chemical reaction (gas phase) | boundary condition at gas−solid interface |
|---|---|---|---|
| Gormely and Kennedy (GK)[319] | X | | $n_g(x,r=R) = 0$<br>$n_g(x=0,r) = n_0$ |
| Cooney et al. (CKD)[324] | X | | $-D_g\ \partial n(x,r)/\partial x\|_{r=R} = k_1 n(x,R) - k_2 n_2$<br>with $k_2$ = constant<br>$n(x=0,r) = n_0$ |
| Ogren,[327] Brown[328] | X | first order | $-D_g\ \partial n(x,r)/\partial x\|_{r=R} = -kn(x,r=R)$<br>$n(x=0,r) = n_0$ |
| Zvára[323] | X | | Monte Carlo model |
| Behr et al.[466] | | | numerical simulation<br>Langmuir kinetics |

[a] Columns indicate physical processes included in the model and boundary conditions at the gas−solid interface. $D_g$, gas-phase diffusion; $R$, tube radius; $n_0$, concentration at tube entry; $k_1$, $k_2$, $k$, first order rate constants at tube wall; $x$, coordinate in flow direction.

**Pressure-Dependent Uptake Coefficients.** Further complications arise if the uptake process is pressure-dependent, as it is for a dissociating gas. Here the uptake coefficient is

$$\gamma(t,p) = \frac{4}{\bar{v}}\left(\frac{k_B T K H_d^0}{p}\right)^{1/2}\sqrt{\frac{D}{\pi t}} \tag{106}$$

The proportionality $\gamma \propto p^{-1/2}$ holds for dissociating gas. As we have discussed above, values between $^1/_2$ and $^1/_3$ may occur for the uptake coefficient for diffusive uptake onto ice. Thus, we solve the continuity equation, eq 95, for the flow tube, ignoring the term for gas-phase diffusion (i.e., for $D_g = 0$). Using the abbreviation

$$\epsilon = \frac{V_c}{A}\sqrt{\frac{\pi t}{K H_d^0 D}} \tag{107}$$

the continuity equation reads

$$0 = \upsilon\frac{dn}{dx} + \epsilon\frac{n^{1-\nu}}{n} \tag{108}$$

This equation can be readily integrated

$$n(x) = \left(n^{\nu}(0) - \frac{\upsilon}{\epsilon}x\right)^{1/\nu} \tag{109}$$

Using the definition of $\epsilon$ and $\nu = ^1/_2$ and converting to units of pressure, we find

$$p(x) = p_0\left(1 - \frac{L}{\upsilon}\frac{A}{V_c}\sqrt{\frac{k_B T K H_d^0}{p_0}}\frac{D}{\pi t}\right)^2 \tag{110}$$

Note that this equation depends solely on the effective Henry's Law constant at partial pressure $p_0$ at the entrance of the flow tube. Thus, it can be used to determine the quantity $k_B T K H_d^0/p_0$. It is noteworthy that this equation shows a distinctly different behavior than the flow tube equation for the nondissociating case. In the case of a nondissociating gas, there will always be some signal immediately after the experiment starts (cf. eq 103) unless the gas adsorbs on the surface as well. In contrast, if the gas dissociates, there will be no signal at the end of the flow tube for $t < (LA/(\upsilon V_c))^2(K H_d^0 D/(n_0\pi))$. This is because the solubility is very high for low partial pressures. Thus, the flow tube is a total sink for the trace gas during the initial period of the uptake experiment.

The equations presented here are useful if gas-phase diffusion does not pose a significant resistance for the transport toward the tube wall. The equations may also be of use in a packed ice column, where the gas passes through a porous material, leading to immediate contact of the trace gas with the ice substrate. In a similar way, more sophisticated equations have been developed to describe the diffusion into the ice spheres of a packed ice bed[264] and for more general geometries.[271]

**Case II: Transport Limitations by Gas-Phase Diffusion.** With rising flow tube pressure and uptake coefficient, the influence of gas-phase diffusion on the measurement increases. Several approaches have been made to solve the quasi-stationary transport eq 95 by numerical or analytical methods.[319−328] To solve the diffusion equation, the Fourier transform technique is used to convert the problem into an eigenvector problem, which allows one to write the solutions as a series of the form

$$n(r,x) = \sum_{i=1}^{\infty} A_i g_i(r)\ e^{-K_i x} \tag{111}$$

where $A_i$ and $g_i(r)$ are determined by the boundary conditions of the problem. The analytical solutions available in the literature differ due to different choices of the boundary conditions (see Table 1).

The possible first solution was derived by Gormley and Kennedy,[319] who solved eq 92 for very fast uptake processes onto the tube walls by assuming that the gas-phase concentration at the tube wall vanishes. Parameters for use in eq 111 are given. A more sophisticated solution with a surface resistance boundary condition (cf. eq 47) was derived by Cooney et al.[324] in cylindrical and planar geometry. Their general solution includes a complex, but straightforward set of equations and parameters for special cases. While originally derived to describe transport processes in blood dialysis, the approach has been used to model the uptake of trace gases as well.[329]

Solutions treating a first-order reaction in the gas phase and on the tube wall but without a resistor boundary condition have been developed by several authors.[325−328] To ease the evaluation of the series expansions, Brown[328] published a widely used Fortran program for analysis of uptake processes in flow tubes.

A very different approach, using Monte Carlo simulations to simulate the transport processes in a laminar flow tube, has been taken by Zvára.[323] He noted that an adsorbed molecule, once desorbing from the tube wall, is very likely to diffuse back to the tube wall in a very short time and

very close to the location of desorption, where it adsorbs again. On the basis of analytical solutions for the transport in laminar flow tubes (e.g., eq 111) and linear gas chromatography, he derived a probability distribution for the distance a molecule is transported between two different adsorption events. This probability distribution together with the residence time of a single adsorption encounter is then used to simulate the distribution and residence time of a molecule in a flow reactor.

A big uncertainty when the influence of the gas-phase diffusion is estimated is associated with the diffusion constants. For an experiment, the diffusion constant of the trace gas in the carrier gas used needs to be estimated. Such binary diffusion constants can be calculated using ideal or nonideal gas theory or using models based on experimental data (see, for example, refs 72, 256, 257, and 260 and citations therein). The gas-phase diffusion constants of acidic gases, which genuinely stick to walls in reaction vessels, are difficult to measure. It is noteworthy that a flow tube reactor can be used to determine gas-phase diffusion constants if the transport to the wall is completely limited by gas-phase diffusion (see, for example, ref 330).

## 6. Evidence for the Existence of Ions upon Trace Gas Uptake on Ice

According to the mechanism originally suggested by Eigen and Kustin,[163] an acidic gas HX dissociates when dissolved in water. Here, the acid HX acts as proton donor when reacting with the readily available water, $HX + H_2O \rightarrow H_3O + X^-$ (cf. eq 12). In ice, the water molecule is chemically bound in the ice lattice; thus it is not as easily available for the dissociation reaction as it is in liquid water. Consequently, it is not necessarily clear whether ions will form when acidic gases interact with ice. This topic has been studied using a variety of experimental and theoretical methods during the last 25 years. The current state of knowledge is reviewed in this section.

### 6.1. Experimental Evidence for Ion Formation

Earliest experimental indication of the dissociation of HCl in ice can be taken from liquid-ice partition coefficient measurements,[167] which showed $p^{1/3}$ dependence for the Henry's Law constant (cf. eq 16). The measurements of the solubility of HCl and $HNO_3$ in ice single crystals by Thibert and F. Dominé,[73,74] who found a solubility $H \propto p^{1/2.73}$ for HCl and $H \propto p^{1/2.3}$ for $HNO_3$ for temperatures above −35 °C, indicate at least a partial dissociation of the dissolving gas in ice. Furthermore, in HCl uptake experiments at 200 K on vapor deposited ice, the relation $H_d D^{1/2} \propto p^{1/2}$ could be shown.[214,250]

The pressure dependence of uptake experiments offers only indirect evidence for the ion formation. Thus, diverse applications of infrared spectroscopy have been employed since the early 1990s (for example, see refs 40, 243, 244, 284, 286, 313, and 331−341) to investigate ions on the ice surface directly. Recently, also other techniques such as reactive ion scattering (RIS)[342−345] or the synchrotron based photo-stimulated desorption near-edge X-ray absorption fine structure spectroscopy (PSD-NEXAFS)[305,313] have been used to verify the existence of ions on HCl-exposed ice.

Most of these studies have been performed at cryogenic temperatures between 20 and 140 K. Higher temperatures are often hard to access experimentally by spectroscopic methods due to the high vapor pressure of ice. For example, the absorption of IR light in water vapor may severely affect the interpretation of solid-phase ice spectra at higher temperatures.

Before presenting the results, we recall the importance of the phase diagram when interpreting uptake experiments. From the HCl phase diagram (Figure 5), it is clear that ice is stable only for finite HCl partial pressures. The lower the temperatures, the lower are the HCl partial pressures needed to form hydrates. With use of an extrapolation as given by Wooldridge,[170] HCl hydrates may be stable at HCl pressures as low as $10^{-8}$ Torr (150 K) or $10^{-10}$ Torr (140 K). A similar picture evolves for HBr and $HNO_3$.

Although hydrate formation is not the predominant topic of this review, we discuss the main results including hydrate formation at low temperatures, because this gives insight into the nature of the acidic trace gas−ice interaction. We focus on HCl; a similar picture is expected for other strong acids.

**Interactions at Cryogenic Temperatures, 20−140 K.** The interaction of adsorbates with small ice nanocrystals of 15−20 nm diameter has been investigated by several authors using FTIR spectroscopy (for example, see refs 285, 331, 338, and 346−353), based on a method developed by Fleyfel and Devlin.[354]

Using small nanocrystals is advantageous because they have relatively more molecules on the surface compared to larger crystals, which enhances the sensitivity of the IR spectra to surface effects. Because nanocrystals consist of only several hundred molecules, numerically expensive simulation methods can be used for complete modeling and comparison with experimental data as has been extensively done by the groups of Buch and Devlin. Furthermore, it is noteworthy that methods have been developed to interpret the spectra in terms of surface, subsurface, and bulk properties.[355]

This research led to general conclusions about adsorbate−ice interactions. One can distinguish between weak (e.g., $H_2$, $N_2$, CO, $CF_4$), intermediate (e.g., $SO_2$, HCN, $H_2S$), and strong adsorbates (e.g., HCl, HBr, $HNO_3$) by considering the adsorption energies.[346−349] Weak adsorbates will not be able to shift the positions of the water molecules on the ice surface but rather adapt to the ice surface structure. For intermediate adsorbates, the binding energy is comparable to the weakest H-bonds, which can be broken by the adsorbing molecules. Strong adsorbates with binding energies on the order of the water−water binding energy will reorder the surface and possibly form hydrates.

From a variety of experimental studies on ice, the principal behavior of the HCl−ice interaction at cryogenic temperatures as function of temperature and amount of HCl exposure can be summarized. In short, the amount of ionization increases with rising temperature and rising amount of HCl. At a temperature around 20 K and a surface coverage around 20%, the HCl is mainly adsorbed as a molecular species.[352] The existence of molecular adsorption at low temperatures has also been confirmed by X-ray absorption spectroscopy.[312] Both reactive ion scattering[343,344] and FTIR spectroscopy combined with theoretical studies[352] showed increasing ion formation when the temperature rose from 20 to 140 K. The RIS study suggests that for temperatures below 80 K molecular adsorption dominates, while the amount of ionic species increases until a temperature of 140 K is reached.[343] Furthermore, at the threshold temperature of about 90−95 K, the ion formation (i.e., of the Eigen and Zundel cations,

$H_3O^+$ and $H_2O_5^+$) is strongly enhanced, and an ion-burst occurs.[352]

These results are corroborated by the use of surface-sensitive PSD-NEXAFS measurements. Here, the H−Cl bond was observed. At a temperature of 150 K, this bond is only visible for pure HCl but not for HCl adsorbed on ice, which directly evidences the dissociation of the HCl molecule.[313] Very recently, using NEXAFS, it could be shown that HCl dissociates on the surface and in the bulk of films of about 100 monolayer thickness for a coverage larger than 1 monolayer of HCl and for temperatures above 90 K.[305]

The amount of HCl on the surface is important for the nature of the interaction. The "ionization burst" at a temperature around 90 K occurs for an HCl coverage higher than 20% and may manifest the formation of a surface phase.[352] In contrast, at lower coverage, the degree of ionization increases smoothly. Similarly, when the adsorption of $NH_3$ on ice at 110 K was studied, it was found that ammonia attaches to the dangling H-bonds. At a higher coverage, it will cleave the $H_2O\cdots H_2O$ bonds and will be located in the surface but not on top of it.

Also, other studies on the acid−ice interaction provide direct and indirect evidence of ion formation at low temperatures. For example, using sputtering with $Ar^+$ ions and SIMS (secondary ion mass spectroscopy), Donsig and Vickermann[356] could show that the number of $H_3O^+$ ions in the sputtered clusters increases after HCl exposure. The authors inferred that there is an ionic film on top of the ice surface, which extends to at least 10 monolayers into the ice for a temperature of 150 K, while the ions are confined to the surface at 135 and 95 K. It could also be shown that the dissociative electron attachment to HCl is greatly enhanced when HCl is adsorbed to the ice surface, compared to gaseous HCl. This result supports the dissociation of HCl.[357]

Very recently, Devlin et al.[353] investigated the mechanism of the HCl dissociation using infrared transmission spectroscopy at temperatures below 100 K. A three stage process was found. First, the HCl molecule attaches to an OH dangling bond, forming Cl−H···O. Then, the Cl atom forms O−H···Cl with another dangling bond. In this state, the HCl molecule is not yet dissociated but stretched to the verge of dissociation. The dissociation occurs only after a third bond attaches at the Cl atom. After dissociation, the proton can diffuse away. The proton forms both the Eigen cation,[163] $H_3O^+$, and the Zundel ion, $H_5O_2^+$,[358,359] on the ice surface. This mechanism was confirmed by both Monte Carlo simulations of HCl uptake onto a flat ice surface and ab initio simulations of the dissolution of HCl in water clusters.

**Results at Stratospheric Temperatures.** The evidence presented so far was made on ice at very low temperatures. Under such conditions, given the amounts of HCl exposure, hydrate formation is highly probable. Unfortunately, experiments at higher temperatures in the ice stability domain are hampered by the high ice vapor pressure and by detection limits as discussed in this section.

For example, Barone et al.[22] investigated the uptake of HCl, HBr, and HI on ice using a Knudsen cell. Using Fourier transform infrared reflection absorption spectroscopy (FTIR−RAS), they monitored the $H_3O^+$ ion. At a low temperature, around 110 K, the $H_3O^+$ ion formed with increasing uptake of acidic trace gas. However, for measurements at higher temperature (202 K) in the ice stability region, no $H_3O^+$ ion could be observed. This was not attributed to the absence of the ion but rather to increasing experimental difficulties, such as rising light scattering from the film during the course of the uptake experiment. The authors suspected that the ice film might have become rougher with time.

Hudson et al.[243] investigated the $HNO_3$ uptake on ice at temperatures between 209 and 214 K and observed the $NO_3^-$ ion using FTIR−RAS. The ion could be clearly shown on ice exposed to $HNO_3$ partial pressure high enough to form NAT. However, for pressures low enough to ensure the thermodynamic stability of ice, the ion could not be observed in the IR spectrum. The authors argued that no $NO_3^-$ is expected due to the low total coverage.

It may be generally expected that acidic gases will dissociate upon uptake onto the ice surface or in a solid solution. However, at present, there is no direct experimental evidence for ion formation in the solid solution regime. Some experiments have been performed[39] on ice condensing with an acidic trace gas present in the gas phase, which results in the formation of a solid phase, which is too highly doped by the trace gas to be thermodynamically stable ice but too low in bulk concentration to form a hydrate. However, under such conditions possibly a phase separation in the overdoped ice may occur and a mixture of doped ice and hydrates may form. While there is evidence that ions form under such conditions, again no inference can be made for ice in the solid solution regime.

There is also experimental information on the dissociation of nonacidic gases after their uptake on ice. For example, the uptake of $ClONO_2$ on ice has been observed using FTIR spectroscopy at a temperature of 180 K.[286,336] It has been argued that $ClONO_2$ will form the intermediate ion $[H_2OCl^+\cdots{}^-ONO_2]$. However, this suggestion has been criticized,[360] and it has been argued that the spectra do not show a $Cl^+$ ion but rather molecular $HNO_3$.

In summary, there is compelling experimental evidence that an acidic gas (HX) forms ions (such as, $H^+$, $X^-$, $H_3O^+$, $H_2O_5^+$) when interacting with ice. However, the experimental evidence is restricted to thermodynamic situations where either hydrates are stable or a liquid solution forms. The lack of direct evidence of ion formation in the solid solution regime is possibly due to the extreme challenge of such experiments or the finite sensitivity of spectroscopic methods, because the solubility of acidic gases in the ice matrix is very low (the mixing ratio of HCl dissolved in solid ice is well below 0.1%, eq 112). Furthermore, the absolute number of molecules on the surface itself is low and may be on the order of a few monolayers or much less, as recent studies indicate.[21,214,217]

It should also be noted that the interpretation of bulk ice spectroscopy might be hampered by the polycrystallinity of the ice, because ions have been found in the triple junctions of polycrystalline ice.[81] Thus ions observed in bulk measurements might be due to liquids in confined aqueous reservoirs and not necessarily associated with their presence as solutes in solid ice.

## 6.2. Theoretical Evidence for Ion Formation

The theoretical methods used to simulate the trace gas−ice interaction have been reviewed by Girardet and Toubin.[361] A variety of studies specifically treated the interaction of acidic gases with ice. The interaction of acidic gas molecules with small clusters[352,362−372] and flat ice surfaces or inside the ice structure[366,373−386] and in water[387] have been studied using classical and quantum mechanical molecular dynamics

methods, ab initio methods, and density functional calculations. One of the earliest molecular dynamics simulations investigated the physisorption of HCl and HOCl on ice.[373] Short residence times for the physisorption processes were found. Furthermore, it was concluded that the adsorption of HCl cannot be explained by assuming the physisorption alone. On the basis of molecular dynamics simulations, Gertner and Hynes[376,377] suggested that HCl is taken up onto the ice surface in two different ways: about 40% is weakly adsorbed onto the ice surface, while about 60% is incorporated into the lattice, where the HCl molecule replaces an O−H unit in the ice lattice and acts as proton donor. Bianco et al.[378] extended the work of Gertner and Hynes[376] by using a quantum rather than a classical treatment and concluded that HCl can only act as proton donor when built into the ice bilayer. Further studies found that the HCl molecule dissolves readily in ice clusters and dissociates without or with very low energy barrier.[362−367,381,383,385]

The attachment of the HCl molecules to several dangling bonds on the ice surface and the start of the dissociation when the third bond is formed as observed by Devlin[353] have been been confirmed in theoretical studies.[366,381,383] On ice clusters with the size of a few hundred water molecules, the formation of the Eigen[163] and the Zundel[359] cations ($H_3O^+$ and $H_5O_2^+$, respectively) could be shown for temperatures above 90 K.[352] Furthermore, theoretical evidence has been found for the existence of the $H_3O^+Br\cdots OH^-$ ion.[364]

In summary, a variety of theoretical studies suggest that HCl readily dissociates in a barrierless process when adsorbing on the ice surface or into water clusters of appropriate size.

## 7. Data 1: Solubility and Diffusion

Trace gases can form a solid solution with ice. The dissolved molecule might be stored in interstitial sites, defects, or vacancies or in the ice lattice itself. For example, for acids with small molecules, such as HF, it has been suggested that HF dissociates and that the $F^-$-ion replaces an O-atom in the ice lattice.[165] Similar arguments have been made for HCl[376] (see also section 6.2). In contrast, for substances such as KOH, a $K^+$-ion is possibly located in the inner part of the hexagonal ring in the ice lattice.[165] The physical mechanism of the diffusion is not the subject of this review and has been reviewed comprehensively elsewhere.[154,165,388]

In many experiments, polycrystalline ice is used. Here impurities may be stored in other reservoirs than the ice matrix. Most notably, there are grain boundaries and triple junctions, where impurities have been found experimentally.[10,11,81] Grain boundaries are less ordered in comparison to the crystal lattice; thus diffusion is expected to be faster than in the crystal lattice. Such reservoirs and other lattice imperfections may serve as shortcuts for the diffusion.[73] However, currently there is no knowledge about the relative importance of the transport velocity and solubility in such reservoirs, which renders the assessment of the relative importance of the different processes difficult.

The measured diffusion constants for impurities in ice show large scatter and seem to lack consistency. For example, for the HCl diffusion in ice, the measured diffusion constants range from values as low as $5 \times 10^{-19}$ to $\sim 10^{-9}$ $m^2$ $s^{-1}$ at temperatures around 190 K. In section 7.2.1, we will try to partially resolve the reason for this scatter.

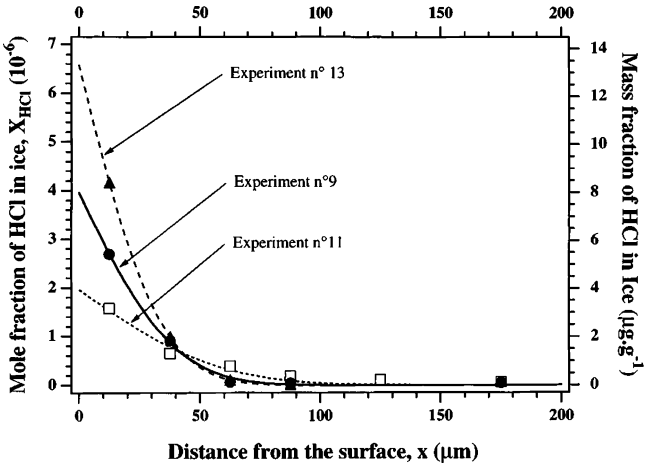


**Figure 19.** HCl concentration profile in ice single crystals as derived by Dominé et al.[291] using the sectioning method. (Reprinted with permission from ref 291. Copyright 1994 American Geophysical Union.)

### 7.1. Solubility of HCl and $HNO_3$ in Single Crystals

We have described the principle of Dominé's sectioning method in section 4.2. In a series of publications, Dominé and co-workers describe measurements of the solubility and diffusivity of HCl and $HNO_3$ in ice at temperatures above −35 °C.[73,74,291] Based on these data, thermodynamic concepts have been used to estimate the solubility of HCl and $HNO_3$ in ice at temperatures as low as −90 °C. However, after an independent repetition of the work by Sommerfeld et al.,[389] a controversy about the method arose, shedding some light on potential experimental pitfalls when uptake experiments on ice are performed.

#### 7.1.1. Determination of the Diffusivity and Solubility

Figure 19 shows HCl concentration profiles in the upper millimeter of an ice single crystal for different temperatures and HCl partial pressures. To analyze these concentration profiles, Thibert, Dominé, and co-workers[73,74] used eq 65. They pointed out that the measured concentration profiles could not be fitted perfectly using eq 65, because the concentrations in the depth of the ice were too high. Thibert and Dominé argued that there are two different diffusive processes in the ice: a slow diffusion through the single-crystal matrix and a fast diffusion along defects. Grain boundaries could be excluded, because single crystals had been used. Microcracks were excluded by annealing experiments. Dominé et al. suspected that the HCl might diffuse along imperfections in the crystal lattice structure, such as small angle boundaries.

#### 7.1.2. Main Results for HCl and $HNO_3$

**Solubility.** From the measured diffusion profiles, Thibert and Dominé[73,74] present parametrizations for the solubility of $HNO_3$ and HCl in ice single crystals as functions of temperature and partial pressure. The mixing ratio of HCl and $HNO_3$ can be parametrized as

$$x_{HCl} = 6.13 \times 10^{-10} \exp(2806.5/T) p^{1/2.73} \quad (112)$$

and

$$x_{HNO_3} = 2.37 \times 10^{-12} \exp(3523.2/T) p^{1/2.3} \quad (113)$$

respectively (acid partial pressure in Pa, temperature in K). The solubility of both trace gases are marked as isosolubility lines in the phase diagrams for the HCl−ice and the $HNO_3$−ice systems (Figures 5 and 6). In general, HCl is more than 1 order of magnitude more soluble than $HNO_3$.

**Pressure Dependence.** Interestingly, for both gases, the exponent $\mu$ for the pressure dependence $x \propto p^{\mu}$ is between the value for a dissociating species ($\mu = 1/2$) and the one for dissolution with defect formation ($\mu = 1/3$), see section 2.1.1. As discussed above, a variety of studies strongly indicate that HCl and $HNO_3$ dissociate when taken up into ice. Thibert and F. Dominé[73] argued that the observed exponent may indicate that the acid is incorporated into interstitial positions in the ice lattice.

**Partition Coefficient Measurements.** The partitioning between ice and the liquid phase is described by the partition coefficient, which is the ratio of the impurity concentration in ice divided by its concentration in the solution. The partition coefficient is measured by slow freezing of an aqueous solution and subsequent chemical analysis of the ice and the remaining aqueous solution. Partition coefficients have been measured in several studies.[136−139,167] Typically, the solubility of impurities in ice is several orders of magnitude lower than the one in water, and partition coefficients may range from $10^{-3}$ to $10^{-7}$. The partition coefficient data for impurities of interest in the atmosphere have been reviewed by Elliot et al.[228]

## 7.2. Data for Diffusion Constants

### 7.2.1. HCl

**Available Data.** Data available on diffusion constants in ice show a large scatter as illustrated in Figure 20 (see also Table 2). The first study on the diffusion of HCl in ice was performed by Krishnan and Salomon,[290] who used the sectioning technique (see section 4.2; filled dots in Figure 20). A mixing ratio on the order of $(1-1.5) \times 10^{-7}$, fairly below the HCl solubility in ice single crystals,[73] was found. Based on these very low amounts of HCl, the validity of these data has been questioned by Dominé et al.,[291] who suspected that the HCl might have diffused between the ice and the adjacent plexiglass tube and suggested that the measured value does not represent the diffusion of HCl in ice but rather a surface diffusion constant.

In 1983, Barnaal and Slotfeldt-Ellingson[390] used pulsed nuclear magnetic resonance to study the diffusion constant of several trace species in ice (cross in Figure 20). The ice preparation was similar to the method used by Krishnan and Salomon:[290] A cap of doped ice was frozen onto an ice single crystal. The samples were stored for up to 4 years to allow diffusion. A change of the NMR signal (the relaxation time, $T_1$) was used to determine the dopant concentration profile in the ice. From this profile, the diffusion constant was derived.

The first measurement of HCl diffusion with HCl taken from the gas phase at a low temperature of 185 K was made by Molina et al.[232] by exposing ice to a $N_2$/HCl mixture and monitoring the HCl content in the solid phase using optical spectroscopy. The HCl partial pressure ranged between 0.01 and 1 Torr. The diffusion into the ice was studied in the thermodynamic regime where ice melts (cf. Figure 5). The high diffusion of $10^{-9}$ m$^2$ s$^{-1}$, which is typical for the diffusion in liquids, suggested that the HCl would diffuse extremely rapidly into the ice under melting conditions. It should be pointed out that this diffusion constant does not reflect the diffusion into the ice lattice, but rather the speed of melting due to the presence of large amounts of HCl.

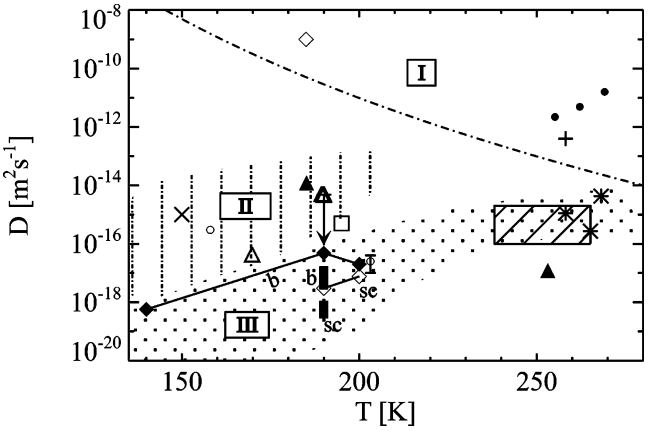


**Figure 20.** Diffusion constants for HCl in ice: I, likely affected by melting of ice (i.e. $D$ is rather a measure of melting and diffusion); II, likely affected by hydrate formation (i.e. $D$ is rather a measure of hydrate growth and migration); III, diffusion of HCl in solid solution (dotted area, estimated values for $D$); solid dots, Krishnan and Salomon;[290] cross, Barnaal and Slootfeldt-Ellingsen;[390] asterisks, Dominé et al.;[291] hatched area, Thibert and Dominé;[73] solid triangle, Wolff et al.;[10] solid rectangle, Flückinger et al.[78,241] (c and b, experiments on condensed and bulk ice; sc, experiments on single crystals); open circle with error bar, Huthwelker et al.;[296] open square, Krieger et al.;[294] open triangles, Livingstone et al.;[394,395,465] arrow, Livingstone et al.;[395] the arrow points toward higher amounts of Na in the ice; open circle without error bar, Koehler et al.;[332] vertical cross (at 150 K), Horn and Sully;[392] open diamond, Molina et al.;[232] for description, see text.

On the basis of the finding that acids can accumulate in the triple junctions of polycrystalline polar ice,[11] Wolff et al.[10] investigated artificially produced HCl doped ice using scanning electron microscopy with X-ray microanalysis. In the experiments, an aqueous HCl solution (∼0.1 M solution) was frozen at liquid nitrogen temperatures and annealed for 24 h at 253 K. The surface was cleaned using a microtome, then cooled to 160 K and investigated. HCl was found in the triple junctions (∼1 $\mu$m diameter) of the ice. The sample was warmed to 185 K for a defined period of time and cooled again. Now, HCl was found again in the triple junction but also in the adjacent ice grain. From these measurements, an upper limit for the diffusion constant of $D = 10^{-14}$ m$^2$ s$^{-1}$ at 185 K was derived. Based on the 24 h storage time at 253 K, an even lower limit of $10^{-17}$ m$^2$ s$^{-1}$ was estimated. Wolff et al.[10] pointed out that their study investigated the diffusion of HCl into the ice grain itself, because they were capable of distinguishing between uptake into the grain boundaries and the grain itself.

It is interesting to investigate the thermodynamic conditions of this diffusion experiment. When an aqueous HCl solution is frozen at liquid nitrogen temperatures, hydrates may form in the ice. However, during the annealing at temperatures around −25 °C, no hydrates are stable. The HCl is expected to be expelled from the ice; thus ice and an aqueous HCl solution are the only stable phases. The observed HCl concentrations of ∼8 M in the triple junctions are close to the ones in a eutectic solution.[391] Due to the curvature in the triple junctions, the chemical potential of the HCl is slightly reduced, that is, below the one in a eutectic solution. Thus, the ice is close to but not at melting conditions. Thibert and Dominé[73] have shown that the

**Table 2. Measurements of HCl Diffusion in Ice by Various Authors**

| author | $x_{HCl}$ ($\times 10^{-6}$) | $T$ (K) | $p$ (Torr) | $D$ ($m^2$ $s^{-1}$) | comment[d] |
|---|---|---|---|---|---|
| Aguzzi et al.[398] | | 140 | | $(5.7 \pm 0.6) \times 10^{-19}$ | b, DP |
| | | 190 | | $(3.0 \pm 0.7) \times 10^{-18}$ | sc, DP |
| | | 190 | | $(2.3 \pm 0.4) \times 10^{-17}$ | c, DP |
| | | 190 | | $(4.8 \pm 0.6) \times 10^{-17}$ | b, DP |
| | | 200 | | $(4.3-8.8) \times 10^{-18}$ | sc, DP |
| | | 200 | | $(1.7-5) \times 10^{-19}$ | b, DP |
| | | 200 | | $(2 \pm 0.6) \times 10^{-17}$ | c, DP |
| Barnaal et al.[467] | | 258 | | $4 \times 10^{-13}$ | NMR, sc |
| Dominé et al.[291] | (0.2−5) | 258−268 | | $(2.6-38) \times 10^{-16}$ | sc, SEC |
| Flückiger[78,241] | | 190−200 | | $8 \times 10^{-15}$ | sc, DP |
| | | 190−200 | | $3.9 \times 10^{-14}$ | c, DP |
| | | 190−200 | | $1.2 \times 10^{-13}$ | b, DP |
| Horn and Sully[392] | | 150 | | $\approx 10^{-15}$ | vp, FTIR |
| Huthwelker et al.[296] | | 203 | $10^{-6}$ | $(1-4) \times 10^{-17}$ | RBS |
| Koehler et al.[332] | | 158 | $8 \times 10^{-7}$ | $2 \times 10^{-16}$ | FTIR |
| Krieger et al.[294] | $2 \times 10^{-4}$ [a] | | | $5 \times 10^{-16}$ to $3 \times 10^{-15}$ | RBS evaporating ice |
| Krishnan and Salomon[290] | $\approx (1-5) \times 10^{-7}$ | 269 | | $1.6 (\pm 0.4) \times 10^{-11}$ | sc[e] |
| | | 262 | | $4.9 (\pm 0.4) \times 10^{-12}$ | |
| | | 255 | | $2.2 (\pm 0.06) \times 10^{-12}$ | |
| Livingston et al.[394,395,465] | ≈0.33[b] to $10^{-3}$ [c] | 190 | | $4.8 (\pm 1.5) \times 10^{-11}$ | LDR, sandwich |
| Molina et al.[232] | | 185 | 0.01−0.1 | $10^{-5}$ | |
| Thibert and Dominé[73] | | 238−265 | | $10^{-16}$ to $10^{-15}$ | sc, SEC |
| Wolff et al.[10] | | 185 | | $10^{-13}$ | |
| | | 253 | | $10^{-17}$ | |

[a] Bulk concentration. [b] In center of sandwich. [c] In ice. [d] sc, single crystals; c, vapor deposited ice; b, bulk ice frozen from water; SEC, sectioning method; DP, dope and probe technique; RBS, Rutherford backscattering; for description of studies see text. [e] It has been criticized that diffusion occurs along the ice−plastic boundary.

partition coefficient rises when the ice melting point is approached, and it might be speculated that also the HCl diffuses faster compared to the diffusion of HCl in a solid solution, because the crystal is on the verge of melting.

Koehler et al.[332] derived the HCl diffusion from the total HCl uptake at $8 \times 10^{-7}$ Torr and 158 K into a film of known thickness. These experiments were performed in the hydrate existence region and thus do not represent the diffusion of HCl into a solid solution.

The most comprehensive work on the diffusion and solubility of HCl in ice single crystals has been performed by Dominé et al. (asterisks in Figure 20) and Thibert and Dominé[73,291] (shaded area in Figure 20). The method has been described in detail in sections 4.2 and 7.1. They performed experiments with uptake from the gas phase at temperatures between 238 and 265 K and partial pressures of HCl between 0.2 and $7 \times 10^{-3}$ Pa. Solubility and the diffusion constants have been determined as functions of temperature and HCl partial pressure. Diffusion constants range from $10^{-12}$ to $10^{-11}$ $cm^2$ $s^{-1}$. No temperature dependence was found.

Horn and Sully[392] (vertical cross in Figure 20) investigated the diffusion of HCl in vapor deposited ice films at a temperature of 150 K. They deposited ice on a polished Ge plate. HCl is brought into the gas phase, and the arrival of HCl at the ice/Ge interface is observed using attenuated internal reflection infrared spectroscopy (ATR−IR).[393] By this method, a diffusion constant of $\sim 10^{-15}$ $m^{-2}$ s was estimated.

A series of investigations about the diffusion of various species in ice has been made by Livingston et al. using LDR.[293,394,395] Here, the diffusion of a trace element in ice is studied in sandwich experiments.[394,394,395] Ice is grown at low temperatures (typically 140 K) by vapor deposition on a Ru(001) single crystal, which has a unit cell of similar size as the one of ice. Therefore, it is assumed that a single crystalline ice layer forms on the surface. On top of this initially deposited ice film, a layer of the trace element (for example, a HCl−water mixture or vapor deposited Na) is deposited. Finally, the sample is covered by depositing an additional layer of water vapor on top. The preparation is made at temperatures that are low enough to prevent diffusion. To study diffusion, the sample is heated to the desired temperature for a defined period of time. Afterward, the sample is cooled to stop the diffusion and to analyze it using LDR. For HCl, the authors confirmed the diffusive kinetics by variation of the diffusion time and comparison of the observed concentration profiles with theoretical models.[394]

Livingston et al.[394] estimated that the amount of HCl exceeds the solubility limit of HCl in ice single crystals by a factor of $10^4$ and concluded that their measurements do not represent the diffusion of HCl in the ice crystal matrix. Because they observed the composition of the HCl trihydrate in the initial middle layer, Livingston et al. argued that they observe the migration of the HCl hydrate in the ice.

Krieger et al.[294] applied Rutherford backscattering to measure the diffusion constant of HCl in ice (open square in Figure 20). In these experiments, a HCl doped solution (0.022 mol %) was frozen at liquid nitrogen temperature and heated to a temperature of 195 K. The sample evaporated with a known evaporation speed, which allows one to determine a diffusion constant of $5 \times 10^{-16} < D < 3 \times 10^{-15}$ $m^2$ $s^{-1}$.

From the temperature dependence between 195 and 220 K, the authors derived a diffusion activation energy of 14.9 ± 2.5 kcal/mol, in good consistency with the result of 15.3 ± 1 kcal/mol from Livingston et al. This consistency indicates that the same diffusive process was observed in both experiments. As in the work of Livingston, HCl concentrations exceeded the solubility limit in ice single crystals as given by Thibert and Dominé, and the ice was prepared at rather low temperatures (77 K by Krieger et al. and between 100 and 160 K by Livingston et al.), which may have led to the formation of hydrates in the ice. Thus, in both experiments, the observed diffusion is presum-

ably not the diffusion of HCl in a solid solution in ice but possibly the diffusive transport of hydrates, as suspected by Livingston.

Flückiger et al.[78,241] used the dope and probe technique in a Knudsen cell experiment to determine the HCl diffusion in ice (filled rectangles in Figure 20). The authors compared different morphologies. Ice was condensed from the gas phase or frozen from liquid water. Also, single crystalline ice was made by slowly freezing the water using a recipe by Knight.[396] The authors found that HCl diffuses up to a factor of 10 slower into single crystalline ice.

The diffusion into bulk ice, which was frozen from liquid water, was studied using RBS by Huthwelker[296] (open dot with errorbar in Figure 20). Here ice was exposed to a HCl vapor of $10^{-6}$ Torr at a temperature of 200 K. A diffusion constant similar to the one of Flückiger et al. was found.

**Data Comparison.** The data for the HCl diffusion show wide scatter. This is impressively demonstrated for the measurements at temperatures around 200 K. The data vary by more than a factor $10^9$. The measurements at HCl partial pressure around 0.1 Torr and higher were made under melting conditions[232] and thus showed a very fast HCl transport in the ice. For the data in the intermediate range,[293,294] no melting occurred. However, the amount of HCl in the ice exceeded the HCl solubility limit in ice single crystals. Furthermore, because the ice was grown at very low temperatures, hydrates may have formed. Thus, the base process might be the diffusion of hydrates, or the diffusion of HCl in an ice/hydrate mixture but not of HCl in a solid solution in ice. The lowest diffusion constants have been determined when the diffusion of gaseous HCl into ice[78,241,296] was investigated in the ice stability regime, where neither melting nor hydrate formation could occur. Thus, these data might represent the most reasonable value for the diffusion of HCl into ice, without melting or hydrate formation. However, because differences between single and polycrystalline ice have been observed by Flückiger,[78,241] care must be taken to distinguish between the diffusion into the ice matrix and that through possible shortcuts such as grain boundaries.

To explain the discrepancies between the different studies at temperatures above 250 K appears less straightforward. Dominé and Xue[397] have suggested that in the Krishan and Salomon experiments surface diffusion between the ice and the plexiglass wall may have lead to rather fast transport. Similar arguments may apply to the data of Barnaal and Slootfeldt-Ellingsen.

Some of the reported diffusivities below 200 K appear relatively high in comparison to the data around 200 K. The measurements of Koehler et al.[332] have been performed at HCl partial pressure in the hydrate stability region as shown spectroscopically. Thus these data may represent the hydrate formation speed. Similar arguments may apply to the data from Horn and Sully.[392]

In summary, when investigating the diffusion of HCl in ice, the thermodynamics of the system must be considered. HCl partial pressures high enough to melt the ice will yield extremely high diffusion constants. Furthermore, hydrate formation can strongly affect the transport of HCl through ice and lead to intermediate values for the diffusion constant. Measurements in the ice stability region yield the lowest values for the diffusion coefficient. At 200 K, the available data for these conditions refer only to the near-surface region, that is, the upper micrometer of the ice surface. These diffusion constants may indeed represent the diffusivity into small micrometer-sized atmospheric ice particles.

However, it is unclear whether these values indeed represent the bulk diffusivity of HCl in ice, because hypothesized surface melting effects may affect the transport speed of HCl in the region close to the ice surface. At present, there is no experimental knowledge about the nature of the near-surface region of ice at temperature around 200 K in the presence of HCl vapors. Furthermore, no direct measurements of the HCl diffusion in the bulk of single crystals are available at temperatures below 243 K.

**Table 3. Measurements of HBr Diffusion in Ice[a]**

| author | $T$ (K) | $D$ ($m^2$ $s^{-1}$) | comment[b] |
|---|---|---|---|
| Aguzzi et al.[398] | 190 | $(1 \pm 0.2) \times 10^{-19}$ | sc, DP |
| | 190 | $(3.3 \pm 0.9) \times 10^{-19}$ | c, DP |
| | 190 | $(5.1 \pm 1.1) \times 10^{-19}$ | b, DP |
| | 205 | $(3.8 \pm 0.3) \times 10^{-18}$ | c, DP |
| | 205 | $(4.8 \pm 0.7) \times 10^{-18}$ | s, DP |

[a] For description of studies see text. [b] sc, single crystals; c, vapor deposited ice; b, bulk ice frozen from water; s, sandwich sample DP: dope and probe technique

### 7.2.2. HBr and HI

Data on the diffusion of HBr and HI in ice are scarce. No data are available for HI and $SO_2$. The only study that provides a direct measurement of the HBr diffusion constant was made in a Knudsen cell using the dope and probe technique.[398] As in previous work with HCl, several types of ice have been investigated: ice single crystals grown from liquid water, polycrystalline bulk ice samples, and vapor deposited ice. Similar to the work on HCl, the diffusion in ice single crystals was slower than the diffusion into polycrystalline ice samples (see Table 3).

### 7.2.3. $HNO_3$

The diffusion of $HNO_3$ in ice has been studied by Thibert and Dominé[74] and by Sommerfeld et al.[389] Both groups apply the sectioning technique to ice single crystals. Based on data taken for temperatures between $-8$ and $-25$ °C and $HNO_3$ partial pressures of $3 \times 10^{-6}$ to $10^{-4}$ Torr, Thibert and Dominé derive a parametrization for the diffusion of $HNO_3$ in ice

$$D_{HNO_3} = 1.37 \times 10^{-2610/T}\ cm^2\ s^{-1} \qquad (114)$$

### 7.2.4. The Sommerfeld–Dominé Controversy

Some controversy evolved around the sectioning method as employed by Dominé and co-workers (hereafter D&C).[73,74,291,399] These experiments have been partially repeated and criticized by Sommerfeld, Knight, and Laird[389,400] (hereafter SKL). This controversy illustrates possible experimental pitfalls when uptake experiments of trace gases on ice are performed. Thus, a detailed presentation of the arguments of both groups might be useful for other researchers when planning and performing experimental work on trace gas uptake onto ice.

**The SKL Results.** Sommerfeld, Knight, and Laird[389] repeated the experimental procedure of D&C in their own setup. The authors used poly- and single-crystalline ice. Single crystals were made using a method suggested by Knight.[396] This method does not rely on the zone refinement as used by D&C. Here, water is cooled to $-1$ °C, and after

spontaneous nucleation, clear and single crystalline ice is made. Polycrystalline ice with about 5 mm large ice grains was made by nucleation of the ice with a cold aluminum sheet.

The results of SKL on $HNO_3$ are significantly different from the D&C study: (1) The amount of $HNO_3$ in the ice found by SKL was about an order of magnitude higher compared to the work of D&C. SKL claimed that the total uptake found in the $HNO_3$ experiments is consistent with the magnitude of total uptake in their previous experiments on $HNO_3$ uptake on ice. (2) The diffusion constant as derived by SKL is about 1 order of magnitude lower than the one estimated by D&C. This is a direct result of the higher observed $HNO_3$ surface concentrations. Furthermore, SKL claimed that (3) the concentration gradient in the ice is an artifact of the serial section technique and that (4) the $HNO_3$ found in the ice can be taken up onto the ice from laboratory air. The later claim was based on an experiment where an ice sheet was brought into contact with laboratory air for 1 h. SKL posed the question whether such contamination effects could be present in any laboratory.

**Fundamental Differences.** SKL acknowledge that contaminations might have affected also their results. However, SKL argue that two independent observations remain striking. First, SKL do not observe a difference of the diffusion constant between poly- and single-crystalline samples. Second, when changing the time scale of the experiment from 73 to 1032 h, SKL observed no changes of the $HNO_3$ concentration profile. Because the diffusion depth should increase with time, SKL concluded that the observed concentration profile cannot be caused by diffusion and suspected that contamination during the sectioning might severely affect the observed concentration profiles. SKL suggested that D&C should measure concentration profiles with different time scales to verify that their work is contamination-free.

**Influence of the Ice Humidification.** Another fundamental difference between the two studies is that D&C aim at ice in equilibrium with the gas phase, while SKL allowed the ice to slowly evaporate. In the SKL experiments, the originally flat surface changed into a slightly curved interface. D&C claimed that this might alter the result for the diffusion constant by up to a factor of 10.

**Contamination When the Ice Is Cut.** SKL also suspected that contaminations could occur during the sectioning. SKL used a microtome to slice the ice into 5 $\mu$m thick slices. To avoid contamination of the microtome, it was wiped with a Kimwipe after each cutting. In a comment, D&C[399] suggested that the Kimwipe could contain traces of $HNO_3$. To avoid such contaminations of the cutting tool, D&C used a stream of pure $N_2$, which is $HNO_3$ free. Furthermore, the microtome might be warmed when it is wiped, and ice particles might melt, which could corrode the microtome blade and effectively lead to contamination. Furthermore, D&C pointed out that they used thicker slices (25 $\mu$m) than SKL (5 $\mu$m), which reduces the risk of contamination. Finally, D&C pointed out that the microtome blade puts much more metal into contact with the ice (up to 8 cm length) compared to a lathe (3 mm), which reduces the risk of contamination.

**Contamination by Laboratory Air.** SKL had argued that laboratory air might contain enough $HNO_3$ to lead to severe contamination of the ice. D&C claimed that they had measured the $HNO_3$ contamination in the laboratory using a denuder technique with $HNO_3$ contaminations around 10 ppt. This is 3 orders of magnitude lower than the $HNO_3$ concentrations used in the actual uptake experiments. D&C pointed out that they had used different rooms for the different steps and that the $HNO_3$ source was in a different wing of the building. Furthermore, D&C noted that in their experiments a stainless steel chamber was used, while SKL used a plastic chamber made of ECTFE with a Teflon lid, and D&C suspected that ambient $HNO_3$ might have diffused through the plastic walls.

**Contamination of the First Slice.** The high amount of uptake in the first slice at the surface posed another severe discrepancy between the studies. D&C suggested a possible experimental pitfall, because the SKL sectioning method provides slices that could be more sensitive to contaminations either by laboratory air or by the microtome blade. Cutting the first slice might have "cleaned" the microtome blade, which leads to lower contaminations when cutting the next sections. However, SKL argued that no high uptake was observed when a blank sample was cut; thus the high uptake could be due to contamination effects.

Furthermore, D&C pointed out that in the SKL experiments the concentrations of the first slice are higher than the solubility limit as determined by D&C and suspected that the $HNO_3$ partial pressures are higher than thought and that the SKL experiments were performed in the ice melting regime. In turn, on the basis of previous work with $HNO_3$ uptake in packed ice beds,[262] SKL stated to have used $HNO_3$ partial pressures in the ice stability domain and suspected that the $HNO_3$ partial pressure used by D&C were lower than thought.

**Open Questions.** The controversy illustrates the experimental difficulties when the diffusivity and solubility of acidic gases on ice are measured. Because very low total amounts have to be detected, contaminations of any kind may pose severe problems to experimental work. To date, no further studies have been published that address these experimental problems explicitly, and the controversy remains somewhat unresolved. However, some general conclusions can be drawn for future experiments with ice. SKL have demonstrated that contaminations may severely hamper experimental work. Clearly, SKL's arguments are weakened by the presence of contaminations in their own experiments, as the authors clearly admit. On the other hand, SKL's argument that their observed diffusion depth is independent from the overall time scale of the experiment may deserve to be tested again to confirm that the interpretation of the surface peaks in terms of diffusion is correct.

## 7.3. Discussion

Data for the diffusion of acidic gases in ice are mainly available for HCl. The data scatter widely and range from values as low as $5 \times 10^{-19}$ to $10^{-9}$ $m^2$ $s^{-1}$ at temperatures around 190 K. The scatter among different data sets cannot easily be resolved because diffusion is influenced by many parameters.

One important aspect is thermodynamic considerations. For HCl, very fast transport processes have been observed in experiments with HCl partial pressures high enough to melt ice. Furthermore, the diffusion is comparably fast once hydrates may form. Considering the thermodynamic aspects leads to some grouping of the data as shown in Figure 20. However, the ice morphology is also of key importance. Here grain boundaries, triple junctions, and other crystal defects

may work as shortcuts, leading to fast transport of the dissolved molecules through the ice. This has been demonstrated by Flückiger et al.,[241] who showed that HCl diffuses much faster in polycrystalline than in single crystalline ice.

We also like to point out that experiments on the diffusion of trace gases into ice are challenging experiments. First of all, very low concentrations need to be detected, because the trace gas solubility in the ice crystals is very low. Furthermore, the ice surface is highly dynamic compared to the speed of diffusion. For example, for a diffusion constant of $10^{-17}$ m$^2$ s$^{-1}$, the characteristic length of diffusion, $\Delta x = \sqrt{Dt}$ is 0.2 $\mu$m for $t = 1$ h and $\sim$1 $\mu$m for a diffusion time of 24 h. From the ice vapor pressure at 200 K, we can calculate that about 580 monolayers per second are exchanged with the gas phase. If the ice is in thermodynamic equilibrium, possibly only the upper molecular layers participate in this exchange. If only the upper monolayer is involved, this implies that the residence time of a water molecule is about 1/580 s on the ice surface.

Such a large volatility has the potential for significant movement of the ice surface position. For a 1% mismatch of the vapor pressure, the surface may move by 0.6 $\mu$m per hour (for an ice vapor pressure of 1 mTorr and for $\alpha_c = 1$), which is on the order of the diffusion depth for a diffusion constant of $10^{-17}$ m$^2$ s$^{-1}$. If this movement is larger than the diffusion depth during experimental time scales, this has to be accounted for when the diffusive uptake into ice is modeled. Thus, to measure the diffusion constant of a gaseous species, the humidity in the gas phase must be adjusted precisely to the ice vapor pressure.

## 8. Data 2: Total Uptake of Different Trace Gases

During the last 20 years, many authors measured the uptake of acidic trace gases on ice using different techniques and different ice morphologies. Despite long-lasting intense research efforts, quantifications of the total uptake on ice scatter widely. The reason for this—though related to the morphology of the ice in the particular investigation—remains largely unexplained.

The experimental results of uptake processes of inorganic acids and organic substances have been reviewed recently by Abbatt.[234] In extension to his review, we will also correlate the available data to explore the reasons for scatter and differences between different studies.

**What Meaning Has the Term "Uptake"?** For comparison of available studies, it is necessary to discuss what the term "uptake" means. Uptake may be given as amount per surface area, where the surface area may refer to the geometric surface area, or to the internal surface area of a porous ice film. In some studies, uptake is given as the amount per ice volume. The way the uptake is given reflects the interpretation of the uptake process, that is, whether the uptake is considered as an adsorption process onto the ice surface itself or as a dissolution process of the trace gas into the ice bulk. In general, no distinction is made between different reservoirs for the uptake of the trace gas, such as the surface itself, the near-surface region, grain boundaries, or triple junctions. Thus, unless otherwise noted, the term uptake refers to the total amount of trace gas transferred from the gas phase to ice, as it is reported in a specific study. This may be the uptake per ice mass, volume, or surface area, as specified. In the literature, the term coverage is used to denote the coverage of the available sites on the surface itself. The net uptake, including bulk and surface contributions is denoted as equivalent coverage, $\theta_{equi}$, which refers to $\theta = 1$ for the uptake of $10^{15}$ molecules cm$^{-2}$, which we define as a formal monolayer.

### 8.1. The Porosity of Vapor Deposited Ice Films

Uptake experiments have been performed on different types of ice. In flow tube experiments, often vapor deposited ice has been used. Before correlating the available data for trace gas uptake, we discuss the nature of vapor deposited ice films. Using environmental scanning electron microscopy (ESEM), Keyser et al.[25] and Leu et al.[79] demonstrated that vapor deposited ice films are not flat and smooth films but rather are highly porous and consist of many micrometer-sized ice crystals. Figure 21 shows an ESEM micrograph of vapor deposited ice. The pictures demonstrate the inhomogeneity of the ice film and that the physical surface area may be larger than the geometric surface area.

**BET Measurements on Vapor Deposited Ice.** The internal surface area density of porous substances can be determined by the BET method. In short, the adsorption isotherm is measured for an inert gas, such as nitrogen, argon,

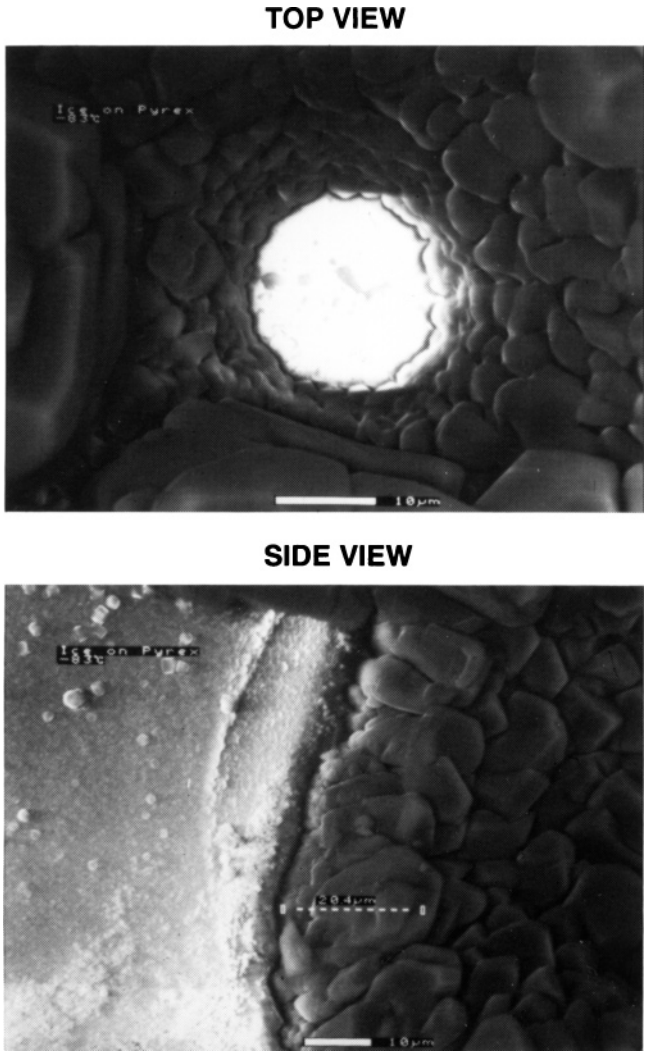


**Figure 21.** ESEM picture of vapor deposited ice taken from Leu et al.[79] Upper panel: ice which was deposited on borosilicate glass. In the middle hole, an ice granule was removed to show the underlying structure. Lower panel: side view of the ice film. The ice film consists of many ice grains. (Reprinted with permission from ref 79. Copyright 1997 American Chemical Society.)

**Table 4. Specific Surface Areas of Vapor Deposited Ice Films as Determined by Different Authors[a]**

| author | $T_{growth}$ (K) | $T_{anneal}$ (K) | gas | $d$ ($\mu$m) | $a_i$ ($m^2$ $g^{-1}$) |
|---|---|---|---|---|---|
| Adamson et al.[401] | 77 | na | $N_2$ | | 2−12[b] |
| Leu et al.[79] | 77 | na | Kr | 1−50 | 250−400 |
| Adamson et al.[401] | 77 | ≈200 | $N_2$ | | 0.2−2 |
| Leu et al.[79] | 196 | na | Kr | | 0.2−2 |
| Keyser and Leu[25] | ∼200 | 180−260 | | 1−20 | 0.2−1 |
| Keyser and Leu[25] | ∼200 | na | | | < 10 |
| Henson et al.[21] | 85 | 190−260 | Ar | 1000[d] | 8−100[c] |

[a] Abbreviations: $a_i$, specific surface area, as determined from BET measurements; $d$, film thickness; $T_{growth}$, deposition temperature; $T_{anneal}$, annealing temperature; gas, gas that was used to measures the BET isotherm; na, not annealed. [b] The authors note poor reproducibility of results. [c] The authors give a range but claim good reproducibility for equal deposition conditions. [d] Calculated from a 50 $cm^2$ sample size and 1 g of deposited water.

krypton, or methane as function of the pressure close to the condensation point of the gas, where multilayer adsorption occurs. Using the BET isotherm,[154,188,216] one may determine the total surface area.

BET measurements on vapor deposited ice surfaces have been performed by several authors,[21,25,79,401] as summarized in Table 4. Clearly, ice that has been deposited at low temperatures may be characterized by large surface area densities. Absolute numbers vary, with some indication that lower deposition temperatures can cause larger surface areas while annealing decreases the surface area. Furthermore, limited reproducibility of absolute numbers[401] for different samples grown at liquid nitrogen temperatures was reported. Performing the BET measurements on ice is a difficult task in itself, because the equilibration between the gas and the porous ice is slow. In addition, it has been argued that best results will be achieved using methane for measuring the specific surface area on ice.[270]

Some consistency between studies of different authors arises when the BET isotherm on vapor deposited ice that was annealed at temperatures around 200 K is considered. Adamson et al.[401] found that the specific surface area of such ice decreases by about an order of magnitude, to values ranging from 0.2 to 2 $m^2$ $g^{-1}$, after the ice is annealed at temperatures between −70 and −80 °C. This result is in reasonable agreement with the result from Leu et al.[79] and Keyser et al.[25] but not with the work of Henson et al.,[21] who report much larger ice surface areas, even after annealing. One might speculate that the comparably large film thickness in the Henson work may have some impact on the size of the internal surface area.

The BET measurements impressively show that vapor deposited films are highly porous with internal surface areas one or more orders of magnitude larger than the geometric surface area. As the comparison of the Leu et al.[79] and the Keyser et al.[25] with the Henson data shows, the morphology may strongly depend on the experimental protocol used, which makes direct comparison of different studies difficult.

### *8.1.1. The Hanson-Keyser controversy*

The influence of the ice porosity on the interaction between trace gases and ice is subject to scientific controversy between Keyser et al.[24−27](hereafter KLM) and Hanson and Ravishankara (hereafter H&R).[28,29] H&R[28] investigated the heterogeneous reactions $ClONO_2 + H_2O \rightarrow HNO_3 + HOCl$ and $N_2O_5 + H_2O \rightarrow 2HNO_3$. They found the reaction rate to be independent of film thickness when the film thickness

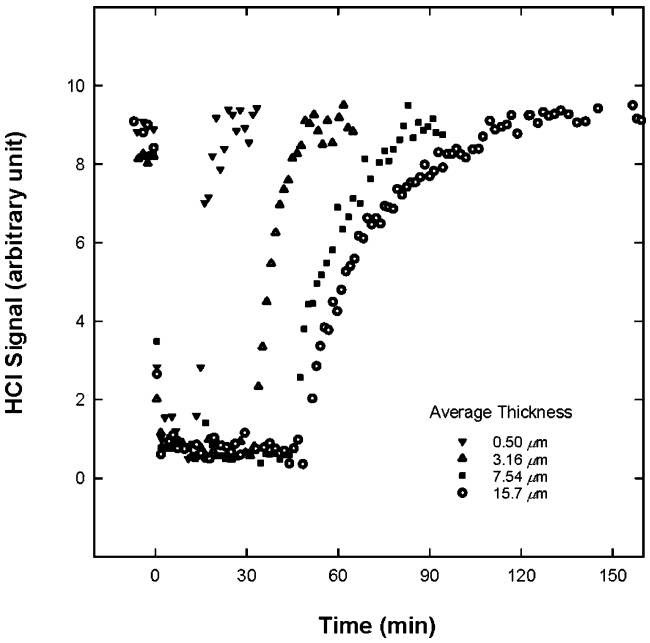


**Figure 22.** Variation of the flow tube signal with changing of the film thickness for an HCl uptake experiment at 188 K and 2.1 × $10^{-7}$ Torr. (Reprinted with permission from ref 252. Copyright 1993 American Chemical Society.)

was varied from 1 to 100 $\mu$m. They concluded that the porosity of the ice would not influence the measured reaction rates and found that the porosity model as proposed by Keyser et al.[24] would not be applicable.

This view has been criticized in a comment by Keyser et al.,[26] who pointed out that the independence of reactive uptake of the film thickness was not a sufficient proof of the nonporosity of the ice film. They argued that there was microscopic evidence of increasing ice granules increasing with film thickness. Including this effect into their porosity model, KLM showed that the observed reaction rate would be independent of the film thickness, as observed by H&R. On the basis of this, KLM argued that an analysis based on the geometric surface area would overestimate the reaction rates.

With further data analysis, H&R[29] corroborated the independence of reactive uptake for a wider range of film thicknesses between 0.2 and 5 $\mu$m. First H&R reported that the total uptake per surface area of HCl was independent of the film thickness between 0.2 and 30 $\mu$m for a partial pressure of HCl of $\sim 10^{-7}$ Torr. Second, when NAT was formed from gaseous $HNO_3$ on both ice and frozen sulfuric acid, about $5 \times 10^{14}$ $HNO_3$ molecules $cm^{-2}$ were needed for surface saturation, which would correspond to a monolayer coverage. H&R argued that equal porosity is unlikely on different substrates, and thus the monolayer uptake would constitute a measurement of the ice surface area. Therefore, they concluded that the geometric surface area is the appropriate choice for the ice in their experiments and suggested that the porosity of the vapor deposited ice might differ between the different studies.

To date, it is still difficult to resolve this controversy. For the uptake of HCl onto vapor deposited ice films, there is compelling evidence that the HCl uptake increases with the ice thickness (see section 8.4.1). Also, the tailing of the breakthrough curves in flow tubes increases with film thickness as shown in Figure 22, which indicates enhanced uptake capacity for thicker films and thus the possible

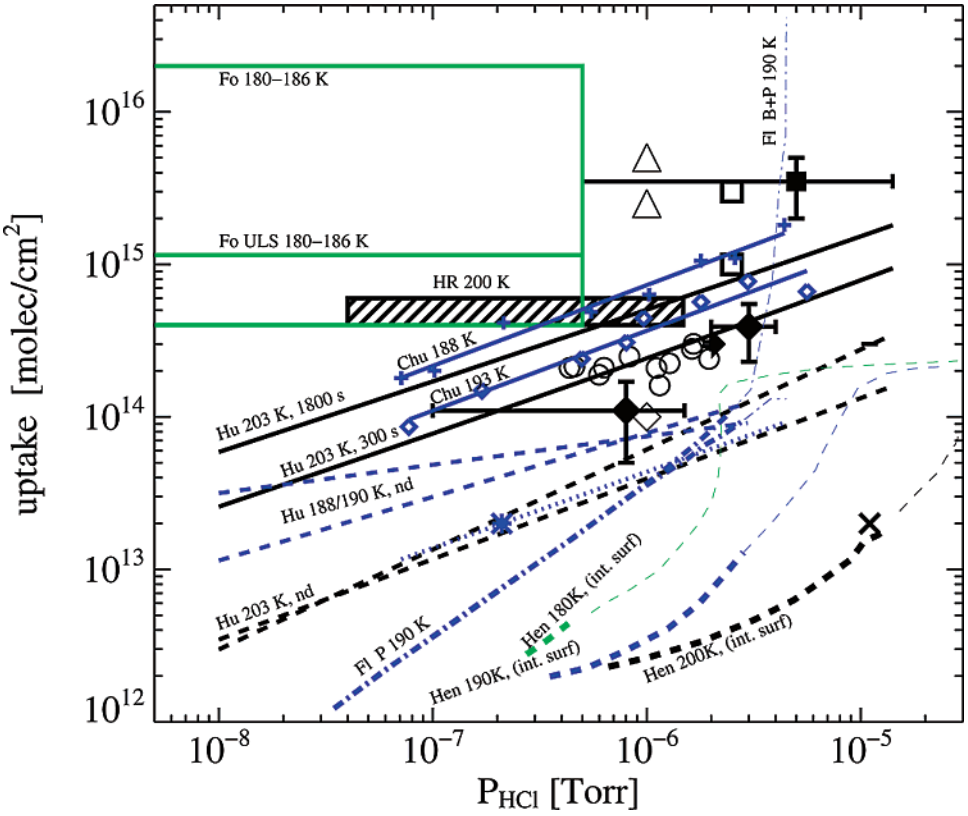


**Figure 23.** HCl uptake per geometric surface area (expressed in molecules per $cm^2$) on ice, as measured by various authors. Colors: black, 200 K; blue, 190 K; green, 180 K; solid lines refer to the reported total uptake per geometric surface area; dashed and dotted lines refer to processed data, such as normalization of the internal surface area, estimates based on asymptotic fitting or numerical modeling of the uptake kinetics. Green rectangle, Foster et al.;[135] solid line labeled Fo ULS Foster et al.[135] upper limit for smooth films; hatched rectangle labeled "HR 200 K", Hanson and Ravishankara;[28] lines labeled Hu 203 K, 1800s and Hu 203 K, 300s, parametrizations for total uptake on porous ice for total time scales of 1800 s or 300 s, respectively;[214] note that this parametrization exhibits only little temperature dependence and is valid for 190 and 203 K; dashed lines labeled Hu 188/190 nd and Hu 203 nd, nondiffusive uptake as derived from asymptotic fitting or numerical modeling;[214] blue crosses and diamonds, raw data from Chu et al.[252] at 188 and 193 K, respectively; solid lines labeled Chu 188 K and Chu 193 K are fits, showing the proportionality $\theta \propto p^{1/2}$ to the data from Chu et al.[252] for 188 and 190 K, respectively; dashed lines labeled Hen 200K, Hen 190K, and Hen 180K, adsorption isotherms at 200, 190, and 180 K, respectively, taken from Henson et al.;[21] thick lines are in the ice stability domain, and thin continuations are in the hydrate stability domain; dashed−dotted line labeled FL P 190 K, uptake (precursor only), as calculated with the kinetic model by Flückiger et al.;[217] the thin continuation to high pressure is in the hexahydrate stability domain; dashed−dotted line labeled FL P+B 190 K, uptake precursor and bulk uptake, as calculated with the kinetic model by Flückiger et al.;[217] note that a strong rise of total uptake occurs in the hexahydrate stability domain; open triangle, Huthwelker et al.[296] RBS on polycrystalline bulk ice, with integrated uptake within the first 0.75 $\mu$m for experimental durations of 2.6 and 6.9 h; filled solid square, Barone et al.;[22] open square, Abbatt et al.[83] for exposure times of ~300 and ~2100 s on vapor deposited ice films; open dots, Hynes et al.[213] data on smooth ice films; filled diamond with error bars, Lee et al.[405] smooth ice films; filled triangle pointing to the right, Lee et al.[405] rough ice films; cross, Lee et al.[405] lower limit for uptake on single crystalline airborne ice particles (~210 K); open diamond, Marti and Mauersberger[275] data from $HCl/HNO_3$ coabsorption in the low $HNO_3$ limit; blue asterisk, derived from Chu's total uptake data using the internal surface area of a porous ice film;[252] the blue dotted line is fixed on Chu's data point at 180 K assuming a $p^{1/2}$ pressure dependence, as observed in the total uptake measured by Chu. For a detailed description, see the text and Table 5.

influence of the porosity on uptake processes. Increasing uptake of HBr on ice under conditions of hydrate formation has also been shown by other authors.[171,402] In contrast, the H&R data do not show any thickness dependence. We will discuss these observations in more detail in section 8.4.4.

## 8.2. HF

Data on HF uptake on ice are scarce. Early studies have shown that HF diffuses readily through ice.[403] Hanson and Ravishankara[404] have performed flow tube experiments to study the uptake per surface area of HF onto ice. The HF partial pressure in the experiment was below $3 \times 10^{-4}$ Torr. Because this pressure is below the estimated HF vapor pressures of an aqueous $HF/H_2O$ solution at the experimental temperature, the authors argued that no HF hydrates have formed in the experiments. An upper limit of 0.05 monolayers of HF on the ice surface has been estimated, which corresponds to an upper limit for the adsorption constant of $3 \times 10^3$ $atm^{-1}$. Assuming a linear dependence of the HF uptake with the HF partial pressure, the authors estimate a surface coverage of less than $10^{-6}$ monolayer on stratospheric ice.

## 8.3. HCl Uptake on Ice: 1. Description of Experimental Studies

The uptake of HCl on ice at temperatures between 180 and 230 K has been measured by numerous authors[21,22,28,35,78,83,135,213,214,232,241,250,252,275,296,314,405,406] using different techniques, mainly flow tubes and Knudsen cells. The reported data for the uptake per surface area of all studies are summarized in Figure 23. Obviously the reported data scatter by several orders of magnitude. To find reasons for

the scatter and to establish some consistency, we will first describe how each individual study has been performed. In section 8.4, we will correlate the available data sets.

### 8.3.1. Measurements of HCl Uptake in Flow Tubes and Knudsen Cells

Based on the low partition coefficient for HCl, the uptake of HCl into ice was considered irrelevant in the atmosphere.[138,136,167,228] This assumption was based on measurements at rather high temperatures, close to the melting point of ice. The first low-temperature data were published in a pioneering work by Molina et al.,[232] who studied the uptake of HCl and $HNO_3$ on ice using an ice coated flow tube reactor and also on macroscopic ice samples. Surprisingly, the authors found a rather high partition coefficient of about 0.3 at low temperatures and fast diffusivity of $10^{-5}$ cm$^2$ s$^{-1}$ at a temperature of 185 K. These results pointed toward the importance of halogen compounds in stratospheric chemistry, especially relevant for conditions during the formation of the spring-time ozone hole. Hence, a series of further studies were made to investigate the HCl−ice interaction. Later it became clear that such high uptake could only be explained in terms of a major change in the ice, namely, the melting of the ice, corresponding to HCl vapor pressures, which cannot be normally reached in the atmosphere.

**Partial Pressure Dependence.** A series of studies aimed to explore the pressure dependence of the HCl uptake on ice, using various approaches to this question. Hanson and Mauersberger[35] investigated the uptake per surface area of HCl onto ice and NAT (nitric acid trihydrate). The authors deposited HCl doped ice films from a mixture of HCl and water vapor on a cold glass surface. Alternatively, the ice was deposited first and the gaseous HCl added in a second step. Using mass spectroscopy, they measured the substrate vapor pressure (HCl and $H_2O$). Afterward, the substrate was evaporated, and the solid-phase composition was inferred by analysis of the evaporation products. The authors noted that care had to be taken to establish equilibrium due to long equilibration times. By this procedure, both the solid- and gas-phase composition, and thus the HCl uptake on ice and NAT, was measured as function of the HCl partial pressure. The uptake on NAT follows the proportionality $p_{HCl} \propto x_{HCl}^2$ as expected for a dissociating gas. However, for HCl uptake on ice, the proportionality $p_{HCl} \propto x_{HCl}$ was found, and the authors concluded that HCl acts as strong electrolyte only on NAT but not on ice. At temperatures around 200 K, HCl mixing ratios of 1−0.1% have been found in the ice, a result distinctively lower in comparison with the Molina study but still much higher than that suggested from the partition coefficient data in previous studies.

Two years later, Hanson and Mauersberger revisited the issue of the HCl/ice interaction[249] with an improved setup. They noted that a partition coefficient of 0.3 as suggested by the Molina group should lead to a HCl concentration in the ice of up to 4 mol %. Such high HCl concentrations should lower the water vapor pressure above ice according to Raoult's law (cf. eq 8). Because no change of the ice vapor pressure was found, the authors concluded that only very little HCl can be taken up into the ice matrix itself. Furthermore, Hanson and Mauersberger discussed possible experimental pitfalls, such as HCl adsorption on glass surfaces and the difficulty to reach thermodynamic equilibrium in the experiment, which, as we will discuss below, might still be an issue of key importance during performance of uptake experiments of acidic gases on ice. Interestingly, after taking these pitfalls into account, Hanson and Mauersberger argued that the observed pressure dependence of $p \propto x$, as observed in their earlier work, did not represent the HCl uptake on ice but was rather influenced by the presence of the glass walls. This demonstrates the challenges in investigation of the uptake of HCl on ice.

Chu et al.[252] studied the uptake of HCl on vapor deposited ice in a flow tube experiment (see Figure 12) at temperatures of 188 and 193 K. The HCl partial pressure was varied from about $8 \times 10^{-8}$ to $4 \times 10^{-6}$ Torr. In this study, for the first time, a clear $\theta_{HCl} \propto p^{1/2}$ dependence of the overall HCl uptake with the HCl partial pressure was found, indicative of dissociation of HCl upon adsorption.

The HCl uptake on vapor deposited ice films was studied in a Knudsen cell by Huthwelker et al.[214] with special emphasis on the tailing often observed in uptake experiments of acidic gases on ice. For equal experimental time scales, the total uptake follows a clear $\propto p^{-1/2}$ dependence. Furthermore, using the asymptotic fitting method, the authors tried to distinguish bulk and surface processes and showed the dependence $H_d\sqrt{D} \propto p^{-1/2}$ for the tailing of the signal.

Using a low-pressure cell and second harmonic generation, Henson et al.[21] studied the uptake of HCl on porous ice. The ice samples were vapor deposited with large, well controlled total surface areas (8 m$^2$ and larger). The specific surface area of the vapor deposited ice was measured by a BET measurement using argon (see Table 4). The experimental approach taken in this study differs from the usual Knudsen cell setup, because the cell did not have a plunger to cover the ice surface. The specific characteristic of this experiment is that due to the very large ice surface area and the very slow pumping speed, essentially all HCl that is introduced into the cell is taken up by the ice before leaving the reaction chamber. Thus the HCl vapor pressure above the ice sample will be governed completely by the absorbed and adsorbed HCl on the ice surface. The adsorption isotherm can then be measured directly by measuring the HCl vapor pressure for a given amount of HCl brought into the cell. This procedure assumes that the HCl has been evenly adsorbed throughout the whole porous film, that is, that there is no enhanced concentration of HCl in the upper layers of the ice films, for example, by the slow chromatography of the highly sticky HCl into the porous ice film.

**Other Measurements of the Total Uptake.** Abbatt et al.[407] used various techniques, such as FTIR spectroscopy, electric conductivity measurements, and a flow tube. High uptake was observed for HCl pressures high enough to melt the ice. The uptake of HCl on vapor deposited ice was investigated at a temperature of 201 K, and an HCl partial pressure of about $10^{-6}$ Torr. In a flow tube experiment, Hynes et al.[213] measured the uptake of HCl on ice. Sokolov et al.[406] studied the uptake of HCl and $HNO_3$ in the presence of organic compounds and $HNO_3$.

In contrast to most previous studies, Hynes et al.[213] used smooth ice, which was made applying a method suggested by Abbatt.[407] In this study, both the temperature and pressure dependence of the uptake was studied. The total HCl uptake was calculated from the breakthrough curve using the two-third criterion (see section 5.2) as introduced by Abbatt.[42] For a temperature of 205 K, the HCl uptake data were analyzed using the adsorption isotherm (eq 58), which assumes that the HCl adsorption depends on the HCl partial pressure. They found good coincidence between the adsorp-

tion isotherm and the data. However, because most data are taken in the saturation regime of the isotherm, the experimental data exhibit only a very weak dependence on the HCl partial pressure. Furthermore, the observed coverage slightly decreased when the temperature was increased for a constant HCl partial pressure of $1.1 \times 10^{-6}$ Torr.

Barone et al.[22] used a Knudsen cell with IR spectroscopy to investigate the interaction of HCl, HBr, and HI with ice at temperatures between 100 and 230 K. Optically polished aluminum was used as substrate holder. Very thin ice films of 10 nm thickness were made by vapor deposition onto the temperature-controlled substrate holder. The total integrated uptake at 202 K was estimated as $3.5 \times 10^{15}$ molecules $cm^{-2}$.

Marti and Mauersberger[275] studied the uptake of HCl into $HNO_3$ doped ice using an experimental setup similar to the one used by Hanson and Mauersberger.[35,249] The $HNO_3$ content was varied from $10^{-5}$ to 2 mol %. The main finding of this study is that the HCl uptake on ice increases with the amount of $HNO_3$ in the ice. From this study, a HCl mixing ratio of 0.002 to 0.004 mol % for a $HNO_3$ content of $10^{-3}$ mol % was determined. Again, as in previous studies, the difficulties to achieve equilibrium were noted and investigated: variation of the exposure time between 30 s and 3 h caused about a factor 3 difference in the amount of HCl dissolved into the vapor deposited ice. Furthermore, a pressure dependence of the mixing ratio $x$ and HCl partial pressure of $p \propto x^{-2.5}$ was suggested.

**Irreversibility of Uptake.** Hanson and Ravishankara[28] used a flow tube to determine the uptake of HCl on vapor deposited ice at 201 K with HCl partial pressures ranging from $4 \times 10^{-8}$ to $1.4 \times 10^{-6}$ Torr HCl. The authors performed subsequent adsorption/desorption cycles, using a three step procedure. First, the injector was kept downstream behind the ice substrate to establish a zero signal for the HCl. Then, the injector was pulled upstream to observe the HCl uptake onto the ice. After saturation, the injector was pushed downstream to its initial position to observe the desorption of HCl from the ice. Interestingly, the amount of desorbed HCl was less than the initial overall uptake. The authors concluded that some of the HCl is irreversibly adsorbed and speculated that the HCl might alter the ice surface. On the basis of a diffusion constant of $D \approx 10^{-11}$ $cm^2$ $s^{-1}$ and a solubility limit of 20 ppm,[249] the authors excluded diffusion of HCl into the ice. No pressure dependence of the HCl uptake per surface area was observed, and the authors noted that the total time of the uptake process changed when the partial pressure was changed.

Similarly, Hynes et al.[213] performed adsorption/desorption cycles. They found that only about 43% of the HCl desorbed back into the gas phase. This confirms a previous finding of Hanson and Ravishankara[28] that some of the HCl is taken up by the ice irreversibly.

**Impact of Roughness, Pores, and Film Thickness.** In addition, the film thickness was varied to investigate the relation between film thickness and HCl uptake. Figure 22 shows the HCl partial pressure in the flow tube during an uptake experiment for films of different thickness. Obviously, the tailing of the signal is more pronounced for thicker ice films, indicating increasing dispersion with increasing thickness.

The authors analyzed the thickness dependence of the HCl uptake for 188 K using the model of Keyser et al.[24,26] for porous ice. The model assumes that the overall uptake capacity is proportional to the physical surface area. On the basis of the model and previous estimates of the ice surface area of vapor deposited ice films using BET measurements,[25,27] the authors derived the internal surface area of their ice films, which may exceed the geometric one by a factor of 25. Thus, assuming that the porous ice film is completely saturated, the uptake per physical ice surface area might be a factor of 25 lower than the uptake related to the geometric surface area.

Foster et al.[135] investigated the HCl uptake and hydrate formation at temperatures ranging from 140 to 186 K with HCl partial pressures ranging from $1 \times 10^{-9}$ to $1 \times 10^{-6}$ Torr using laser-induced thermal desorption spectroscopy (LITD). The HCl uptake was found to be independent of the ice temperature and the HCl partial pressure. It is noteworthy that the authors found increasing total uptake with increasing ice preparation time, which included the time needed for vapor deposition, annealing, and equilibration with the vapor phase. To explain this effect, Foster et al.[135] suggested that the ice surface might become rougher with time, thus providing more surface area for adsorption.

For ice films prepared at temperatures between 180 and 186 K, a total HCl uptake of $(7.2 \pm 1.6) \times 10^{15}$ molecules $cm^{-2}$ was found for pressures of $1 \times 10^{-9}$ to $10^{-6}$ Torr. The error range was attributed to shot-to-shot variation of the laser pulse. For the smoothest ice films, that is, for the experiments with shortest ice preparation times, a total uptake of about $1.15 \times 10^{15}$ molecules $cm^{-2}$ was found, in agreement with other studies.

Leu et al.[79] studied the HCl uptake on vapor deposited ice films at 196 K and a HCl partial pressure of $5 \times 10^{-7}$ Torr using a flow tube setup. The main finding of this study is that the total amount of HCl taken up onto ice increases linearly with the amount of deposited ice.

**Experiments with Very Short Time Scale.** Rossi and co-workers[78,241,247,398] used very short HCl gas pulses to probe the HCl/ice interaction using a wide range of HCl partial pressures. Because these experiments last only a few milliseconds, they are highly surface-sensitive. Flückiger and Rossi[217] used a precursor model to simulate the uptake kinetics of short HCl pulses taken up by ice in a Knudsen cell. Conceptually, their model is equal to the one described by eqs 59 and 60, the only difference being that now two precursor states are involved for the general case. By fitting the model to pulses made under various experimental conditions, they derived kinetic parameters to describe the surface kinetics of the HCl uptake on ice. The HCl uptake derived from the model was found in reasonable agreement with the measured HCl uptake on ice, which was determined by integrating the initial, 10 s long period of a breakthrough curve. For measurements at 190 K, the HCl uptake was found to rise strongly, once the HCl partial pressure rises above $3 \times 10^{-6}$ Torr. At this HCl partial pressure, the HCl−hexahydrate, and not ice, is the thermodynamically stable phase.[174]

### *8.3.2. Measurements within the Bulk Phase and Evidence for Bulk Uptake*

In the studies discussed so far, uptake has been given either as mixing ratio of HCl in ice or as uptake per geometric or physical surface area (cf. Table 5). Thus, the data have been interpreted either as pure surface or as pure volume uptake. However, both volume and surface processes may occur simultaneously. In a series of recent studies, attempts have been made to separate bulk and surface processes, either

**Table 5. Studies of the HCl Surface Uptake on Ice in Chronological Order[a]**

| author | method | $T$ (K) | $p$ ($\times 10^{-6}$ Torr) | uptake ($\times 10^{15}$ molecules cm$^{-2}$) | exp time scale | ice type | ice thickness ($\mu$m) |
|---|---|---|---|---|---|---|---|
| Marti and Mauersberger[275] | KN | 200 | 0.1−1 | 0.1[h] | 30 s | vp | 1 |
| Abbatt et al.[83] | FT | 201 | 1−4 | 1−3 | 5−35 | vp | 5−40 |
| Hanson and Ravishankara[28] | FT | 201 | 0.04−1.5 | 0.4−0.6[e] | | vp | 3−30 |
| | | 201 | 0.2 | 0.5 | 5 | vp | |
| Chu et al.[252] | FT | 188, 193 | 0.07−4 | 0.1−0.2 | 15−90 | vp | 1.4 ± 0.2 |
| | FT | 188 | 0.21 | 0.02[b] | | vp | 0.5−15.7 |
| Chu et al.[252] | FT | 188 | not given | 0.8−11 | | vp | 3.7−34.1 |
| Foster et al.[135] | LITD | 180−186 | 0.001−0.6 | 0.4−20[c] | | vp | |
| | | | - | 1.15[d] | | | |
| Flückiger et al.[314] | KN | 190−210 | 0.5−200 | | ms to ∼40 min | vp | >0.3 |
| Barone et al.[22] | KN | 202 | 50−10000[o] | 3.5 | 30−60 | vp | 0.051 |
| Leu et al.[79] | FT | 196 | 0.5 | 0.1−1[n] | | vp | 1−45 |
| Foster et al.[135] | LITD | 180−186 | 0.001−0.5 | 0.4−20[j] | | vp | *i* |
| Foster et al.[135] | LITD | 180−186 | 0.001−0.5 | 0.4−1.15[k] | | vp | *i* |
| Lee et al.[405] | TFT | 201 | 0.15−4 | 0.1−0.4 | | s | |
| | | 201 | 2 | ∼0.3 | | vp | |
| Lee et al.[405] | TFT | ∼210 | 5−20 | >0.02[g] | | scp | 1−5 |
| Huthwelker et al.[214,250] | KN | 188−203 | 0.08−10 | 0.03−1 | <3 h | vp | 3−50 |
| Flückiger et al.[78,241] | KN | 190−210 | - | 0.4−1 | | b, vp, sc | |
| Hynes et al.[213] | FT | 205 | 0.4−2 | ∼0.2 | ∼5 min | s | |
| | | 205−230 | 1.2 | ∼0.3−0.1 | | s | |
| Sokolov and Abbatt[406] | FT | 228 | 1−4 | 0.15 | | b | |
| Flückiger et al.[217] | KN | 190 | 0.6−2.7 | 0.1−0.4 | some 10 s | b | ∞ |
| Flückiger et al.[217] | KN | 190 | 2.8−3.2[m] | 1.5−41 | some 10 s | b | ∞ |
| Huthwelker et al.[296] | RBS | 200 | 1 | 0.03−2[f] | 3−7 h | s | |
| Henson et al.[21] | KN/SHG | 180, 190, 200 | 0.5−40 | 0.001−0.1 | hours | vp | 100[l] |

[a] Abbreviations: FT, flow tube; KN, Knudsen cell; TFT, turbulent flow tube; RBS, Rutherford backscattering; vp, vapor deposited ice; s, smooth ice film, grown from distilled water; b, bulk ice grown from water; sc, single crystalline ice; scp, single crystalline airborne ice particles. [b] Data point derived using the internal surface area of the ice film. [c] Data vary with ice preparation time. [d] For smooth ice film. [e] Observed uptake varies by a factor of 2 with thickness.[25,27] [f] In upper 0.75 $\mu$m depth of bulk ice. [g] Lower limit only. [h] Derived from $HNO_3$/HCl codeposition; the data point is the limit for low $HNO_3$ content and short exposure. [i] 520 Å for experiments on HCl trihydrate, not specified for experiments on ice. [j] Range for all data. [k] $1.15 \times 10^{15}$ molecules cm$^{-2}$ is the upper limit for smooth films. [l] Calculated from 0.5 g of water spread over the sample holder of 50 cm$^2$ size. [m] These data are probably taken at HCl partial pressures in the stability domain of HCl hexahydrate as $p > 3 \times 10^{-6}$ Torr. [n] Calculation based on ice mass and thickness as given in original publication. [o] No pressure dependence reported.

by analysis of the kinetics in Knudsen cell experiments[78,241,247,250,398] or by direct investigation of the solid phase.[296]

Huthwelker et al.[296] used Rutherford backscattering to study the near-surface region of ice. In these experiments, polycrystalline ice was frozen from liquid water at temperatures around −5° C. The concentration profile in the near-surface region, that is, in the outermost micrometer, has been monitored in situ as function of time (see Figure 24). The study shows that the HCl mixing ratio rises with time and extends into a depth of at least 0.75 $\mu$m. These subsurface profiles constitute the only direct subsurface investigation to date of gas uptake into ice, which do not rely on the indirect analysis via gas-phase measurements and apart from those done off-line by slicing and analyzing the ice.

In a series of Knudsen cell studies[78,241,247,398] using both gaseous HCl (and also HBr) pulses and the dope and probe technique (see section 5.1), the occurrence of diffusive processes has been further corroborated. In short, first the ice surface is doped with gaseous HCl. Then the plunger is closed, the HCl flow is stopped, and after a certain time delay, the exposure to $ClONO_2$ starts, and the reaction $ClONO_2 + HCl \rightarrow Cl_2 + HNO_3$ occurs. Because the ice surface is consumed by both evaporation and hydrolysis reaction, $ClONO_2(g) + H_2O(s) \rightarrow HOCl(g) + H^+NO_3^-$, of the ice, the reaction product $Cl_2$ is considered as a measure of the HCl concentration profile on the ice surface itself. Thus, the $Cl_2$ burst shown in Figure 18 is interpreted as measure of the HCl concentration profile in the ice. The

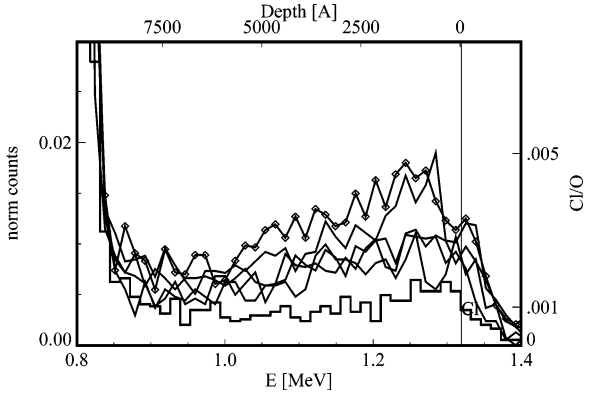


**Figure 24.** HCl diffusion profile in polycrystalline ice as a function of depth and backscattered energy for temperatures of 70 ° C and a HCl partial pressure of $10^{-6}$ Torr. The lowermost spectrum ($t$ = 0 min) shows the initial contamination of the ice due to residual HCl. Subsequent spectra are taken $t$ = 45, 166, 266, 350, and 416 min after the first spectrum. (Reprinted with permission from ref 296. Copyright 2002 American Institute of Physics.)

longer the time delay between doping and probing, the less HCl is found on the ice surface, which indicates that the HCl indeed diffuses into the depth of the ice. The dotted line in Figure 18, where the four concentration profiles cross, was interpreted as the limit of a surface layer of defined thickness. The authors argued that HCl accumulates in the near-surface region of the ice and estimated a layer range of 17−210 nm.[398]

### 8.3.3. Summary

The uptake of HCl on ice has been studied by many authors using various techniques. Clearly, HCl is readily taken up on ice, but the published data show extensive scatter as illustrated in Figure 23. When the data are interpreted, several issues are of importance. The porosity of ice films is a key parameter, because it has been shown impressively that vapor deposited ice films are highly porous and that the HCl uptake increases with film thickness. However, because the quantification of the internal surface area is difficult, estimates for the uptake per physical surface area differ widely. Furthermore, recent studies, such as the kinetic analysis of breakthrough curves[214] and the dope and probe experiments, indicate that at least some of the adsorbed HCl is taken up into the bulk of the ice.

## 8.4. HCl Uptake on Ice: 2. Data Correlation

The available data for HCl uptake on ice at temperatures between 180 and 220 K are summarized in Figure 23. Clearly, there is quite some scatter among the published data. It is important to note that the data have been measured using various techniques, under very different experimental conditions, such as experimental time scales or different types of ice. In this and the following sections, we will investigate the impact of such parameters on the overall uptake and test the consistency of the data set with models of the uptake process.

### 8.4.1. Dependence of HCl Uptake on Film Thickness

In an attempt to correlate the uptake with film thickness, Figure 25 shows the HCl uptake per geometric surface area on vapor deposited ice films as a function of the film thickness at a temperature of 200 K and for an HCl partial pressure of $10^{-6}$ Torr. For these conditions, most data are available. Calculations necessary for data comparison are described in footnote 408. The extensive scatter will be further analyzed in the following sections. First, we consider only data from a single data set (Leu et al.,[79] asterisks in Figure 25). These data show that the HCl uptake per surface area, as determined from the breakthrough curve in a flow tube, increases with film thickness, when the film thickness rises from 0.3 to 3 $\mu$m.

Rising HCl uptake with increasing film thickness has also been demonstrated for lower temperatures (188 K) and lower HCl partial pressures ($2.1 \times 10^{-7}$ Torr) by Chu.[252] However, this study cannot be compared quantitatively with the data presented in Figure 25 because temperatures and HCl partial pressure differ.

The HCl uptake has often been interpreted as surface uptake, that is, as uptake per geometric surface area. Conversely, one can also calculate the net mixing ratio

$$x_{\mathrm{HCl}} \equiv \frac{\text{moles of HCl taken up}}{\text{moles of water in the ice film}} \qquad (115)$$

in the film. This representation allows one to compare the overall uptake with various solubility limits for HCl in ice. From Figure 25, top panel, we can estimate an equivalent surface uptake of 0.1 formal monolayers as a rough estimate for the lower limit of the uptake at $10^{-6}$ Torr HCl and 200 K if we consider only studies based on the analysis of breakthrough curves in flow tubes or Knudsen cells or by co-deposition experiments.

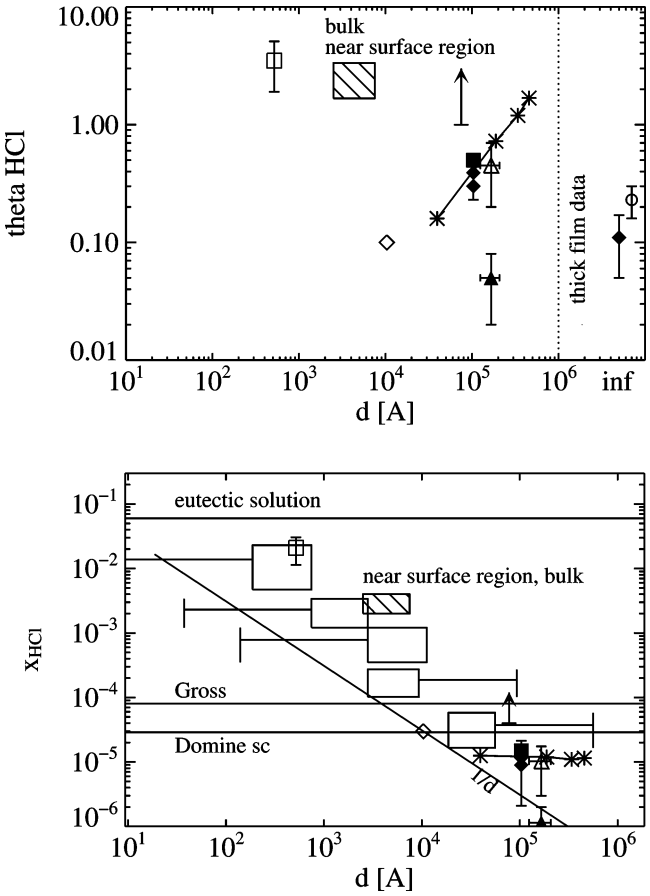


**Figure 25.** HCl uptake on ice at 200 K and $10^{-6}$ Torr. Top panel: HCl surface coverage per geometric surface area as a function of film thickness. Data points to the right of the dotted lines (for $d > 10^6$ Å) are taken on thick films, such as films frozen from liquid water. Bottom panel: Net HCl mixing ratio in ice films as a function of film thickness. Big open rectangles: Hanson and Mauersberger[249] calculated from their Figure 4, assuming an ice surface area of 1 cm$^2$ for data for the three thinnest films and 10−20 cm$^2$ for data for the two thickest films. Error bars show the full error range for full ranges of surface areas from 1 to 20 cm$^2$. Note that errors in surface area lead to rather large uncertainties in surface coverage, which makes determination of surface coverage impossible. Solid line ("Gross"): partition coefficient as measured by Gross, as cited in Hanson.[249] Solid line ("Dominé"): mixing ratio in single crystalline ice. Solid line labeled as 1/*d*: lower limit of the net mixing ratio estimated from the net uptake of $0.1 \times 10^{15}$ molecules cm$^{-2}$ for a film thickness of 3.1 Å. Symbols for both plots: open square with error bar, Barone et al.;[22] filled square, Hanson and Ravishankara;[28] asterisks, from Figure 3 in Leu et al.;[79] vertical arrow, Abbatt et al.[83] (the arrow starts at the $t = 5-10$ min experimental duration and points toward the 35 min experimental duration); open triangle, total uptake after 1800 s from Figure 7 in Huthwelker et al.;[214] filled triangle, surface uptake from Figure 7 in Huthwelker et al.;[214] open diamond, Marti and Mauersberger;[275] filled diamonds, Lee et al.;[405] open circle, Hynes et al.[213] on smooth ice; hatched square ("bulk surface"), HCl mixing ratio in the near-surface region of bulk polycrystalline ice as measured with RBS.[296]

For this lower limit, we can calculate the net mixing ratio in films of different thickness by $x_{\mathrm{HCl}} = 0.1\mathrm{ML} \times 3.1\ \text{Å}/d$, where we assume an average thickness of 3.1 Å for a monolayer of ice. This thickness can be calculated from the density of ice, see footnote 209. This representation allows quantitative comparison with the study of Hanson and Mauersberger[249] (open rectangles with error bars in Figure 25). The Hanson and Mauersberger data[249] have larger errors in our representation compared to the original work, where

the data are given in terms of total amounts of HCl and water, independent of the area of the deposited film. The conversion to an average film thickness for representation in Figure 25 requires knowledge of the ice surface area. The authors report large errors, ranging from 1 to 20 $cm^2$, which are represented by the error bars. For the rectangles in Figure 25, we have used the estimate 10−20 $cm^2$ for the two thicker films and 1 $cm^2$ for the thin film data, in accordance with the information given in the original paper.

In summary, Figure 25 does not allow one to arrive at a consistent picture concerning the HCl uptake in vapor deposited ice. First, when only the Leu data are considered, the HCl seems to be uniformly distributed over the whole deposited ice film, because $x_{HCl}$ is constant while $\theta_{HCl}$ increases. This could be interpreted in terms of an increasing internal surface area in the vapor deposited ice film, if the porosity was independent of the film thickness and the internal surface area was completely saturated.

In contrast, despite large errors, the Hanson and Mauersberger data suggest a different picture. Here, the observed mixing ratio rises with a $1/d$ law, which would be consistent with the HCl being taken up onto the geometric surface area. The Hanson and Mauersberger data are among the oldest data, where the investigations of the HCl uptake on ice were real pioneering work, and one might be tempted to disregard this study, especially because error bars are large and newer studies may have implemented newer knowledge and technology. However, results similar to the ones reported by Hanson and Mauersberger on thin films have also been reported in a recent study by Barone et al.,[22] who found HCl mixing ratios in the percent range on thin films. Interestingly, also in the near-surface region of bulk ice samples (i.e., within the first tenth of a micrometer or less), surprisingly high mixing ratios, comparable to the thin film results from Hanson and Mauersberger have been found by Rossi and co-workers[78,241,247,398] and by Huthwelker et al.[296] using RBS (see sections 5.1 and 4.4). Given this coincidence with recent studies, the Hanson and Mauerberger data should not easily be disregarded.

Thus, the overall picture remains disturbing: For films thicker than roughly a micrometer, there is a clear dependence of the HCl uptake with film thickness with constant mixing ratio independent from the film thickness, and a lower limit of 0.1 formal monolayer (per geometric surface area at $10^{-6}$ Torr HCl and 200 K) total uptake. Once films get smaller, the effective mixing ratio increases with still 0.1 formal monolayer as lower limit (at $10^{-6}$ Torr HCl and 200 K) but with surprisingly high net HCl mixing ratios in the very thin films or in the near-surface region of ice. To further explore these issues, we will first consider the magnitude of uptake and then discuss the dependence of the HCl uptake on pressure and temperature.

### 8.4.2. Magnitude of Uptake

**Uptake in Terms of Mixing Ratio.** When the magnitude of the uptake is discussed, it is instructive to compare the net mixing ratio of HCl in the ice film with the overall uptake or with estimates for the solubility in ice. In Figure 25 (bottom panel), horizontal lines mark the mixing ratio of HCl estimated in ice single crystals at 200 K and $10^{-6}$ Torr as derived from Thibert and Dominé,[73] from ice/liquid partition coefficient measurements as reported by Gross,[139] and in an aqueous HCl solution in equilibrium with ice at 200 K. Clearly, the thick film data show a net mixing ratio lower than the solubility of HCl in single crystals. Interestingly, studies on very thin ice films exhibit an overall mixing ratio that exceeds the solubility limit as estimated from the solubility in ice single crystals or from the partition coefficient data. Thus, not the bulk ice crystal, but surfaces and interfacial reservoirs, such as the ice/gas interface, grain boundaries or triple junctions, or the internal surface area (which might be very different on ultrathin ice films, compared to thicker ones) in the porous ice must play the key role for uptake processes of HCl on ice.

**Surface Uptake at 200 K and $10^{-6}$ Torr.** In contrast to the Hanson and Mauersberger[249] data, the Leu data,[79] which are measured on thicker films, show rising uptake with increasing film thickness (Figure 25, top panel). Trend and absolute value of the Leu data[79] in this study appear to be in reasonable agreement with the data measured by Lee et al.[405] (filled diamonds) and also by Hanson and Ravishankara[28] (filled square), both on vapor deposited ice films. The study by Abbatt[407] shows about a factor of 4−10 higher total HCl uptake compared to the other studies on films of comparable thickness. This study points to the difficulty of equilibration processes on vapor deposited ice films, because the total uptake increases by a factor of 3 when the total experimental time scale is increased from about 5 to 35 min. Similar observations have been reported by Huthwelker et al.[214] The overall uptake in this study coincides with the Leu data if the total time scale of the uptake process is about 1800 s (open triangle).

Interestingly, the uptake on the thinnest film as reported by Leu (asterisks), the nondiffusive uptake as derived by Huthwelker et al. using the asymptotic fitting method[214] (see section 5.1) from experiments on thick ice films (filled triangle), and the data from Marti and Mauersberger[275] (1 $\mu$m ice films, open diamond) indicate an uptake of about 0.1 formal monolayers of HCl on the geometric ice surface area. All these data points are quite close to the $1/d$ line (bottom panel in Figure 25).

Thus, on the basis of these studies,[79,214,249,275,405] one might consider the following picture of uptake processes on vapor deposited ice. The lower limit of roughly 0.1 formal monolayers per geometric surface area is observed in studies on vapor deposited ice. This result is consistent with the data on macroscopically thick, smooth ice films (data from Hynes et al.[213] and Lee et al.[405]). Only for films thicker than a micrometer thickness, the uptake rises due to the increasing porosity of the ice films. To some extent, this picture is corroborated by Hanson and Mauersberger.[249] The mixing ratio rises according to the relation $x_{HCl} \propto 1/d$, as expected if the HCl was residing on the surface of a homogeneous ice film. However, even on very thin films, the total uptake can exceed the limit of 0.1 monolayer, as observed by Barone[22] (open square with error bar), which contradicts this concept. In this specific study,[22] the ice was not grown on glass, as in all other studies. Thus, one might argue that the ice morphology is significantly different, which might have lead to a higher internal surface area compared to ice films grown on glass substrates, leading to higher apparent uptake. However, also on smooth nonporous bulk ice samples, high mixing ratios of about $10^{-4}$−$10^{-3}$ have been observed in the near-surface region of ice using RBS[296] (upper 0.75 $\mu$m) and the dope and probe technique[78,241,398] (upper some hundred nanometers). These observations indicate that the overall uptake of HCl may well exceed 0.1 formal monolayers, even on nonporous smooth ice samples.

**Surface Uptake for Other Conditions.** In the previous section, we considered studies made at 200 K and $10^{-6}$ Torr HCl only. Studies based on the analysis of breakthrough curves in flow tubes and Knudsen cells seem to indicate an uptake per geometric surface area of 0.1 formal monolayer as the lower limit. However, when larger ranges of HCl partial pressures are considered, it becomes clear that this is not the full picture. In three recent studies, much lower amounts of HCl uptake were found.

At 190 K, for HCl partial pressures from $3 \times 10^{-8}$ to $10^{-6}$ Torr, Flückiger and Rossi[217] derived a surface uptake of 0.001−0.1 formal monolayers (Figure 23), much lower than the one flow tube studies report. Furthermore, the uptake strongly rises with HCl partial pressure. This result is based on kinetic analysis of pulsed valve experiments on time scales shorter than a second. It is corroborated by the analysis of breakthrough curves for HCl. Here, for a short period of a few seconds, strong HCl uptake occurred before the HCl uptake became almost constant. The fact that in the Flückiger and Rossi[217] work only interactions on short time scales are considered may partially explain why the estimated amount of uptake is small compared to the one reported in most other studies, which last at least a few minutes or even hours. Due to the short time scales of the Flückiger and Rossi[217] work any diffusion into the ice bulk or into micropores should be of minor importance. Also, any restructuring of the ice surface should not be relevant during the short time scales of the Flückiger and Rossi[217] experiment.

Lee et al.[405] reported a lower limit of $\theta > 0.02$ at 210 K (Figure 23) for the uptake on airborne ice single crystals without giving any description of the experimental setup. Explanations for the comparably low uptake might be the single crystalline state of the ice particles but also the possibly short experimental duration in comparison to the flow tube studies.

For 200 K, Henson[21] reported a total HCl uptake as low as $\theta = 0.002-0.02$ (Figure 23). This result is by far the lowest estimate of the HCl uptake on ice. In this experiment, the uptake was measured on vapor deposited ice films of about 1 mm thickness (based on the amount of deposited water and the sample holder size). Because the uptake is given per internal surface area of the ice film, which was determined by BET measurements (Table 4), direct comparison of the Henson data with studies that report the uptake per geometric surface area is difficult. The only exception is the study by Chu et al.,[252] who used their porosity model (which is also based on BET measurements), to estimate the uptake per internal surface area. For temperature around 190 K, they arrived at about $\theta \approx 0.02$ (for $2 \times 10^{-7}$ Torr, asterisk in Figure 23), which is still about a factor of 10 higher than the Henson data. Thus, the Henson data seem to pose the lower limit of all measured data.

It is unclear why the Henson data are comparably low. For this study, the exact time scale is unknown, but it is probably long compared to the Flückiger[217] (less than a second for pulsed valve experiments and a few 10 s for breakthrough curves) and Lee[405] on experiments on airborne ice particles. As Henson et al.[21] noted problems to establish equilibrium between the gas phase and the ice film, their time scales are possibly comparable with the one in flow tube and Knudsen cell studies.

We note that the method of the Henson study is quite different from the approach used in flow tubes and Knudsen cells, as Henson did not measure a breakthrough curve but rather the vapor pressure above the ice, which has been exposed to gaseous HCl. The films are thicker compared to the micrometer thin films in other kinetic studies. We also note that the specific surface area of the ice film was given as $8-100$ m$^2$ g$^{-1}$ for ice that was deposited at 85 K and annealed at temperatures between 190 and 260 K. This is much higher than the estimate of $0.2-2$ m$^2$ g$^{-1}$, as measured by Leu[79] and Adamson[401] for ice grown under similar conditions. Thus, we speculate that there might be some unresolved systematic differences between the Henson study and the other ones. It might be that the time scales of the experiment and the way the HCl migrates through the ice films are worth considering. The authors claim that the BET experiments using argon showed that the transport into the ice film occurs within experimental time scales and concluded that there will be no transport limitation for the HCl to penetrate the ice film within the longer time scales for the equilibration of the HCl with the ice. It might be worth performing experiments with the Henson setup and systematically varying the film thickness to explore this question. Analysis as in Figure 25 will allow one to determine whether the HCl is evenly distributed over the whole ice film.

### *8.4.3. Pressure Dependence of HCl Uptake*

So far we have discussed the consistency of the available data in terms of magnitude. The pressure dependence can give further clues on the nature of the uptake process. For example, a $p^{1/2}$ dependence may indicate dissociation, while pressure independence may indicate surface saturation.

The pressure dependence of the HCl uptake has been studied by some authors.[21,213,214,217] Early estimates for the pressure dependence range from $p_{HCl} \propto x_{HCl}^2$ (ref 35) to $p_{HCl} \propto x_{HCl}^{2.5}$ (ref 275) to no pressure dependence of the HCl uptake.[28] Hanson and Mauersberger[249] argued that wall effects may have hampered some of the early results of the pioneering first studies, which posed a substantial experimental challenge.

Generally, it is difficult to determine the pressure dependence of the uptake without variation of pressure over large ranges. For justification of a $p^{-1/2}$ dependence, varying the pressure by an order of magnitude will lead to a factor of 3 change in uptake. Because the reproducibility between two experiments might be on the order of a factor of 2, it is clear that the partial pressure has to be varied over ranges large enough to override the scatter between single experiments to get reliable results. In 1993, Chu et al.[252] did such an experiment using a sophisticated flow tube setup and investigated the HCl uptake at 188 and 193 K for HCl pressures ranging from $8 \times 10^{-8}$ to $5 \times 10^{-5}$ Torr (see Figure 23). Here a clear pressure dependence $\theta_{HCl} \propto p^{1/2}$ was found over the whole pressure range.

For a temperature of 200 K, we compare the uptake per geometric surface area as function of the HCl partial pressure for all available studies in Figure 26. Open circles are taken from Hynes et al.[213] These data show a weak pressure dependence. The shaded area shows the data from Hanson and Ravishankara,[28] who found the HCl uptake independent of the HCl partial pressure. Horizontal arrows show the total uptake measured in a Knudsen cell by Huthwelker et al.[214] within an experimental duration of 300 s, which is comparable to the duration of the experiments by Hynes.[213] The data are shown as arrows. The arrow starts at a pressure $p_0$ in the cell with the plunger closed. The tip of the arrow points to the pressure in the Knudsen cell after an experimental

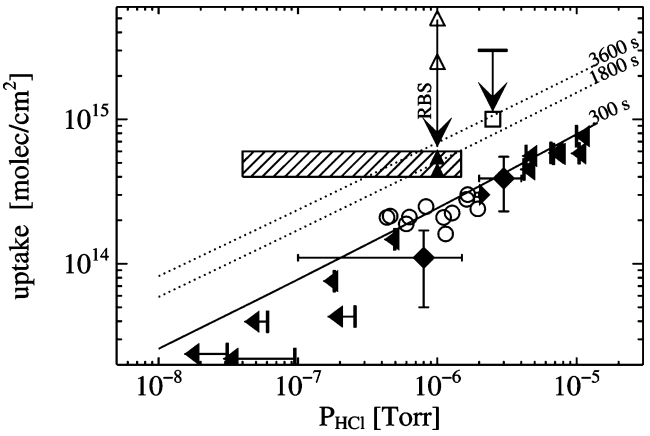


**Figure 26.** Comparison of total HCl uptake on ice at temperatures around 200 K: open dots, from Hynes et al.[213] at 205 K; hatched area, Hanson and Ravishankara;[28] diamonds, Lee et al.[405] at 201 K, average of several experiments; open square, Abbatt et al.;[83] the vertical arrow shows the correction for diffusive kinetics; the arrow starts at the original data $n(t_{exp})$, and the tip of the arrow points toward the time corrected point $n(t{=}300s) = n(t_{exp})(t_{norm}/t)^{1/2}$; open triangles, integrated amount of Cl in the near-surface region (upper 0.75 $\mu$m) of bulk ice measured with RBS for 6.9 and 2.6 h HCl exposure times; the arrow points to data corrected for diffusion-like kinetics to the time scale of 300 s (filled triangles); horizontal arrows, ref 214, total integrated uptake after 300 s; the end of the arrow marks $p_0$; the tip of the arrow marks $p_r$ after 300 s; dotted lines, parametrization for total HCl uptake, as given in ref 214 for experimental times of 1800 and 3600 s respectively; solid line, parametrization for total HCl uptake, as given in ref 214 for experimental times of 300 s. (Adapted with permission from ref 214. Copyright 2004 American Chemical Society.)

duration of 300 s, which is roughly comparable to the duration of the experiments by Hynes.[213] The data from Lee et al. are given as filled diamonds. Interestingly, after taking the total experimental time into account, these three studies coincide within a factor of 2−3 in total uptake, despite the fact that we compare experiments on smooth and vapor deposited ice.[213,214,405] This observation may indicate that under such short time scales the diffusion into the porous ice film is of less importance.

While the data from Huthwelker et al.[214] suggest a $p^{1/2}$ dependence of the total uptake, Hynes et al.[213] found a slightly weaker dependence. This was interpreted as the onset of the surface saturation of a Langmuir isotherm, and Hynes et al. derived a Langmuir constant by fitting the dissociative Langmuir adsorption isotherm, eq 58, to their data based on this assumption.

Less coincidence occurs when the data from Abbatt et al. (open square) and Hanson and Mauersberger (hatched area) are considered. The Abbatt and the Barone data are shown as arrows. The arrow starts at the original data point. The tip points toward a rescaled value using a $t^{1/2}$ law. The rescaled value was calculated by $N_{scaled} = N_{orig}(t_0/t_{exp})^{1/2}$ ($N_{scaled}$ = the rescaled value; $N_{orig}$ = the originally published data point; $t_0$ = the reference time of 300 s; $t_{exp}$ = the duration of the experiment). After rescaling, both the Barone and the Abbatt data come closer to the other data; however a factor of 3 remains as difference.

In contrast to all other studies, Hanson and Ravishankara (hatched area in Figure 26) reported the HCl uptake to be independent from HCl partial pressure. For a HCl partial pressure of $2 \times 10^{-7}$ Torr, the time scale is given as 5 min, which may allow comparison with the other data. Here, the HCl uptake is about a factor of 4 higher compared to other studies.

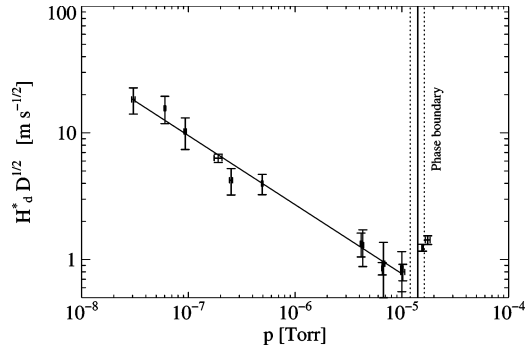


**Figure 27.** Pressure dependence of uptake kinetics on vapor deposited ice. $H_d^* D^{1/2}$, as derived from an asymptotic fitting method[214] as a function of HCl partial pressure at 203 K. The solid line marks the ice−liquid phase boundary. The dotted lines mark the uncertainty of the phase boundary due to the error in the pressure measurement. Note that the relation $H_d^* D^{1/2} \propto p^{-1/2}$ is valid over the whole range of HCl partial pressure in the ice stability domain. Once the HCl partial pressure rises to the liquid stability domain, $H_d^* D^{1/2}$ rises, which indicates enhanced uptake of HCl due to the melting of ice. (Reprinted with permission from ref 214. Copyright 2004 American Chemical Society.)

It is important to note that also stronger dependencies than $\theta \propto p^{1/2}$ have been observed, most notably in the work of Henson[21] and Flückiger,[78] as it is shown in Figure 23. In both studies, sophisticated models have been used to simulate the adsorption isotherm. The work of Flückiger is based on the analysis of pulsed valve experiments, designed to study the adsorption−desorption kinetics on time scales of seconds or less, which is very short compared to the previously mentioned studies. Thus, one may speculate that Flückiger et al. have investigated the interaction of HCl with fresh, unexposed ice. It is conceivable that HCl, which has a strong interaction with hydrogen bonds, may restructure the surface. Thus, experiments with a longer time scale will give a different answer, because with time the HCl−ice interaction may change the nature of the ice surface.

A different approach to study the pressure dependence is to investigate the kinetics of the tailing. As further described in the following section, there is a body of experimental evidence (see refs 22, 42, 83, and 214) that the tailing of the breakthrough curve has a diffusion-like kinetics. Based on experimental observation, the kinetics of the tailing can be described by eq 84, and the quantity $H_d D^{1/2}$ can be determined. For HCl uptake, it could be shown that the proportionality $H_d D^{1/2} \propto p^{-1/2}$ holds, as shown in Figure 27. This result corroborates the concept that all HCl may indeed be taken up by diffusion into a yet unknown reservoir and that the HCl dissociates upon uptake into that reservoir.

In summary, experiments on the pressure dependence give an inconclusive picture. However, except the observation that the HCl uptake rises with HCl partial pressure, there seems to be not even a convergence of the observed pressure dependence in recent work: Hynes (2001) observed only a very weak pressure dependence (but on a limited range of HCl partial pressures); Huthwelker (1999, 2004) reported $p^{1/2}$ for the total uptake and for $H_d D^{1/2}$; Flückiger et al. (2003) and also Henson et al. (2004) reported that the total uptake rises stronger than a $p^{1/2}$ law, but both groups report different pressure laws.

This is a very unfortunate situation for applications in atmospheric research. Often laboratory experiments are

performed at pressures higher than those in the atmosphere, and extrapolations are needed to assess the surface coverage under atmospheric conditions. Thus, knowledge of the correct pressure dependence is of crucial importance to derive the uptake for real atmospheric conditions. Furthermore, models for surface reactions often depend on estimates of the surface coverage to calculate reaction rates. Again, extrapolations are needed to calculate reaction rates for atmospheric conditions. These parametrizations may be doomed without knowing the correct surface coverage and the correct kinetic parameters for the trace gas/ice interaction.

### 8.4.4. Implications from the HCl Uptake Kinetics

**Experimental Observation of Tailing in Breakthrough Curves.** Abbatt[42] was the first to note that the tailing of the breakthrough curve for $HNO_3$ uptake on ice in a flow tube experiment displays similarity with the kinetics of diffusive processes and could be fitted using eq 103. Similarly, for HCl uptake on ice, long-lasting tailing of the breakthrough curve has been observed as well by several authors. Examples can be found in both flow tube (refs 22 and 407, Figure 28) and Knudsen cell studies on thick ice films (ref 214, Figure 17), but also on very thin films (~50 nm; ref 22, Figure 28). Interestingly, in the flow tube study of Chu et al.,[252] the observed tailing was less but increased with increasing film thickness (see Figure 22).

Tailing and diffusion-like kinetics poses important questions. First, what is the physical nature of the tailing, and what is the reservoir for this slow uptake process? With the nature of the tailing unexplained, the practical question arises how to analyze measured breakthrough curves and how to interpret the total observed HCl uptake. Clearly, this question can only be answered once we understand the nature of the uptake process. In the absence of a generally accepted understanding, several approaches have been taken.

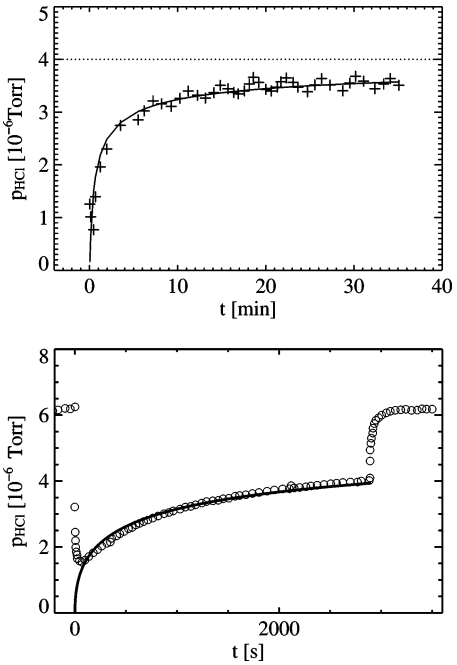


**Figure 28.** Tailing of breakthrough curves with diffusion-like kinetics during HCl uptake on ice. Bottom panel: Breakthrough curve in a Knudsen cell taken from Figure 6A in Barone et al.[22] (open circles); the HCl pressure is calculated from the total flow into the cell ($3.5 \times 10^{14}$ molecules $s^{-1}$) and $A_e = 0.17$ $cm^2$; solid line, kinetic model for diffusive kinetics in the Knudsen cell simulated with eq 83 for $H_d^* D^{1/2} = 14$ m $s^{-1/2}$. Top panel: Breakthrough curve in a flow tube taken from Figure 5 in Abbat et al.[83] (crosses); solid line, simulated breakthrough curve for diffusion-like uptake kinetics as calculated with eq 103 for $H_d^* D^{1/2} = 3.5$ m $s^{-1/2}$ assuming $A_{ice} = 90$ $cm^2$, gas speed $\upsilon = 7$ $ms^{-1}$, and ice length = 50 cm. These values are chosen such that the integrated uptake within 35 min yields $3 \times 10^{15}$ molecules $cm^{-2}$, as is stated in the original paper. For comparison, see Figure 17.

**Two-Third Criteria.** A pragmatic approach to this problem has been suggested by Abbatt[42] and is used by other authors[213] as well. The surface uptake is considered to be finished once the breakthrough curve rises to two-thirds of its initial value. This point was chosen because here a strong change in the shape of the breakthrough curve occurs. This may indicate a transition point from the dominance of the initial fast uptake on the ice surface to slower processes dominating during the tailing period.

However, if the tailing follows a diffusion-like uptake kinetics, the impact of the tailing may depend on the specific setup of the flow tube or Knudsen cell. For a pure diffusive kinetics, the time for the breakthrough curve to recover to $^2/_3$ of its final value is $t_{2/3,FT} = (xA_S H_d D^{1/2}/(\ln(^2/_3)\upsilon V\pi))^2$ in a flow tube (eq 103) and $t_{2/3,KN} = (4A_S H_d D^{1/2}/(V_c k_e))^2$ for a Knudsen cell (eq 84). In both cases, the characteristic time depends on instrument parameters, such as ice surface area $A_s$, gas velocity $\upsilon$, or escape rate $k_e$. The total uptake per surface area, $n_s$, becomes independent from instrument parameters only in the diffusive limit, where the total uptake follows the time dependence $n_s = 2n_0 H_d D^{1/2}(t/\pi)^{1/2}$ (see Figure 17). Therefore, when the total uptake is calculated by integrating the breakthrough curve to the instrument-dependent characteristic time $t_{2/3}$, the result will also depend on instrument parameters (i.e., on $A_S/(V_c k_e)$ in a Knudsen cell or $xA_S/(\upsilon V)$ in a flow tube). As a consequence, investigating the same system with different instrumentation may lead to different results, that is, the contribution of the tailing period to the measured uptake will be different in different setups. This effect has been demonstrated when experiments on $SO_2$ uptake into packed ice beds that were performed on different experimental time scales were compared.[172]

Furthermore, it must be noted that the impact of a diffusion-like $t^{1/2}$ tailing on the overall uptake can be strong compared to a tailing with exponential decay. An uptake coefficient with a kinetic law $\gamma(t) \propto t^{-1/2}$ leads to infinite total uptake $N_{tot} \propto \int_0^\infty \gamma(t')\,dt' \approx t^{1/2}$ (only prior to saturation of the reservoir). In contrast, if the tailing is governed by first-order kinetics, the tailing obeys an exponential time law, $\gamma(t) \propto e^{-\lambda t}$, and the integrated tailing leads to a finite contribution to the total uptake: $N_{tot} \propto \int_0^\infty \gamma(t')\,dt' = 1/\lambda$. Thus, on instruments with high sensitivity, the relative contribution to the overall uptake can be much higher in systems with diffusion-like kinetics compared to systems where the tailing follows a first-order kinetics. At present, this aspect of uptake kinetics is widely unexplored.

**Asymptotic Fitting.** Based on such arguments, an alternative approach was taken by Huthwelker et al.,[214,250] who analyzed the tailing of the breakthrough curve using a diffusive model. Figure 17 shows the breakthrough curve for HCl in an uptake experiment on vapor deposited ice in a Knudsen cell. The slow recovery of the signal can be fitted by the kinetic equation for diffusive uptake processes (see eq 85 for $t > 1000$ s (dotted line in Figure 17, see ref 409). From this procedure, the quantity $H_d^* D^{1/2} = (k_B T K H_d^0 D/p_0)^{-1/2}$ was derived (see also section 8.4.3).

**Table 6. Estimated Values for $H_d^* D^{1/2}$ for HCl Uptake on Ice, Calculated from Data Taken from the Literature[a]**

| author | $T$ (K) | ice type | $d$ ($\mu$m) | $p_{HCl}$ ($\times 10^{-6}$ Torr) | $H_d^*$ | $D$ ($m^2\ s^{-1}$) | $H_d^* D^{1/2}$ ($ms^{-1/2}$) |
|---|---|---|---|---|---|---|---|
| Thibert and Dominé[73] | 200 | sc | $\infty$[b] | 5 | $7.2 \times 10^6$ | $10^{-16}$ [c] | $7.2 \times 10^{-2}$ |
| Thibert and Dominé[73] | 200 | sc | $\infty$[b] | 5 | $7.2 \times 10^6$ | $4 \times 10^{-18}$ [d] | $4.5 \times 10^{-3}$ |
| Abbatt et al.[83] | 200 | vp | 35 | 4 | | | 3.5[e] |
| Barone et al.[22] | 200 | vp | 0.051 | 6 | | | 14[f] |
| Huthwelker et al.[214] | 200 | vp | 3−50 | 5 | | | 4[g] |
| HCl in water | 200 | liq water | | 1 | $5.5 \times 10^{10}$ [h] | $1.6 \times 10^{-12}$ [i] | $7 \times 10^4$ |

[a] Key to columns: $T$, temperature; $d$, ice thickness. Ice types: sc, single crystalline ice (note that different methods were used to grow single crystals in refs 73 and 78, 241); vp, vapor deposited ice; bulk, polycrystalline ice, grown from liquid water. $p_{HCl}$, HCl partial pressure in the Knudsen cell; $H_d^*$, dimensionless Henry's Law constant; $D$, diffusion constant. [b] From diffusion into the upper 20 $\mu$m, by slicing the ice. [c] Calculated from HCl solubility and diffusion constant as given in Thibert and Dominé.[73] [d] Calculated from HCl solubility as given by Thibert and Dominé,[73] with single-crystal diffusion constant at 190 K taken from Flückiger.[241] [e] Calculated from Figure 5 in Abbatt et al.,[83] see Figure 28. [f] Calculated from Figure 6A in Barone et al.,[22] see Figure 28. [g] See Figure 27. [h] Henry's Law constant calculated from Ref. 17. [i] Diffusion constant for HCl diffusion in 35 wt % sulfuric acid solution at 200 K from Ref. 410, the diffusivity in water is possibly even larger. Unless otherwise stated, all calculations assume an ice density of 1 g $cm^{-3}$.

The authors determined the nondiffusive uptake using several methods, by taking the difference between total and diffusive uptake, by numerical simulation of a Langmuir type adsorption on the surface and simultaneous diffusion into the ice bulk, and by application of the two-third criteria. Interestingly, the results of all three methods coincided within a factor of 4. While this approach uses a physical and kinetic model to treat the tailing, quite difficult experimental problems may occur. To determine $H_d^* D^{1/2}$, the kinetics of a small difference $p_0 - p_r$ in the tailing region of the breakthrough curve has to be measured with accuracy. For a practical matter, this is only possible if the experimental setup allows very high accuracy and stability.

**Interpretation of $H_d^* D^{1/2}$.** While it appears probable that the observed tailing is due to diffusion, this has not yet been proven in direct experiments, which analyze the solid phase. At present, the reservoir for the uptake during the tailing period is not established, and the question is how to interpret the kinetic quantity $H_d^* D^{1/2}$. In Table 6, we compare $H_d^* D^{1/2}$ as derived from flow tubes or Knudsen cells (refs 22, 83, and 214; Figure 28). Typical values are between 1 and 10 for 200 K and about $5 \times 10^{-6}$ $ms^{-1/2}$ Torr HCl. This is about 2 orders of magnitude larger than $H_d^* D^{1/2}$ if estimated from the solubility and diffusivity of HCl in single crystalline ice. Thus, the tailing cannot be due to the diffusion of HCl into the bulk ice matrix.

A possible process could be the diffusion of HCl into the grain boundaries or veins of the polycrystalline sample. Such reservoirs are possibly liquidlike, as it has been shown for triple junctions at higher temperatures.[81,141,142] We also note that the accumulation of HCl in grain boundaries and veins has been shown on ice samples frozen from HCl solutions.[10] However, from a thermodynamic point of view, this is a quite different situation. When an HCl solution is frozen, a two phase system will form, consisting of a bulk HCl solution and ice. In contrast, for uptake experiments in the ice stability regime, a macroscopic aqueous HCl solution would not be stable, unless surface forces lower the chemical potential of the solution in the confined reservoir, similar to the ones responsible for the formation of surface disorder on ice (cf. section 2.2).

Grain boundaries are interfacial reservoirs, and the diffusivity in these reservoirs is possibly higher than that on solid ice but lower than that in liquid water. This has been shown for the self-diffusion of water in the quasi-liquid layer on pure ice at temperatures close to the ice melting point.[106] However, no data are available for the diffusion of HCl into ice grain boundaries at 200 K.

Assuming the solubility[17] and diffusivity[410] of HCl in water would lead to $H_d^* D^{1/2} = 7 \times 10^4$ $ms^{-1/2}$, about a factor of 100 larger than the value for $H_d^* D^{1/2}$ derived for the uptake on ice. Assuming the solubility and diffusivity of HCl in the grain boundary or triple junction system to be close to the one in water, one might explain the tailing, because these reservoirs cover only a small fraction, $\epsilon$, of the ice surface. Thus, the effective value for $H_d D^{1/2}$ will be reduced by the factor $\epsilon$, if we neglect any transport by surface diffusion from the crystal surface to the grain boundary. For $\epsilon \approx 10^{-2}$−$10^{-3}$, one would arrive in the correct order of magnitude for $H_d^* D^{1/2}$ in the kinetic studies.

This interpretation will hold for the measurements in refs 83 and 214 because these experiments have been made on thick ice films. The diffusion time through the ice film can be calculated by $\Delta t = (\Delta x)^2/D$, which must be small compared to the experimental duration; otherwise the tailing should deviate from a $t^{1/2}$ law. Thus, the maximum diffusion constant $D_{max}$ is about $6 \times 10^{-13}$ $m^2\ s^{-1}$ (for ref 83, based on 35 $\mu$m, 2100 s duration) and $3 \times 10^{-14}$ $m^2\ s^{-1}$ (for ref 214, based on 10 $\mu$m thickness and 3000 s duration). Although these values are a factor of 10−100 smaller than the estimate for the diffusion in an aqueous sulfuric acid solution, this might be consistent, because the diffusion in confined liquid reservoirs could be slow compared to the diffusion in bulk water. However, the work of Barone et al.[22] was performed on films of 51 nm thickness. From the experimental duration of 3000 s, we calculate a maximum diffusion coefficient of $9 \times 10^{-19}$ $m^2\ s^{-1}$, which is as low as the diffusion constant of HCl in ice single crystals. If grain boundaries were the reservoir for the uptake process also on thin films, the effective diffusion constants would have to be on the order of the solid-state diffusion, which would be somewhat surprising.

In the picture of a diffusive uptake, the overall rate of uptake during the tailing is solely determined by the product $H_d^* D^{1/2}$. Thus, even for very slow diffusion, the rate of uptake remains constant, if the solubility is high enough. In consistency, the study by Barone et al.[22] shows a comparably large total amount of HCl taken up, both in terms of uptake per geometric surface area and also in terms of mixing ratio in the ice film (see Figure 25). In this work, and also in the experiments on vapor deposited ice by Hanson and Mauersberger[249] (see Figure 25), HCl mixing ratios well exceeding the solubility limit in ice single crystals[73] have been observed. While both these studies were performed on thin films, there is also evidence for similarly high HCl mixing ratios in the near-surface region of ice on thicker ice films and even on

single crystalline ice. The measurements by Flückiger et al.[78,241] and Aguzzi et al.[398] using the dope and probe technique yield information about the HCl concentration in the near-surface region and demonstrated that the HCl diffuses from the near-surface region into the ice bulk. Here also, high HCl mixing ratios in the upper 10−300 nm of order $10^{-3}$ to $10^{-4}$ have been found.

In addition, the RBS study of Huthwelker et al. determined the HCl composition in the ice using Rutherford backscattering. In the RBS study, ice was frozen from liquid water and the HCl concentration in the upper 0.75 $\mu$m was measured. Also here, high concentrations of some 0.1% have been found.

Based on these observations, a slightly different picture from the one derived in the previous section would emerge: HCl is readily taken up onto the ice. It diffuses into the near-surface region, where the HCl solubility is much higher than the one in ice single crystals, but with a diffusion constant as typical for the diffusion in ice single crystals. One may speculate that a possible explanation could be that the HCl slowly restructures the near-surface region of the ice surface, which leads to a high solubility, while the kinetics of this process is effectively limited by solid-state diffusion.

**Controversy about Bulk and Surface Processes.** In summary, the occurrence of a diffusion-like kinetics is a well established observation. Interestingly, it has been observed on both macroscopically thick and ultrathin ice films, with comparable kinetic constants. However, the nature of this process remains unexplained. One might speculate that one explanation could be the formation of a surface layer with enhanced solubility for HCl in the near-surface region. This layer would form on the surface of any type of ice, leading to similar kinetics, independent from the ice morphology. But also the diffusion into grain boundaries and triple junctions would be conceivable, if one assumes that the diffusion into grain boundaries and triple junctions is very slow. Because these microscopic reservoirs possibly contain highly concentrated solutions, the net mixing ratio in the near-surface region would be higher than that expected for HCl dissolved in ice single crystals. Now, if the solubility and diffusion are roughly equal in these reservoirs, one would also observe a similar diffusion-like kinetics, independent of the ice morphology.

Currently, none of these potential bulk processes have been shown in direct experiments. Thus, in short, the nature of the high HCl concentrations in the near-surface region and the diffusion-like kinetics remains unexplained. Indeed, the whole topic is controversial. The uptake has been interpreted as pure adsorbate on smooth or porous ice surfaces (e.g. refs 75, 217, 255, 406, and 411), or in terms of diffusive processes into the bulk or the near-surface region of ice (e.g. refs 214, 217, and 241). The answer to this question is of key importance to this research field. It affects not only the interpretation of uptake experiments but also the formulation of models to parametrize uptake processes and chemical reactions in atmospheric models. The authors of this review suggest that further research should be devoted to exploring this question.

### 8.4.5. Temperature Dependence

**Consistency of Data.** As most data are available at a HCl pressure of $10^{-6}$ Torr, we restrict our consideration to this pressure. The temperature dependence of the HCl uptake data is shown in Figure 29. For the total uptake, the overall trend

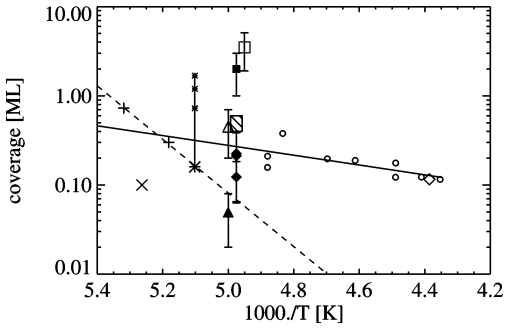


**Figure 29.** HCl surface coverage per geometric surface area (expressed as equivalent coverage on ice as a function of inverse temperature for HCl partial pressures close to $10^{-6}$ Torr): crosses, Chu et al.;[252] asterisks, Leu et al.,[79] with the biggest asterisk marking data on the thinnest ice film; filled diamonds, Lee et al.,[405] rescaled to an HCl partial pressure of $10^{-6}$ Torr, assuming a $\theta \propto p^{1/2}$ dependence; filled triangle, Huthwelker et al.,[214] nondiffusive component, as derived from asymptotic fitting; open triangle, Huthwelker et al.,[214] maximum total uptake in the experiment for 1800 s duration; shaded area, Hanson and Ravishankara;[28] open circles, uptake on smooth ice, taken from Hynes et al.;[213] filled square, Abbatt et al.,[83] with the point marking an average of 5 and 35 min experimental duration data, which define the error limit shown; open diamond, Sokolov et al.[406] (average data point from all data between 1 and $4 \times 10^{-6}$ Torr HCl); solid line, Arrhenius type fit to Hynes et al. data only (note that this fit slightly deviates from the best fit suggested by Hynes et al.,[213] which is based on the precursor mediated uptake model); dashed line, Arrhenius type fit to the data set from Chu et al.[252] and the data on the thinnest films by Leu.[79]

shows slightly rising uptake toward lower temperatures. For simplicity and guidance of the eye, we have fitted an Arrhenius type temperature dependence to the Hynes et al.[213] data. From the temperature dependence, the authors derived the free energy of adsorption as $-(48.9 \pm 2)$ kJ/mol. Within a factor of 3, several data sets, mainly the ones on thin films, appear consistent (i.e. Chu et al.,[252] Leu et al.[79] for the data on the thinnest films, the Lee et al.[405] data, the total uptake within 1800 s experimental time as determined by Huthwelker et al.,[214] the data from Hanson and Ravishankara,[28] and the data from Sokolov and Abbatt[406]).

Chu et al.[252] measured the HCl uptake on thin vapor deposited films at two different temperatures, lower than those in the studies discussed so far. For both temperatures, a wide range of pressures was studied. As the observed pressure dependence shows a very clear $p^{1/2}$ dependence, with very little scatter (Figure 23), the temperature dependence within the Chu data appears to be well established. Again, fitting an Arrhenius dependence (dashed line) to the Chu data and the data on the thinnest films from Leu, we find these two data sets to be in good agreement. Furthermore, the Arrhenius line is close to the lower error limit for one of the Lee et al. data points and also the nondiffusive uptake as determined by Huthwelker et al.[214]

Thus, by taking data subsets, two different temperature dependencies may be derived: a weak one, as suggested from the Hynes et al. data for temperatures above 200 K, and a strong one, based on the Chu data for temperatures below 200 K. The reason for this observation remains unclear. In principle, the HCl uptake does not need to follow a simple Arrhenius-like $1/T$ dependence. Such complex non-Arrhenius-like temperature dependencies occur, if the overall process is governed by several individual processes.

The temperature dependence of $H_d^* D^{1/2}$ was investigated for temperatures between 190 and 203 K,[214] and within this

small temperature range no temperature dependence was found. This might be due to the fact that the temperature trends of solubility and diffusion are opposite. For HCl, the trends of these individual processes are not known. Based on measurements of the $HNO_3$ diffusion into ice single crystals, $H_d^* D^{1/2}$ should rise toward lower temperatures.[74] We note that $H_d^* D^{1/2}$ does not show any temperature dependence for the dissolution of HCl in cold sulfuric acid solutions.[318]

Currently the nature of the experimentally observed temperature dependence is not well understood, and there are several possible explanations. There might be two different states for HCl on the ice surface, which lead to a non-Arrhenius-like temperature dependence. Also, a different degree of diffusion at different temperatures may lead to such effects. In some way, this explanation is closely related to the concept of two different adsorbed states, as the stronger bound state would correspond to HCl diffusing into the ice. We note that Flückiger et al.[78] have pointed to such an interpretation. Furthermore, in section 2.3.4 we show the mathematical equality of the kinetic precursor model with a surface model assuming a Langmuir type adsorption and subsequent diffusion into the bulk. Another possibility could be that different setups have different sensitivities to different elementary processes. For example, experiments with longer time scales may be more sensitive to slow, diffusion-like processes, while experiments on short time scales are more surface sensitive. Furthermore, we note that the Hynes data were taken on smooth ice, while all other data were taken on vapor-deposited ice films. Thus, it might be that data on vapor-deposited ice are more surface sensitive and exhibit a stronger temperature dependence than data on smooth ice films.

### 8.4.6. Uptake in Melting and Hydrate Stability Regimes

This review is restricted to uptake processes in the ice stability regime. But as the formation of hydrates, or the melting of ice, may sometimes occur in experiments once sufficiently high HCl partial pressures are used, we briefly discuss some aspects of uptake experiments of HCl under conditions where ice is no longer the stable phase. This regime is defined by a set of temperatures and HCl partial pressures as shown in the HCl phase diagram (Figure 5; see also ref 170). From a thermodynamic point of view, there is a fundamental difference between uptake processes inside and outside the ice stability regime. In the ice stability regime, ice remains a stable solid phase, with a certain amount of HCl taken up on the ice surface and/or dissolving into the ice. In contrast, at higher pressures, hydrates may form.

However, the situation is more complex due to the nucleation barrier, which has to be overcome to form a new phase. For entropic reasons, transitions from the solid to the liquid phase have very low nucleation barriers. This is especially true, if surface premelting occurs, as the nucleation germ already exists on the ice interface even in the ice stability domain. In contrast, the transition from the liquid to the solid phase, or between two solid phases, is often kinetically limited. A famous example is the abundance of supercooled liquid aerosols in the stratosphere.[34,412,413] (For discussion of hydrate formation in the HCl/ice system, see refs 21, 170, and 337 and references therein.)

Indeed, the phase transition of solid ice to an aqueous HCl solution induced by high HCl partial pressures occurs easily and a strongly accelerated uptake kinetics has been observed by many authors[83,214,232] (see also Figure 27).

In principle, an adsorption isotherm of HCl on ice may be defined even in the hydrate existence regime, if the new phase has not nucleated and ice still exists as a metastable phase. For example, based on spectroscopic evidence, Henson et al.[21] demonstrated that the hexahydrate will nucleate only if HCl partial pressures range far into the hydrate stability region. Also, Flückiger et al.[217] analyzed gas pulses for very different thermodynamic conditions, including HCl partial pressures high enough to form hydrates, and derived an adsorption isotherm which extends well into the hydrate regime (Figure 23).

Both groups derived adsorption isotherms from their data, and it is obvious that both isotherms do not coincide (Figure 23, lines labeled Hen 190 and Fl P+B 190). While the Flückiger data suggest a rise by 2 orders of magnitude at $3 \times 10^{-6}$ Torr, the Henson data show only a modest increase of the uptake. Furthermore, the Henson isotherm levels off at a maximum surface coverage of $(2-3) \times 10^{14}$ molecules $cm^{-2}$, which is the surface coverage where the nucleation of a new phase occurs. The interpretation of this difference is unresolved and might be due to very different experimental protocols used in both studies.

## 8.5. HBr and HI

**Hydrate Stability.** For HBr and HCl, a similar behavior is expected upon uptake on ice. Both acids readily dissolve and dissociate in water according to the Eigen−Kustin mechanism.[163] This physicochemical similarity is also reflected by the similar shapes of the HCl/ice and the HBr/ice phase diagrams (see Figures 5 and 7). For the same temperature, the amount of HBr dissolved in an HBr solution at the ice/liquid coexistence point is similar to the one of the HCl solution at the ice/liquid coexistence point.[174] However, as HBr is much more soluble in water than HCl, the acid vapor pressure at the ice/solution coexistence line is much lower for HBr than for HCl. Consequently, ice can coexist with HCl vapors of pressures up to $10^{-4}$ Torr (at −20 °C), while HBr vapors as low as $\sim 10^{-7}$ Torr will melt ice.

At low temperatures (below ~205 K for $10^{-7}$ Torr of HBr) or at higher HBr partial pressures, hydrates can form. The location of the $HBr \cdot 2H_2O$, $HBr \cdot 3H_2O$, and $HBr \cdot 4H_2O$ hydrates in the phase diagram has been determined experimentally by Chu and Chu.[171] The $HBr \cdot 5H_2O$ hydrate has been proposed to fill the region between ice and the $HBr \cdot 4H_2O$ hydrate, but this has not yet been experimentally verified.[402] Stratospheric hydrobromic acid partial pressures are around $10^{-11}$ Torr.[414] Thus, in the atmosphere, ice and not HBr hydrates is the stable phase in the presence of atmospheric HBr vapors.

When investigating the HBr/ice interaction, care must be taken to ensure the thermodynamic stability of the ice substrate by establishing sufficiently low HBr partial pressures. This experimental challenge is reflected by the fact that there are no data on the HBr uptake on ice in the ice stability domain available (see Figure 30). This review is concerned with uptake processes in the ice stability domain. However, for illustrative purposes, we briefly discuss the available studies on HBr uptake on ice. Studies on the HBr uptake in the hydrate regime illustrate the nature of the acid/ice interaction under these specific thermodynamic conditions and apply also to other acidic gases such as $HNO_3$ or HCl.

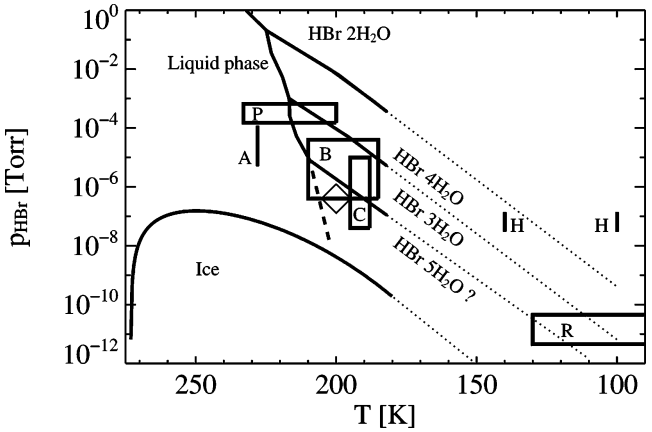


**Figure 30.** Thermodynamic conditions of HBr uptake experiments. Diamond, Hanson et al.;[404] P, Percival et al.;[411] A, Abbatt et al.;[415] B, Barone et al.;[22] C, Chu and Chu;[402] R, Rieley et al.;[416] H, Hudson et al.[417] For details, see the text and Table 7. Dotted lines, approximate hydrate coexistence curves, calculated by linear extrapolation of the phase boundaries taken from Chu and Chu.[202]

**Available Data.** The uptake of HBr on ice has been studied by several authors.[22,171,314,402,404,411,415−417] In practically all studies, a continuous steady-state uptake of HBr has been observed. In flow tube[404,415] and Knudsen cell studies,[314] the HBr partial pressure dropped to the vapor pressure of the eutectic solution, once HBr partial pressures were in the liquid stability domain. This indicates that the HBr vapor readily melts the ice. Steady-state uptake, with uptake coefficients between 0.03 and 0.3 (see Table 7), has also been observed in the hydrate stability domain in uptake experiments with HBr,[171,402] $HNO_3$,[242] and HCl.[22] During steady-state uptake conditions in the hydrate stability domain, ions, such as the $H_3O^+$ ion, form readily[22] (see section 6). However, this does not necessarily imply that hydrates indeed nucleate, as has been demonstrated for the $HNO_3$/ice system by Hudson et al.[243] using FTIR spectroscopy.

**Evidence for Hydrate Formation in Flow Tube Experiments.** The formation of HBr hydrates during the exposure of ice to HBr was shown by Chu and Heron[402] and Chu and Chu[171] in a flow tube study. The principle of the experiment is illustrated in Figure 31, where we show a sketch of the HBr and $H_2O$ signals at the flow tube exit. The experiment

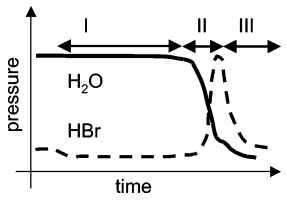


**Figure 31.** Principle of HBr uptake with subsequent hydrate formation. Solid line, water partial pressure; dashed line, HBr partial pressure. Phase I: steady-state uptake of HBr onto ice, with $p_{H_2O}$ given by the evaporating ice. Phase II: after all ice is evaporated, $p_{H_2O}$ decreases, while $p_{HBr}$ rises according to the Gibbs−Duhem relation[35] ($p_{HBr}p^n_{H_2O}$ = constant, which allows determination of the HBr hydrate composition). Phase III: evaporation of the entire sample.

has three stages. During phase I, steady-state uptake of HBr is observed. Note that the flow tube is not humidified. Thus, evaporating ice at the tube inlet serves as humidity source for the ice in the downstream region. As long as ice exists in the flow tube, it has a water vapor pressure higher than any of the possibly forming hydrates, thus forcing the water partial pressure to the value of the ice vapor pressure. As long as there is enough ice in the tube to define the water partial pressure in the tube, only a eutectic solution or the hypothesized $HBr·5H_2O$ hydrate could form on top of the ice surface.

Phase II starts when the water partial pressure in the flow tube decreases, due to complete evaporation of the ice. Now the water partial pressure is defined by the remaining hydrate in the flow tube. For thermodynamic reasons, the HBr vapor pressure of the hydrate is related to the HBr vapor pressure of the hydrate by the Gibbs−Duhem relation[35] $K = p_{HBr}p^n_{H_2O}$, with $n$ being an integer and $K$ a constant which depends only on temperature. By observing the integer $n = 2$ or $n = 3$, the formation of the di- and the trihydrate on the ice surface could be shown.[171] As the total amount of absorbed HBr is very low, the hydrate evaporates readily during phase III. By this method, Chu and Chu[171] constructed the hydrate locations in the HBr/ice phase diagram.

**Total Uptake Measurements of HBr and HI and Coadsorption.** Chu and co-workers performed several studies to determine the total uptake of HBr[171] and HI[418] and also the coadsorption of HBr with HCl.[171] In their experi-

**Table 7. HBr Uptake on Ice**

| author | method[a] | $T$ (K) | $p_{HBr}$ ($\times 10^{-6}$ Torr) | $\theta_{equi}$ ($\times 10^{15}$ cm$^{-2}$) | $\gamma$ | thermodynamic regime[b] |
|---|---|---|---|---|---|---|
| Hanson and Ravishankara[404] | FT | 200 | 0.4[c] | >5[d] | | melting |
| Abbatt[415] | FT | 228 | 5−12 | 50[d] | ∼0.3 | melting |
| Rieley et al.[416] | *e* | 80−130 | 0.0000045−0.000045[f] | | 1 ± 0.05 | hydrate |
| Chu and Heron[402] | FT | 188, 195 | 0.37−6.4 | 0.11−11[g] | | hydrate[j] |
| Seisel and Rossi[428] | KN | 190 | not given | | 0.25−0.6 | |
| Chu and Chu[171] | FT | 188 | 0.04−10 | ∼1−100[g] | | hydrate |
| Barone et al.[22] | KN, IR | 185−210 | 20−4000[h] | | >0.02 | melting/hydrate |
| | | 110 | | | | hydrate (?)[i] |
| Hudson[417] | LITD | 140 | (0.03−0.14) | | 0.61 ± 0.05 | hydrate |
| | | 100 | | | 0.24 ± 0.05 | hydrate |
| Percival[411] | FT | 200−233 | 150−660 | | 0.03 ± 0.005 | melting |
| | | <212 | | | >0.1 | hydrate (?) |

[a] Abbreviations: FT, flow tube; KN, Knudsen cell; LITD, laser-induced thermal desorption. [b] The thermodynamic regime is estimated on the basis of temperatures and HBr partial pressures used in the experiment; it is often not clear which hydrates indeed nucleated in the experiment. [c] HBr pressure of inflowing gas; pressure dropped during steady-state uptake as low as $6 \times 10^{-9}$ Torr. [d] Unlimited uptake, steady-state signal. [e] Ice was exposed to a molecular beam of acid molecules. [f] The total influx of gas molecules directly onto the surface of $10^{12}$ to $10^{13}$ molecules cm$^{-2}$ was used to estimate the HBr partial pressure. [g] Total uptake before evaporation of sample starts; see text. [h] Pressure calculated from orifice size assuming a temperature of 202 K. [i] Hydrate formation at high HBr flow rates. [j] HBr phase diagram not established at these low temperatures and partial pressures; hydrate stability region estimated on the basis of extrapolations in Figure 30.

ments the authors report clear relations of the form $\theta \propto p^f$ for the equivalent coverage as a function of the applied partial pressure, with $f$ being a number which is characteristic for the specific system. The observed uptake often exceeded more than a monolayer. Chu and Chu[171] also studied the co-uptake of HCl and HBr on the same ice films. Here, the authors found that the total amount of HBr is anti-correlated to the amount of HCl on the ice surface and vice versa.

As ice is not thermodynamically stable under the experimental conditions, there are several interpretations of the reported total surface coverage. First of all, the observed coverage might be interpreted as the equilibrium surface coverage of the trace gas on metastable ice. However, the authors reported that in most experiments a final peak occurred, which indicated hydrate formation (see Figure 31). Thus, one might speculate whether the total amount of trace gas taken up in the time prior to hydrate formation should be interpreted as the amount needed for forming the nucleation germ for the hydrate on the ice surface.

**Summary.** Hydrobromic acid vapor readily reacts with ice, and hydrates or liquid solutions form easily. It is to be expected that HBr uptake processes are very similar to the ones of HCl. However, as there are no uptake experiments in the ice stability domain, the adsorption isotherm in the ice stability domain, and thus for atmospheric conditions, remains unknown.

## 8.6. $HNO_3$

Nitric acid, $HNO_3$, has similar properties as the strong halogen acids. It is a strong acid, which dissolves in water, where it rapidly dissociates.

$$H_2O + HNO_3 \rightarrow H_3O^+ + NO_3^- \qquad (116)$$

The ice/$HNO_3$ phase diagram has similar properties as the one of HCl or HBr (see Figure 6). As $HNO_3$ solutions have very low $HNO_3$ vapor pressures, ice melts already in the presence of $HNO_3$ partial pressures as low $10^{-4}$ Torr. For higher $HNO_3$ partial pressures and for lower temperatures, hydrates,[249] most notably nitric acid trihydrate (NAT), which is also found in polar stratospheric clouds, may form.

### 8.6.1. Studies on $HNO_3$ Uptake on Ice

The gas/solid partitioning between $HNO_3$ and ice has been investigated in laboratory studies (see Table 8), using packed ice beds,[262] flow tubes,[42,215,255,406,419] and Knudsen cells.[243] Furthermore, the gas/solid partitioning was inferred from field studies.[420−423]

**Flow Tube Studies.** The uptake of $HNO_3$ on ice has been investigated in several very similar flow tube experiments.[42,215,255,406] In all studies, smooth ice films were used, which were frozen from deionized water following a procedure originally described by Abbatt.[42] In all studies, a strong initial uptake with some tailing was observed, similar to the results of uptake experiments on HCl. The tailing was treated by the two-third criterion, or related approaches, to infer the end of the surface uptake. As shown below, these studies yield a quite consistent picture.

**Reversibility of $HNO_3$ Uptake.** Another issue of investigation is the question of whether the trace gas is absorbed reversibly. Ullerstam and Abbatt[215] performed adsorption/desorption cycles in a flow tube experiment. In these experiments, the injector was first moved upstream to expose the ice. As a consequence, a strong uptake of $HNO_3$ was observed. After a certain time period, the injector was moved downstream to the end of the flow tube. For a very short time period of the initial exposure, no desorption of the absorbed $HNO_3$ was observed, which led the investigators to conclude that a part of the $HNO_3$ is taken up irreversibly. However, the larger the initial exposure time (i.e. once the tailing of the breakthrough curve starts), the larger the amount of $HNO_3$ desorbing from the ice.

A second important observation is that less $HNO_3$ is taken up onto the ice surface, in a second exposure on already exposed ice.[42,215] Similar observations have been reported for HCl,[214] which indicates the similarity of the HCl/ice and the $HNO_3$/ice interaction. This observation corroborates that part of the $HNO_3$ is taken up irreversibly into a strongly bound state at the ice surface, where the $HNO_3$ remains and blocks further adsorption onto those strongly bound sites.

Those strongly bound states could, in principle, be caused by alkaline impurities on the ice surface, which react with the acid. The impact of impurities on the uptake process has been addressed by Ullerstam and Abbatt,[215] who performed $HNO_3$ uptake experiments on ice films, which were frozen on different types of water, such as deionized water and ordinary tap water. Larger uptake of $HNO_3$ was observed on ice frozen from tap water, but the authors noted also that the morphology of the tap water films was somewhat different. Thus, differences in uptake could also be caused either directly by differences in impurity concentrations or by differences in the ice morphology.

**Other Laboratory Studies.** Several other approaches have been taken in laboratory experiments. Arora et al.[419] studied the uptake of $HNO_3$ on submicron sized ice particles. The ice particles were produced by condensing water vapor on dried $Na_2SO_4$ aerosols. These aerosols were exposed to $HNO_3$ while passing through a flow tube. The amount of $HNO_3$ was determined by analysis of the nitrate in the collected aerosols. From the measured size distribution, the $HNO_3$ surface coverage was inferred.

**Table 8. Laboratory Studies on $HNO_3$**

| author | method[a] | $T$ (K) | $p$ (Torr) | uptake ($\times 10^{15}$ molecules cm$^{-2}$) | exp time scale | ice type |
|---|---|---|---|---|---|---|
| Hanson and Ravishankara | FT | 191.5, 200 | 0.08, 0.3 | 0.05−0.15 | | vp |
| Abbat[42] | FT | 208−248 | 3.1−13 | 0.07−0.3 | minutes | b[b] |
| Arora et al.[419] | IPFT | 230 | 4.5−7 | 0.1−1.2 | | ap[c] |
| Hudson et al.[243] | KN | 209−220 | 0.2−8 | 1 ($T$ > 213 K) | some 10 min | vp |
| | | | | >1 ($T$ < 213 K) | some 10 min | vp |
| Hynes et al.[255] | FT | 210−250 | 0.3−2.4 | 0.2−0.4 | minutes | b[b] |
| Sokolov and Abbatt[406] | FT | 228 | 1−5 | 0.16 ± 0.2 | minutes | b[b] |
| Ullerstam et al.[215] | FT | 200−239 | 0.008−0.8 | 0.01−0.2 | minutes | b[b] |

[a] FT, flow tube; KN, Knudsen cell; IPFT, flow tube with airborne ice particles. [b] Ice film frozen on walls of flow tube. [c] Airborne ice particles.

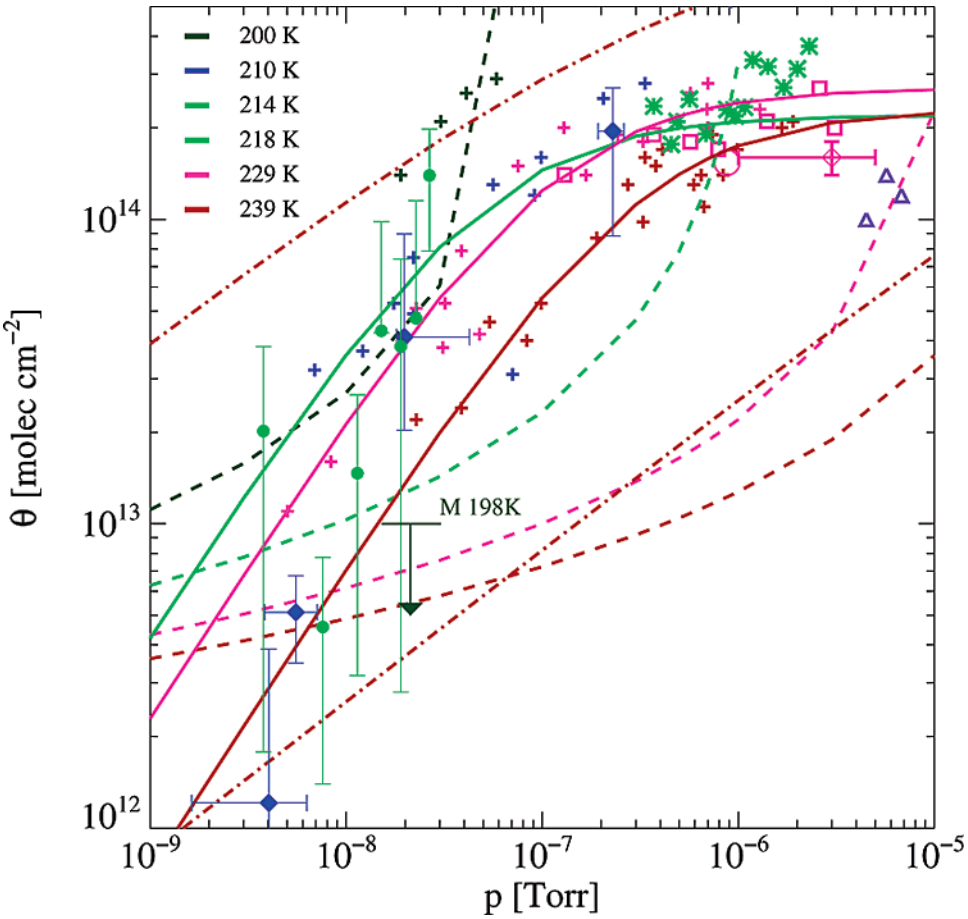


**Figure 32.** Equivalent $HNO_3$ surface coverage ($\theta_e$) on ice as a function of $HNO_3$ partial pressure. Colors label different temperatures, as coded in the figure. Crosses and open symbols, laboratory data; filled symbols, field studies. Laboratory studies: crosses, Ullerstam and Abbatt;[215] open squares, Abbatt et al.;[42] open triangles, Arora et al.;[419] open diamonds, Sokolov and Abbatt;[406] asterisks, Hynes et al.;[255] open circle, Hynes et al.;[255] solid lines, nondissociative Langmuir adsorption isotherms as given by Ullerstam and Abbatt;[215] dashed lines, multilayer adsorption isotherm as given by Hudson et al.;[243] dashed−dotted line, adsorption isotherm after Tabazadeh et al.[77] for different adsorption enthalpies (upper line 14.2 kcal mol$^{-1}$ from ref 77; lower line 10.5 kcal mol$^{-1}$ from ref 265). Field studies: filled circles, Ziereis et al.;[422] filled diamonds, Kondo et al.;[421] arrow labeled "M 198", upper limit as given by Meilinger et al.[420]

In a study using a Knudsen cell and FTIR spectroscopy, Hudson et al.[243] studied the $HNO_3$ uptake on ice, which was made by vapor deposition on a gold substrate. The internal ice surface area of the porous ice film was determined by a BET measurement using butene. In the study, continuous uptake was found, once the $HNO_3$ partial pressure was in the stability domain of NAT, consistent with previous studies and similar to measurements of HCl and HBr uptake in hydrate stability domains. Spectroscopic investigation of the ice surface during uptake in the hydrate stability domain revealed the existence of the asymmetric $NO_3^-$ stretch and, thus, the formation of the $NO_3^-$ ion. The spectroscopic probe of the ice surface also revealed that there was no NAT formation during uptake in the NAT stability domain, i.e., that, despite continuous uptake of $HNO_3$, NAT did not nucleate.

The study also showed that the uptake per surface area strongly rises with lowering of the temperature to reach a total uptake of several monolayers. Based on this finding, the authors suggested modeling the $HNO_3$ uptake using the Frenkel−Halsey−Hill (FHH) adsorption model, which accounts for multilayer adsorption.

Further studies include thermochromatography experiments for determination of the adsorption enthalpy of nitrogen oxides,[265] and packed ice bed studies at higher temperatures.[262,263]

**Field Studies.** In contrast to studies with HCl, HBr, $SO_2$, or HONO, the amount of $HNO_3$ on atmospheric ice particles has also been determined in several field studies.[420−423] In these studies, the partioning of $HNO_3$ between the gas and the ice phase was determined from the measured $HNO_3$ concentration in the gas phase and the amount of $HNO_3$ found when evaporating the collected ice particles.[420−423] As outlined in section 1.2, uptake of $HNO_3$ by cirrus clouds and uptake of $HNO_3$ on polar stratospheric aerosols are issues of major interest in atmospheric science. Results from field studies and from laboratory experiments will be compared in the following subsection.

### *8.6.2. Data Comparison*

**Pressure Dependence.** The available data from laboratory and field studies of $HNO_3$ uptake on ice are summarized in Figure 32, where we plot the overall uptake of $HNO_3$ as function of the $HNO_3$ partial pressure. Crosses mark the most comprehensive data set from Ullerstam and Abbatt.[215] These data show a slow rise of coverage with $HNO_3$ partial pressure until a saturation occurs with about 0.2 formal monolayers. The observed pressure dependence is consistent with a nondissociative Langmuir adsorption isotherm (solid lines in Figure 32). This is surprising, as $HNO_3$ is expected to dissociate on ice. However, as Ullerstam and Abbatt pointed out, the dissociative Langmuir adsorption isotherm assumes

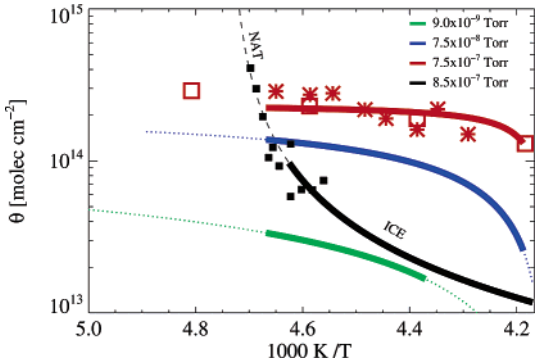


**Figure 33.** $HNO_3$ surface coverage on ice as a function of temperature for different $HNO_3$ partial pressures. Colors label different partial pressures, as coded in the figure. Solid lines, nondissociative Langmuir adsorption isotherms, calculated from Ullerstam and Abbatt[215] using their parametrization for a temperature-dependent Langmuir constant and the average saturation coverage for all pressures of $2.4 \times 10^{14}$ molecules $cm^{-2}$; bold colored lines mark the region were data are available; dotted extensions are extrapolations; solid black line, FHH multilayer adsorption isotherm as suggested by Hudson et al.;[243] the bold part marks the ice coexistence regime ("ICE"); the thin dashed extension marks the NAT stability domain ("NAT"); the phase boundary is calculated according to Hanson and Mauersberger;[35] filled squares, Hudson et al.,[243] only data points where saturation occurred are shown; open squares, Abbatt et al.[42] ($6-9 \times 10^{-7}$ Torr $HNO_3$); asterisks, Hynes et al.[255] ($8.5 \times 10^{-7}$ Torr $HNO_3$).

that two different sites, i.e., one for the $NO_3^-$ ion and one for the $H^+$ ion, are consumed upon dissociative adsorption. If the two ions are not forming independent adsorbates competing for the same site, but rather a larger complex covering a certain area, the overall process may be considered adsorption into a single site. This would justify using a nondissociative adsorption isotherm.

The data from Ullerstam and Abbatt show good consistency with results from previous flow tube studies (Abbatt,[42] Sokolov and Abbatt[406]) and also to a lesser extent with the aerosol flow tube study by Arora et al.,[419] which showed somewhat lower values for the total uptake.

Furthermore, there is also reasonable consistency with results derived from field studies by Kondo et al.[421] on Arctic clouds and by Ziereis et al.[422] on cirrus clouds at low latitudes. Furthermore, the observed saturation coverage of about 0.22−0.27 formal monolayers is consistent with the maximum coverage determined in the CRYSTAL-FACE field campaign above Florida, where a maximum $HNO_3$ uptake of 0.14 formal monolayers was observed.[423]

**Temperature Dependence.** The temperature dependence of the measured total uptake for $HNO_3$ on ice is summarized in Figure 33. Here we compare the suggested adsorption isotherms from Ullerstam and Abbatt[215] with other data and the FFH isotherm, which was suggested by Hudson et al.[243] There is good consistency among the flow tube data. Because the saturation of the adsorption isotherm at about $0.24 \times 10^{14}$ molecule $cm^{-2}$ is independent of the temperature, there is only a weak temperature dependence at, or close to, the saturation regime, and a stronger one in the unsaturated regime.

In contrast to the adsorption isotherm by Ullerstam and Abbatt, the FFH multilayer adsorption isotherm by Hudson et al.[243] does not show any saturation, but rather a strong uptake toward lower temperatures. The Hudson isotherm is plotted as a thick black solid line in the ice stability domain and as a thin dashed line in the NAT stability domain. The raw data as reported by Hudson et al.[243] (filled squares) are also shown. Clearly, the strong rise occurs once temperatures are low enough to allow for NAT stability. However, it must be pointed out that Hudson et al. explicitly addressed this question by spectroscopic investigation, which revealed the existence of the $NO_3^-$ ion, but not the formation of NAT. Thus, these data show that the $HNO_3$ uptake strongly rises, once hydrates can form. This observation is consistent with other studies and also with other gases. For example, Flückiger and Rossi demonstrated strongly rising HCl uptake, once HCl pressures are high enough to form the HCl hexahydrate.

## 8.7. HONO

Another acidic gas of interest is nitrous acid (HONO). It has a slightly more complex chemistry compared to $HNO_3$. It is instructive to consider the fate of HONO in aqueous solutions upon dissolution in water, where it dissociates[424]

$$HONO(aq) \rightleftharpoons H^+ + NO^-_2 \qquad (117)$$

In addition, it decomposes reversibly to $NO_2$, which hydrolyzes irreversibly to nitric and nitrous acid by the reactions

$$H^+ + 2NO_2^- \rightleftharpoons NO(g) + NO_2(g) + H2O(l) \qquad (118)$$

$$2NO_2(g) + H_2O \rightleftharpoons 2H^+ + NO_3^- + NO_2^- \qquad (119)$$

The effective solubility of HONO in aqueous solutions depends on the pH, especially for low pH, where the presence of protons shifts the equilibrium in the solution toward the formation of $NO^+$ by

$$HONO(aq) + H^+ \rightleftharpoons H_2O + NO^+ \qquad (120)$$

As a consequence, the effective solubility of HONO in sulfuric acid rises dramatically, once the presence of protons (eq 120) dominates.[425−427] The shift of the equilibrium according to reaction 120 possibly drives the formation of ClNO when HONO reacts with HCl doped sulfuric acid[236,428] or ice[429,430] by

$$HONO + HCl \rightarrow ClNO + H_2O \qquad (121)$$

This reaction occurs in aqueous solutions and on ice, which indicates that the interaction mechanisms of acidic gases on ice surfaces are often comparable to the ones in liquid environments. We also note that the uptake coefficient of HONO on ice rises, if HBr is present in the gas phase.[428] However, as this review focuses on nonreactive uptake processes, we will not further explore this topic.

**Available Data.** Data on nonreactive uptake of HONO on ice are scarce, which is surprising, given the importance of HONO for atmospheric and especially polar snow chemistry. Two studies report data for the total uptake of HONO on ice under typical stratospheric temperatures. Chu et al.[429] measured the equilibrium coverage of HONO in a flow tube on vapor deposited ice and determined the adsorption enthalpy from the temperature dependence of the total uptake. Fenter and Rossi[236] determined the uptake of HONO in a Knudsen cell experiment. The data are summarized in Figure 34. In contrast to studies on other acidic gases, such as $HNO_3$ or HCl, only very little tailing was observed. However, as the total amount of HONO uptake is

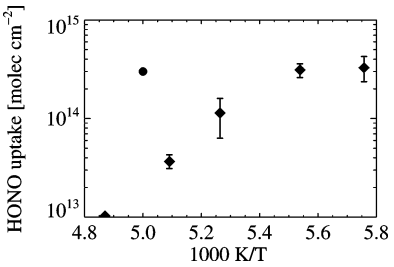


**Figure 34.** HONO uptake on ice: diamonds, total uptake for a HONO partial pressure of $1.9 \times 10^{-7}$ Torr, measured on vapor deposited ice in a flow tube (Chu et al.[429]); solid dot, from Fenter and Rossi,[236] measured in a Knudsen cell.

small compared to the uptake of HCl or $HNO_3$, it might well be that the tailing was not visible with the experimental sensitivity, as discussed in section 8.4.4. Another approach to study the uptake of HONO on ice was taken by Bartels-Rausch et al.,[265] who used radioactively labeled HONO and performed thermochromatography on a packed ice bed of about 400 $\mu$m sized ice spheres. For temperatures around 160 K they derived the adsorption enthalpy ($\Delta H = -32$ kJ mol$^{-1}$) and entropy ($\Delta S = -42$ J mol$^{-1}$K$^{-1}$, which refers to a standard surface area of $6.7 \times 10^{10}$ cm$^{-2}$). This enthalpy value is in good agreement with the enthalpy as determined by Chu et al.,[429] who report $\Delta H = -33.8$ kJ mol$^{-1}$.

## 8.8. Sulfur Dioxide, $SO_2$

The uptake of $SO_2$ onto ice has been studied using a variety of different techniques, such as packed ice bed experiments with artificial ice[59,60,84,261,431,432] and natural snow,[266] and in flow tube experiments on both vapor deposited and smooth ice films.[62,433,434] Also, uptake processes on individual ice spheres and snowflakes[435] and the impact of riming and ice growth in clouds[436,437] have been investigated. Finally, it was shown that oxidants[60,62,84,433,434] and salts[60,84] strongly influence the amount of $SO_2$ uptake on ice. For direct environmental application, several field experiments and modeling studies[57,438−445] were designed to investigate the dry deposition of $SO_2$ on snow and land surfaces.

It is instructive to recall the behavior of sulfur dioxide in an aqueous solution. It dissociates in a two step process[56,446] by

$$SO_2(aq) + H_2O \rightleftharpoons H^+ + HSO_3^- \quad (122)$$

$$HSO_3^- \rightleftharpoons H^+ + SO_3^{2-} \quad (123)$$

Compared to strong acids such as HCl, $SO_2$ is a comparably weak acid. Thus, its degree of dissociation depends strongly on the acidity of the solvent. In very acidic solutions (pH < 2), there is very little dissociation and the molecular solubility dominates. The $HSO_3^-$ ion dominates for 3 < pH < 6.5. The second dissociation step, when the $SO_3^{2-}$ ion forms, occurs for pH > 7. When dissolved in water, the proportionality for the solubility $H_d^* \propto p^{-1/2}$ evolves (see eq 130), indicating the dominance of the first dissociation stage.

The solubility of sulfur dioxide in water is almost 3 orders of magnitude lower than the one of HCl: The molecular solubility, which ignores the subsequent dissociation, is 1.23 M atm$^{-1}$ for $SO_2$ and 727 M atm$^{-1}$ for HCl.[56] For 1 ppb of the trace gas, the effective Henry's Law constant for $SO_2$ is about 450 times smaller compared to that for HCl (4000 M atm$^{-1}$ and $2 \times 10^6$ M atm$^{-1}$ for $SO_2$ and HCl, respectively[17,56]).

The effective solubility of $SO_2$ in aqueous solutions can be dramatically enhanced, if oxidants, such as ozone, $O_3$, or hydrogen peroxide, $H_2O_2$, oxidize the bisulfite ion to the sulfate ion, $SO_4^{2-}$,[56] in an acid−base-catalyzed reaction, $HSO_3^- + H^+ + H_2O_2 \rightarrow SO_4^{2-} + 2H^+ + H_2O$. Similar processes seem to occur, when $SO_2$ is taken up onto ice. The presence of hydrogen peroxide, $H_2O_2$, enhances the overall uptake of sulfur dioxide on ice. This was demonstrated in uptake experiments on vapor deposited ice at stratospheric temperatures,[433,434] and for tropospheric conditions in packed ice bed experiments[60] and uptake experiments on snow.[266]

Similarly, bases, such as ammonia, $NH_3$, can increase the uptake of sulfur dioxide on ice.[432] Enhanced sulfate in the presence of ammonia has also been found in field studies (for example, see ref 447). However, as this review is concerned with nonreactive processes, we will not further explore this topic.

The relatively weak interaction of $SO_2$ with water and ice is also reflected in the sulfur dioxide/ice phase diagram (see Figure 4). Due to the low solubility of $SO_2$ in water, there is no significant reduction of the ice melting point when sulfur dioxide dissolves in water at typical atmospheric $SO_2$ partial pressures. Even $SO_2$ partial pressures as high as several hundred torr will reduce the ice melting point by less than three degrees kelvin. Only for higher partial pressures will hydrates form. In contrast, ice will melt in the presence of HCl vapors of more than $10^{-4}$ Torr (see Figure 5).

The moderate adsorption of $SO_2$ on ice in comparison with the cases of strong acids is shown in Figure 35. It is an intermediate adsorbate on the ice surface according to a classification introduced by Devlin and co-workers.[346−349] Thus, $SO_2$ is able to break some single weak H-bonds, but not the water−water bonds themselves.

The mechanism of the $SO_2$ adsorption on ice has been studied using FTIR spectroscopy at a temperature of 120 K.[355] Interestingly, a very slow, three step adsorption process was found. In a first, about 2−3 h long period, the ice surface is saturated by adsorbing $SO_2$. During this period, some of the H-bonds are strained. In a second 2−3 h long period, the $SO_2$ molecule is inserted into the strained H-bonds. In the last stage, the $SO_2$ is built into the subsurface layer below the ice surface. The main conclusion from this work is that gaseous $SO_2$ will slowly restructure the ice surface. Similar effects have been reported for other strongly H-bonding adsorbates.[448]

**Available Data.** In this section we will compare the measurements concerning the sulfur dioxide uptake on ice in the absence of oxidants and other chemical reactions (see Table 9). The uptake of sulfur dioxide has been studied at high temperatures using packed ice beds[59,60,261] and small individual ice spheres.[61] Recently, flow tube studies have been performed at stratospheric temperatures between 190 and 228 K.[62,433]

Sommerfeld and Lamb[261] were the first to study the uptake of sulfur dioxide on ice with packed ice bed experiments (see section 3.3). These early experiments illustrated the feasibility of the method and demonstrated that the uptake of sulfur dioxide increases with temperature,[261] a result which was previously found in field studies of the dry deposition of sulfur dioxide in snow[442] and confirmed in later studies.

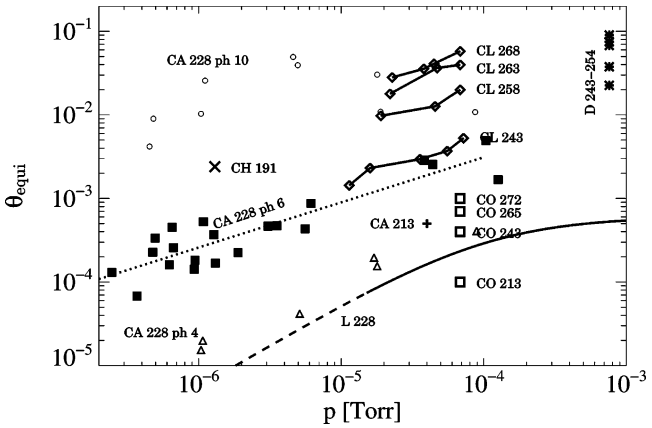


**Figure 35.** Uptake of sulfur dioxide on ice as a function of $SO_2$ partial pressure by various authors; for details see Table 9. Open diamonds, Clapsaddle and Lamb[59] (CL) raw data converted to uptake per surface area using a mean ice surface area of 3.17 $m^2$ and numerical integration of the breakthrough curve following ref 172; open squares, Conklin et al.[60] (CO); asterisks, Diehl et al.[61] (D) converted to uptake per surface area using the surface area of the ice spheres used in the experiment (note that the experimental time scales range from 10 to 30 min and no saturation was observed); solid line (L 228), Langenberg[449] measured region; dashed line, extrapolation based on fitting parameters given in the original study; CA, Clegg and Abbatt[62] uptake onto films of different acidities at 228 K; filled squares, on ice frozen from deionized water (pH 6); open triangles, on ice frozen from $H_2SO_4$ solution (pH 4.1); open circles, on ice frozen from NaOH solution (pH 10.4); dotted line, best fit ($\theta = ap_{SO_2}^b$) to pH 6 data taken from Clegg and Abbatt,[62] resulting in $b = 0.53$, as expected for dissociation; cross (CA 213), ice frozen from deionized water (pH 6) (213 K) from Clegg and Abbatt;[62] cross labeled "CH 191", Chu et al.;[429] $\theta = 1$ means an uptake of a formal monolayer of $10^{15}$ molecules $cm^{-2}$; numbers in the plot denote the temperature in K during uptake.

As the adsorption usually increases when lowering the temperature, this result points toward a more complex mechanism for the adsorption of the trace gas. This general finding was confirmed in the more detailed packed ice bed studies by Clapsaddle and Lamb[59] (CL) and Conklin et al.[60] (CO), who studied the sulfur dioxide uptake for temperatures approaching the ice melting point.

In these studies, the breakthrough curve for sulfur dioxide in the packed ice bed was measured under very similar experimental conditions. In the Conklin study, the ice was melted at the end of the experiment and the amount of sorbed sulfur dioxide was determined by liquid-phase analysis. In contrast, in the CL study, the total uptake of sulfur dioxide was determined by integrating the breakthrough curve. The main difference between the two studies was the different lengths of the packed ice beds and the different experimental time scales (in the hour range for the Co study and up to 2 days for the CL study).

Diehl and co-workers[61] (D) exposed small ice spheres to 1 ppmv of sulfur dioxide for time scales of 10−30 min and determined the uptake by liquid-phase analysis of the melted ice.

Langenberg[449] (L) studied the uptake of sulfur dioxide on ice using an ice coated capillary.[450] In this work, small pulses of a mixture of sulfur dioxide and $SF_6$ pass an ice coated capillary. The different retention times of $SF_6$ and $SO_2$ in the ice column allow inference of the adsorption isotherm for $SO_2$ using theoretical methods commonly used in gas chromatography.[451] In contrast to the case of measuring a breakthrough curve, no saturation of the ice column has to be awaited. Rather, the migration of the $SO_2$ molecules along the ice surface is studied directly, as the shortened time of a $SO_2$ molecule to pass the ice column, the retention time, is measured directly. In the analysis, it was assumed that the $SO_2$ uptake is governed by a Langmuir isotherm, which allows determination of the Langmuir adsorption constant.

Recently, the uptake of sulfur dioxide on ice has been studied using flow tube reactors at stratospheric temperatures between 190 and 228 K. Two studies have been performed with very similar setups. A major difference is the ice preparation method: Chu et al.[429] used vapor deposited ice, while Clegg and Abbatt[62] produced ice films by freezing a wetted flow tube.

**Data Comparison.** When comparing the results of the diverse studies, one must keep in mind that very different types of ice, such as vapor deposited ice,[429] smooth ice films,[62] packed ice beds,[59,60] or frozen ice spheres,[61] have been used. Furthermore, the experimentally applied exposure times range from a few seconds[62,429] to several days.[59] Thus, differences in morphology and time scale render a direct quantitative comparison difficult. However, a quantitative correlation of the presently available data illustrates our limited understanding of the nature of the sulfur dioxide/ice interaction.

Figure 35 shows all available data for $SO_2$ uptake on ice as a function of the $SO_2$ partial pressure for various temperatures. The data are given as uptake per surface area, as it is given in most of the original studies. There are two exceptions. Clapsaddle and Lamb (CL)[59] gave their data in terms of volume uptake. We have converted these numbers to a surface coverage using the average surface area of 3.17 $m^2$ for conversion, as was done in ref 172. Also, the data from Diehl et al.[61] were given as amount of $SO_2$ dissolved in small ice spheres. We have converted these data to a net uptake per surface area by using the surface area of the ice substrate, which was an ice half sphere in the experiment.

**Table 9. Studies on Sulfur Dioxide Uptake on Ice**

| author | method[a] | $T$ (K) | $p$ (Torr) | uptake ($\times 10^{15}$ molecules $cm^{-2}$) | time scale |
|---|---|---|---|---|---|
| Sommerfeld and Lamb[261] | PB | 243−270 | $7.6 \times 10^{-4}$ to $3.8 \times 10^{-3}$ | | |
| Clapsaddle and Lamb[59] | PB | 243−268 | $1.4 \times 10^{-5}$ to $7 \times 10^{-5}$ | $10^{-3}$ to 0.04[b] | up to 2 days |
| Conklin et al.[60] | PB | 213−272 | $5 \times 10^{-5}$ to $6.8 \times 10^{-5}$ | $10^{-4}$ to $10^{-3}$ | hours |
| Langenberg[449] | ICC | 210−260 | $7.6 \times 10^{-3}$ to $1.5 \times 10^{-5}$ | $\approx 10^{-6}$ to $10^{-5}$ | <5 s |
| Diehl et al.[61] | IS | 254, 243 | $7.6 \times 10^{-4}$ | 0.02−0.08[c] | 10−30 min |
| Chu et al.[429] | FT | 191 | $1.3 \times 10^{-6}$ | $10^{-3}$ | <30 s |
| Clegg and Abbatt[62] | FT | 228 | $10^{-4}$ to $10^{-6}$ | $10^{-4}$ to $10^{-3}$ | <5 s |

[a] IS, uptake on ice spheres of 3.6 mm diameter; PB, packed ice bed studies; ICC, ice coated capillary; FT, flow tube. [b] Original work, 1−50 nmol/g; converted to surface coverage using the average ice surface area as described in ref 172. [c] Original work, 0.1−0−0.3 mg/L: converted to surface coverages by distributing the absorbed amount of $SO_2$ onto the ice sphere surface.

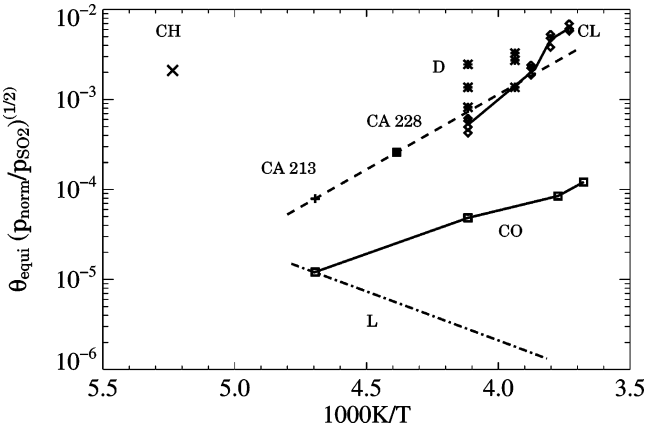


**Figure 36.** Sulfur dioxide uptake on ice, normalized to $p_{norm} = 10^{-6}$ Torr, assuming a $p_{SO_2}^{1/2}$ dependence on $SO_2$ partial pressure by $\theta_p = \theta(p_{SO_2})(p_{norm}/p_{SO_2})$. Symbols are as in Figure 35. Filled square, uptake on ice frozen from deionized pH 6 water as given by Clegg and Abbatt;[62] point, taken from dotted line in Figure 35 for $p_{SO_2} = 10^{-6}$ Torr; dashed line, extrapolated temperature dependence, as given by Clegg and Abbatt,[62] solely based on their measurements at 213 and 228 K; dashed−dotted line (L), Langenberg.[449]

**Dependence on $SO_2$ Partial Pressure.** Some general trends of the data can be observed immediately. Most pronounced, the proportionality $\theta \propto p^{1/2}$, as expected for a dissociating gas, has been shown in the CA study for 228 K. This corroborated the finding of CL for temperatures between 243 and 268 K. However, because these latter data cover less than an order of magnitude of variation in $SO_2$ partial pressure, a $p^{1/2}$ dependence could not be determined with certainty. Furthermore, the Diehl (D) data might be considered as roughly consistent with the CL data, by extrapolating the $\theta \propto p^{1/2}$ proportionality from the CL data toward higher pressures. Similarly, the work of Langenberg (L)[449] showed rising uptake with increasing $SO_2$ partial pressure.

The general trend of rising uptake with sulfur dioxide partial pressure can be found *within* a specific data set. However, when comparing the absolute amounts of uptake as reported in different studies, large disagreements occur. For example, there is a factor of 70 difference between the reported amounts of uptake in the two packed ice bed studies (CO and CL). Similarly, at low temperatures, the data of the CA, CH, and L studies scatter widely.

**Impact of Ice Acidity.** The impact of impurities on the total amount of $SO_2$ uptake on ice has been demonstrated by Conklin,[60] who investigated the $SO_2$ uptake on ice, which was frozen from salt solutions. Also, the acidity of the ice plays a key role. Clegg and Abbatt[62] performed uptake experiments on different ice films, which were frozen from deionized water and from acid and basic solutions. They could show that there is less $SO_2$ uptake on ice which is grown from acidic solutions while the uptake rises under basic conditions (see Figure 35).

**Anomalous Temperature Dependence.** Because the dissociation of sulfur dioxide can be expected and the proportionality $\theta \propto p^{1/2}$ has been shown for the data sets from CL and CA on pure ice, we normalize the data sets to a pressure of $p_{norm} = 10^{-6}$ Torr by $\theta_p = \theta(p)(p_{norm}/p_{SO_2})^{1/2}$ in Figure 36.

This representation enhances the consistency among the different studies. The possibly most interesting feature in this plot is that the $SO_2$ uptake increases with rising temperature (data from CO, CL, and CA), which is in contrast to the behavior of typical adsorptive gas−solid equilibria. The equilibrium uptake is expected to rise toward lower temperatures, unless energy is needed to transfer molecules from the gas to the solid phase. It has been pointed out by CA that assuming an Arrhenius temperature dependence allows the data from CL and CA to be brought into consistency. Given the scatter, the D data could also be considered in consistency with this assumption. However, it must be pointed out that neither in the CL nor in the D experiment was equilibrium reached. Thus, the good coincidence between the CA, CL, and D data would be less if the experiments had been performed for longer exposure times.

In contrast, the data from CO, CH, and L differ by more than an order of magnitude from the CL, D, and CA data. This difference is quite surprising for the CO data, as both CL and CO performed packed ice bed experiments using almost identical experimental setups. This difference can in part be explained in terms of different exposure times: see the next subsection. The comparably high uptake observed by CH could, in principle, be attributed to a high porosity of the vapor deposited ice films used in this study. However, the overall difference of a factor of $10^4$ between CA and CO appears very high, compared with the reported porosities, which suggests a factor of 10−100 difference at most[79] between the internal and the geometric surface areas.

In contrast to all other studies, the L data show a classical temperature dependence: the uptake of $SO_2$ rises with lowering the temperature. Currently, there is no explanation for this contradictory observation. It is conceivable that the measurements of the retention time probe a different process compared to the breakthrough curve approach, which is used in all other studies. Langenberg also observed a strong impact of impurities on the $SO_2$ uptake. He observed an anomalous temperature dependence, once he changed the chemical treatment of the glass capillary, which hosts the ice film. Currently, there is no generally accepted explanation for the anomalous temperature dependence. There is some limited evidence that the anomalous temperature behavior merges into a normal adsorption behavior ($\partial\theta/\partial T < 0$) at low temperatures.

**Evidence for Diffusive Processes.** It has been noted that, in the experiments from CL, thermodynamic equilibrium has never been reached,[172] even in experiments which lasted up to 2 days. Furthermore, a long-lasting tailing with diffusion-like kinetics has been observed. Thus, the CL experiments do not necessarily manifest a measurement of the equilibrium coverage. The tailing has been analyzed using eq 103.[172] The results were comparable to those of a similar analysis of HCl uptake experiments.[214] The data display a proportionality $H_d^* D^{1/2} \sim p^{-1/2}$, as expected for the diffusion of a dissociating gas. Furthermore, as shown in Figure 37, the experimentally observed temperature dependence of $H_d^* D^{1/2}$ is consistent with the temperature dependence of the product $H_d^* D^{1/2} \times r_v$, where $H_d^*$ and $D$ are the solubility and diffusivity of $SO_2$ in liquid water and $r_v$ is the vein radius (see eq 42).

This analysis suggests that the tailing regime of the CL data is dominated by the diffusion of $SO_2$ into the veins of polycrystalline ice, based on these arguments:[172] First, the tailing shows a diffusion-like kinetics. Second, the kinetic parameter $H_d^* D^{1/2}$ shows a $p^{-1/2}$ dependence, as expected for a trace gas diffusing into a liquid or liquidlike environment. Third, the temperature dependence of $H_d^* D^{1/2} \times r_v$ can be

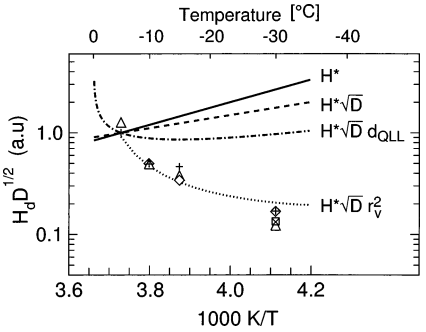


**Figure 37.** Temperature dependence of $H_d^* D^{1/2}$ for $SO_2$ uptake into packed ice beds. Data are normalized to the value at −5 °C. Symbols: $H_d D^{1/2}$, as derived from breakthrough curves of the CL study;[59] solid line, solubility of $SO_2$ in water; dashed line, $H_d^* D^{1/2}$ for $SO_2$ in water; dashed−dotted line, $H_d^* D^{1/2} \times d_{QLL}$ for uptake into a quasi-liquid layer (QLL), assuming $d_{QLL} = T_0/(T - T_0)^{1/3}$ (see eq 38); dotted line, $H_d^* D^{1/2} \times r_v^2$ for uptake into veins (see eq 42). (Reprinted with permission from ref 172. Copyright 2001 Elsevier.)

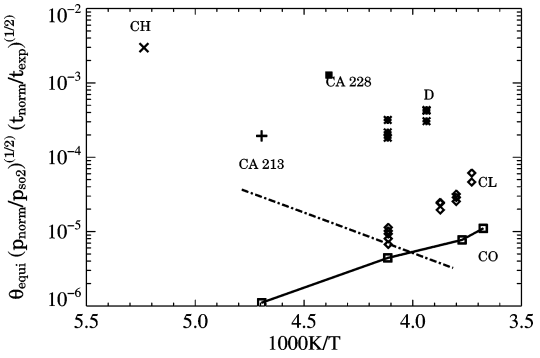


**Figure 38.** Sulfur dioxide uptake on ice, normalized assuming a $p_{SO_2}^{1/2}$ dependence on $SO_2$ partial pressure and a diffusion-like uptake kinetics by $\theta_p = \theta(p_{SO_2})(p_{norm}/p_{SO_2})(t_{norm}/t_{exp})^{1/2}$ with $p_{norm} = 10^{-6}$ Torr and $t_{norm} = 30$ s. Symbols are as in Figure 35. Assumptions for the experimental time scale for different studies: CA and CH, 5 s; CL, taken from raw data; CO, 1 h; D, 10−30 min, taken from Figure 6 in ref 61; L, 5 s. Note that the time scales for CA, CO, and CH are order of magnitude estimates based on the information given in the original studies. For guidance of the eye, the CO data have been connected by a line.

explained by the temperature-dependent size changes of triple junctions.

**Time Dependence of the Uptake.** A diffusion-like kinetics often occurs in $SO_2$ uptake experiments. For example, long-lasting tailing has been observed in the CL study with experimental exposure times of up to 2 days. Similarly, the data in the Diehl study did not saturate within experimental time scales. In contrast, only very little tailing was reported in the CA study where experimental times in the 30 s range were used. These very different time scales, and moreover the difficulties of establishing a surface saturation in the CL and D study, cast doubt on the attempt to compare experiments ranging from a few seconds to several days quantitatively without taking the time dependence into account.

To explore the impact of diffusion-like processes, one might try to further normalize the existing data by calculating the quantity $\theta(p_{norm}/p_{SO_2})^{1/2}(t_{norm}/t_{exp})^{1/2}$. Here the last term accounts for the diffusion-like kinetics. If the system was governed completely by diffusion and dissociation, for a given temperature, all data points should collapse onto one line as a function of temperature. Figure 38 shows that this model brings the packed ice bed data, which differed by up to a factor of 80, into better consistency within a factor of 2 to 8. Also, the scatter within the data points of the Diehl data set is reduced. However, it is obvious from Figure 38 that the simple assumption of diffusive kinetics is not sufficient to bring all studies into consistency.

**Summary.** This section offers a systematic comparison of all presently available data for $SO_2$ uptake on ice. First, the total uptake follows a $p^{1/2}$ law, as expected of a dissociating species. This enables elimination of the partial pressure dependence.

Second, there is compelling evidence that there is an anomalous temperature dependence when $SO_2$ is taken up by ice: the uptake per surface area rises toward higher temperatures ($\partial\theta/\partial T > 0$). This effect has been observed for a large temperature range from 213 to 273 K both in long-lasting packed ice bed experiments and in flow tube experiments on a much shorter time scale.

For quantitative comparison, the data may be grouped into subsets. The flow tube data (CH, CA) at temperatures below 228 K were obtained within time scales of less than a minute. In contrast, there are data sets at temperatures above 240 K with long time scales of minutes to hours (D, CO) and even days (CL). In the latter experiments, the gas−solid equilibrium was possibly never completely established, despite the long exposure time.

Based on the available data, there are arguments which favor the dominance of diffusive processes and others which point against it. The consistency between the CL, CA, and, to a lower extent, D data, in terms of the temperature dependence (dotted line in Figure 36), could be interpreted as due to $SO_2$ being taken up onto the surface with some complex, yet unknown, uptake processes with anomalous temperature dependence following an Arrhenius type law. The fact that these studies cannot be brought into consistency by assuming a diffusive kinetics does not support the importance of diffusive processes. The observed tailing in the packed ice bed studies would then have to be interpreted as the dispersion of the gas when flowing through the porous packed ice bed. This picture leaves the anomalous temperature dependence unexplained.

However, there is also evidence for diffusive processes, based on the packed ice bed experiments, which use highly polycrystalline ice. The packed ice bed experiments from CO and CL can be brought into close (but not complete) agreement by assuming a diffusion-like kinetics. The quantity $H_d^* D^{1/2}$ follows a $p^{1/2}$ law, as expected for the diffusion of a dissociating species. Furthermore, the anomalous temperature dependence could be explained with the uptake into veins. However, in this picture the difference in magnitude between the packed ice bed studies and the flow tube studies remains unexplained.

Thus, both pictures cannot fully explain the differences between the existing data sets. The analysis presented so far does not take into account that the ice has been made in very different ways in different studies. Important morphological parameters, such as the degree of polycrystallinity, may be very different in the flow tube studies by CA and the packed ice bed studies by CO and CL. Thus, these experiments might have been sensitive to very different physical processes, which may explain the differences. Furthermore, it is conceivable that different physical processes are dominant at different temperatures. For example, as veins and grain boundaries might dominate at higher

temperature, their impact is expected to be larger at higher temperatures, as used in the packed ice bed experiments. In the flow tube studies, which were performed at lower temperatures and on smooth, and possibly less polycrystalline, ice films, less impact of such confined reservoirs may be expected. Also, it has been shown that the ice purity may play an important role for uptake processes. Such parameters may explain why the results of the different studies are so different.

Clearly, it is not possible to resolve these issues on the basis of the currently available data sets. For resolution, uptake experiments with one setup and ice of similar purity and well defined morphology over larger temperature and pressure regimes would be needed.

## 8.9. Impact of Other Impurities on the Trace Gas Uptake

An important but often ignored aspect is how the uptake of one trace gas is influenced by the presence of a second trace gas or by impurities already present in the ice. There are mechanisms by which different absorbed impurities may interact with each other on the ice surface or in the ice bulk. First of all, for adsorbed species, only a limited number of sites is available and the different adsorbed species may compete for the same sites. An example for such competitive adsorption may be found in the work of Hynes et al.,[255] who showed that the presence of $HNO_3$ may displace already adsorbed HCl from the ice surface. Similarly, Chu and Chu[171] showed that the adsorption of HCl decreases with increasing HBr partial pressure. However, as this study was performed in the hydrate stability domain, it is unclear whether the formation hydrates had any impact on the measurements. In contrast to such displacement effects, Marti and Mauersberger[275] showed that the amount of HCl dissolved into ice increases with increasing amount of $HNO_3$ in the ice.

Besides the competition for the same surface sites, there are many reasons why acids may interact with each other when taken up onto ice. First of all, acids likely dissociate on the surface. They are surrounded by ions and mobile water molecules. Therefore, acid−base equilibria may play an important role in uptake processes. Such effects are supported by several studies, such as the observed pH dependence of the $SO_2$ uptake on ice[62] or the experiments of Hynes et al.[255] and Chu et al.[171] which showed the displacement of one acidic trace gas by the presence of another one.

Another issue is the potential impact of confined reservoirs, such as grain boundaries, veins, or a premelt surface layer, on the trace gas uptake. The size of these reservoirs strongly depends on the temperature but also on the amount of dissolved nonvolatile impurities.[80,113,132,141,142,147] When ice freezes, nonvolatile impurities accumulate in grain boundaries or triple junctions to high concentrations and it has been shown experimentally that these impurities indeed govern the reservoir size[141,142] at temperatures close to the ice melting point. Furthermore, it has been argued that, due to the high concentrations in confined reservoirs, the oxidation of dissolved nitrogen oxides[452,453] is enhanced during the freezing of ice. Thus, it is clear that confined reservoirs affect impurities in ice and that, in turn, confined reservoirs are affected by impurities. Also, the anomalous temperature dependence of the $SO_2$ uptake into ice, which may be explained with the dissolution of $SO_2$ into impurity filled triple junctions,[172] indicates the importance of such reservoirs.

Based on this evidence, it may be speculated that these reservoirs may act as a chemical buffer for the trace gases taken up. Therefore, it must be suspected that the ice purity also plays an important role in uptake experiments of trace gases on ice.

## 8.10. Impact of Nonequilibrium Processes during Trace Gas Uptake on Ice

Due to its high vapor pressure, the ice surface is highly dynamic. For example, at 200 K the ice vapor pressure is around 3 mTorr. In nature, ice is seldom in thermodynamic equilibrium. For example, in lee-waves of ice clouds, temperature changes of as fast as 10 degrees per hour may occur.[454] Such fast changes of the thermodynamic conditions strongly affect the composition of aerosol ensembles.[454] The impact of the ice growth rate on trace gas uptake has been modeled by Dominé and Thibert,[455,456] who suggested that the mixing ratio in the ice can be calculated by considering the kinetic limit $x_{HCl} = (\alpha_{c,HCl}/\alpha_{c,water})[p_{HCl}/p_{water}(M_{water}/M_{HCl})^{1/2}]$, while, for slower growth rates, a model involving the growth of steps on the ice surface was formulated. Very recently, Kärcher and Basko[457] suggested a theoretical model which describes the trapping of adsorbed trace gases in the bulk of growing ice for a whole range of growth rates including the kinetic limit. For HCl, this effect has been shown in Knudsen cell experiments.[250] Here, the net uptake of HCl into growing ice was investigated under steady state conditions. It could be shown that the HCl mixing ratio in the ice rises with increasing growth rate (see Figure 39). Furthermore, for very fast ice growth rates, the kinetic limit is observed, where the uptake of water and HCl is solely limited by the rate of HCl and water molecules hitting the ice surface, in consistency with the model developed by Domine et al.[455] Ice and hydrates, which are grown from various gaseous HCl/water mixtures, have been investigated spectroscopically, and it could be shown that the HCl likely dissociates and that the structure of the solids has some disorganized character.[458]

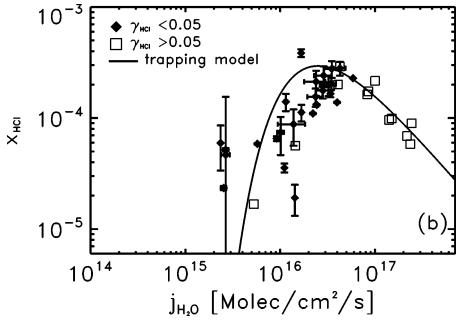


**Figure 39.** Mixing ratio of HCl in ice as a function of the net ice growth rate under steady-state growth conditions at 203 K: filled diamonds, data with $\gamma_{HCl} < 0.05$; open squares, data with $\gamma_{HCl} > 0.05$; solid line, trapping model for uptake in growing ice assuming that adsorbed molecules are buried in the ice after a finite residence time on the ice surface. The decreasing mixing ratio for high growth rates is consistent with the kinetic uptake limit as suggested by Dominé and Thibert.[455] (Reprinted with permission from ref 250. Copyright 1999 Cuvillier-Verlag.)

# 9. Outlook

In this review, we have detailed the state of the art of experimental findings about the uptake of acidic gases on

ice. Here we summarize the main findings, formulate open questions, and suggest future avenues of research.

During recent years, major technical improvements of the experimental techniques have been made. Today, sophisticated flow tubes and Knudsen cells, in combination with improved ice preparation techniques, allow highly reproducible experiments, as the survey of flow tube studies on $HNO_3$ demonstrates. These improvements will allow performance of uptake studies with accuracy sufficient to explore both the overall magnitude of the uptake and the detailed kinetics. Particular emphasis should be placed on new techniques, which allow distinguishing of bulk and surface processes, such as nonlinear optical techniques.[115,287,289] Also, nondestructive profiling techniques for the near-surface region, such as Rutherford backscattering,[294,295] might be useful.

As the processes involved are a complex interplay of surface adsorption, dissociation, and possibly diffusion, new numerical models will be required. For example, coupling of Langmuir adsorption and diffusion into the bulk could be used to describe the kinetics of the HCl uptake into vapor deposited ice.[214] Such models should be developed to further analyze the kinetics of uptake experiments in flow tubes and Knudsen cells, to address issues such as the irreversibility of uptake processes or to aim toward improved interpretation of complex promising experiments, such as the dope and probe technique developed by Rossi and co-workers.[241]

## 9.1. Key Experimental Results and Open Questions

**Impact of Ice Morphology.** There is clear evidence that the morphology of ice is important for uptake processes on and into ice. Key results are the faster diffusion of HCl and HBr in polycrystalline ice compared to single crystalline ice[241,398] and the observation that the amount is strongly dependent on the thickness of porous ice films.[24,25,79,252] The consistency in measured uptake between different studies on HCl uptake on porous ice films is limited. This may be due to uncertainties in the internal surface area, which may be determined by BET measurements (see Table 4) or porosity models.[21,24,79,252] To limit the impact of the ice morphology in uptake experiments, future work should be pursued on well controlled ice samples. One approach was suggested by Abbatt,[42] who produced smooth ice films by freezing water on the walls of a glass flow tube. Future studies should also aim to use single crystals to exclude the impact of diffusion into grain boundaries.

**Uptake Kinetics and Shape of Breakthrough Curves.** The breakthrough curve has a similar shape for all strong acids (i.e. for HCl and $HNO_3$) on all types of ice. An initial period of high uptake is followed by a long-lasting tail with diffusion-like kinetics. Different methods, such as using the two-third criterion or asymptotic fitting, have been used to treat the tail. Less evidence for the formation of a tail exists for the weaker acids $SO_2$ and HONO in flow tube studies. Conversely, for $SO_2$, a diffusion-like tail has been observed in packed bed experiments.

Little is known about the physical nature of the diffusion-like part of the uptake. The kinetics by itself does not unambiguously reveal the physical nature of the uptake process, as the reservoir is not yet identified. Transport processes into confined large reservoirs, such as grain boundaries, veins (triple junctions), or pores, are slow processes that are conceivably responsible for the persistent uptake. But also, slow nondiffusive processes, such as surface roughening or restructuring of the surface, might be an explanation for the tail. In the case of HCl, the parameter $H_d^* D^{1/2}$, which would represent the diffusion-like kinetics of the tail, is quite similar for uptake processes on vapor deposited ice films, whether they are several micrometers thick[83,214] or as thin as a few nanometers.[22] Based on this observation, one may argue against diffusion into confined reservoirs, as the density of confined reservoirs should be very different in these different types of experiments. Because the nature of the tail remains unresolved, the question arises whether it could be an experimental artifact which has to be excluded in the analysis of uptake experiments or whether it is rather an essential feature of the acid/ice interaction.

A diffusion-like uptake was observed in very different experimental designs probing the gas phase (flow tubes,[42,83] packed beds,[59,295] Knudsen cells[214]). Also, experiments probing the condensed phase showed that significant amounts of HCl are distributed in the near-surface region of ice (using RBS[294−296] and the dope and probe technique[241,398]). This wide range of observations suggests that the tailing is not an experimental artifact.

Depending on the experimentally applied exposure times, the overall uptake in the tail can amount to as much as several monolayers[22,214,243] and may substantially exceed the uptake during the initial period, which is dominated by adsorption processes with typically 0.1 monolayer for HCl and $HNO_3$. The importance of this phenomenon for natural systems will ultimately depend on the lifetime of the ice. The lifetimes of natural ice vary from minutes in clouds, to days and weeks in snow and firn, to many years in glaciers and ice cores. Thus, when using results from laboratory experiments in atmospheric models, the lifetime of the ice—next to its morphology—could be a key factor when including parametrizations of uptake processes on ice in atmospheric models.

In summary, the issue of diffusion-like uptake should again be addressed in future laboratory research. This should be pursued by forcing those techniques which did not show a diffusive uptake tail to longer time scales, by analyzing the condensed phase concerning the total amount taken up, by spectroscopic investigation of the near surface region of ice, and by intercomparing different experimental setups working on ice with the same morphology.

**Reversible and Irreversible Uptake.** Irreversible uptake has been found in uptake experiments on HCl[28,213] and $HNO_3$.[42,215] For $HNO_3$, it could be shown that the uptake during the tailing period is largely reversible, while this is not the case for the initial uptake period.[215] Furthermore, in uptake experiments with HCl[214] and $HNO_3$,[42,215] it was found that there is less adsorption in a second repeated uptake onto previously exposed ice. For HCl, the kinetics of the repeated uptake was shown to be almost perfectly diffusion-like.[214]

These observations support the concept that the long-lasting tail and the initial uptake are indeed two different processes. Possibly, the trace gas is first adsorbed irreversibly into a strongly bound state at the surface. The experimental observation that HCl and $HNO_3$ can displace each other suggests that both acids compete for the same sites on the ice surface.

It is noteworthy that the observation of irreversibility in the early uptake violates the simple physical picture of physisorption, e.g. as assumed for Langmuir type adsorption. This should reveal simple first order kinetics between the gas phase and the surface. In the low coverage regime, as was experimentally observed at low partial pressures for HCl

and $HNO_3$, detailed balance at the surface requires that a kinetic equilibrium will be established after a short time with equal adsorption and desorption rates at the surface, which implies reversible desorption of adsorbed molecules. Conversely, one would argue that signs of irreversibility in a fraction of the uptake call for a few adsorption sites which differ considerably (i.e. bind the adsorbate much more strongly) compared to the other sites, or reconstruct the ice surface itself.

Basically, the adsorbate would be required to form a bound state with the ice molecules with stronger binding than the $H_2O-H_2O$ bond. Given the highly dynamic nature of the ice surface (due to its high volatility), such states should immediately be subject to burial of the adsorbed molecules, which effectively should correspond to a slow diffusion process of these molecules into the depth of the ice. Clearly, here also, some theoretical work is required to achieve progress in understanding.

**Acid Displacement and Impact of Ice Purity on Uptake Processes.** There is experimental evidence that the ice purity may affect the trace gas uptake. Flow tube studies have demonstrated acid−base displacements on the ice surface for the HCl/$HNO_3$ system[255,406] in the ice stability domain and for the HCl/HBr system[171] in the hydrate stability domain. In contrast, it has also been shown that the presence of $HNO_3$ can enhance the amount of HCl when dissolving into vapor deposited and $HNO_3$ doped ice.[275] Furthermore, studies of $SO_2$ uptake on ice showed that the amount of $SO_2$ taken up onto ice is strongly influenced by the presence of salts[60,84] or oxidants, such as $H_2O_2$.[60,62]

Further research on this issue is important, because atmospheric ice is never clean but, rather, several acids, such as $HNO_3$, HCl, HBr, organic acids, and other trace gases, adsorb simultaneously on the ice surface. These gases compete for free sites and, furthermore, may interact with each other, e.g. by acid−base equilibria.

A second, possibly important, but widely unexplored issue is the purity of the ice sample used in an uptake experiment. When ice is frozen from liquid water, remaining impurities will be largely expelled from the ice grains and accumulate in grain boundaries, in veins, and also on the ice surface itself. As these confined reservoirs are very small compared to the volume of the total ice sample, very high impurity concentrations occur in the confined reservoirs. It is possible that such effects have some influence on uptake processes and are part of the explanation why different studies find different results. There is also evidence that these effects may play a role in chemical reactions, such as the oxidation of nitrogen oxides.[452]

**Impact of Nonequilibrium at the Ice Surface.** It has been suggested theoretically[455,457] and investigated experimentally[250,456] that growth and evaporation processes affect the uptake of trace gases on ice. Under natural conditions, ice is only seldom at equilibrium with the gas phase. Therefore, such effects may be of high importance in nature and are an important theme for future studies.

## 9.2. Quantitative Comparison of Different Studies

Sections 7 and 8 provide quantitative comparison of different studies. There are major differences in measured total uptake, in the observed pressure and temperature dependencies, and in the observed uptake kinetics. We summarize the main results of this comparison.

**Magnitude of Uptake.** For both HCl and $HNO_3$, there is a consistent picture about the amount of uptake among the newer flow tube studies. For $HNO_3$, about 0.2 formal monolayers are the maximum uptake.[215,255] For HCl, the uptake during the initial period is about 0.1 formal monolayers at a partial pressure of $10^{-6}$ Torr and a temperature of 200 K. This result is derived from flow tubes with smooth ice films. In the case of HCl, this result holds for experiments on smooth ice films,[213] but also on thin vapor deposited ice films, as long as the uptake is calculated during the initial period, which occurs before any long-lasting tailing.[79,214,217,249,275,405]

While there is good convergence in measurements at 200 K and $10^{-6}$ Torr HCl partial pressure, less consistency is found when considering larger pressures and temperature ranges. Moreover, very recent results,[21,217] dating from 2003 and 2004, disagree with previous work in magnitude and pressure dependence (see Figure 23). The reasons for the disagreements in magnitude between the different studies are unclear, but possible reasons are shorter experimental exposure time scales,[217,405] scaling of the data on the internal surface area,[21] and using single crystalline ice particles.[405]

**Pressure Dependence.** In short, for both HCl and $HNO_3$ uptake on ice, there are two competing results. Flow tube studies which evaluate the initial part of the overall uptake point toward a Langmuir type isotherm, with a saturation coverage of 0.1−0.2 formal monolayers. For $HNO_3$, a recent flow tube study suggests using a nondissociative adsorption isotherm.[215] In contrast, a multilayer adsorption isotherm without any saturation has also been used to model the results of Knudsen cell experiments, for pressures high enough to allow hydrate formation.[243] In experiments with HCl on vapor deposited ice, a pronounced $p^{1/2}$ law without any saturation effects has been observed for the total uptake[214,252] and also for the quantity $H_d^* D^{1/2}$,[214] which is consistent with diffusive kinetics. Furthermore, two recent studies suggested adsorption isotherms with very strong pressure dependencies (i.e. stronger than $x \propto p^{1/2}$).[21,217] It is noteworthy that strong rises of the adsorption are frequently observed, once acid pressures are (almost) high enough to form hydrates.[21,217,243] However, it must be pointed out that this does not imply the formation of hydrates. For example, Hudson et al.[243] reported strongly rising uptake under such conditions but did not find any spectroscopic evidence for hydrate formation.

Thus, there is limited agreement among the different studies, except that similar results are obtained when using the same setups and similar data evaluation procedures. For example, the flow tube studies for $HNO_3$ uptake on ice demonstrate the reproducibility of such experiments.

**Temperature Dependence.** The temperature dependence of uptake processes of strong acids, such as HCl and $HNO_3$, shows increasing uptake with increasing temperature, but the observed temperature trends differ considerably between different studies. In contrast, the weak acid $SO_2$ was shown in several studies to have an anomalous temperature dependence; that is, the uptake increases with rising temperature. While it has been suggested that this could be explained by the temperature dependence of the vein system in polycrystalline ice,[214] there is currently no direct experimental evidence for this hypothesis.

**Reasons for Differences between Different Studies.** The reasons for the discrepancies between different studies are unclear. The notion that the uptake process is a composite process, consisting of a bulk (diffusive) and a surface

component, may be key to the explanation. These two components of the uptake may have quite different dependencies on temperature and pressure. For example, the solubility of a dissociating species in the ice crystal matrix follows roughly a $p^{1/3}$ dependence,[73,74,167] and the dissolution into liquidlike reservoirs is expected to obey a $p^{1/2}$ law. In contrast, there might be a nondiffusive component, showing a saturation for higher HCl partial pressures, as has been suggested by Hynes et al.[213]

Thus, it is likely that experiments with long exposure times are more sensitive to bulk processes, while short time scales of seconds are sensitive to the adsorption on the ice surface itself. Furthermore, different ice morphologies, such as different densities of grain boundaries and different roughnesses of the ice surface, may lead to different sensitivities to a specific process. We also note that it has been argued that applying different methods to treat the tailing from the breakthrough curve when analyzing breakthrough curves from the same data set may lead to different results for the pressure dependence.[214]

We like to stress that there is no generally accepted explanation for the quantitative differences between the different studies. Different authors invoked arguments about the ice porosity and different relative importances of bulk and surface processes. Moreover, even the nature of the uptake process is discussed controversially, as the physical concepts include Langmuir type adsorption, uptake into a surface premelt layer, which may form under the influence of trace gases, or diffusion into confined reservoirs.

## 9.3. Conceivable Reservoirs and Uptake Processes

From this review, it is clear that the physical nature of a trace gas uptake on ice is surprisingly poorly understood. There are several conceivable reservoirs and basic processes for the trace gas uptake on ice. In this section we will briefly summarize the consistency of the various possible reservoirs within the experimental observations.

**Adsorption on the Ice Surface.** The adsorption of trace gases on the ice surface appears to be an important uptake process. However, different adsorption isotherms have been invoked, for example, for $HNO_3$, the nondissociative Langmuir adsorption isotherm with surface saturation[215] and a multilayer isotherm without saturation.[243] Similarly, theoretical and experimental concepts have been used for HCl which are incompatible with each other.[21,213,217] It should also be noted that solid surfaces are not necessarily flat on an atomic scale. Interfaces have some degree of roughness: steps, kink sites, and terraces form, each with a different adsorption energy. Currently, little is known about the impact of such microscopic structure on the adsorption process, but one may speculate whether such sites may also be a reason for disagreement between different studies.

**Grain Boundaries and Veins.** In addition to surface defects, such as steps and kink sites, there are also defects in the bulk ice. Grain boundaries and veins occur naturally in polycrystalline ice and may host impurities.[11,81,459] The diffusion into such reservoirs is a likely candidate to explain the tailing of the breakthrough curve. In this picture, the first part of the breakthrough curve would be due to uptake on the ice surface itself. The tailing would be due to the diffusion into the grain boundary and veins, with kinetics governed by $H_d^* D^{1/2}$, where $H_d^*$ would be the average solubility in the ice, including grain boundaries. The experimentally observed proportionality $H_d^* D^{1/2} \propto p^{-1/2}$ supports this model, which is consistent with the dissociation of HCl in a liquidlike reservoir. However, the fact that the tailing is also observed on very thin ice films may be taken as an argument against grain boundaries and veins as reservoirs, simply because the diffusion through such thin films should be sufficiently fast to penetrate the entire film.

**Surface Disorder (QLL) and Surface Restructuring.** At temperatures around 200 K, there is no or only very little surface disorder[93,115,361] (see section 1.4). Furthermore, there is theoretical evidence that surface melting is strongly influenced by impurities.[129,132,147] Thus, the strong interaction of HCl with the ice surface may induce surface disorder, which is a thermodynamically stable layer on the ice surface. If the formation kinetics of this layer is slow, for example limited by solid state diffusion, this concept might also explain the slow development of the breakthrough curves and why a quantitatively similar tailing is observed both on vapor deposited ice and on ice which is grown from liquid water. Closely related, or possibly equivalent, is the picture that the ice surface is slowly restructured by the presence of the gaseous HCl. We note that, for the $SO_2$ ice system, long-lasting restructuring processes have been reported at low temperatures.[355]

However, despite the frequent notion that trace gases dissolve into a quasi-liquid layer on the ice surface, currently there is no experimental evidence for this process, and without very slow continuous restructuring, the QLL is by far too thin to explain the kinetics. If trace gases induce surface disorder, the concept of surface adsorption might become invalid, because the trace gas would change the nature of the interface during the interaction. If the time scale for reconstruction is very slow, the uptake of trace gas on ice should not only be given in terms of total uptake but should also contain information about the time scale of the uptake process (see ref 214).

**Roughening of the Ice Surface.** We also note that, based on optical techniques, a roughening of the ice surface has been reported.[22,135] The nature and kinetics of such processes on the ice surface are widely unexplored. However, the kinetics of surface roughening, and hence the formation of a new microscopic ice surface, is controlled by stochastic processes, such as surface diffusion, and the ongoing fluctuations of the ice surface due to condensation and evaporation of the water molecules. Thus, also, the overall kinetics may turn out to follow a $t^{1/2}$ law, as characteristic for such processes. While such processes have been investigated on solids of low volatility,[460] such effects are widely unexplored on the ice surface.

**Summary.** In summary, several conceivable reservoirs and processes may play an important role when acidic trace gases are taken up onto ice. Apparently, none of these concepts can explain all experimental observations. This lack of understanding may be one of the reasons why uptake experiments have been interpreted in terms of surface adsorption by some authors, while other authors invoke bulk processes or a mixture of both. Thus, the nature of the uptake process of acidic gases on ice appears unresolved and further research is needed to decipher the fundamental processes, to determine the relative importance of bulk and surface processes, and to resolve scientific controversy on this issue.

### 9.4. Future Lines of Research

Clearly, despite intense efforts, there is a surprising lack of understanding of the physical nature of the uptake processes. One reason for our limited understanding is the technical challenges associated with the required laboratory experiments. During the past 15 years, many obstacles have been resolved and future research has a good chance to answer open questions.

**Variation of Parameters over Wider Ranges.** It would be of interest to perform flow tube or Knudsen cell experiments with variation of several parameters, such as the partial pressure, the temperature, and the experimental time scale, over wider ranges to constrain the different physical processes. For example, short exposure times would lead to stronger surface sensitivity; longer time scales would be more bulk sensitive. The importance of such thorough approaches has been demonstrated in a recent study by Ullerstam and Abbatt.[215]

**Exploring the Nature of the Acid−Ice Interaction: Bulk or Surface Processes?** Uptake experiments have been interpreted in terms of both surface adsorption and diffusion. Future research may aim to explore the relative importance of pure surface (adsorption) and bulk processes (diffusion). In kinetic experiments, the uptake kinetics should be compared with the various physical processes. Also, other, nonkinetic techniques (e.g. surface sensitive spectroscopy) might directly address the question of whether acids are adsorbed on the ice surface itself, taken up into the near-surface region, or taken up into confined reservoirs, such as grain boundaries or triple junctions.

**Closer Look at the Ice Surface Stability.** Several authors observed changes of ice films with time during the uptake process.[22,135] Here it was argued that the ice surface may become rougher with time. Such effects are widely unexplored, but they are of potential importance, as they may also occur on natural ice surfaces. The development of techniques specifically designed for this purpose would be especially promising.

**More Emphasis on Nonequilibrium Conditions.** Natural ice undergoes continuous growth and evaporation. The impact of the growth is widely unexplored, but recent modeling efforts[455,457] suggested the importance of such effects under tropospheric and stratospheric conditions. Measurements of the trace gas uptake into growing ice indeed indicate that the HCl uptake changes once the ice grows.[250,456] For future work, these issues should be systematically addressed.

**Studies on Ice Purity.** The presence of impurities in the ice may affect the trace gas uptake, as has been shown for the $SO_2$/ice system,[60,434] and to a lower extent for the $HNO_3$/ice system.[215,275] As ice in nature is never pure, it would be very important to systematically study such effects.

**Better Modeling Strategies for Environmental Applications.** From an environmental point of view, one might wonder whether a thorough understanding of the individual fundamental processes is really required. However, many parametrizations depend on extrapolations from laboratory data over wide ranges. Thus, a proper knowledge of the pressure and temperature dependencies is essential in order to avoid detrimental misrepresentations and loss of prognostic capabilities.

**Using New Techniques.** To explore the nature of the trace gas−ice interaction, further experimental developments are needed. Here the use of new techniques that allow the nondestructive investigation of the condensed phase is required with both high depth resolution below the surface and analysis of the surface itself. Here, spectroscopic techniques, such as surface-sensitive nonlinear optical techniques, may play a key role in investigation of surface processes. Nondestructive profiling techniques, such as Rutherford backscattering,[294,296,297] are suited to gaining depth resolution. For lateral resolution, synchrotron based X-ray microspectroscopy may be a very promising tool.[461,462] Furthermore, new third generation synchrotron sources will allow use of tomographic techniques to directly determine the distribution of impurities in three dimensions with micrometer resolution.[463]

## 10. Symbols

*Greek Symbols*

| | |
|---|---|
| $\alpha_c$, $\alpha_{c,i}$ | mass accommodation coeficient, - |
| $\alpha_w$ | partial molar volume of water, - |
| $\epsilon$ | ratio of ice surface covered by confined reservoirs, - |
| $\gamma$ | uptake coefficient, - |
| $\Phi$ | grand canonical potential, J molecule$^{-1}$, J mol$^{-1}$ |
| $\sigma$ | surface energy, J m$^{-2}$ |
| $\sigma_{sv}$ | surface energy of solid vapor interface, J m$^{-2}$ |
| $\sigma_{lv}$ | surface energy of liquid vapor interface, J m$^{-2}$ |
| $\sigma_{ls}$ | surface energy of liquid solid interface, J m$^{-2}$ |
| $\mu$ | chemical potential, J molecule$^{-1}$, J mol$^{-1}$ |
| $\mu^0$ | chemical potential of a standard state, J molecule$^{-1}$, J mol$^{-1}$ |
| $\mu_i^\infty$ | chemical potential, standard state of an infinitely dilute solution, J molecule$^{-1}$, J mol$^{-1}$ |
| $\Delta\mu_{ad}$ | chemical potential of adsorption, J molecule$^{-1}$, J mol$^{-1}$ |
| $\rho$ | density, kg m$^{-3}$ |
| $\rho_p$ | density of porous ice, kg m$^{-3}$ |
| $\sigma_0$ | area of an adsorbed molecule, m$^2$ |
| $\theta$ | surface coverage, - |
| $\theta_e$ | surface coverage on a surface in thermodynamic equilibrium, - |
| $\theta_{equi}$ | equivalent coverage, expressed as net uptake, including bulk and surface uptake |

*Indices*

| | |
|---|---|
| c | condensed phase |
| b | bulk |
| g | gas phase |
| *i* | species number |
| ice | ice phase |
| l | liquid phase |
| q | quasi-liquid layer |
| s | solid phase |
| v | vapor phase |

*Latin Symbols*

| | |
|---|---|
| $a_i$ | specific surface area, m$^2$ kg$^{-1}$ |
| $A$ | surface area, m$^2$ |
| $A_i$ | ice surface area, m$^2$ |
| $A_e$ | size of exit aperture |
| $A_F$ | cross section of flow tube, m$^2$ |
| $A_S$ | sample area in Knudsen cell, m$^2$ |
| $c$ | concentration, mol/L, M, molecule cm$^{-3}$ |
| $D$ | diffusion constant, m$^2$ s$^{-1}$ |
| $E$ | energy, J |
| $f^\infty$ | activity coefficient for an infinitely dilute solution, - |
| $\Delta h_{ad}$ | specific enthalpy of adsorption, J molecule$^{-1}$, J mol$^{-1}$ |
| $h$ | Henry's Law constant defined by $hp = x$, Pa$^{-1}$ |
| $\hat{h}$ | Henry's Law constant defined by $\hat{h}p = x$, for dissociating species, Pa$^{-1}$ |
| $H$ | Henry's Law constant defined by $Hp = n$, m$^{-3}$ Pa$^{-1}$, M atm$^{-1}$ |
| $H_d$ | dimensionless Henry's Law constant defined by $Hn_g = n_c$, - |

| | |
|---|---|
| $H_d^0$ | molecular Henry's Law constant, describes dissolution set prior to dissociation, - |
| $K$ | dissociation constant for the reaction $HY \rightleftharpoons H^+ + Y^-$, $K \equiv n_{H^+} n_{Y^-} n_{HY}^{-1}$, $m^{-3}$ |
| $j$ | molecular flux density, $s^{-1}$ $cm^{-2}$ |
| $k_e$ | escape rate in Knudsen cell, $s^{-1}$ |
| $k_d$ | desorption constant, $s^{-1}$ |
| $k_{ad}$ | adsorption constant $k_{ad} \equiv \alpha_c \bar{v}/4$, $ms^{-1}$ |
| $K_L$ | Langmuir constant, $K_L = k_d/k_{ad} n_{sites}$ |
| $k_B$ | Boltzmann constant |
| $l_m$ | latent heat of melting, J $mol^{-1}$ |
| $m$ | molecular mass, kg |
| $n$ | particle density, $m^{-3}$ |
| $n_s$ | surface density, $m^{-2}$ |
| $n_{sites}$ | density of available surface sites, Pa, Torr, atm |
| $p$ | total pressure, Pa, Torr, atm |
| $p_i$ | partial pressure, Pa, Torr, atm |
| $p_i^s$, | $p_{g,i}^s$ partial pressure just above the surface, Pa, Torr, atm |
| $p_c$ | pressure in Knudsen cell, Pa, Torr, atm |
| $p_v^0$ | vapor pressure of pure condensed phase, Pa, Torr, atm |
| $p_w(x_i)$ | water vapor pressure of condensed phase with dissolved impurity of mixing ratio $x_i$, Pa, Torr, atm |
| $p_0$ | Knudsen cell pressure with closed plunger, Pa, Torr, atm |
| $p_r$ | Knudsen cell pressure with open plunger, Pa, Torr, atm |
| $r$ | radius coordinate, m |
| $R$ | flow tube radius, m |
| $r_p$ | pore radius, m |
| $R$ | rate, $s^{-1}$ |
| $T$ | temperature, K |
| $T_m$ | melting temperature, K |
| $t$ | time, s |
| $t_q$ | reduced temperature, - |
| $\bar{v}$, $\bar{v}_i$ | mean thermal velocity, m $s^{-1}$ |
| $V$ | volume, $m^3$ |
| $x$ | mixing ratio |

## 11. Glossary

| | |
|---|---|
| BET method | method to determine the internal surface area of porous media by gas adsorption and analysis of the adsorption isotherm using the multilayer adsorption isotherm as derived by Brunnauer, Emmet, and Teller (BET)[216] |
| chemical potential | the chemical potential of the $i$th species $\mu_i$ is the Gibbs free energy per mole: $\mu = \partial G/\partial N_i|_{T,p}$ |
| formal monolayer | we consider a formal monolayer as a unit; a formal monolayer of 1 means $10^{15}$ molecules per $cm^2$ |
| equivalent coverage | total uptake per surface area, including both uptake on the surface itself (surface adsorption) and uptake into the bulk ice (e.g. dissolution into the bulk ice, grain boundaries, and veins |
| grain boundary | in polycrystalline matter the surface where two single crystallites meet |
| hydrate | a hydrate is a molecular solid, consisting of water molecules and another molecular species; it has a defined stoichiometry; examples for hydrates in the atmosphere are sulfuric acid trihydrate ($H_2SO_4 \cdot 3H_2O$ or SAT) or nitric acid trihydrate ($HNO_3 \cdot 3H_2O$ or NAT) |
| Henry's Law constant | the dimensionless Henry's Law constant $H_d$ describes the dissolution of a gas into an ideal, infinitive dilute solution, $H_d n_g = n_c$, where $H_d$ is the dimensionless Henry's Law constant and $n_g$ and $n_c$ are the concentrations in the gas and the condensed phases, respectively; here only the first step of the dissolution process, i.e., the molecular dissolution, without any further steps such as reaction or dissociation, is included. |
| effective Henry's Law constant | in contrast to the Henry's Law constant $H_d$, the effective Henry's Law constant $H_d^*$ includes the total amount of dissolved matter, including all products; e.g., for HCl, $H_d^* n_{g,HCl} = (n_{l,HCl} + n_{Cl^-})$, while $H_d n_{g,HCl} = (n_{l,HCl})$; we use $H_d$ also to describe the total amount of gas taken up into the ice bulk, by defining $H_d^* n_g = n_i$, where $n_i$ is the total amount of dissolved matter in the ice averaged over all reservoirs |
| partition coefficient | when freezing ice from an aqueous solution, the ratio of impurity in the ice to the initial solution is called the partition coefficient |
| Pitzer model | thermodynamic model to describe concentrated multicomponent electrolyte solutions; by assigning interaction parameters between different ions, the properties of a ternary solution can be derived from two known binary systems; the Pitzer model has been used with great success to model the properties of supercooled $H_2SO_4$/$HNO_3$/HCl solution in stratospheric aerosols |
| triple junction, vein | in polycrystalline matter, the line where three grain boundaries meet. |

## 12. Acknowledgment

We thank Drs. B. F. Henson, U. K. Krieger, D. A. Knopf, M. M. Miedaner, and M. Kerbrat for valuable comments on the manuscript. The help of P. Forney in many practical matters and careful proofreading of the manuscript is gratefully acknowledged. Many discussions with colleagues helped to shape our understanding of topics treated in this review. We are thankful to Dr. M. J. Rossi for helpful discussions about the nature of the trace gas uptake on ice and the interpretation of experimental work. We are thankful for many weeks of intense discussion with Drs. M. B. Baker, D. Lamb, and B. Swanson during several visits of T.P. and T.H. in Seattle. Partial funding of this work by the European integrated project SCOUT O3 is gratefully acknowledged.

## 13. Appendix A: Units for Solubility Constants

**Dimensionless Henry's Law Constant.** The introduction of solubility concepts has been based on mixing ratios, because the term $k_B T \ln x$ relates directly to the entropy of an ideal gas. However, for practical reasons, often, other units such as concentration (symbol $c$, with unit M or mol $L^{-1}$), molecular particle density (symbol $n$, with unit $m^{-3}$), molality (moles per kg of water in the solution, mol $kg^{-1}$), or weight percent (symbol $w$, kg of solute per kg of solution) are used when calculating solubilities. In this review, we will mostly quantify concentration as molecular density, in units of molecules $cm^{-3}$. Mixing ratios and molecular densities are related by $x_i \rho = n_i \bar{m}$, where the mean molecular mass is $\bar{m} = \sum N_j m_j / \sum N_j$ and the mass density of the condensed phase is $\rho = \sum N_j m_j / V$. This allows rewriting of Henry's Law as

$$H_{d,i} n_{g,i} = n_{c,i} \tag{124}$$

where the dimensionless Henry's Law constant is related to $h_i$ by

$$H_{d,i} = h_i \left( \rho \frac{k_B T}{\bar{m}} \right) \tag{125}$$

by virtue of the ideal gas law $p_i = n_i k_B T$. Another common way of expressing solubility is to use the molecular Henry's

Law constant $H$ (in units of mol $L^{-1}$ $atm^{-1}$)

$$H_i p_i = c_i \tag{126}$$

where $H_i = H_{d,i}/(N_A k_B T)$.

Similarly, the dimensionless Henry's Law constant can be retrieved for species which partly dissociate upon dissolution. To calculate the overall solubility of such species, the equilibrium between the dissolved molecules and the dissociated ions

$$HX \rightleftharpoons H^+ + X^- \tag{127}$$

has to be considered. Under equilibrium conditions, the law of mass action yields

$$K(T) \equiv \frac{n_{H^+} n_{X^-}}{n_{HX}} \tag{128}$$

where $K(T)$ is a temperature-dependent equilibrium constant. The total dissolved acid $n_{tot} = n_{X^-} + n_{HX}$ can be described by the effective Henry's Law

$$H_d^* n_g = n_{tot} \tag{129}$$

with the effective Henry's Law constant

$$H_d^* = H_d^0 + \sqrt{\frac{K H_d^0 k_B T}{p_i}} \approx \sqrt{\frac{K H_d^0 k_B T}{p_i}} \tag{130}$$

## 14. References


(1) Barbante, C.; Schwikowski, M.; Döring, T.; Gäggeler, H. W.; Schotterer, U.; Tobler, L.; van der Velde, K.; Heferrai, C.; Cozzi, G.; Turetta, A.; Rosman, K.; Bolshov, M.; Capodaglio, G.; Cescon, P.; Boutron, C. *Environ. Sci. Technol.* **2004**, *38*, 4085.
(2) Petit, J. R.; et al. *Nature* **1999**, *399*, 429.
(3) Watson, R. T. *Climate Change 2001: Synthesis Report*; Cambridge University Press: Cambridge, 2001.
(4) Peter, Th. *Annu. Rev. Phys. Chem.* **1997**, *48*, 785.
(5) Zondlo, M. A.; Hudson, P. K.; Prenni, A. J.; Tolbert, M. A. *Annu. Rev. Phys. Chem.* **2000**, *51*, 473.
(6) Solomon, S. *Nature* **1990**, *347*, 347.
(7) Legrand, M. R.; Delmas, R. L.; Charlson, R. J. *Nature* **1988**, *334*, 418.
(8) Legrand, M.; Mayewski, P. *Rev. Geophys.* **1997**, *35* (3), 219.
(9) Wolff, E. W. Location, movement and reaction of impurities in solid ice. In *Chemical Exchange between the atmosphere and polar snow*; NATO ASI series. Serie I: Global environmental change, Vol. 43; Wolff, E. W., Bales, R. C., Eds.; Springer: New York, 1995.
(10) Wolff, E. W.; Mulvaney, R.; Oates, K. *Geophys. Res. Lett.* **1989**, *16*, 487.
(11) Mulvany, R.; Wolff, E. W.; Oates, K. *Nature* **1988**, *331*, 247.
(12) Dominé, F.; Shepson, P. B. *Science* **2002**, *23* (24), 1506.
(13) McElroy, C. T.; McLinden, C. A.; McConnell, J. C. *Nature* **1999**, *397*, 338.
(14) Wennberg, P. O.; et al. *Science* **1998**, *279*, 49.
(15) Bottenheim, J. W.; Dibb, J. E.; Honrath, R.; Shepson, P. *Atmos. Environ.* **2002**, *36* (Special issue: Alert 2000), 15−16.
(16) Finlayson-Pitts, B.; Pitts, J. *Chemistry of the upper and lower atmosphere*; Academic Press: San Diego, CA, 2000.
(17) Carslaw, K. S.; Clegg, S. L.; Brimblecombe, P. *J. Phys. Chem.* **1995**, *99*, 11557.
(18) Crutzen, P. J.; Arnold, F. *Nature* **1986**, *324*, 651.
(19) Peter, Th.; Crutzen, P. J., *J. Aerosol Sci.* **1993**, *24*, 119.
(20) Peter, Th.; Crutzen, P. J., *NATO ASI Ser.* **1994**, *I* 21, 500.
(21) Henson, B. F.; Wilson, K. W.; Robonson, J. M.; Noble, C. A.; Cason, J. L.; Worsnop, D. R. *J. Chem. Phys.* **2004**, *121*, 8468.
(22) Barone, S.; Zondlo, M. A.; Tolbert, M. *J. Phys. Chem.* **1999**, *103*, 9717.
(23) Carslaw, K. S.; Peter, Th. *Geophys. Res. Lett.* **1997**, *24* (14), 1743.
(24) Keyser, L. F.; Moore, S. B.; Leu, M. T. *J. Phys. Chem.* **1991**, *95*, 5496.
(25) Keyser, L. F.; Leu, M. T. *Microsc. Res. Technol.* **1993**, *25*, 434.
(26) Keyser, L. K.; Leu, M. T.; Moore, S. B. *J. Phys. Chem.* **1993**, *97*, 2800.
(27) Keyser, L. F.; Leu, M. T. *J. Colloid Interface Sci.* **1993**, *155*, 137.
(28) Hanson, D. R.; Ravishankara, A. R. *J. Phys. Chem.* **1992**, *96*, 2682.
(29) Hanson, D. R.; Ravishankara, A. R. *J. Phys. Chem.* **1993**, *97*, 2802.
(30) Vogt, R.; Sander, R.; Glasow, R.; Crutzen, P. J. *J. Atmos. Chem.* **1999**, *32*, 375.
(31) Wagner, T.; Platt, U. *Nature* **1998**, *395*, 486.
(32) McConnell, J. C.; Henderson, G. S.; Barrie, L.; Bottenheim, J.; Niki, H.; Langford, C. H.; Templeton, E. M. J. *Nature* **1992**, *355*, 150.
(33) Luo, B. P.; Carslaw, K. S.; Peter, Th.; and Clegg, S. M. *Geophys. Res. Lett.* **1995**, *22*, 274.
(34) Carslaw, K. C.; Th. Peter,; Clegg, S. L. *Rev. Geophys.* **1997**, *35* (2), 125.
(35) Hanson, D.; Mauersberger, K. *Geophys. Res. Lett.* **1988**, *15* (13), 1507.
(36) Waibel, A. E.;; Peter, Th.,; S.Carslaw, K.; Oelhaf, H.; Wetzel, G.; Crutzen, P. J.; Poeschl, U.; Tsias, A.; Reimer, E.; Fischer, H. *Science* **1999**, *283*, 2064.
(37) Deshler, T.; Peter, Th.,; Müller, R.; Crutzen, P. *Geophys. Res. Lett.* **1994**, *21*, 1327.
(38) Peter, Th.,; Müller, R.; Crutzen, P. J. *Geophy. Res. Lett.* **1994**, *21*, 1331.
(39) Biermann, U. M.; Crowley, J. N.; Huthwelker, T.; Crutzen, G. K. M. P. J.; Peter, Th. *Geophys. Res. Lett.* **1998**, *25*, 3939.
(40) B. G. Koehler, B. *Int. J. Chem. Kinet.* **2001**, *33*, 295.
(41) Lawrence, M. G.; Crutzen, P. J. *Tellus* **1998**, *50B*, 263−289.
(42) Abbatt, J. P. D. *Geophys. Res. Lett.* **1997**, *24*, 1479.
(43) Zondlo, M. A.; Barone, S. B.; Tolbert, M. A. *Geophys. Res. Lett.* **1997**, *24*, 1391.
(44) Davis, D. D.; et al. *Atmos. Environ.* **2004**, *38*, 5363.
(45) Zhou, X. L.; Beine, H. J.; RE, R. E. H.; Fuentes, J. D.; Simpson, W.; Shepson, P. B.; Bottenheim, J. W. *Geophys. Res. Lett.* **2001**, *28* (21), 4087.
(46) Zhou, X. L.; Gao, H. L.; He, Y.; Huang, G.; Bertram, S. B.; Civerolo, K.; Schwab, J. *Geophys. Res. Lett.* **2003**, *30*, Art. No. 2217.
(47) Dibb, J. E.; Huey, L. G.; Slusher, D. L.; Tanner, D. J. *Atmos. Environ.* **2004**, *38* (32), 5399.
(48) Stutz, J.; Alicke, B.; Ackermann, R.; Geyer, A.; Wang, S.; White, A. B.; Williams, E. J.; Spicer, C. W.; Fast, J. D. *J. Geophys. Res.* **2004**, *109*, D03307, http://dx.doi.org/10.1029/2003JD004135.
(49) Ammann, M.; Kalberer, M.; Jost, D. T.; Tobler, L.; Rössler, E.; Piguet, D.; Gäggeler, H. W.; Baltensperger, U. *Nature* **1998**, *395*, 157.
(50) Kleffmann, J.; Becker, K. H.; Lackhoff, M.; Wiesen, P. *Phys. Chem. Chem. Phys.* **1999**, *1* (24), 5443.
(51) Leu, M. T. *Int. Rev. Phys. Chem.* **2003**, *22* (2), 341.
(52) Arnold, F.; Scheid, J.; Stilp, T.; Schlager, H.; Reinhardt, M. E. *Geophys. Res. Lett.* **1992**, *1926*, 2421.
(53) Lu, R. E. H. Y.; Peterson, M. C.; Dibb, J. E.; Arsenault, M. A.; Cullen, N. J.; Steffen, K. *Atmos. Environ.* **2001**, *28* (21), 4087.
(54) Jacobi, H. W.; Bales, R. C.; Honrath, R. E.; Peterson, M. C.; Dibb, J. E.; Swanson, A. L.; Albert, M. R. *Atmos. Environ.* **2004**, *38* (12), 1687.
(55) Beine, H. J.; Honrath, R. E., D. F. S. W. F. J. *J. Geophys. Res. A* **2002**, *107* (D21), Art. No. 4584.
(56) Seinfeld, J. H. *Atmospheric chemistry and physics of air pollution;* Wiley-Interscience: New York, 1986.
(57) Voldner, E. C.; Barrie, L. A.; Sirois, A. *Atmos. Environ.* **1986**, *20* (11), 2101.
(58) Wesely, M. L.; Hicks, B. B. *Atmos. Environ.* **2000**, *34*, 2261.
(59) Clapsaddle, C.; Lamb, D. *Geophys. Res. Lett.* **1989**, *16*, 1173.
(60) Conklin, M. H.; Sommerfeld, R. A.; Laird, S. K.; Villinski, J. E. *Atmos. Environ.* **1993**, *27A*, 159.
(61) Diehl, K.; Mitra, S. K.; Pruppacher, H. R. *Atmos. Res.* **1998**, *47*−*48*, 235.
(62) Clegg, S. M.; Abbatt, J. P. D. *J. Phys. Chem. A* **2001**, *105*, 6630.
(63) Schwartz, S. E.; Freiberg, J. E. *Atmos. Environ.* **1981**, *15*, 1129.
(64) Schwartz, S. E. Mass-transport considerations pertinent to aqueous phase reactions of gases in liquid-water clouds. In *Chemistry of Multiphase Atmospheric Systems*; NATO ASI Series, Vol. G6; Springer-Verlag: Berlin Heidelberg, 1986.
(65) Danckwerts, P. V. *Gas*−*liquid reactions*; McGraw-Hill Chemical Engineering Series; New York, 1970.
(66) Hanson, D. R.; Ravishankara, A. R. *J. Phys. Chem.* **1994**, *98*, 5728.
(67) Hanson, D. R. *J. Phys. Chem. B* **1997**, *101*, 4998.
(68) Jayne, J. T.; Davidovitz, P.; Worsnop, D. R.; Zahniser, M. S.; Kolb, C. E. *J. Phys. Chem.* **1990**, *94* (15), 6041.
(69) Davidovitz, P.; J. T. Jayne, J.; Duan, S. X.; Worsnop, D. R.; Zahniser, M. S.; Kolb, C. E. *J. Phys. Chem.* **1991**, *95*, 6337.
(70) Hanson, D. R.; Ravishankara, A. R.; Solomon, S. *J. Geophys. Res.* **1994**, *99*, (D2), 3615.

(71) Pöschl, U.; Rudich, Y.; Ammann, M. *Atmos. Chem. Phys. Discuss.* **2005**, *5*, 2111.
(72) Andrussow, L. Diffusion. In *Landolt-Börnstein: Zahlenwerte und Funktionen aus Physik, Astromonie, Geophysik und Technik*; Transportphänomene I, Vol. 6Bd II; Springer Verlag: Berlin, 1969; p 5.
(73) Thibert, E.; Dominé, F. *J. Phys. Chem. B* **1997**, *101*, 3554.
(74) Thibert, E.; Dominé, F. *J. Phys. Chem. B* **1998**, *102*, 4432.
(75) Ravishankara, A. R. *Science* **1997**, *276*, 1058.
(76) Tabazadeh, A.; Turco, R. P. *J. Geophys. Res.* **1993**, *98D7*, 12727.
(77) Tabazadeh, A.; Toon, O. B.; Jensen, E. J. *Geosphys. Res. Lett.* **1999**, *2614*, 2211.
(78) Flückiger, B.; Chaix, L.; Rossi, M. *J. Phys. Chem. A* **2003**, *107*, 2768.
(79) Leu, M. T.; Keyser, L. F.; Timonen, R. S. *J. Phys. Chem. B* **1997**, *101*, 6259.
(80) Paren, J. G.; Walker, J. C. F. *Nature Phys. Sci.* **1971**, *230*, 77.
(81) Fukazawa, H.; Sugiyama, K.; Mae, S. *J. Phys. Chem.* **1998**, *102* (D2), 4794.
(82) Molina, M. J. The probable role of stratospheric 'ice' clouds: heterogeneous chemistry of the 'ozone hole'. In *Chemrawn VII: The Chemistry of the atmosphere: Its impact on global change*; Blackwell Sci. Publ.: Oxford, U.K., 1992.
(83) Abbatt, J. P. D.; Beyer, K. D.; Fucaloro, A. F.; McMahon, J. R.; Wooldridge, P. J.; Zhang, R.; Molina, M. J. *J. Geophys. Res.* **1992**, *97* (D14), 15918.
(84) Conklin, M. H.; Bales, R. C. *J. Geophys. Res.* **1993**, *98*, 16851.
(85) Molina, M. J. In *Chemistry of the atmosphere: Its impact on global change*; Calvert, J. G., Ed.; Blackwell Sci.: Oxford, 1994.
(86) Chen, J. P.; Crutzen, P. J. *J. Geophys. Res.* **1994**, *99D9*, 18847.
(87) Faraday, M. *Athenaeum* **1850**, 640.
(88) Faraday, M. *Philos. Mag.* **1859**, *17*, 162.
(89) Oxtoby, D. W. *Nature* **1990**, *347*, 725.
(90) Pluis, B.; Taylor, T. N.; Frenkel, D.; van der Veen, J. F. *Phys. Rev. B* **1989**, *40*, 1353.
(91) van der Veen, J. F. *Surf. Sci.* **1999**, *433*−*435*, 1.
(92) Dosch, H. *Critical phenomena at surfaces and interfaces*; Springer Tracts in modern Physics, Vol. 126; Springer: Berlin, Heidelberg, New York, 1992.
(93) Dash, J. G.; Fu, H.; Wettlaufer, J. S. *Rep. Prog. Phys.* **1995**, *58*, 115.
(94) Wettlaufer, J. S. *Philos. Trans. R. Soc. London A* **1999**, *357*, 3403.
(95) Dash, J. G. *Rev. Mod. Phys.* **1999**, *71*, 1737.
(96) Pluis, B.; van der Gon, A. W. D.; van der Veen, J. F. *Surf. Sci.* **1990**, *239*, 282.
(97) Pluis, B.; van der Gon, A. W. D.; van der Veen, J. F. *Surf. Sci.* **1990**, *239*, 265.
(98) van der Gon, A. W. D.; Smith, R. J.; Gay, J. M.; O'Connor, D. J.; van der Veen, J. F. *Surf. Sci.* **1990**, *227*, 143.
(99) Tolla, F. D. D.; Ercolessi, F.; Tosatti, E. *Phys. Rev. Lett.* **1995**, *74*, 3201.
(100) Herman, J. W.; Elsayed-Ali, H. E. *Phys. Rev. Lett.* **1992**, *69*, 1228.
(101) Akhter, J. I.; Jin, Z. H.; Lu, K. *J. Phys.: Condens. Matter* **2001**, *13*, 7969.
(102) Ocampo, J.; Klinger, J. *J. Phys. Chem.* **1983**, *87*, 4167.
(103) Furukawa, Y.; Yamamoto, M.; Kuroda, T. *J. Cryst. Growth* **1987**, *82*, 665.
(104) Elbaum, M.; Lipson, S. G.; Dash, J. G. *J. Cryst. Growth* **1993**, *129*, 491.
(105) Beaglehole, D.; Nason, D. *Surf. Sci.* **1980**, *96*, 357.
(106) Mizuno, Y.; Hanafusa, N. *J. Phys. C1* **1987**, *48*, 511.
(107) Lied, A.; Dosch, H.; Bilgram, J. H. *Physica* **1994**, *B198*, 92.
(108) Lied, A.; Dosch, H.; Bilgram, J. H. *Phys. Rev. Lett.* **1994**, *72*, 3554.
(109) Dosch, H.; Lied, A.; Bilgram, J. H. *Surf. Sci.* **1995**, *327*, 145.
(110) Döppenschmidt, A.; Butt, H. J. *Langmuir* **2000**, *16*, 6709.
(111) Pittenger, B.; Jr. S. C. F.; Cochran, M. J.; Donev, J. M. K.; Robertson, B. E.; Szuchmacher, A.; Overney, R. M. *Phys. Rev. B* **2001**, *63*, 13102.
(112) Sadtchenkeo, V.; Ewing, G. E. *J. Chem. Phys.* **2001**, *116*, 4686.
(113) Bluhm, H.; Ogletree, D. F.; Fadley, C. S.; Hussain, Z.; Salmeron, M. *J. Phys.: Condens. Matter* **2002**, *14*, L227.
(114) Golecki, I.; Jaccard, C. *Phys. Lett. A* **1977**, *63*, 374.
(115) Wei, X.; Miranda, P.; Shen, Y. *Phys. Rev. B* **2002**, *66*, art. no. 085401.
(116) Fletcher, N. H. *Philos. Mag.* **1962**, *7*, 255.
(117) Fletcher, N. H. *Philos. Mag.* **1968**, *18*, 1287.
(118) Lackmann, R.; Stranski, I. N. *J. Cryst. Growth* **1972**, *13/14*, 236.
(119) Nenow, D.; Trayanow, A. *J. Cryst. Growth* **1986**, *79*, 801.
(120) Stoltze, P.; Norskov, J. K.; Landman, U. *Phys. Rev. Lett.* **1988**, *61*, 440.
(121) Karim, O. A.; Haymet, A. D. J. *J. Chem. Phys.* **1988**, *89*, 6889.
(122) Karim, O. A.; Haymet, A. D. J. *Chem. Phys. Lett.* **1987**, *138*, 531.
(123) Kroes, G. J.; Clary, D. C. *Surf. Sci.* **1992**, *365*, 365.
(124) Nada, H.; Furukawa, Y. *J. Phys. Chem. B* **1997**, *101*, 6163.
(125) Vlot, M. J.; Huinink, J.; van der Eerden, J. P. *J. Chem. Phys.* **1999**, *110*, 55.
(126) Nada, H.; Furukawa, Y. *Surf. Sci.* **2000**, *446*, 1−16.
(127) Mantz, Y. A.; Geiger, F. M.; Molina, L. T.; Molina, M. J. *J. Chem. Phys.* **2000**, *113*, 10733.
(128) Gao, G. T.; Zeng, X. C. *J. Chem. Phys.* **2000**, *112*, 8534.
(129) Beaglehole, D. *J. Cryst. Growth* **1991**, *112*, 663.
(130) Israelachvili, J. *Intermolecular & surface forces*, Vol. 2; Academic Press Inc.: San Diego, CA 92101, 1991.
(131) Israelachvilli, J. N.; McGuiggan, P. M. *Science* **1988**, *241*, 795.
(132) Wettlaufer, J. S. *Phys. Rev. Lett.* **1999**, *83* (12), 2516.
(133) Orem, M. W.; Adamson, A. W. *J. Colloid Sci.* **1969**, *31* (2), 278.
(134) Bolton, K. *J. Mol. Struct.* **2004**, *632*, 145.
(135) Foster, K. L.; Tolbert, M. A.; George, S. M. *J. Phys. Chem.* **1997**, *101*, 4979.
(136) Gross, G. W. *J. Colloid Sci.* **1967**, *25*, 270.
(137) Gross, G. W.; McKee, C.; Wu, C. H. *J. Chem. Phys.* **1975**, *62*, 3080.
(138) Gross, G. W.; Wu., C.; Bryant, L.; McKee, C. *J. Chem. Phys.* **1975**, *8*, 3085.
(139) Gross, G. W.; Wong, P. M.; Humes, K. *J. Chem. Phys.* **1977**, *67*, 5264.
(140) Bronsteyn, V. L.; Chernov, A. A. *J. Cryst. Growth* **1991**, *112*, 129.
(141) Mader, H. *J. Glaciol.* **1992**, *38*, 359.
(142) Mader, H. *J. Glaciol.* **1992**, *38*, 333.
(143) Colbeck, S. C. *J. Colloid Interface Sci.* **1979**, *72* (3), 371.
(144) Rempel, A. W.; Waddington, E. D.; Wettlaufer, J. S.; Woster, M. G. *Nature* **2001**, *411*, 568.
(145) Rempel, A. W.; Wettlaufer, J. S.; Waddington, E. D. *J. Geophys. Res.* **2002**, *107* (B12), 2330.
(146) Rempel, A. W.; Wettlaufer, J. S.; Woster, M. G. *Phys. Rev. Lett.* **2001**, *87*, 088501.
(147) Benatov, L.; Wettlaufer, J. S. *Phys. Rev. E* **2004**, *70*, 061606.
(148) Fukuta, N.; Lu, Q. J. *Atmos. Res.* **1995**, *38*, 101.
(149) Knight, C. A. *J. Geophys. Res.* **1996**, *101*, 12921.
(150) Baker, M. B.; Dash, J. G. *J. Geophys. Res.* **1996**, *101* (D8), 12929.
(151) Knight, C. A. *J. Geophys. Res.* **1996**, *101* (D8), 12933.
(152) Baker, M.; Nelson, J. *J. Geophys. Res.* **1996**, *101* (D17), 23035.
(153) Makkonen, L. *J. Phys. Chem. B* **1997**, *101*, 6196.
(154) Hobbs, P. V. *Ice physics*; Clarendon Press: Oxford, 1974.
(155) Chen, J. P.; Crutzen, P. J. *J. Geophys. Res. A* **1996**, *101* (D17), 23037.
(156) Davy, J. G.; Somorjai, G. A. *J. Chem. Phys.* **1971**, *55*, 3624.
(157) Chaix, L.; van den Berg, H.; Rossi, M. J. *J. Phys. Chem. A* **1998**, *102*, 10300.
(158) Delval, C.; Flückiger, B.; Rossi, M. J. *Atmos. Chem. Phys.* **2003**, *3*, 1131.
(159) Sadtchenko, V.; Brindza, M.; M, M. C.; Palmore, B.; Eom, R. *J. Chem. Phys.* **2004**, *121*, 11980.
(160) Guggenheim, E. A. *Thermodynamics. An advanced treatment for chemists and physicists*; North-Holland Publishing Company: 1949.
(161) Pitzer, K. S.; Simonson, J. M. *J. Phys. Chem.* **1986**, *90*, 3005.
(162) Pitzer, K. *J. Phys. Chem.* **1970**, *77*, 268.
(163) Eigen, M.; Kustin, K. *J. Am. Chem. Soc.* **1962**, *94*, 1355.
(164) There has been some controversy whether the term Henry's Law should be applied also to the quadratic law describing the dissolution of dissociating electrolytes in eq 15, which describes the ideal behavior of the dissolution of dissociating electrolytes. However, historically the term Henry's Law was originally used only for the linearity between gas-phase pressure and the amount of dissolved matter. For discussion of the controversy, see refs 468 and 469 and references therein.
(165) Petrenko, V. F.; Whithworth, R. W. *Physics of ice*; Oxford University Press: Oxford, 1999.
(166) The corresponding Henry's Law constant is $\hat{h}_{\mathrm{HX}x_{\mathrm{L}}} = p^{-1} \exp[-(\mu^0_{\mathrm{g},i} - \mu^{\infty}_{\mathrm{c,H^+}} - \mu^{\infty}_{\mathrm{c,Cl^-}} - \mu^{\infty}_{\mathrm{c},x_{\mathrm{L}}})/k_{\mathrm{B}}T]$.
(167) Seidensticker, R. G. *J. Chem. Phys.* **1972**, *56*, 2853.
(168) Kemball, C.; Rideal, E. K. *Proc. R. Soc. London, Ser. A: Math. Phys. Sci.* **1946**, *187*, 53.
(169) de Boer, J. H. *The Dynamical Character of Adsorption*; Clarendon Press: 1968.
(170) Wooldridge, P. J.; Zhang, R. Y.; Molina, M. J. *J. Geophys. Res., [Atmos.]* **1995**, *100*, 1389.
(171) Chu, L. T.; Chu, L. *J. Phys. Chem. A* **1999**, *103*, 384.
(172) Huthwelker, T.; Lamb, D.; Baker, M.; Swanson, B.; Peter, Th. *J. Colloid Interface. Sci.* **2001**, *238*, 147.
(173) Gmelin, J. F. *Gmelin's Handbuch der anorganischen Chemie, Schwefel*, 8th ed.; Verlag Chemie: Weinheim, 1960; Vol. Part B, No. 2.
(174) Carslaw, K. S.; Peter, Th. Air pollution research report. *Proceedings of the third european workshop*, 18 to 22 September 1995; European Commission: 1995; Vol. 56, p 726.
(175) Pickering, S. U. *Ber. Dtsch. Chem. Ges.* **1893**, *26*, 277.
(176) Rupert, F. *J. Am. Chem. Soc.* **1909**, *31*, 851.
(177) Vuillard, G. C. *R. Acad. Sci.* **1955**, *241*, 1308.
(178) Fritz, J.; Fuget, C. *Ind. Eng. Chem., Chem. Eng. Data Ser.* **1956**, *1*, 10.

(179) Jaecker-Voirol, A.; Ponche, J.; Mirabel, P. *J. Geophys. Res.* **1990**, *95*, 11857.
(180) Ji, K. Etude de la composition des aérosols stratosphériques polaires au moyen de diagrammes de phase stables, métastables et cinétique des systemes: $HNO_3/H_2O$, $HCl/H_2O$ et $H_2SO_4/H_2O$. Thesis, Université de Paris VII, Paris, 1994.
(181) Koop, T.; Carslaw, K. S. *Science* **1996**, *272*, 1638.
(182) Kuste, H.; Kremann, R. *Z. Anorg. Chem.* **1904**, *41*, 1.
(183) Biltz, W.; Hülsmann, O. *Nachr. Götting. Ges.* **1935**, *2* (1), 99.
(184) Potier, J.; Potier, A. *C. R. Acad. Sci.* **1956**, 1474.
(185) Pickering, S. U. *Philos. Mag.* **1893**, *36*, 11.
(186) Haase, R.; Naas, H.; Thumm, H. *Z. Phys. Chem. Frankfurt* **1963**, *37*, 210.
(187) *International Critical Tables of Physics, Chemistry and Technology*; McGraw-Hill: New York, 1929; Vol. 3, p 177.
(188) Adamson, A. W. *Physical chemistry of surfaces*; John Wiley and Sons: New York, 1990.
(189) Bhatt, D.; Newmann, J.; Radtke, C. J. *J. Phys. Chem. B* **2003**, *107*, 13076.
(190) Baker, M. B.; Dash, J. D. *J. Geophys. Res.* **1994**, *99*, 10621.
(191) From the standard thermodynamic relations $\mu = h - Ts$ and $d\mu = -s\ dT + v\ dp$, which implies $s = -\partial\mu/\partial T$, follows $\Delta\mu = \Delta h + T\ \partial\Delta\mu/\partial T$. At the triple point, where we have $\Delta\mu = 0$, the relation $\partial\Delta\mu/\partial T|_{T_0,p_0} = \Delta h(T_0,p_0)/T$ follows.
(192) Surface energy data for ice show large uncertainty; for example, data[154] for $\gamma_{ls}$ vary from 10 to 40 mJ $m^{-2}$. If we adopt the measurement of Ketcham and Hobbs[470] ($\gamma_{sv} = 109 \pm 3$ mJ $m^{-2}$, $\gamma_{ls} = 33$ mJ $m^{-2}$, $\gamma_{gb} = 65$ mJ $m^{-2}$) and use $\gamma_{lv} = 75 \pm$ mJ $m^{-2}$ (*Hobbs Ice Physics* p 434), we find $\Delta\gamma = 75 + 33 - 109$ mJ $m^{-2} = 1$ mJ $m^{-2} \pm 5$ mJ $m^{-2}$. Thus, available data are not sufficient to predict the existence or nonexistence of the surface premelt layer.
(193) Nye, J. F. *J. Glaciol.* **1991**, *37* (127), 401.
(194) Walford, M. E. R.; Nye, J. F. *J. Glaciol.* **1991**, *37* (101), 1107.
(195) Kirchner, W.; Welter, F.; Bongarts, A.; Kames, J.; Schweighoefer, S.; Schurath, U. *J. Atmos. Chem.* **1990**, *10*, 427.
(196) Roth, C. M.; Goss, K. U.; Schwarzenbach, R. P. *J. Colloid Interface Sci.* **2002**, *252* (1), 21.
(197) Jayne, J. T.; Duan, S. X.; Davidovitz, P.; Worsnop, D. R.; Zahniser, M. S.; Kolb, C. E. *J. Phys. Chem.* **1991**, *95*, 6337.
(198) Nathanson, G. M.; Davidovits, P.; Worsnop, D. R.; Kolb, C. E. *J. Phys. Chem.* **1996**, *100* (31), 13007.
(199) Kelly, C.; Cramer, C. J.; Truhlar, D. G. *J. Phys. Chem. B* **2004**, *108* (34), 12882.
(200) Andersson, P. U.; Nagard, M. B.; Pettersson, J. B. C. *J. Phys. Chem. B* **2000**, *104*, 1596.
(201) Isakson, M. J.; Sitz, G. O. *J. Phys. Chem. A* **1999**, *103*, 2044.
(202) Berland, B. S.; Tolbert, M. A.; George, S. M. *J. Phys. Chem. A* **1997**, *101*, 9954.
(203) Chu, L.; Chu, L. T. *J. Phys. Chem. A* **1999**, *103*, 8640.
(204) Pruppacher, H. R.; Klett, J. D. *Microphysics of clouds and precipitation*; D. Reidel Publishing Company: Dordrecht, Holland, 1980.
(205) Monchick, L.; Reiss, H. *J. Chem. Phys.* **1954**, *22*, 831.
(206) Monchick, L.; Blackmore, R. *J. Aerosol Sci.* **1988**, *19*, 273.
(207) Monchick, L. *J. Chem. Phys.* **1983**, *78* (4), 1808.
(208) L'vov, B. V. *Spectrochim. Acta, Part B* **1997**, *52*, 1.
(209) Assuming an ice density of 1 g $cm^{-3}$, we calculate the average number of molecules $N_{ML}$ in a monolayer by $N_{ML} = N_{cube}^{2/3} = 1.04 \times 10^{15}$ molecules $cm^{-2}$, where $N_{cube}$ is the number of water molecules in a cubic centimeter of ice. From the ice density, we calculate the average thickness of this monolayer as 3.1 Å. These numbers represent only average values for thickness and density of a monolayer, which differ from the crystallographic data. As we do not consider the detailed crystal lattice structure, the average numbers are sufficient for all calculations. See also footnote 408.
(210) Trapnell, B. M. W. *Chemisorption*; Butterworth Scientific Publications: London, 1955.
(211) Mozurkewich, M. *Geophys. Res. Lett.* **1993**, *20*, 355.
(212) Henson, B. F.; Wilson, K.; Robinson, J. *Geophys. Res. Lett.* **1996**, *23*, 1021.
(213) Hynes, R. G.; Mössinger, J. C.; Cox, R. A. *Geophys. Res. Lett.* **2001**, *28*, 2827.
(214) Huthwelker, T.; Malmström, M. K.; Helleis, F.; Peter, Th.; Moortgat, G. *J. Phys. Chem. A* **2004**, *108*, 6302.
(215) Ullerstam, M.; Thornberry, T.; Abbatt, J. P. D. *Faraday Discuss.* **2005**, *130*, 211.
(216) Brunnauer, S.; Emmet, P. H.; Teller, E. *J. Am. Chem. Soc.* **1938**, *60*, 309−319.
(217) Flückiger, B.; Rossi, M. *J. Phys. Chem. A* **2003**, *107*, 4103.
(218) In ref 214, the saturation term for the transport from the bulk to the surface was omitted, because the condition $\theta < 0.1$ was fulfilled.
(219) We note that eq 61 has been used to model the mass accommodation coefficient as defined for liquid interfaces (see section 2.3.1). To do so, $\gamma$ needs to be replaced with $\alpha_c$ and $S_0$ takes the role of $\alpha_c$ in eq 61.
(220) Crank, J. *Mathematics of diffusion;* Oxford University Press: London, 1956.
(221) Carslaw, H. S.; Jaeger, J. C. *Conduction of heat in solids*; Clarendon Press: Oxford, 1959.
(222) For a complete derivation, the change of the Henry's Law constant must be considered when solving the diffusion equation. Therefore, the expression $\gamma(t,p) \approx (4/\bar{v})(k_B T K H_d/p)^{1/2} t^{1/2}$ is an approximation, which allows estimation of the influence of small pressure changes during an uptake experiment in a Knudsen cell or a flow tube. To the best of our knowledge, currently there is no full analytical solution for the uptake kinetics into liquids for a dissociating species.[471]
(223) Worsnop, D. R.; Zahniser, M. S.; Kolb, C. E. *J. Phys. Chem.* **1989**, *93*, 1159.
(224) Ammann, M.; Poeschl, U.; Rudich, Y. *Phys. Chem. Chem. Phys.* **2003**, *5*, 351.
(225) Ammann, M.; Poeschl, U. *Atmos. Chem. Phys. Discuss.* **2005**, *5*, 2193.
(226) Often, the diffusion depth is approximated by the expression $x = (Dt)^{1/2}$. Here we use the mathematically correct expression of $x = (Dt/\pi)^{1/2}$. It should be noted that in the early work on this topic[223] the factor of $\pi^{1/2}$ was missing.
(227) Huthwelker, T.; Peter, Th. *J. Chem. Phys.* **1996**, *105*, 1661−1667.
(228) Elliot, S. E.; Turco, R. P.; Toon, O. B.; Hamill, P. *Geophys. Res. Lett.* **1990**, *17*, 425.
(229) Golden, D. L.; Spokes, G. N.; Benson, S. W. *Angew. Chem.* **1973**, *14*, 602.
(230) Howard, C. J. *J. Phys. Chem.* **1979**, *83*, 3.
(231) Kaufmann, F. *J. Phys. Chem.* **1984**, *88*, 4909.
(232) Molina, M. J.; Tso, T. L.; Molina, L. T.; Wang, F. C. Y. *Science* **1987**, *238*, 1253.
(233) Tolbert, M. A.; Rossi, M. J.; Malhotra, R.; Golden, D. M. *Science* **1987**, *238*, 1258.
(234) Abbatt, J. P. D. *Chem. Rev.* **2003**, *103* (12), 4783.
(235) Williams, L. R.; Golden, D. M. *Geophys. Res. Lett.* **1993**, *20* (20), 2227.
(236) Fenter, F. F.; Rossi, M. J. *J. Phys. Chem.* **1996**, *100*, 13765.
(237) Williams, L. R.; Golden, D. M.; Huestis, D. L. *J. Geophys. Res.* **1995**, *100* (D4), 7329.
(238) Caloz, F.; Fenter, F. F.; Tabor, K. D.; Rossi, M. J. *Rev. Sci. Instrum.* **1997**, *68* (8), 3172.
(239) Allanic, A.; Oppliger, R.; Rossi, M. J. *J. Geophys. Res., [Atmos.]* **1997**, *102*, 23529.
(240) Chaix, L.; Allanic, A.; Rossi, M. J. *J. Phys. Chem. A* **2000**, *104*, 7268.
(241) Flückiger, B.; Chaix, L.; Rossi, M. J. *J. Phys. Chem. A* **2000**, *104*, 11739.
(242) Aguzzi, A.; Rossi, M. J. *Phys. Chem. Chem. Phys.* **2001**, *3*, 3707.
(243) Hudson, P. K.; Shilling, J. E.; Tolbert, M. A.; Toon, O. B. *J. Phys. Chem. A* **2002**, *106*, 9874.
(244) Hudson, P. K.; Zondlo, M.; Tolbert, M. A. *J. Phys. Chem. A* **2002**, *106*, 2882.
(245) Fenter, F. F.; Caloz, F.; Rossi, M. J. *Rev. Sci. Instrum.* **1997**, *68* (8), 3180.
(246) Susa, A.; Koda, S. *Meas. Sci. Technol.* **2004**, *15*, 1230.
(247) Flückiger, B. Laboratory kinetics and mechanistic studies of heterogeneous reactions on ice relevant to the stratosphere. Thesis No. 2158; EPLF: Lausanne, Switzerland, 2000.
(248) Kleffmann, J.; Benter, T.; Wiesen, P. *J. Phys. Chem. A* **2004**, *108*, 5793.
(249) Hanson, D. R.; Mauersberger, K. *J. Phys. Chem.* **1990**, *94*, 4700.
(250) Huthwelker, T. Experimente und Modellierung der Spurengasaufnahme in Eis. Dissertation, Universität Bonn, Cuvillier Verlag Göttingen, 1999, ISBN 3-89712-675-3.
(251) Knopf, D. A.; Zink, P.; Schreiner, J.; Mauersberger, K. *Aerosol Sci. Technol.* **2001**, *35*, 924.
(252) Chu, L. T.; Leu, M. T.; Keyser, L. F. *J. Phys. Chem.* **1993**, *97*, 7779.
(253) Bartels-Rausch, T.; Huthwelker, T.; Gäggeler, H. W.; Ammann, M. *J. Phys. Chem. A* **2005**, *109*, 4531.
(254) Winkler, A. K.; Holmes, N. S.; Crowley, J. N. *Phys. Chem. Chem. Phys.* **2002**, *4*, 5270.
(255) Hynes, R. G.; Fernandez, M. A.; Cox, R. A. *J. Geophys. Res.* **2002**, *107*, http://dx.doi.org/10.1029/2001JD001557.
(256) Hirschfelder, J. O.; Curtiss, C. F.; Curtis, R. B. *Molecular theory of gases and liquids*; John Wiley & Sons, Inc.: 1954.
(257) Mason, E. A.; Monchick, L. *J. Chem. Phys.* **1961**, *36*, 2746.
(258) Monchick, L.; Mason, E. A. *J. Chem. Phys.* **1961**, *35*, 1676.
(259) Schäfer, K., Ed.; *Landolt-Börnstein: Zahlenwerte und Funktionen aus Physik, Astromonie, Geophysik und Technik. Transportphänomene*; 1969; Vol. Bd, p 5a.

(260) Massmann, W. J. *J. Phys. Chem. B* **2003**, *107*, 3871.
(261) Sommerfeld, R. A.; Lamb, D. *Geophys. Res. Lett.* **1986**, *13*, 349.
(262) Laird, S. K.; Sommerfeld, R. A. *Geophys. Res. Lett.* **1995**, *22*, 921.
(263) Laird, S. K.; Buttry, D. A.; Sommerfeld, R. A. *Geophys. Res. Lett.* **1999**, *26*, 699.
(264) Conklin, M. H.; Sigg, A.; Neftel, A. *J. Geophys. Res.* **1993**, *98*, 18367.
(265) Bartels-Rausch, T.; Eichler, B.; Zimmermann, P.; Gäggeler, H. W.; Ammann, M. *Atmos. Chem. Phys.* **2002**, *2*, 235.
(266) Choi, J.; Conklin, M. H.; Bales, R. C.; Sommerfeld, R. A. *Atmos. Environ.* **2000**, *34*, 793.
(267) Jellinek, H. H. G.; Ibrahim, S. H. *J. Colloid Interface Sci.* **1967**, *25*, 245.
(268) Hoff, J. T.; Gregor, D.; Mackay, D.; Wania, F.; Jia, C. Q. *Environ. Sci. Technol.* **1998**, *32*, 58.
(269) Dominé, F.; Cabanes, A.; Taillander, A. S.; Legagneux, L. *Environ. Sci. Technol.* **2001**, *35* (4), 771.
(270) Legagneux, L.; Cabanes, A.; Dominé, F. *J. Geophys. Res., [Atmos.]* **2002**, *107* (D17), art. no. 4335.
(271) Van Genuchten, M. T.; Wirenga, P. J. *J. Soil Sci. Soc. Am.* **1976**, *40*, 473−480.
(272) de Hoffmann, E.; Stroobant, V. *Mass spectroscopy—Principles and applications*; J. Wiley & Sons: Chichester, New York, 2002.
(273) Mauersberger, K. *Rev. Sci. Instrum.* **1977**, *48*, 1169.
(274) Mauersberger, K.; Finstad, R. *Rev. Sci. Instrum.* **1979**, *50*, 1612.
(275) Marti, J.; Mauersberger, K.; Hanson, D. *Geophys. Res. Lett.* **1991**, *18* (10), 1861.
(276) Schreiner, J.; Voigt, C.; Kohlmann, A.; Arnold, F.; Mauersberger, K.; Larsen, N. *Science* **1999**, *283*, 968.
(277) Voigt, C.; et al. *Science* **2000**, *290*, 1756.
(278) Helleis, F.; Crowley, J. N.; Moortgat, G. K. *J. Phys. Chem.* **1993**, *97*, 11464.
(279) Arijs, E.; Barassin, A.; Kopp, E.; Amelynck, C.; Catoire, V.; Fink, H. P.; Guimbaud, C.; Jenzer, U.; Labonnette, D.; Luithard, W.; Neefs, E.; Nevejans, D.; Schoon, N.; Bavel, A. M. V. *Int. J. Mass. Spectrom.* **1998**, *181*, 99.
(280) Ferguson, E. E.; Fehsenfeld, F. C.; Schmeltekopf, A. L. *At. Mol. Phys.* **1969**, *5*, 1.
(281) Gleason, J. F.; Sinha, A.; Howard, C. J. *J. Phys. Chem.* **1987**, *91*, 719.
(282) Hanson, D. R.; Ravishankara, A. R. *J. Geophys. Res.* **1991**, *96*, 5081.
(283) Bevilacqua, T. J.; Hanson, D. R.; Howard, C. J. *J. Phys. Chem.* **1993**, *97*, 3750.
(284) Koehler, B. G.; McNeill, L. S.; Middlebrook, A. M.; Tobert, M. A. *J. Geophys. Res.* **1992**, *97*, 8065.
(285) Delzeit, L.; Rowland, B.; Devlin, J. P. *J. Phys. Chem.* **1993**, *97*, 10312.
(286) Banham, S. F.; Horn, A. B.; Koch, T. G.; Sodeau, J. R. *Faraday Discuss.* **1995**, *100*, 123.
(287) Du, Q.; Superfine, R.; Freysz, E.; Shen, Y. R. *Phys. Rev. Lett.* **1993**, *No. 15*, 2313.
(288) Geiger, F. M.; Pibel, C. D.; M., J.; Hicks, *J. Phys. Chem. A* **2001**, *105*, 4940.
(289) Richmond, G. L. *Chem. Rev.* **2002**, *102*, 2693.
(290) Krishnan, P. N.; Salomon, R. E. *J. Phys. Chem.* **1969**, *73*, 2680.
(291) Dominé, F.; Thibert, E.; Landeghem, F. V.; Silvente, E.; Wagnon, P. *Geophys. Res. Lett.* **1994**, *21*, 601.
(292) Berland, B. S.; Hynes, D. R.; Foster, K. L.; Foster, M. A.; George, S. M. *J. Phys. Chem.* **1994**, *98*, 4358.
(293) Livingston, F. E.; Smith, J. A.; George, S. M. *Anal. Chem.* **2000**, *72*, 5590.
(294) Krieger, U. K.; Huthwelker, T.; Daniel, C.; Weers, U.; Peter, Th.; Lanford, W. *Science* **2002**, *295*, 1048.
(295) Huthwelker, T.; Krieger, U.; Weers, U.; Peter, Th.; Lanford, W. *NIMS B* **2002**, *B190*, 47.
(296) Huthwelker, T.; Krieger, U. K.; Peter, Th.; Lanford, W. In *Proccedings of the 17th International conference on the Application of Accelerator in Research and Industry*; Duggan, J. L., Morgan, I. L., Eds.; American Institute of Physics: Melville, NY, 2002; Vol. 680, p 400.
(297) Chu, W. K.; Mayer, J. M.; Nicolet, M. A. *Backscattering spectrometry*; Academic Press: 1978.
(298) Tesmer, J. R.; Nastasi, M. *Handbook of modern ion beam analysis*; Material Research Society: 1995.
(299) Doolittle, L. R. *Nucl. Inst. Methods* **1985**, *B9*, 344.
(300) Ammann, M. *Radiochim. Acta* **2001**, *89*, 831.
(301) Baltensperger, U.; Ammann, M.; Bochert, U. K.; Eichler, B.; Gäggeler, H. W.; Jost, D. T.; Kovacs, J. A.; Türler, A.; Scherer, U. W.; Baiker, A. *J. Phys. Chem.* **1993**, *97*, 12325.
(302) Eichler, B.; Zvara, I. *Radiochim. Acta* **1982**, *30*, 233.
(303) Huthwelker, T.; Ammann, M. Manuscript in preparation.
(304) Wilson, K. R.; Rude, B. S.; Catalano, T.; Schaller, R. D.; Tobin, J. G.; Co, D. T.; Saykally, R. J.-T. *J. Phys. Chem. B* **2001**, *105*, 3346.
(305) Bournel, F.; Mangeney, C.; Tronc, M.; Laffon, C.; Parent, P. *Surf. Sci.* **2003**, *528*, 224.
(306) Wernet, P.; Nordlund, D.; Bergmann, U.; Cavalleri, M.; Odelius, M.; Ogasawara, H.; Naslund, L. A.; Hirsch, T. K.; Ojamae, L.; P. Glatzel, P.; Pettersson, L. G. M.; Nilsson, A. *Science* **2004**, *304*, 995.
(307) Ruan, C. Y.; Lobastov, V. A.; Vigliotti, F.; Chen, S. Y.; Zewail, A. H. *Science* **2004**, *304*, 80.
(308) Bragg, A. E.; Verlet, J. R. R.; Kammrath, A.; Cheshnovsky, O.; Neumark, D. M. *Science* **2004**, *306*, 669.
(309) Paik, D.; Lee, I.-R.; Yang, D.-S.; Baskin, J. S.; Zewail, A. H. *Science* **2004**, *306*, 672.
(310) Maria, S. F.; Russell, L. M.; Gilles, M. K.; Myneni, S. C. B. *Science* **2004**, *306*, 1921.
(311) Ghosal, S.; Hemminger, J. C.; Bluhm, H.; Mun, B. S.; Hebenstreit, E. L. D.; Ketteler, G.; Ogletree, D. F.; Requejo, F. G.; Salmeron, M. *Science* **2005**, *307*, 563.
(312) Parent, P.; Laffon, C. *J. Phys. Chem. B* **2005**, *109*, 1547.
(313) Bournel, F.; Mangeney, C.; Tronc, M.; Laffon, C.; Parent, P. *Phys. Rev. B* **2002**, *65*, art. no. 201404.
(314) Flückiger, B.; Thielmann, A.; Gutzwiller, L.; Rossi, M. J. *Ber. Bunsen-Ges. Phys. Chem. Chem. Phys.* **1998**, *102*, 915.
(315) Yasumoto, I. *J. Phys. Chem.* **1980**, *84*, 589.
(316) For quasi-stationarity in a flow tube, the condition

$$2v\left(1-1\frac{r^2}{R^2}\right)\frac{\delta n(x,r,t)}{\delta x}+D_g\left(\frac{\delta^2}{\delta r}+\frac{1}{r}\frac{\delta}{\delta r}+\frac{\delta^2}{\delta^2 x}\right)n(x,r,t)+S(x,r,t)\gg\frac{\mathrm{d}n(x,r,t)}{\mathrm{d}t} \quad (131)$$

must hold.

(317) By Taylor expansion, it can be shown that

$$\lim_{x\to 0}\left(-\frac{\alpha}{x}+\sqrt{\left(\frac{\alpha}{x}\right)^2-\frac{\beta}{x}}\right)=-\frac{\beta}{2\alpha} \quad (132)$$

The limit of the positive branch of eq 97 is $-\infty$. Thus, one of the exponential terms in eq 96 disappears.

(318) Hanson, D. R.; Ravishankara, A. R. *J. Phys. Chem.* **1993**, *97*, 12309.
(319) Gormley, P. G.; Kennedy, M. *Proc. R. Soc.* **1949**, *52*, 163.
(320) Aris, R. *Proc. R. Soc.* **1956**, *A235*, 67.
(321) Taylor, G. *Proc. R. Soc.* **1954**, *A235*, 473.
(322) Taylor, G. *Proc. R. Soc.* **1953**, *A219*, 186.
(323) Zvára, I. *Radiochim Acta* **1985**, *38* (2), 95.
(324) Cooney, D. O.; Kim, S. S.; Davis, E. J. *Chem. Eng. Sci.* **1974**, *29*, 1731.
(325) Walker, R. E. *Phys. Fluids* **1961**, *4*, 1211.
(326) Poirier, R. V.; Carr, J. R. W. *J. Phys. Chem.* **1971**, *75*, 1593.
(327) Ogren, P. *J. Phys. Chem.* **1975**, *79*, 1749.
(328) Brown, R. L. *J. Res. Natl. Bur. Stand.* **1978**, *83*, 1.
(329) Msibi, I. M.; Shi, J. P.; Harrison, R. M. *J. Atmos. Chem.* **1993**, *17*, 339.
(330) Fickert, S.; Adams, J. W.; Crowley, J. N. *J. Geophys. Res.* **1999**, *104* (D19), 23719.
(331) Ritzhaupt, G.; Devlin, J. P. *J. Phys. Chem.* **1991**, *95*, 90.
(332) Koehler, B. G.; McNeill, L. S.; Middlebrook, A. M.; Tobert, M. A. *J. Geophys. Res.* **1993**, *98*, 10563.
(333) Toon, O. B.; Tolbert, M. A.; Koehler, B. G.; Middlebrook, A. M. *J. Geophys. Res.* **1994**, *99*, 25361.
(334) Middlebrook, A. M.; Berland, B. S.; George, S. G.; Tolbert, M. A. *J. Geophys. Res.* **1994**, *99*, 25655.
(335) Peil, S.; Seisel, S.; Schrems, O. *J. Mol. Struct.* **1995**, *348*, 449.
(336) Sodeau, J. R.; Horn, A. B.; Banham, S. F.; Koch, T. G. *J. Phys. Chem.* **1995**, *99*, 6258.
(337) Banham, S. F.; Sodeau, J. R.; Horn, A. B.; McCoustra, M. R. S.; Chesters, M. A. *J. Vac. Sci. Technol., A* **1996**, *14* (3), 1620.
(338) Delzeit, L.; Powell, K.; Uras, N.; Devlin, J. P. *J. Phys. Chem. B* **1997**, *101*, 2327.
(339) Koch, T. G.; Banham, S. F.; Sodeau, J. R.; Horn, A. B.; McCoustra, M. R. S.; Chesters, M. A. *J. Geophys. Res., [Atmos.]* **1997**, *102*, 1513.
(340) Pursell, C. J.; Zaidi, M.; Thompson, A.; Fraser-Gaston, C.; Vela, E. *J. Phys. Chem. A* **2000**, *104*, 552.
(341) Pursell, C. J.; Everest, M. A.; Falgout, M. E.; Sanchez, D. D. *J. Phys. Chem. A* **2002**, *106*, 7764.
(342) Using reactive ion scattering (RIS), $Cs^+$ ions of low energy (10−30 eV) are scattered on a surface. Ions on the surface react with the incoming $Cs^+$ ion and leave the surface. These scattered molecule ions are analyzed by mass spectroscopy.

(343) Kang, H.; Shin, T. H.; Park, S. C.; Kim, I. K.; Han, S. J. *J. Am. Chem. Soc.* **2000**, *122*, 9842.
(344) Park, S. C.; Maeng, K. W.; Pradeep, T.; Kang, H. *Nucl. Instrum. Methods Phys. Res., Sect. B: Beam Interact. Mater.* **2001**, *182*, 193.

(345) Park, S. C.; Maeng, K. W.; Pradeep, T.; H. Kang, H. *Angew. Chem., Int. Ed.* **2001**, *40*, 1497.
(346) Buch, V.; Delzeit, L.; Blackledge, C.; Devlin, J. P. *J. Phys. Chem. B* **1996**, *100*, 3732.
(347) Buch, V.; Delzeit, L.; Blackledge, C.; Devlin, J. P. *J. Phys. Chem.* **1996**, *100*, 3732.
(348) Devlin, J. P.; Buch, V. *J. Phys. Chem. B* **1997**, *101*, 6095.
(349) Devlin, J. P.; Uras, N.; Rahman, M.; Buch, V. *Isr. J. Chem.* **1999**, *39*, 261.
(350) Uras, N.; Rahman, M.; Devlin, J. P. *J. Phys. Chem. B* **1998**, *102*, 9375.
(351) Uras-Aytemiz, N.; Devlin, C. J. J. P. *J. Phys. Chem. A* **2001**, *105*, 10497.
(352) Buch, V.; Sadlej, J.; Aytemiz-Uras, N.; Devlin, J. P. *J. Phys. Chem. A* **2002**, *106*, 9374.
(353) Devlin, J. P.; Uras, N.; Sadlej, J.; Buch, V. *Nature* **2002**, *417*, 269.
(354) Fleyfel, F.; Devlin, J. P. *J. Phys. Chem.* **1989**, *93*, 7292.
(355) Delzeit, L.; Devlin, J. P.; Buch, V. *J. Chem. Phys.* **1997**, *107*, 3726.
(356) Donsig, H. A.; Vickermann, J. C. *J. Chem. Soc., Faraday Trans.* **1997**, *93*, 2755.
(357) Lu, Q. B.; Sanche, L. *J. Chem. Phys.* **2001**, *115*, 5711.
(358) Zundel, G.; Metzger, H. *Phys. Chem. (Munich)* **1968**, *58*, 225.
(359) Zundel, G. *Adv. Chem. Phys.* **2000**, *111*, 1.
(360) Bianco, R.; Thompson, W. H.; Morita, A.; Hynes, J. T. *J. Phys. Chem. A* **2001**, *105*, 3132.
(361) Girardet, C.; Toubin, C. *Surf. Sci. Rep.* **2001**, *44*, 163.
(362) Buesnel, R.; Hillier, I. H.; Masters. *Chem. Phys. Lett.* **1995**, *247*, 391.
(363) Planas, M.; Lee, C.; Novoa, J. J. *J. Phys. Chem.* **1995**, *99*, 14323.
(364) Ramondo, F.; Sodeau, J. R.; Roddis, T. B.; Williams, N. A. *Phys. Chem. Chem. Phys.* **2000**, *2*, 2309.
(365) Packer, M. J.; Clary, D. C. *J. Phys. Chem.* **1995**, *99*, 14323.
(366) Svanberg, M.; Pettersson, J. B. C.; Bolton, K. *J. Phys. Chem. A* **2000**, *104*, 5787.
(367) Milet, A.; Struniewicz, C.; Moszynski, R.; Wormer, P. E. S. *J. Chem. Phys.* **2001**, *115*, 349.
(368) Shevkunov, S. V. *Colloid J.* **2004**, *66* (2), 216.
(369) Shevkunov, S. V. *Colloid J.* **2004**, *66* (2), 230.
(370) Shevkunov, S. V. *Colloid J.* **2004**, *66* (4), 495.
(371) Shevkunov, S. V. *Colloid J.* **2004**, *66* (4), 506.
(372) Shevkunov, S. V.; Lukyanov, S. I.; Leyssale, J.-M.; Millot, C. *Chem. Phys.* **2005**, *310*, 97.
(373) Kroes, G. J.; Clary, D. C. *J. Phys. Chem.* **1992**, *96*, 7079.
(374) Wang, L. C.; Clary, D. C. *J. Chem. Phys.* **1996**, *104*, 5663.
(375) Clary, D. C.; Wang, L. C. *J. Chem. Soc., Faraday Trans.* **1997**, *93*, 2763.
(376) Gertner, B. J.; Hynes, J. T. *Science* **1996**, *271*, 1563.
(377) Gertner, B. J.; Hynes, J. T. *Faraday Discuss.* **1998**, *110*, 301.
(378) Bianco, R.; Gertner, B. J.; Hynes, J. T. *Ber. Bunsen-Ges. Phys. Chem.* **1998**, *102*, 518.
(379) Liu, Z. F.; Siu, C. K.; J. S. Tse, J. *Chem. Phys. Lett.* **1999**, *309*, 335.
(380) Allouche, A.; Couturier-Tamburelli, I.; Chiavassa, T. *J. Phys. Chem. B* **2000**, *104*, 1497.
(381) Bolton, K.; Pettersson, J. B. C. *J. Am. Chem. Soc.* **2001**, *123*, 7360.
(382) Toubin, C.; Picaud, S.; Hoang, P. N. M.; Girardet, C.; Demirdjian, B.; Ferry, D.; J. Suzanne, J. *J. Chem. Phys.* **2002**, *116*, 5150.
(383) Mantz, Y. A.; Geiger, F. M.; Molina, L. T.; Molina, M. J.; Trout, B. L. *J. Phys. Chem. A* **2002**, *106*, 6972.
(384) Al-Halabi, A.; Kleyn, A. W.; J., G.; Kroes. *J. Chem. Phys.* **2001**, *115*, 482.
(385) Calatayud, M.; Courmier, D.; Minot, C. *Chem. Phys. Lett.* **2003**, *369*, 287.
(386) Bolton, K. *Int. J. Quantum Chem.* **2004**, *96*, 607.
(387) Ando, K.; Hynes, J. T. *J. Phys. Chem.* **1997**, *101*, 10464.
(388) Fletcher, N. H. *The chemical physics of ice*; Cambridge University Press: London, 1970.
(389) Sommerfeld, R. A.; Knight, C. A.; Laird, S. K. *Geophys. Res. Lett.* **1998**, *25*, 935.
(390) Barnaal, D.; Slootfeldt-Ellingsen, D. *J. Phys. Chem.* **1983**, *87*, 4321−4325.
(391) The melting point of ice in the grain boundary region is depressed by two effects. First of all, by Raoult's Law, that is the melting point depression by the present impurities. Second, the curvature of the ice causes an additional reduction of the melting points. In essence, this effect follows the same thermodynamic principles as the formation of the quasi-liquid layer. Here the Kelvin effect replaces the surface energy of the quasi-liquid layer. This effect has been investigated in detail by several authors.[80,141−143,193,194]
(392) Horn, A. B.; Sully, J. *J. Chem. Soc., Faraday Trans.* **1997**, *93*, 2741.
(393) In this experiment, an ice film is condensed onto an optically polished germanium plate. To perform attenuated total internal reflection infrared spectroscopy (ATR-IR), a beam of infrared radiation is brought into the polished germanium plate, such that total reflection occurs inside the plate at the germanium−ice interface. Along the surface where total reflection occurs, an evanescent field extends into the other phase, which in this case is the back side of the ice film. Thus, the back side of the ice film is investigated with IR spectroscopy.
(394) Livingston, F. E.; George, S. M. *J. Phys. Chem. A* **2001**, *105*, 5155.
(395) Livingston, F. E.; George, S. M. *J. Phys. Chem. B* **2002**, *106*, 5114.
(396) Knight, C. A. *J. Glaciol.* **1996**, *42*, 585.
(397) Dominé, F.; Xueref, I. *Anal. Chem.* **2001**, *73*, 4348.
(398) Aguzzi, A.; Flückiger, B.; Rossi, M. J. *Phys. Chem. Chem. Phys.* **2003**, *3*, 4157.
(399) Dominé, F.; Thibert, E. *Geophys. Res. Lett.* **1998**, *25*, 4389.
(400) Sommerfeld, R. A.; Knight, C. A.; Lair, S. K. *Geophys. Res. Lett.* **1998**, *25*, 4391.
(401) Adamson, A. W.; Dormant, L. M.; Orem, M. *J. Colloid Interface Sci.* **1967**, *25*, 206.
(402) Chu, L. T.; Heron, J. W. *Geophys. Res. Lett.* **1995**, *22*, 3211.
(403) Hobbs, P. V.; Scott, W. D. *J. Colloid Interface Sci.* **1967**, *25*, 223−230.
(404) Hanson, D. R.; Ravishankara, A. R. *J. Phys. Chem.* **1992**, *96*, 9441.
(405) Lee, S.-H.; Leard, D. C.; Zhang, R. Z.; Molina, L. T.; Molina, M. J. *Chem. Phys. Lett.* **1999**, *315*, 7.
(406) Sokolov, O.; Abbatt, J. P. D. *Geophys. Res. Lett.* **2002**, *29*, 1851 (http://dx.doi.org/10.1029/2002GL014843).
(407) Abbatt, J. P. D.; Molina, M. J. *J. Phys. Chem.* **1992**, *96*, 7674.
(408) For all conversions, such as from the ice mass to the film thickness, we use a specific weight of 1 g $cm^{-3}$ for ice. We are aware that the density of vapor deposited ice is lower than this value, but for the sake of comparison, it is important to use the same density in all calculations. In Figure 25, open squares mark the ranges as derived from Figure 4 in ref 249. The authors do not explicitly give a film thickness, but they give the ice mass and the mixing ratio of HCl in the ice. We have converted the ice mass into a film thickness, by assuming a total ice surface area between 10 and 20 $cm^2$ for the two thickest films and 1 $cm^2$ for the three thinnest films. The ranges in the figure take this uncertainty of the ice surface area into account. The open square is taken from ref 22 and is based on a film thickness of 50 nm and a measured uptake of $(3.5 \pm 1.6) \times 10^{15}$ molecules $cm^{-2}$. The filled square is taken from ref 28 using a film thickness of 10 $\mu$m. The crosses are taken from Abbatt et al. Here a total uptake of $3 \times 10^{15}$ and $10^{15}$ is converted to mixing ratio units using a film thickness of 7.5 $\mu$m, which is the average value of the estimate of 5−10 $\mu$m in the original publication. Asterisks mark the data from Figure 3 in ref 79. The conversion of the ice mass to a film thickness uses the fact that a total mass of 496 mg corresponds to a film thickness of 44 $\mu$m. Open and closed circles are taken from Figure 7 in ref 214. The open circle marks the range of total uptake as measured for a total experimental time of 1800 s. The filled circle marks the surface uptake as calculated from the asymptotic fitting procedure. The impressive thickness dependence as measured by Chu et al.[252] is omitted in Figure and 25, as these data were taken at the lower temperatures 193 and 188 K (see also Figure 22), while the figure refers to a temperature of 200 K. See also footnote 209.
(409) For practical matters, the quantity $\gamma(t,p)$ is plotted as function of $t^{1/2}$ and a linearity $1/\gamma(t,p) \approx (\bar{v}/4)(p_0/k_B TKH_d)^{1/2}(\pi t/D)^{1/2}$ is used.
(410) Luo, B. P.; Clegg, S. L.; Peter, Th.; Müller, R.; Crutzen, P. J. *Geophys. Res. Lett.* **1994**, *21*, 49.
(411) Percival, C. J.; Mössinger, J. C.; Cox, R. A. *Phys. Chem. Chem. Phys.* **1999**, *1*, 4565.
(412) Carslaw, K. S.; Luo, B. P.; Clegg, S.; Peter, T.; Brimblecombe, P.; Crutzen, P. J. *Geophys. Res. Lett.* **1994**, *21*, 2479.
(413) Koop, T.; Biermann, U. M.; Raber, W.; Luo, B. P.; Crutzen, P. J.; Peter, Th. *Geophys. Res. Lett.* **1995**, *22*, 917.
(414) Brasseur, G. P.; Orlando, J. J.; Tyndall, G. S. *Atmospheric chemistry and global change*; Oxford University Press: New York, 1999.
(415) Abbatt, J. P. D. *Geophys. Res. Lett.* **1994**, *21*, 665.
(416) Rieley, H.; Aalin, H. D.; Haq, S. *J. Chem. Soc., Faraday Trans.* **1995**, *91*, 2349.
(417) Hudson, P. K.; Foster, K. L.; Tolbert, M. A.; George, S. M.; Carlo, S. R.; V. H. Grassian, V. *J. Phys. Chem. A* **2001**, *105*, 694.
(418) Chu, L. T.; Chu, L. *J. Phys. Chem. B* **1997**, *101*, 6271.
(419) Arora, O. P.; Cziczo, D. J.; Morgan, A. M.; Abbatt, J. P. D.; Niedziela, R. F. *Geophys. Res. Lett.* **1999**, *26*, 3621.
(420) Meilinger, S. K.; Tsias, A.; Dreiling, V.; Kuhn, M.; Feigl, C.; Ziereis, H.; Schlager, H.; Curtius, J.; Sierau, B.; Zöger, M.; Schiller, C.; Peter, Th. *Geophys. Res. Lett.* **1999**, *26* (14), 2207.
(421) Kondo, Y.; et al. *Geophys. Res. Lett.* **2003**, *30* (4), 1154 (http://dx.doi.org/10.1029/2002GL016539).
(422) Ziereis, H.; Minikin, A.; Schlager, H.; Gayet, J. F.; Auriol, F.; Stock, P.; Baehr, J.; Petzold, A.; Schumann, U.; Weinheimer, A.; Ridley, B.; Ström, J. *Geophys. Res. Lett.* **2004**, *31*, http://dx.doi.org/10.1029/2003GL018794.

(423) Popp, P. J.; et al. *J. Geophys. Res.* **2004**, *109D*, 06302 (http://dx.doi.org/10.1029/2003JD004255).
(424) Park, J. Y.; Lee, Y. W. *J. Phys. Chem.* **1988**, *92*, 6294.
(425) Becker, K. H.; Kleffmann, J.; Kurtenbach, R.; Wiesen, P. *J. Phys. Chem.* **1996**, *100*, 14984.
(426) Longfellow, C. A.; Imamura, T.; Ravishankara, A. R.; Hanson, D. R. *J. Phys. Chem. A* **1998**, *102*, 3323.
(427) Riordan, E.; Minogue, N.; Healy, D.; O'Driscoll, P.; Sodeau, J. R. *J. Phys. Chem. A* **2005**, *109*, 779.
(428) Seisel, S.; Rossi, M. J. *Ber. Bunsen-Ges. Phys. Chem.* **1997**, *101*, 943.
(429) Chu, L.; Diao, G. W.; Chu, L. T. *J. Phys. Chem. A* **2000**, *104*, 3150.
(430) Diao, G. W.; Chu, L. T. *J. Phys. Chem. A* **2005**, *109*, 1364.
(431) Santachiara, G.; Prodi, F.; Vivarelli, F. *Atmos. Environ.* **1995**, *9*, 983.
(432) Santachiara, G.; Prodi, F.; Udisti, R.; A. Prodi, A. *Atmos. Res.* **1998**, *48*, 209.
(433) Chu, L.; Diao, G. W.; Chu, L. T. *J. Phys. Chem. A* **2000**, *104*, 7565.
(434) Clegg, S. M.; Abbatt, J. P. D. *Atmos. Chem. Phys.* **2001**, *1*, 73.
(435) Diehl, K.; Mitra, S. K.; Pruppacher, H. R. *Atmos. Environ.* **1995**, *29*, 975.
(436) Iribarne, J. V.; Pyshnov, T.; Naik, B. *Atmos. Environ.* **1990**, *24A*, 389.
(437) Valdez, M. P.; Dawson, G. A.; Bales, R. C. *J. Geophys. Res.* **1989**, *44D1*, 1096.
(438) Welpdale, D. M.; Shaw, R. W. *Tellus* **1974**, *1*−*2*, 196.
(439) Dovland, H.; Eliasson, A. *Atmos. Environ.* **1976**, *10*, 783.
(440) Barrie, L. A.; Walmsley, J. L. *Atmos. Environ.* **1978**, *12*, 2321.
(441) Granat, L.; Johanson, C. *Atmos. Environ.* **1983**, *17*, 191.
(442) Cadle, S. H.; Dash, J. M.; Mulva, P. A. *Atmos. Environ.* **1985**, *19*, 1819.
(443) Dash, J. M.; Cadle, S. H. *Water, Air, Soil Pollut.* **1986**, *29*, 297.
(444) Valdez, M. P.; Bales, R. C.; Stanley, D. A.; Dawson, G. A. *J. Geophys. Res.* **1987**, *D8*, 9779.
(445) Bales, R. C.; Valdez, M. P.; Dawson, G. A. *J. Geophys. Res.* **1987**, *D8*, 9789.
(446) Goldberg, R.; Parker, V. B. *J. Res. Natl. Bur. Stand.* **1985**, *90*, 341.
(447) Maupetit, F.; Delmas, R. J. *Tellus* **1994**, *46B*, 304.
(448) Delzeit, L.; Rowland, B.; Devlin, J. P.; Buch, V. *J. Phys. Chem.* **1996**, *100*, 10076.
(449) Langenberg, S. Anwendung der Kapillar-Gaschromatographie zur Untersuchung von Spurengas-Aerosolwechselwirkungen. Dissertation, Universität Bonn, http://www2.chemie.uni-erlangen.de/services/dissonline/nnav/d_kat0.html, 1997.
(450) Langenberg, S.; Schurath, U. *Geophys. Res. Lett.* **1999**, *26*, 1695.
(451) Giddings, J. C. *Unified separation analysis*; Wiley: 1991.
(452) Takenaka, N.; Ueda, A.; Maeda, Y. *Nature* **1992**, *358*, 736.
(453) Takenaka, N.; Ueda, A.; Daimona, T.; Banwow, H.; Dohmaru, T.; Maeda, Y. *J. Phys. Chem.* **1996**, *100*, 13874.
(454) Meilinger, S. K.; Koop, T.; Luo, B. P.; Huthwelker, T.; Carslaw, K. S.; Krieger, U.; Crutzen, P. J.; Peter, Th, *Geophys. Res. Lett.* **1995**, *22*, 3031.
(455) Dominé, F.; Thibert, E. *Geophys. Res. Lett.* **1996**, *24*, 3627.
(456) Dominé, F.; Rauzy, C. *Atmos. Chem. Phys.* **2004**, *4*, 2513.
(457) Karcher, B.; Basko, M. M. *J. Geophys. Res. D* **2004**, *109*, Art. No. D22204.
(458) Xueref, I.; Dominé, F. *Atmos. Chem. Phys.* **2003**, *3*, 1779.
(459) Wolff, E. W.; Mulvany, R. *Geophys. Res. Lett.* **1991**, *18* (No. 6), 1007.
(460) Xiao, R.-F.; Ming, N.-B. *Phys. Rev.* **1994**, *49*, 4720.
(461) Russell, L. M.; Maria, S. F.; Myneni, S. C. B. *Science* **2002**, *16*, art. no. 10.1029/2002GL014874.
(462) Marcus, M. A.; MacDowell, A. A.; R, R. C.; Manceau, A.; Miller, T.; Padmore, H. A.; Sublett, R. E. *J. Synth. Rad.* **2004**, *11*, 239.
(463) Miedaner, M. M.; Huthwelker, T.; Enzmann, F.; Stampanoni, M.; Ammann, M.; Kersten, M. Manuscript in preparation.
(464) Schick, M.; Shih, W. H. *Phys. Rev.* **1987**, *B35*, 5030.
(465) Livingston, F. E.; George, S. M. *J. Phys. Chem. B* **1999**, *103*, 4366.
(466) Behr, P.; Terziyski, A.; Zellner, R. *Z. Phys. Chem.: Int. J. Res. Phys. Chem. Chem. Phys.* **2004**, *18* (11), 1307.
(467) Barnaal, D.; Kopp, M.; Lowe, I. *J. Chem. Phys.* **1976**, *65*, 5495.
(468) Schwartz, S. E. *Atmos. Environ.* **1988**, *10*, 2331.
(469) Clegg, S. L.; Brimblecombe, P. *Atmos. Environ.* **1988**, *10*, 2332.
(470) Ketcham, W. M.; Hobbs, P. V. *Philos. Mag.* **1969**, *19*, 1161.
(471) To properly solve this problem, the diffusion equation must be solved with a boundary condition of the form

$$D\frac{\delta n(x{=}0,t)}{\delta x} = \text{constant} \times (p_g - n^j) \qquad (133)$$

with $j = {}^3/_2$. The case $j = 1$ describes the case without dissociation, which can be solved analytically. The case $j = {}^3/_2$ leads to nonlinear equations which cannot be solved easily.

CR020506V